CHARACTERISING A TRANSMISSION LINE CONDUCTOR SUBJECT TO FREE AND FORCED VIBRATIONS

by

Malwande Babalo Sityoshwana

Dissertation submitted in fulfilment of the requirements for the degree

Master of Engineering in Mechanical Engineering

in the Faculty of Engineering and the Built Environment

at the Cape Peninsula University of Technology

Supervisor: Professor Modify Andrew Elton Kaunda

Co-Supervisor: Dr Tiyamike Ngonda

Bellville Campus

Date submitted September 2020

DECLARATION

I, Malwande Babalo Sityoshwana, declare that the content of this dissertation represents my unaided work and that the dissertation has not been previously submitted for academic examination towards any qualification. Furthermore, it represents my own opinions and not necessarily those of the Cape Peninsula University of Technology.

Signed Date

ABSTRACT

Aeolian vibration is caused by vortex shedding due to the laminar flow of wind. It has low amplitude vibrations and is characterised by frequencies of between 3 and 150 Hz. It is the most common kind of vibrations in transmission lines. Since it occurs in the vertical plane, it causes alternating bending stresses, leading to eventual failure of the conductor cable.

The study characterised free and forced vibrations of the Tern and ACSR Bersfort conductors. This was done according to IEEE Standards and general research on line conductors according to CIGRE guidelines. The characterisation experiments were conducted at the University of KwaZulu-Natal's Vibration Research and Testing Centre (VRTC).

The study was conducted to confirm the findings of a 2011 study by Mokeretla, which suggested that the Tern and ACSR Bersfort conductors' self-damping characteristics could not be able to suppress Aeolian vibrations.

The study found that the damping factors for forced and free vibrations on the Tern conductor were ≤ 0.02181 and ≤ 0.236, respectively. Also, it found that the damping factors for forced and free vibrations for the ACSR Bersfort were ≤ 0.024807 and ≤ 0.232, respectively. These findings suggest that the natural damping of the Tern and ACSR Bersfort conductors cannot suppress aeolian vibrations. Thus, this study collaborates the findings of Mokeretla.

ACKNOWLEDGEMENT

I thank the Lord Almighty for giving me strength and the passion for completing the study. I would also like to thank the following people who have played different roles in reaching this achievement.

I thank my supervisor Prof M.A.E Kaunda for encouraging me to further my studies, guide and advise me throughout this journey.

I also thank my co-supervisor, Dr Tiyamike Ngonda, for standing in as my supervisor while Prof Kaunda was sick. This made it possible for me to submit my proposal within the prescribed period.

I express gratitude to Mr Pravesh Moodley and Prof David Dorrell of the University of KwaZulu-Natal for providing me access to their facilities for the testing portion of my study.

I thank my parents (Thembinkosi Sityoshwana and Nomsa Sityoshwana) for the valuable support and words of encouragement when needed the most.

I make special mention of my siblings, starting with Zamikhaya Mlakalaka and his wife Ndileka Barnes-Mlakalaka for helping me choose this career and being most supportive, Olwethu Sityoshwana and my home supervisor Vuyiseka Sityoshwana for the kind assistance you gave me through this journey and my wife Mama ka Unako (Sisipho Mngeni-Sityoshwana) for the words of encouragement and being a support system.

I thank my children (Lisolethu Phuza, Unako Sityoshwana and Amise Sityoshwana) for being there for me and my friends and colleagues who took some of their time assisting me, ndiyabulela.

I acknowledge the support I received from the University of KwaZulu-Natal, Eskom's Tertiary Education Support Programme (TESP) of Eskom, the National Research Foundation (NRF) and the Cape Peninsula University of Technology.

Ndiyabulela…

TABLE OF CONTENTS

LIST OF TABLES

LIST OF FIGURES

CHAPTER 1
INTRODUCTION

1.1 Introduction

Transmission lines (see Figure 1.1) play an essential role in distributing electricity to various places. Wind-induced (Aeolian) vibrations of transmission lines can produce damage that can significantly influence the functionality of these lines.

Mokeretla, (2011) explains that Aeolian vibration is the most common vibration of transmission lines, arising from vortex shedding beneath a laminar stream of wind. Aeolian vibration is often a low-amplitude vibration which usually occurs at 3 - 60 Hz for wind speeds of (1-8 m/s). These vibrations occur in the vertical plane, applies nonstop substituting bowing stresses on the conductor strands, and may, in the long run, lead to weariness disappointment of the conductor (Bukhari et al, 2008).

Conductors damaged by Aeolian vibration need to be resized or even taken out of service until repairs can be made. This loss of conductors could significantly affect an entire network because conductors are the power carrying component of the transmission lines (Diana et al., 2000).

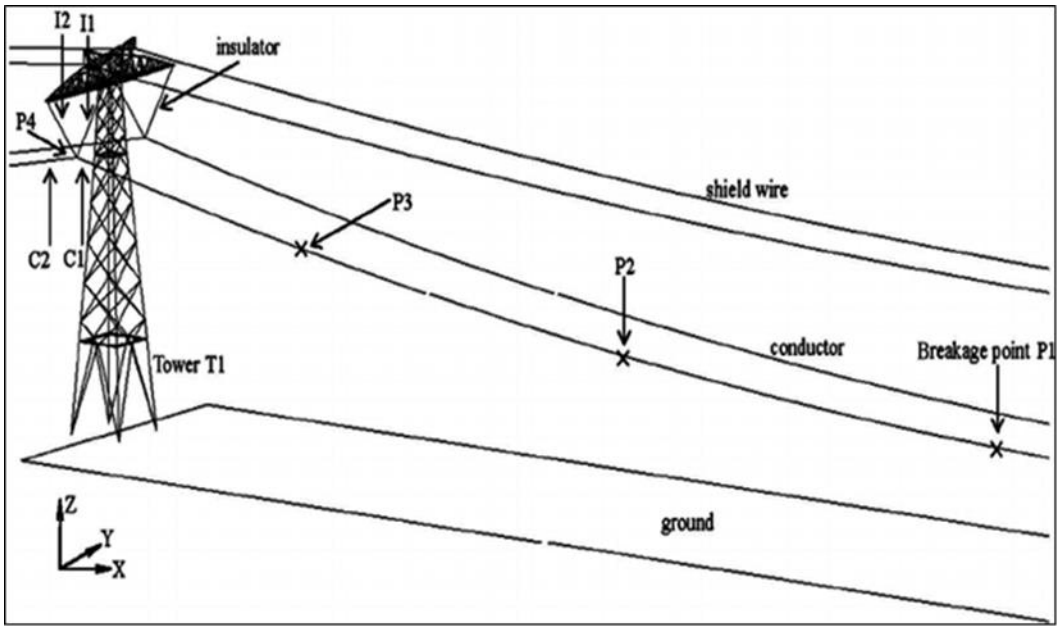

Figure 1. 1: A sketch of transmission lines

The overhead transmission lines are continuously exposed to wind forces, making them liable to repeated alternating stresses that are the source of absolute damage to the power network. These stresses are known as "wind-induced conductor motion". They take the form of conductor galloping, wake-induced oscillations, and Aeolian vibration (Chan et al., 2006). These motions are mainly distinguished by their frequencies and amplitudes of vibration (Barry, 2014).

Table 1.1 below gives a summary of these three types of vibration.

Table 1. 1: Summary of three types of vibrations (Doucy et al., 1979).

	Vibration Category		
Parameter	**Aeolian**	**Galloping**	**Wake-Induced**
Sort of overhead lines affected	All	All	Bundle conductors
Recurrence range	3 Hz to 150 Hz	0.08 Hz to 3 Hz	0.15 Hz to 10 Hz
Peak-peak conductor amplitude	0.01 to 1 D	5 to 300 D	0.5 to 80 D
Sort of wind inciting motion	Consistent	Consistent	Consistent
Velocity of wind	1 m/s to 7 m/s	7 m/s to 18 m/s	4 m/s to 18 m/s
The surface of the conductor.	Uncovered or uniform frosted	Asymmetrical ice deposit	Bare, dry

In South Africa, transmission lines usually fail (break, unwind) due to either the harsh environment as excessive wind or overtime usage under a particular environment. The consequence of such unpredicted failure is generally a power outage that subsequently leads to excessive consumer complaints and massive loss of valuables. Electric power suppliers in South Africa face this unwanted situation regularly and therefore decided to look into possible ways of avoiding or limiting failures of their transmission lines.

In terms of failure due to excessive wind, the source of the predicament is that the transmission line users (Eskom and Municipalities) do not have sufficient information from the transmission

line manufacturers regarding the maximum wind that these transmission lines can withstand without failure. Similarly, in terms of failure due to overtime usage, the transmission line users do not also have the transmission lines manufacturers' information regarding their life span on the South African environment. It could be said that the mechanical failure of the transmission lines is due to a lack of sufficient knowledge of the vibration characteristics of transmission conductors.

In South Africa, the transmission lines are exposed to the wind speed of approximately 5 to 15 km/h. These winds force the transmission lines to gallop, which causes reversed stresses in the cable that makes up the transmission lines. Some of the consequences of transmission line failure can be avoided if Eskom and Municipalities could predict the failure from the onset. These entities' prediction potential is hampered by the absence of transmission lines dynamic and onsite characteristics of the transmission line. This results from the lack of numerical and physical models that could predict the failure of the transmission lines exposed to South African conditions.

1.1.1 The ACSR conductors used in transmission lines

In transmission lines, the Aluminium Conductor Steel Strengthened (ACSR) is generally utilised as uncovered overhead transmission conductor. The ACSR is used as an essential, auxiliary dissemination conductor and flag-bearer back because it offers ideal quality for line plan without relinquishing ampacity (Fletcher et al., 2018). Fletcher et al. (2018) explain that another reason for the ACSR conductor's preference is that it is an economical design.

The ACSR is concentrically stranded conductor with one or more layers of drawn electrolytic aluminium wire on galvanised tall malleable steel wire centre (see Figure 1.2) (Fletcher et al, 2018). The centre can be single wire or stranded depending on the estimate of the conductor. Steel centre wire of the ACSR is galvanised to minimise corrosion. ACSR is mostly used for long-span transmission lines because of its high tensile strength.

Figure 1. 2: Strand structure of ACSR conductor (Fletcher et a., 2018)

Like other transmission conductors, the ACSR fail due to harshness of the environment, particularly thundering, rain, lightning, phenomena, flashover, winter ice, fog, fog stick on the insulator, and pollution cause poor contact insulators and transmitters (Panth, 2014). Excessive vibrations of conductors facilitate these failures. Examples of failed ACSR conductors are shown in Figure 1.3.

(a) **(b)**

Figure 1. 3: Pictures of failed ACSR conductors (Trujillo et al., 2018)

1.2 Problem statement

Mokeretla (2011) points out that conductor manufacturers do not give the self-damping characteristics of conductors. This is a challenge because it forces users of transmission conductors to investigate conductors' damping characteristics to enable them to specify relevant mass absorbers. Also, since conductors' self-damping characteristics are not known, mathematical modelling of conductor vibration behaviour cannot be successfully executed.

It is imperative to know if a particular conductor's self-damping characteristics will minimise the vibration-induced failures, especially those caused by Aeolian vibration on the transmission line. For South Africa, this is crucial because this will mean that the transmission line can be installed on the areas where the self-damping characteristics can suppress the estimated maximum wind's effects. Furthermore, this will save Eskom and government funds by not putting additional dampers where it is not necessary.

1.3 Objectives of the study

The study's primary objective was to determine if ACSR Bersfort and Tern conductors' natural vibration damping behaviour are sufficient to suppress wind-induced Aeolian vibrations.

To achieve the primary objective, the following secondary objectives were pursued.

1.3.1 To experimentally determine the vibration behaviour of ACSR Bersfort and Tern conduction when excited with an electrodynamic shaker, to examine the damping constant, stress profile and natural frequencies.

1.3.2 To numerically determine the damping behaviour of ACSR Bersfort and Tern conduction when exposed to free and forced vibrations of between 10 Hz and 300 Hz.

1.4 Limitation of the study

In South Africa, electricity supply companies and municipalities use various types of conductors for the transmission line. However, this study focuses on ACSR Bersfort conductor and Tern conductor.

1.5 Outline of the dissertation

Chapter 1 presents a background of the problem, the study's objectives, and a summary of the facilities and equipment used.

Chapter 2 presents a review of literature that was undertaken encompassing theory of vibration of conductors and previous studies of vibrations of transmission lines.

Chapter 3 presents the theory of free and forced vibrations of conductors as relevant to the study.

Chapter 4 presents the experimental procedures that were used.

Chapters 5 to 8 present the results from the experimental work.

Chapter 9 presents the conclusion that was drawn from the findings of the study.

Chapter 10 presents the recommendations for further work arising from the lessons learnt in the present study.

.

CHAPTER 2
LITERATURE REVIEW

2.1 Introduction

This chapter presents a literature review on the effects of weather conditions on transmission lines. It will also present literature on the vibration of conductors, particularly types of conductor vibration that affect ACSR and Tern conductors used in transmission lines.

2.2 Weather conditions

Panth (2014) showed that transmission lines suffer from different types of failure because they are generally uncovered and exposed to the environment. The landscape influences the way particular transmission lines are arranged. This makes them prone to transmission line halfway flashover failure. This failure of line fault-prone shapes the ordinary control supply of the control system where the danger becomes quite large within the occasion of failure, caused by partial wind trip (Panth, 2014).

Therefore, it becomes clear that certain conductors are designed for certain standards and allocated as per the weather conditions. The conductor situated in a hot but low wind environment cannot be the same as that in an environment with heavy wind. Some conductors fail because they are misplaced or placed in an environment that does not match the conductor material criteria. Therefore, the study reflected on the need for the supplier to specify the condition that the conductor can withstand. This will help Eskom save funds and not place additional dampers to stop vibration where it is not necessary.

Operation of the multi-circuit overhead lines interfacing huge generation and stack centres are often affected by the crisis loading, which produces high conductor temperature. In the past, the conductor's most extreme emergency temperature has been constrained to 80°C to 120°C depending on the conductor sort and size. Nigol and Barrett (1981) suggest that the trend has been to extend these operational temperatures further. Since the prevailing temperature influences conductors' vibration response, it is of utmost importance that the researchers consider the temperature when conducting the vibration experiments to determine conductor response under free and forced vibration.

.

2.3 Vibrations of conductors

Three major types of conductor movements influence ACSR conductor to breaking point:

a) Aeolian vibration

b) Conductor galloping

c) Wake-induced vibration

2.3.1 Aeolian vibration

Alderton et al. (2015) explain that aeolian vibration is low amplitude and high-frequency vibration of conductors due to vortex shedding. Aeolian vibration is caused by the wind. As the wind passes over an uncovered, tensioned conductor or cable, vortices develop, as shown in Figure 2.1. The developed vortices are shed on the tail end of the conductor. The shedding of the vortices is cyclic, and this causes the conductor to vibrate.

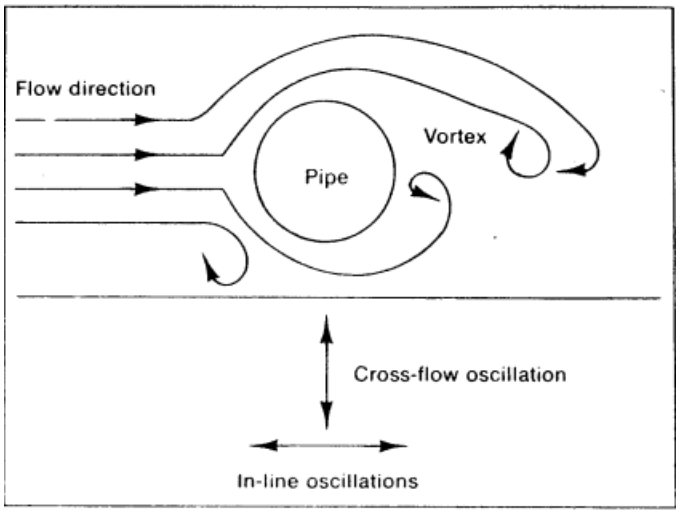

Figure 2. 1: Aeolian Vibration (Darmasaputra, 2016)

According to Alderton et al. (2015), Aeolian vibration is the major cause of conductor strands' fatigue failure. Figure 2.2 shows an example of the type of fatigue failure Aeolian vibration causes to ACSR conductor strands. In case of extreme the conductor vibration, fatigue of individual conductor strands can result. Aluminium strands are especially prone to fatigue, particularly when fretting is involved.

Figure 2. 2: ACSR Fatigue Failure & Broken Aluminium Strands (Alderton et al., 2015)

Kubelwa et al. (2018) argue that wind-induced conductor vibrations such as Aeolian vibrations are still a significant issue of concern to transmission-line engineers. If unmitigated, wind-induced conductor vibrations can cause severe conductor damage. In the installation of transmission lines., it is preferred to prevent conductor failure before it occurs. This is a challenge because it is difficult to estimate the amount of wind in different places. Thus, conductors must be installed to withstand heavy wind conditions. If the conductor cannot withstand wind-induced vibration in a particular area, dampers must be attached to reduce vibration.

2.3.2 Conductor galloping

Chan et al. (2006) describe conductor galloping as a very low-frequency, high amplitude, primarily vertical conductor motion. Conductor galloping occurs in snowy weather, accompanied by moderate to strong wind (Chan et al., 2006). It is most common when there is hail covering the cable. This coating of ice makes sporadic edges and surfaces, disturbing the air stream, which breaks away at these points to initiate a certain self-excitation (Mokeretla,2011).

2.3.3 Wake-induced vibration

Wake-induced vibration happens in bundle conductors may occur due to the swinging movement, like a pendulum that is caused when the wind blows over a bundle conductor. In an event, the two transmission lines, side-by-side, isolated by a spacer are considered. The wake from the windward line actuates lower drag and makes lifting strengths on the leeward line. The lines shared by a

spacer affect each other motion through a combination of the spacer (Irvine, 2006). Figure 2.3 shows wake-induced vibration of conductors.

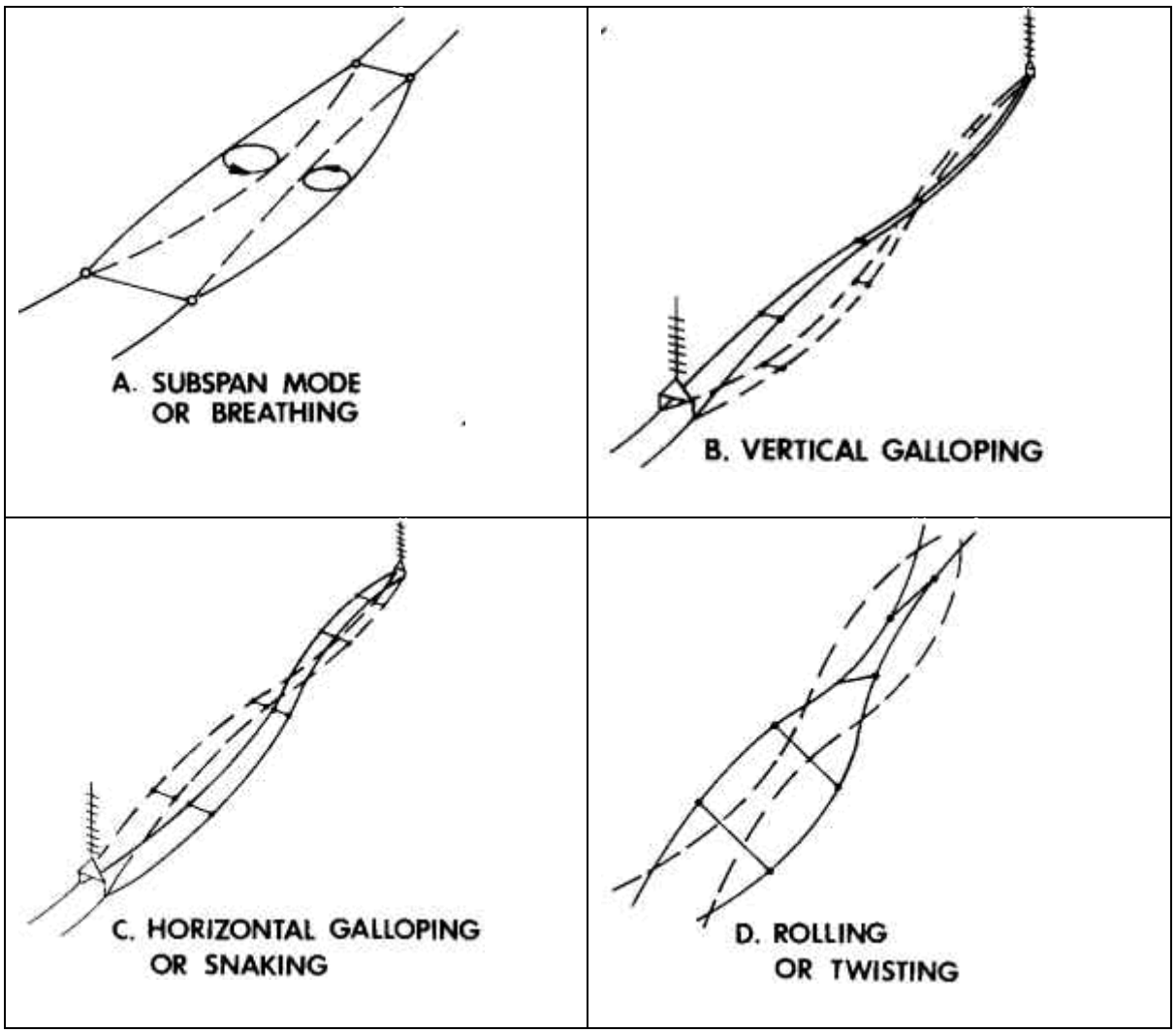

Figure 2. 3: Waked Induced Vibration (Diana & Milano, 2018)

2.4 Review of literature on experimental research on conductor vibration

Several experimental studies, such as Mokeretla (2011), Panth,2014 and Eshiemogie (2011), have focused on transmission lines' damping characteristics. Mokeretla (2011) studied self-damping of the transmission lines and found that conductor vibration does depend on tuned absorbers such as Stockbridge dampers but on viscous or contact damping. Despite this, Mokeretla (2011) found that the transmission lines' self-damping is usually insufficient to suppress Aeolian vibration. Furthermore, Mokeretla study showed that it is not compulsory to have dampers on transmission lines. Considering Mokeretla's findings, it is worth noting that

the study was conducted on TERN and Aero-Z IEC62219-REV240609 conductors, not ACSR conductors.

Eshiemogie (2011) evaluated the bare conductor self-damping. This study evaluated damping at different tensions for free and forced vibration for Aero-Z and Tern conductors. It found that the self-damping of Aero-Z conductor is higher than that of Tern conductor. This finding alludes to the need to study the characteristics of the various conductors. Also, Eshiemogie's study showed that two parameters need to be considered, the highest wind speed in the environment where a transmission line will be installed and the type of conductor that could suppress the wind effects in that particular environment. Understanding this would help power utilities such as ESKOM to reduce costs, as there will not be a need to install dampers were there are not needed. This is particularly useful in new transmission line development. Still, for the existing installations that were done without considering wind speed, dampers can minimise vibration.

Tsimberg *et al*. (2014) showed that overhead conductors' condition could not be satisfactorily determined by age or visual inspection. The study used a set of 14 conductors to determine if they were still functional. The study found significant differences between conductor well-being determined utilising the "Basic" and "Comprehensive" Relief List equations. The study also found no correlation between the chronological age of transmission lines and their functional life span. This indicates that inspection or life stage modelling has limited usefulness in determining various conductors' functional capacity. This finding puts pressure on designers to address factors that would prolong the functional life of transmission lines during transmission line design, thus, conductor selection should consider the environmental condition in which the conductors will be placed.

Another study by Wayer (2016) focused on five spans classified as borderline during an inspection testing in April 2013. The declined sections were removed in 2015 with a couple of hundred feet of new ACSR that were merged in the span. Out of the 54 wire spans inspected, 30 spans contained a compression joint. In comparison, the remaining 24 spans did not include any compression connection. This study showed that:

- 96% of spans with compression sleeve splices had corrosion present in various stages.
- 83% of these spans were found to be in good condition.

- 42% of spans without compression sleeves had corrosion present in various stages.
- 91% of these spans were considered “Good” or “Very Good”
- About 40% of the spans in the system have localised areas of corrosion that are Category 3 or worse.
- 33 of 36 maximum corrosion locations (91%) occurred within 150 ft. of the low point of the span.

Figure 2. 4: Transmission line electromagnetic testing (Wayer, 2016)

With the assumption that these results are representative of the system, the following generalisation can be made:

- Almost all spans with compression splices have corrosion at some location.
- About ½ of spans without compression splices have corrosion at some location.
- The point of maximum corrosion occurs within 150 feet of the low point of the span.
- None of the conductors were appraised as fatigue-prone, which would lead to ineviTable failures. Since none of these localised zones was in a destitute condition, it may be a few years before more frequent discoveries of broken wire and related issues are watched. However, a plan/program needs to be developed to start addressing this deteriorating conductor.

Rawlins (2008) examined the vibration of tensioned cables amid flexure by transverse vibration. The flexure caused relative developments between the wires or strands of the cable, movements which were obliged by grinding between them. Beneath conditions common to the

vibration of overhead transmission line conductors the contact was incredible sufficient to avoid net sliding.

Moreover, there was a small scale slip at the edges of the connect strand contacts, so there was frictional scattering. In expansion, the frictional strengths caused shear strains at the contacts with coming about fabric damping. Investigation showed that interfaces the conductor's substantial flexure with the inner connect strand developments and powers with scattering sums that happen self-damping. Comparison of gauges based on the examination with measured information on self-damping uncovers sensible assertion, for a constrained extend.

Kubelwa et al. (2018) presented the experimental results of bending stresses on aluminium conductors and steel-reinforced ACSR that was rigidly clamped and subjected to Aeolian vibration in an indoor span. The tests were conducted on four different conductors widely used by a utility to determine the relationship between bending stress and bending amplitude, which is an important parameter for conductor fatigue.

Diana et al. (2000) worked around a modern strategy for deciding the overhead transmission line conductor self-damping by applying tests on a research facility span. The process depended on the converse standing wave proportion strategy but presented an estimation strategy to restrain a few of the issues associated with the strategy's straightforward application. It has been considered and tried particularly given its application to estimate specific conductors' self-damping, such as the optical ground wires and the generally unused all-dielectric self-supporting optical cables, whose self-damping is exceptionally low.

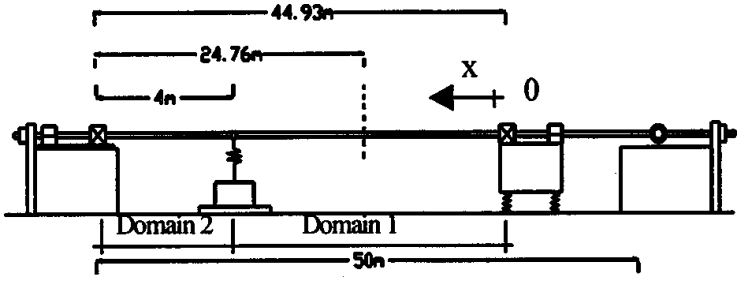

Figure 2. 5: Laboratory Span (Diana et al., 2000)

Test results from Diana et al. (2000) showed a non-linear dependence on the bending amplitude, particularly for smaller-sized conductors. This differs significantly from the

bending stresses as calculated by the Poffenberger-Swart formula. This can be noted in Figure 2.6 below. Bending amplitude and bending stress data, plotted using curve-fitting with third-order polynomials, gave excellent correlation with experimental data. Thus, Diana et al. (2000) may be used to assess the vibration severity for these conductors. This approach may then easily be applied for further investigations, such as estimating the lifetime expectancy, and/or the fatigue endurance limits of these conductors undergoing Aeolian vibrations.

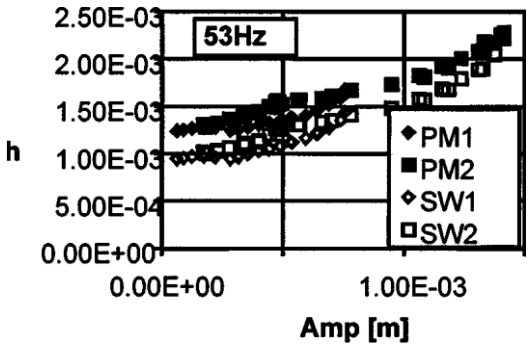

Figure 2. 6: Comparison control method-ISWR strategy: 34 Hz (1, 2 diverse test runs; ACST cable, distance across 24.15 mm). (Diana et al., 2000)

Koh and Rong (2004) investigated three-dimensional cable movement, bookkeeping for pivotal, flexural and torsion distortions, as well as geometric nonlinearity due to expansive displacements and revolutions. Their study used numerical techniques whose findings were verified by experimental work. Cable movement due to support excitation was utilised to demonstrate the asymmetry and sensitivity of the energetic pressure reaction related to geometric non-linearity of large-displacement cable movement. The shaking Table tests collaborated the numerical outcomes for both two-dimensional and three-dimensional cases. This study's key finding was that conductors are much weaker in the out-of-plane motion than the in-plane motion.

Wolf et al. (2008) developed an energy balance-based estimation of overhead transmission line Aeolian vibrations. Their method estimated bending stresses, amplitude and strains at the middle of the span, the suspension clamp and the damper clamp. When they compared the parameters estimated by their numerical method with field data, they found a reasonable agreement between them. Their findings suggest that it is possible to develop numerical models that would replace field data collection to estimate life spans of various transmission lines.

Another key finding from Wolf et al. (2008) relates to the damper's efficiency. They found that a Stockbridge damper's efficiency depends on its position, which means that there is a need to determine optimal damper position; otherwise, the dampers might cause more damage to points on the span.

Another study that explored the influence of dampers was done by Bukhari et al. (2018). They investigated the effect of a moving damper on the vibration behaviour of overhead transmission lines. The damper or absorber comprises of the mass-spring-damper-mass framework. The absorber is associated with a single conductor subjected to demand and wind drive. They found that a moving absorber can be more viable than a settled absorber. It is additionally illustrated that the vibration uprooting diminishes with expanding driving recurrence and diminishing safeguard speed. Even though dampers' stated purpose is to reduce Aeolian vibration, most studies show that the damper's movement causes some damage to transmission lines.

Munaswamy and Haldar (2000) investigated self-damping characteristics of three ACSR conductors, circular cross-section, trapezoidal cross-section and self-damping ACSR. In their tests, they used seven different sizes of conductors. They found that the power dissipation of a conductor is proportional to the size of the conductor. They also found that at high frequencies, the power dissipation of ACSR conductors with trapezoidal cross-section was large than equivalent ACSR conductors with circular cross-sections for same diameters. This finding shows that the geometry strands influence the damping characteristics of conductors.

2.5 Conclusion

Firstly, this chapter presented a background on the causes and types of vibrations undertaken by transmission lines. It started by looking at one of the causes of vibration of transmission lines, the weather. It then appraised the various types of transmission line vibration caused by weather such as Aeolian vibration, conductor galloping and wake-induced vibration. After the background, the chapter reviewed literature on the damping characteristics of transmission lines, focusing on both experimental and numerical studies.

CHAPTER 3
THEORETICAL BACKGROUND ON THE FREE AND FORCED VIBRATIONS

3.1 Introduction

This chapter presents the theory that was the basis for calculations of various parameters related to free and forced vibration of conductors, as utilised in the processing of experimental data investigation of the results.

3.2 Damping and its analysis for free vibration

De Silva (2007) explains that damping is a phenomenon by which a dynamic system dissipates its mechanical energy by converting the energy into internal thermal energy. In a vibrating system, this dissipation is crucial in minimizing the amplitude/strength of the vibrations which the system experiences. Thus, the damping characteristics of a given system determines the maximum dynamic excitation the system can withstand. When the damping inherent in a system is not sufficient to withstand the excitation that the system would experience, external damping devices such as Stockbridge dampers for transmission lines, may be added to increase the level of damping that is present.

There are several types of damping inherent in mechanical systems such as Coulomb (dry friction), structural (material), magnetic and viscous damping (de Silva, 2007). This study focuses on viscous damping. Viscous damping occurs when a vibrating system is resisted by a force, whose direction is opposite to the direction of the vibration, the magnitude of which is constant and independent of displacement and velocity of the vibrating system (Thomson, 1986).

The level of damping that is present in a particular system is usually expressed as a damping factor. A damping factor, which is sometimes represented by the Greek letter zeta, ζ is the proportion of actual damping coefficient to critical damping coefficient (Maurya, Sharma & Khan, 2020)

For free vibration, the damping factor was calculated using the least-square approach based on the equation below.

When zeta, ζ, is less than 1:

$$\zeta = \frac{\delta}{\sqrt{(2\pi)^2 + \delta^2}} \quad 3.1$$

Else,

$$\zeta = \frac{\delta}{2\pi} \quad 3.2$$

where:

ζ = is the damping factor (zeta)

δ = logarithmic decrement.

3.3 Damping and the analysis of forced vibration

The quality factor is utilised as a degree of damping on the forced vibration for both conductors (Tern and ACSR Bersfort).

3.3.1 The quality factor (Q)

The quality factor (Q) is regularly utilised to measure damping in forced vibration (Meirovitch, 2008)

$$Q = \frac{1}{2\zeta} \quad 3.12$$

The quality factor is associated with excitation of variable at point 1 and point to correspond on magnification factor (see Figure 11).

f1= variable that is lower than resonant Fn

Fn = is described as half power-point.

f2 = is the higher than resonant Fn (described as half power-point).

The magnification factor is defined as:

$$\text{Magnification factor} = \frac{0.707}{2\zeta} \qquad 3.13$$

A bigger Q value indicates a smaller damping factor; a delicately damped framework would be portrayed as having an elevated Q calculate.

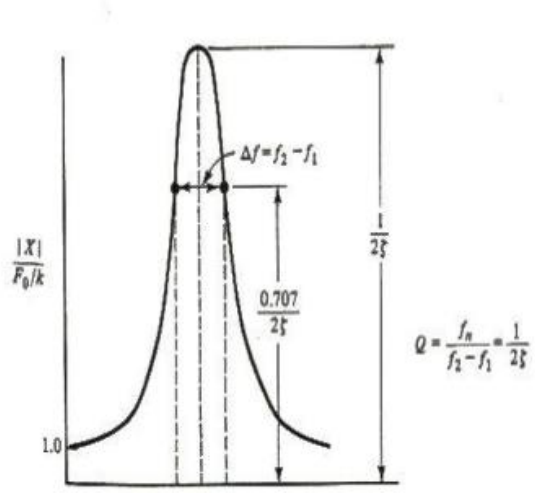

Figure 3. 1: Determination of the Q factor

At F= Fn

$$\frac{|X|}{F_0/k} = Q = \frac{1}{2\zeta} \qquad 3.14$$

$$\Delta f = f_2 - f_1 \qquad 3.15$$

Where:

Δf is described as the bandwidth of the system)

3.3.2 Determining the quality factor (Q)

Therefore, the Quality Factor is calculated as:

$$Q \cong \frac{f_n}{\Delta f} = \frac{f_n}{f_2 - f_1} \quad 3.16$$

Thus:

$$Q = \frac{1}{2\zeta} \cong \frac{f_n}{\Delta f} \quad 3.17$$

3.4 Conclusion

This chapter presented the theory that governs the computations that were used to process the experimental data. The next chapter will describe the procedures that were followed in the experimental work.

CHAPTER 4
EXPERIMENTAL PROCEDURE AND THE APPARATUS USED

4.1 Introduction

Chapter 4 describes the experimental procedures used to characterise the ACSR BERSFORT DISSCAAY5 / BS215 / IEC61089 and Tern transmission conductors. The procedures described were developed by Makeretla (2011) to characterise the self-damping characteristics of the TERN and Aero-Z IEC62219-REV240609 conductors.

4.2 The facility where the experiments were conducted

The characterisation experiments were conducted at the University of Kwa-Zulu Natal's (UKZN) Vibration Research & Testing Centre (VRTC).

Figure 4. 1: UKZN VRTC Laboratory

The VRTC is a temperature-controlled facility that was specially built for testing vibrations of transmission line conductors. Regarding the transmission lines, all the experimental work are carried out according to IEEE 563 STD 1978. The characterised transmission lines and the tests were carried out at the KZN VRTC. The VRTC is one out of four transmission line vibration testing stations globally, and it is state of the art in understanding wind-induced vibration issues (Moodley, 2018). The facility can test conductors of up to 84.6 m span, see Figure 4.1 (external) and Figure 4.2 (internal).

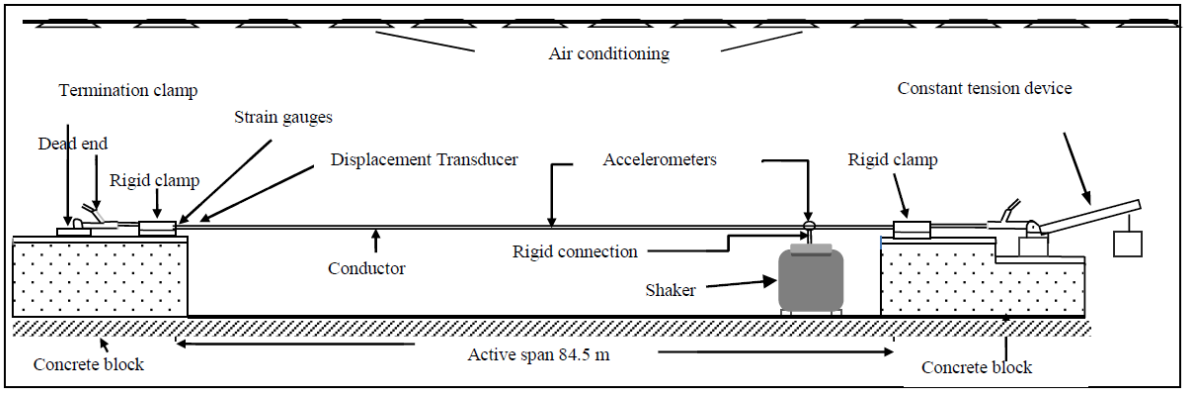

Figure 4. 2: UKZN VRTC Interior (Kubelwa et al., 2018)

VRTC's functions focus on the following:

- Vibration testing of power lines according to IEEE 563 STD 1978
- Vibration testing of Stockbridge type of Vibration Dampers according to IEEE 664 STD and IEC 61897
- Resonance Frequency search & vibration testing of samples

4.2 Experimental Set up of a conductor (Free Vibration).

The experimental set-up proceeded as follows, the researcher:

- Selected conductor (ACSR Bersfort/ Tern) that was clamped between two rigid supports (see Figure 4.3 below).

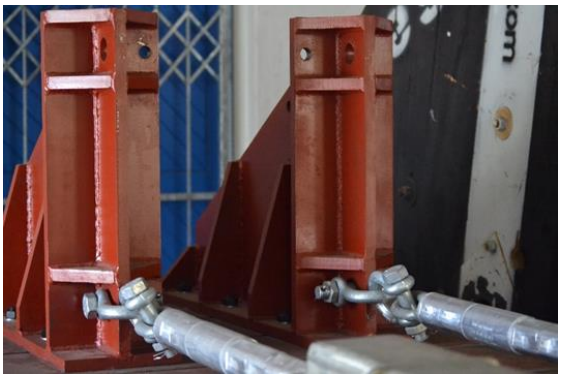

Tensioned the conductor, Figure 4. 3: Rigid Support

Figure 4. 4: Tensioned Conductors (Taken by: Sityoshwana, 2019

- Tension the conductor, which was required in the experiment (see Figure 4.4 above).
- Tightened the hold-down block, the conductor was fastened, and the load cell value was recorded (see Figure 4.5).
- Measured and marked the distance for the accelerometers and the hammering point (see Figure 4.6).

Figure 4. 5: Hold Down Block

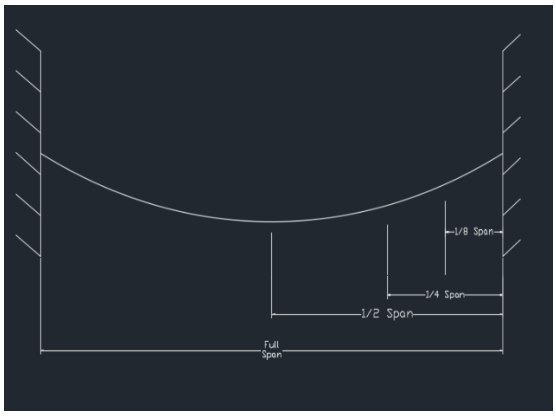

Figure 4. 6: Conductor Configuration

- Selected the accelerometers and attached it to the measured distance (see Figure 4.7).

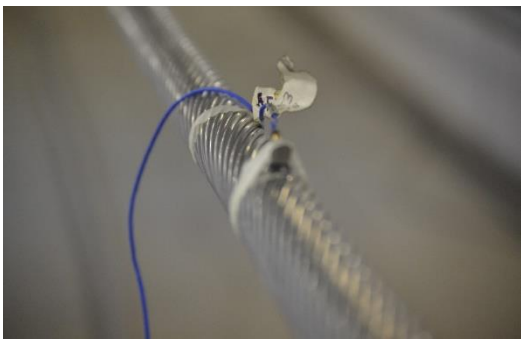

Figure 4. 7: Accelerometer

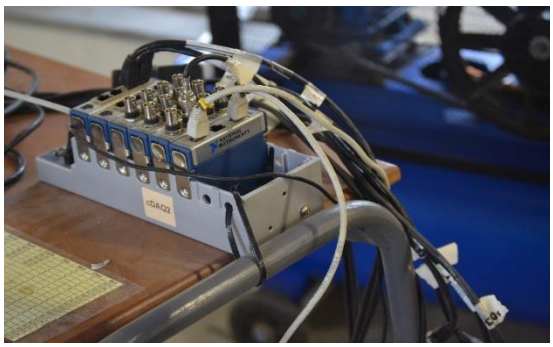

Figure 4. 8: National Instrument Desk (Accelerometer Connector)

- Connected the accelerometers to the National Instrument Desk system for recording purposes (see Figure 4.8).
- Switched on the National Instrument Desk for test purpose and run the system to see if all accelerometers are connected properly.
- Checked the sensitivity or calibration value using the calibration exciter for each accelerometer for accuracy purposes (see Figure 4.9).

Figure 4.9: Calibration Exciter

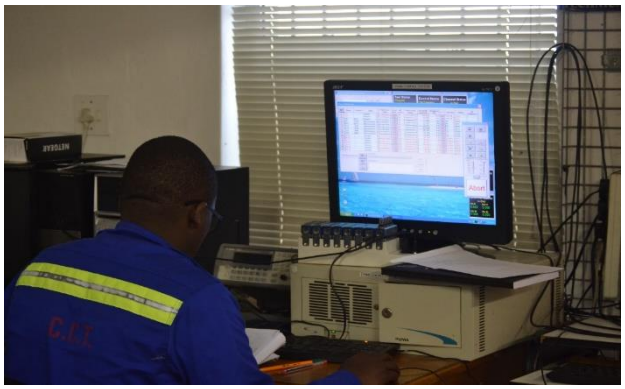

Figure 4.10: Insert Sensitivity Values

- Inserted the sensitivity or calibration values (see Figure 4.10) to the National Instrument Desk and run the system to check if all accelerometers were connected. The configuration is presented in Table 4.1.

Table 4. 1: Initial Configuration-Measured Results

		Tension (ACSR Bersfort)			**Tension (Tern)**		
		T1	**T2**	**T3**	**T1**	**T2**	**T3**
Position	**Distance**	**36 kN**	**45 kN**	**54 kN**	**26 kN**	**33 kN**	**39 kN**
2m span	2 m	101.7 mV/g			97.565 mV/g		
½ span	42.3 m	99.5 mV/g			102.6296 mV/g		
1/3 span	28.2	N/A			102.369 mV/g		
¼ span	21.150 m	97.1 mV/g			99.539 mV/g		
1/8 span	10.575 m	99.7 mV/g			101.33 mV/g		

4.3 Free vibration procedure for ACSR Bersfort and Tern conductors

The free vibration experimental procedures described in this section were adapted from Makeretla (2011). The researcher proceeded as follows:

1. Started with a conductor (ACSR Bersfort or Tern)

2. Tightened the conductor to the required tension (T1) and verified the reading from the load cell (see Figure 4.11below).

3. Measured the range from the floor at ½ length, ¼ length, and 1/8 range away from the fixed side.

4. Struck the conductor at any appropriate position x away from the non-fixed sid(see Figure 4.12).

Figure 4.11: Loading Cell

Figure 4.12: Hammering

5. Recorded the vibration value for amplitude versus time utilising piezo-ceramic sensor device and the accelerometer device etc.

6. After each test, a waiting period was ensured hourly to allow the vibration to stop before doing another test.

7. The procedure was repeated multiple times.

8. Step 2 was redone above, and the tension was changed to T2, T3 etc.

9. After each changed tension, steps 3 followed to 7 multiple times.

10. The test ended.

4.4 Experimental set up for forced vibration tests

The experimental set-up procedures for forced vibration tests proceeded as follows

- The chosen conductor (ACSR Bersfort/Tern) was fixed between two unbending backings.
- The chosen conductor was tightened to the required tension, which was required in the experiment.
- The hold-down block was tightened, and the value from the load cell was recorded.
- The Tira Vib Shaker (Electro-dynamic exciter shaker) was connected (see Figure 4.13).
- The shaker was connected to the flexi-connection (see Figure 4.14).

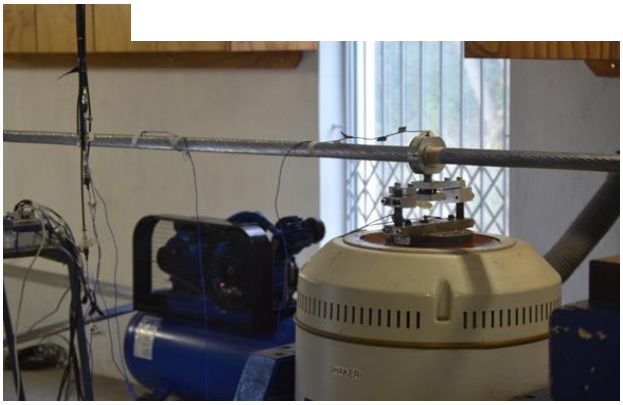

Figure 4.13: Shaker

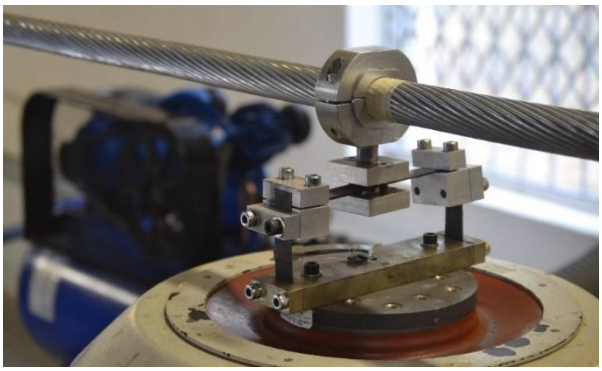

Figure 4.14: Flexi-Connection

- The distance of the accelerometers and force transducer were measured and marked.
- The selected accelerometers and force transducer were attached to measure distance.
- The Puma Control System was switched on for test purpose and run the system to see if all accelerometers and force transducer were correctly connected.
- The sensitivity or calibration value was checked using the calibration exciter for each accelerometer for accuracy purposes.
- The sensitivity or calibration value was inserted and ran the system to check if all accelerometers and force transducer were connected.

4.5 Forced vibration procedure

The forced vibration tests proceeded as follows:

1. Started with the conductor (ACSR Bersfort or Tern).

2. Tightened the conductor to the required tension (T1) and verified the load cell reading.

3. Measured the range from the floor at 1/2 length, 1/4 length, and 1/8 range away from the fixed side.

4. The Tira Vib Shaker was used for the forced vibration experiment.

5. Started the shaker to vibrate the conductor to determine resonant frequencies.

6. The conductor was vibrated for several seconds and recorded the velocity, displacement, phase angle, applied force at the shaker and acceleration.

7. The procedure was repeated multiple times.

8. Step 2 was redone above, and the tension was changed to T2, T3, etc.

9. After each change of Tension, steps 1 to 8 followed multiple times.

10. Test was finally completed.

3.2.1 Logarithmic decrement, frequency and damping factor

The viscous damping factor can be determined from using:

$$Zj = aYj + b \qquad 3.3$$

where:

Zj= corresponds to lnx_j

a = $-\delta_j$

j= -1

b= lnx_1

It is important to determine the constants **"a**" and **"b"** by diminishing the whole of the square of the varieties among the normal logarithm of the measured relocation and the straight line. The total of the squares of the distinction as the error is:

$$\epsilon = \sum_{j=1}^{6}(lnPj - aYj - b)^2 \qquad 3.4$$

The above can be re-written within the least complex frame to undertake and reduce the error, which the two logarithmic conditions within the unknowns **"a"** and **"b"** to be written as:

$$\left(\sum_{j=1}^{6} Y^2 j\right)a + \left(\sum_{j=1}^{6} Yj\right)b = \sum_{j=1}^{6}(lnPY)Yj \qquad 3.5$$

$$\left(\sum_{j=1}^{6} Yj\right)a + 6b = \sum_{j=1}^{6} lnPY \qquad 3.6$$

Once values are taken from the measurements of the peak amplitudes (X1, Y1), (X2, Y2), (X3, Y3) are taken simultaneous equation can be used to determine the values of **a** and **b**.

where:

Y = acceleration (m/s^2)

X = Time (seconds)

The value of **a** will be:

$$\delta = -a \qquad 3.7$$

The value of viscous damping can be substituted for equation 3.1 to identify damping Figure of the conductor. Once the damping factor is known the wave equation on equation 3.8 can be used to determine the wave frequency.

$$y(x,t) = Asin(2\pi kx - \omega t) \qquad 3.8$$

Where:

$$k = \frac{1}{\lambda} \qquad 3.9$$

Where "k" is know as wave number

$$\omega = c\frac{2\pi}{\lambda} \qquad 3.10$$

Where "ω" is frequency of wave

Equation 3.10 can be further be simplified as follows:

$$\tau = \frac{2\pi}{\omega} = \frac{\lambda}{c} = \frac{t_n - t_o}{n-1} \qquad 3.11$$

4.6 Conclusion

This chapter described the test facilities where the free and forced vibration tests were conducted. It also described the experimental set-up and testing procedures for both free and forced vibration tests.

CHAPTER 5
RESULTS

5.1 Introduction

Chapter 5 presents the results of free and forced experiments for ACSR Bersfort DISSCAAY5 / BS215 / IEC61089 and Tern transmission conductors.

5.2 Free Vibration results for the ACSR Bersfort

As indicated in the previous chapter, for free vibration experiment, the ACSR Bersfort DISSCAAY5 / BS215 / IEC61089 conductors were struck with the rubber hammer shown in Figure 4.12.

5.2.1 Results of free vibration tests for ACSR Bersfort conductor

Four accelerometers placed were on the following positions from the tension side, as shown in Figure 4.6.

Mr Moodley, the technician responsible for the VRTC, connected and calibrated the accelerometers used in free vibration tests. The ACSR conductor calibration set-up is shown in Table 5.1.

Table 5. 1: Accelerometer set-up and calibration for ACSR conductor free vibration tests

Accelerometer	Channel Connection	Calibration Value/ Sensitivity	Serial Number	Distance from Tension side.
1	0	101.7 mV/g	6963	2 m
2	1	99.7 mV/g	6964	10.575 m
3	2	97.1 mV/g	6729	21.15 m
4	3	99.5 mV/g	6519	42.3 m

Test 1

For accuracy, it was essential to calibrate the measuring equipment. This is so because all measuring devices' accuracy degrades over time due to normal wear and tear (Brei, 2013).

The set up's calibration was recorded on Table 5.2 below using the following accelerometer, tension, and the hammering point.

Table 5. 2: The values that were used in the calibration using accelerometer 1

Accelerometer	Channel Connection	Calibration Value/ Sensitivity	Serial Number	Distance from Tension side.	Tension	Hammering Point
1	0	101.7 mV/g	6963	2 m	53.88 kN	1m (from tension side.)

Procedure:

The procedure to do the free vibration was discussed in chapter 4, and some aspects are repeated here for convenience.

- The researcher used the hammer to hit the conductor at a point that is 1 meter from the tension side and 1 meter from the accelerometer (see Figure 4.12).
- National Instrument Desk was used to record the graphs. The data was displayed at seconds per interval (see Figures 5.1).

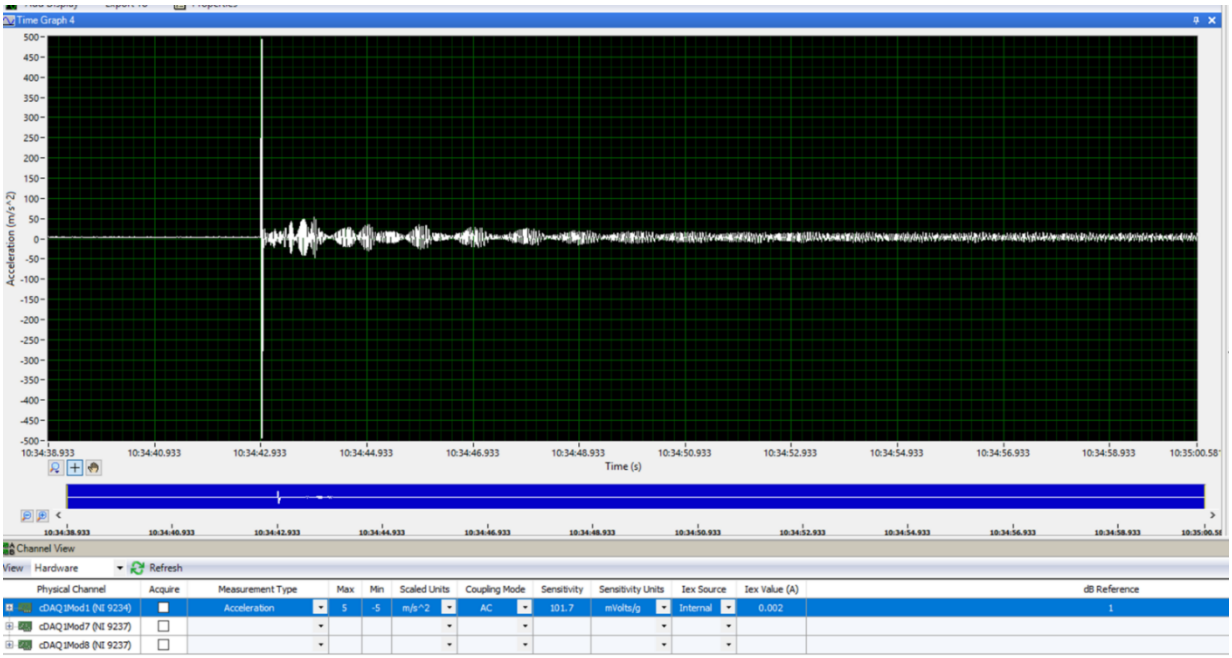

Figure 5.1: Free Vibration on 53.88 kN, Excitation on 2m

Figure 5.1 above showed that the accelerometer next to the hitting point received high vibrations, which decayed over a period. The first graph was used to assess the damping for the first decay region.

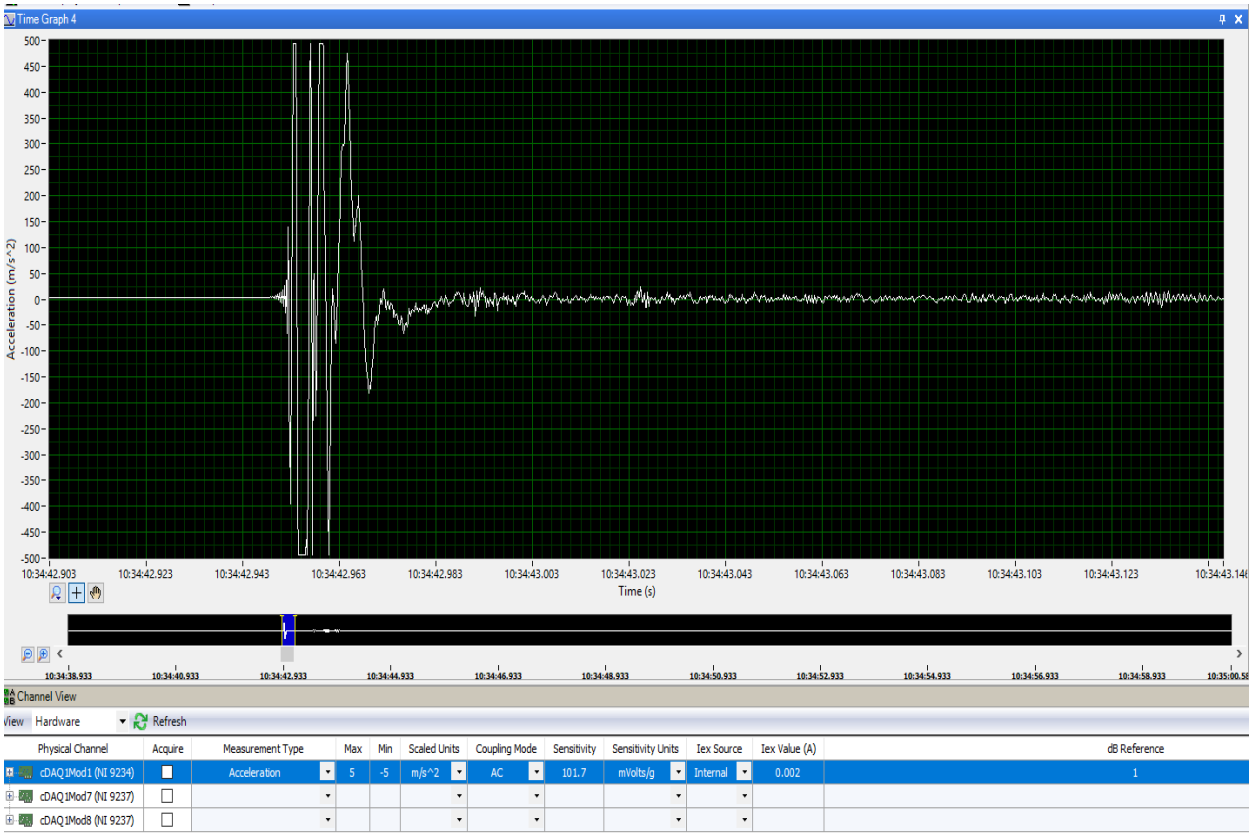

Figure 5.2: Close view of Figure 5.1

Test 2

The transmission line tension was changed to 44.91 kN for further testing. As seen in Table 5.3 (Experiment Connection), three more accelerometers were connected when the vibrations were measured at different points simultaneously.

The following results were obtained:

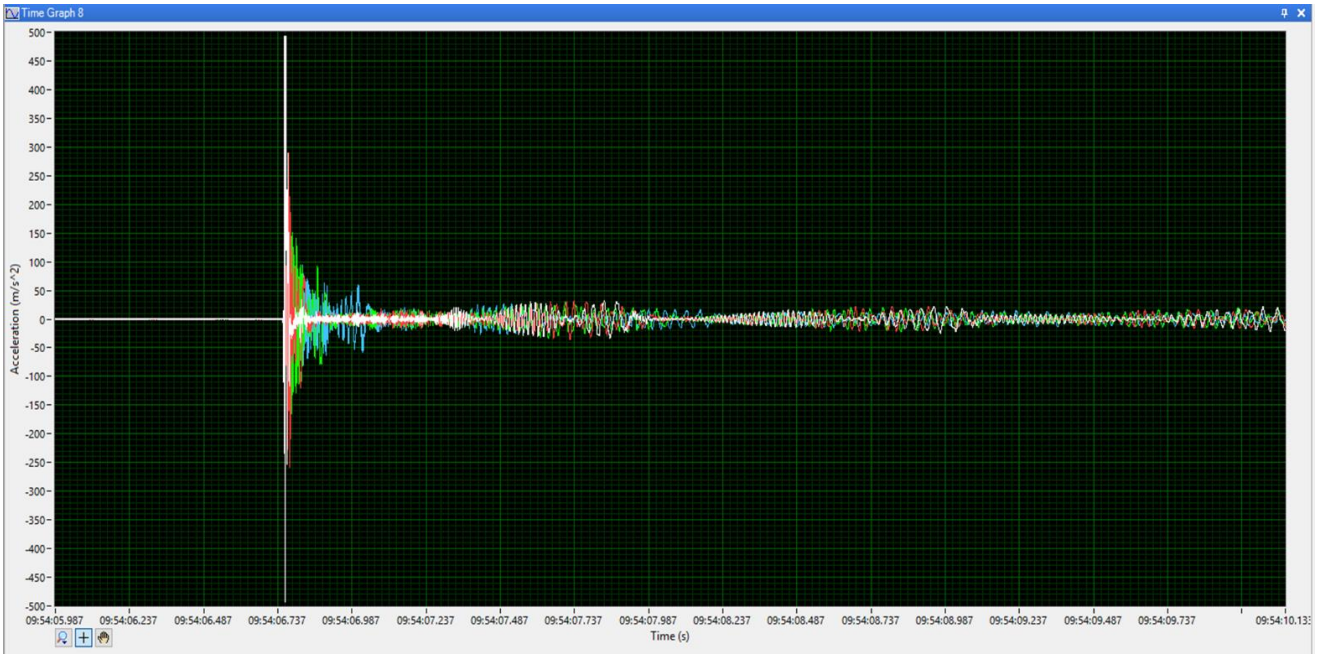

Figure 5.3: Free Vibration on 44.91 kN

The above graph represents the excitement of all points at the same time, the colour for each graph, as indicated in Table 5.3 below:

Table 5. 3: Calibration sensitivity and graph colours for various accelerometers

Accelerometer	Channel Connection	Calibration Value/ Sensitivity	Colour	Distance from Tension side.
1	0	101.7 mV/g	White	2 m
2	1	99.7 mV/g	Pink	10.575 m
3	2	97.1 mV/g	Green	21.15 m
4	3	99.5 mV/g	Blue	42.3 m

Figure 5.3 (Free vibration on 44.91 kN) showed that the highest vibration happens on the closest accelerometer closer to the hitting point and followed the distance as per the furthest location. The high acceleration started from channel zero (white) located at 2 meters, channel

one (pink) located at 10.575 meters, channel two (green) located at 21.15 meters, and lastly channel three located at mid-point at 42.3 meters.

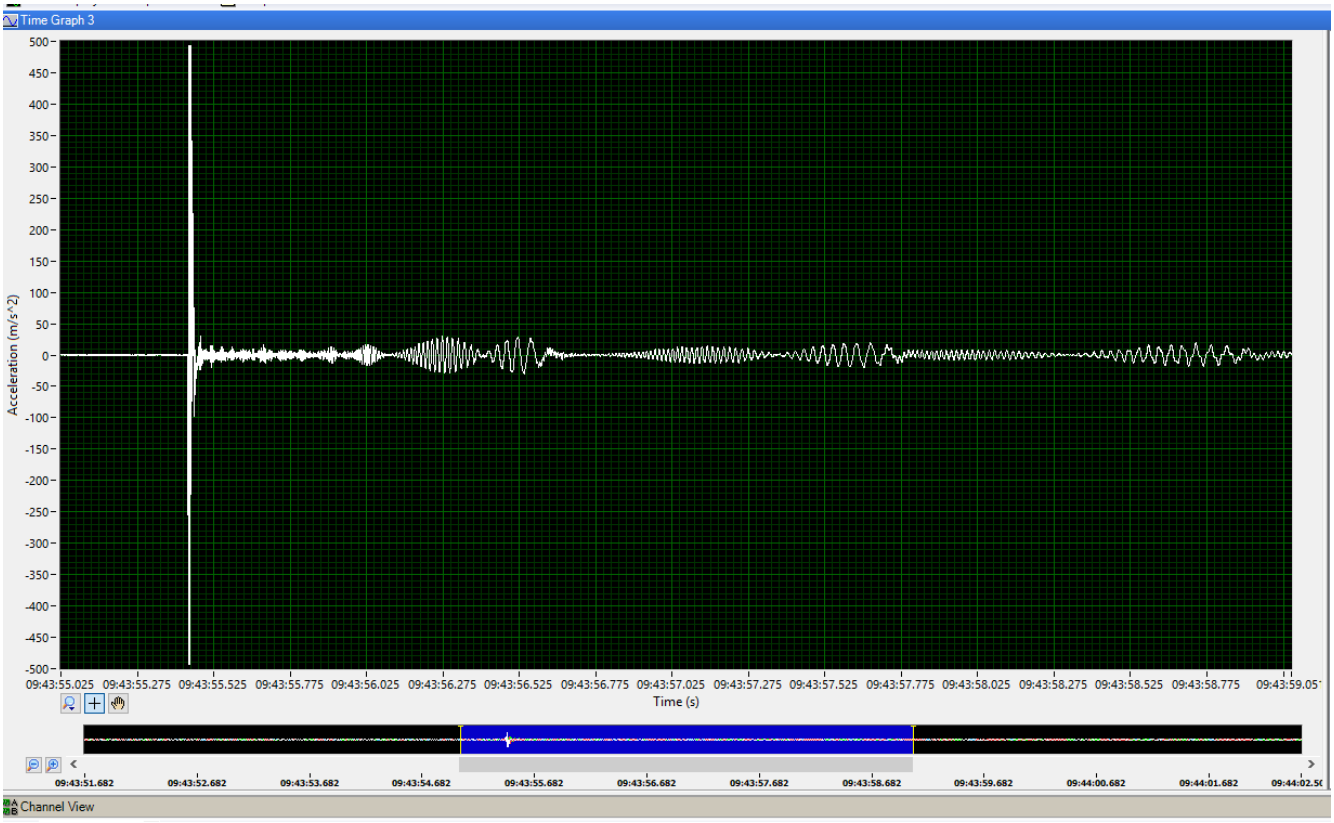

Figure 5.4: Excitation at 2 m, cable tension reading 44.91 kN, as per load cell.

Figure 5.4 is the same graph as Figure 5.6, but it focused on the excitation located at 2 meters. The difference helped to identify and determine the frequency and the degenerating portion:

- frequency of degenerating oscillations
- log decrement
- damping coefficient.

The results for the free vibration will be discussed more in chapter 6.

5.2.2 Forced Vibration Results for ACSR Bersfort

Puma Controlled System was used to conduct the forces vibration method to obtain response when the conductor was subjected to repetitive forcing functions. The set up for the experiment was changed to fit the PUMA Controlled system and was as follow:

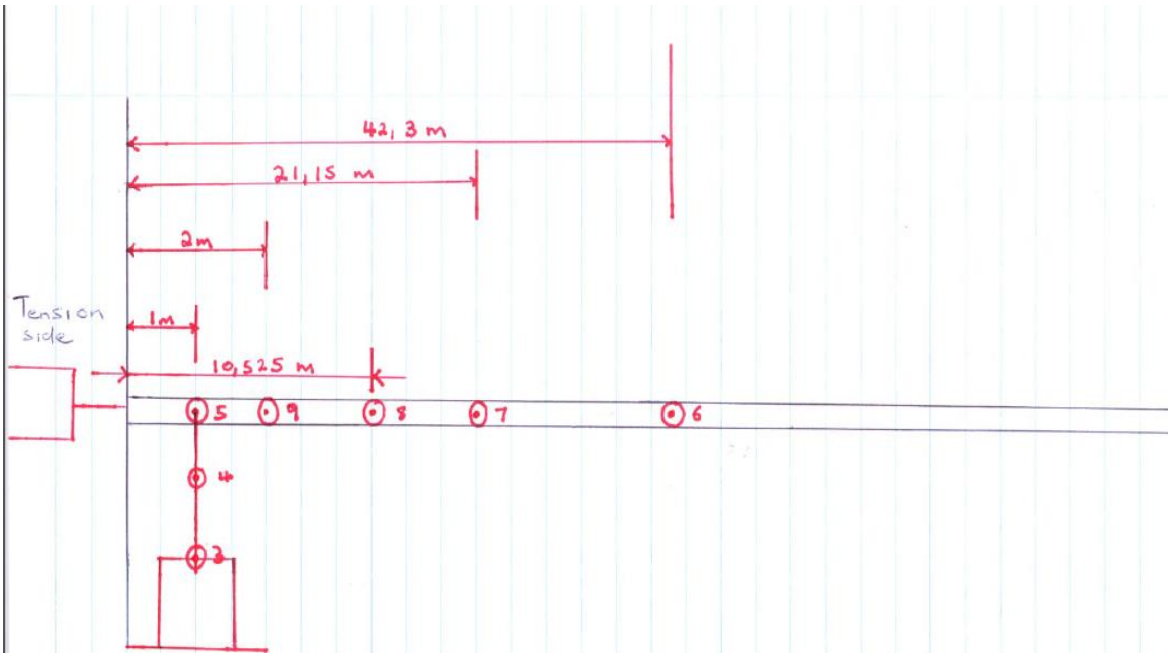

Figure 5.5: Forced vibration setup

The details of the above diagram are detailed in Table 5.4 below:

Table 5. 4: Forced Vibration accelerometer and forced transducer positioning and sensitivity

Item	Description	Channel Line	Sensitivity	Serial Number	Distance from Tension
3	The accelerometer on flexi connection	3	98.3 mV/g	6519	1m
4	The force Transducer	4	21.43 mV/g	55807	1m
5	An accelerometer on a shaker base	5	95.4 mV/g	6523	1m
6	An accelerometer at ½ span	6	99.5 mV/g	6518	42.3m

7	An accelerometer at ¼ span	7	97.1 mV/g	6729	21.15m
8	The accelerometer at 1/8 span	8	99.7 mV/g	6964	10.525m
9	The accelerometer at 2m of the span	9	98.3 mV/g	6963	2m

The experiment was conducted using a constant speed of 0.05 m/s, and the sweep test was done from 5-300 Hz at an interval of 30 minutes.

The data shown in Figure 5.6 was extracted from a force transducer located at 1 meter from the fixed tension side. It displays the results of the sweep test plotted using PUMA system for cable tension of 35.97 kN. The results were taken and transferred to the excel spreadsheet and will be discussed in the next chapter.

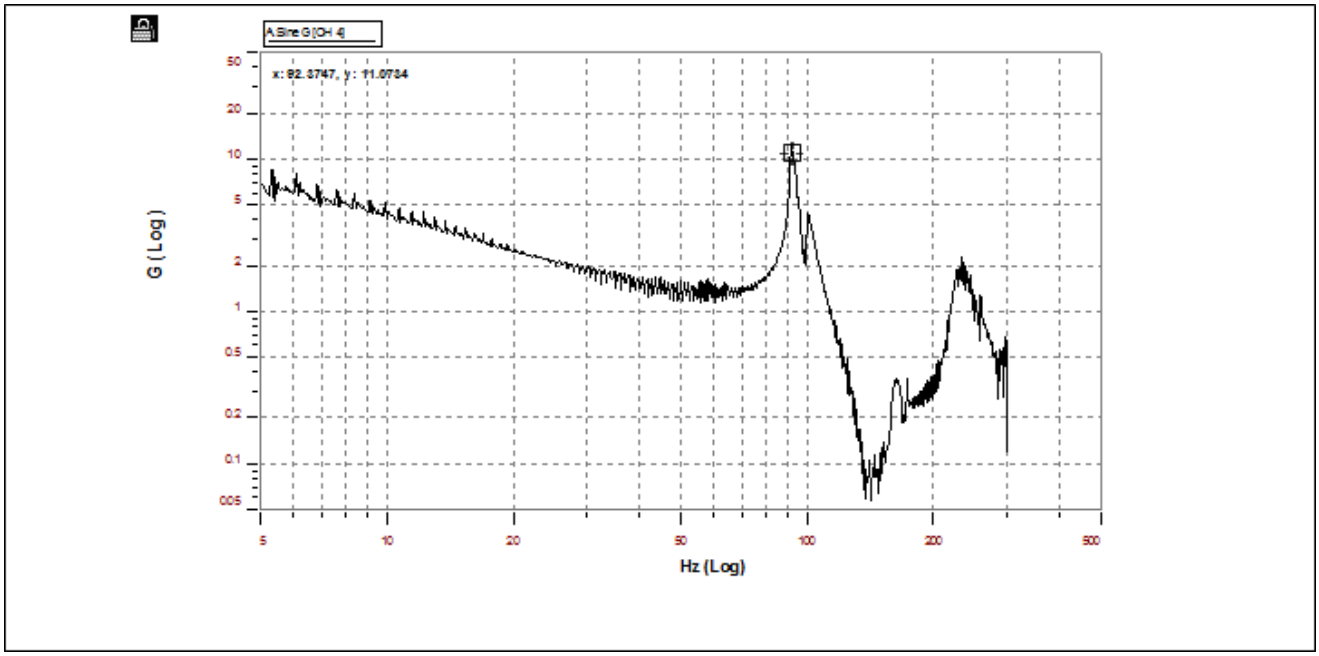

Figure 5.6: Results at 1 m (force transducer), cable tension = 35.97 kN

The data shown in Figure 5.7 was extracted from an accelerometer located at ½ a span from the fixed tension side. It displays the results for the sweep test plotted using PUMA system for cable tension of 35.97 kN.

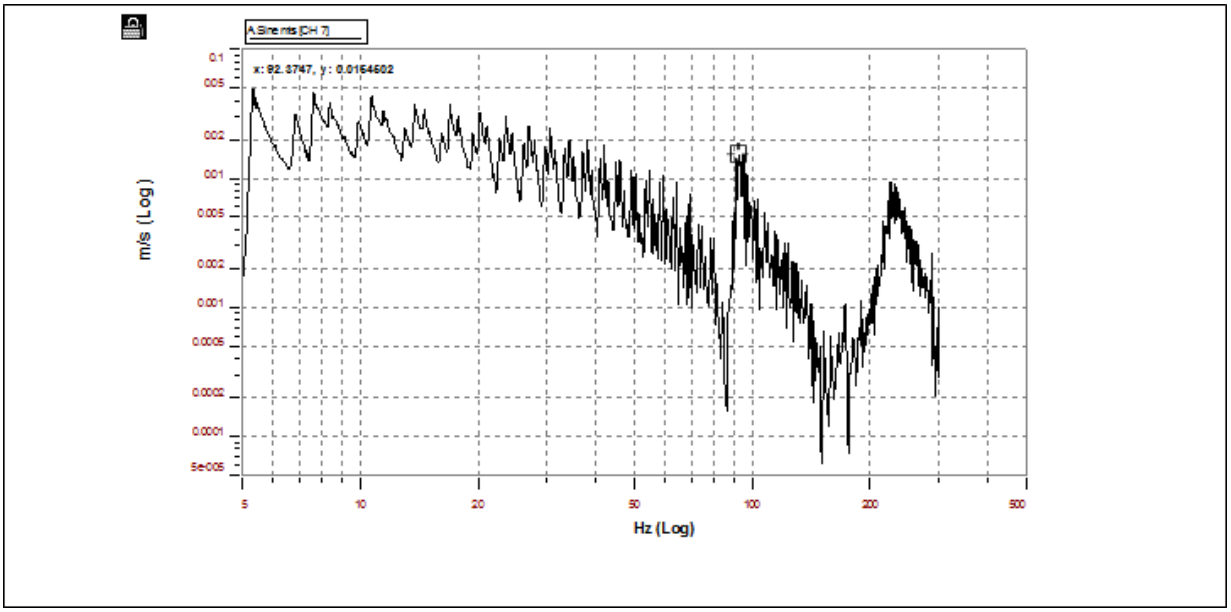

Figure 5.7: Shaker, ACSR conductor, an accelerometer at Flexi connection

The results shown in the graphs were transferred to the excel spreadsheet and will be discussed in the following chapter. Figure 5.8 shows the researcher recording the results on the PUMA system.

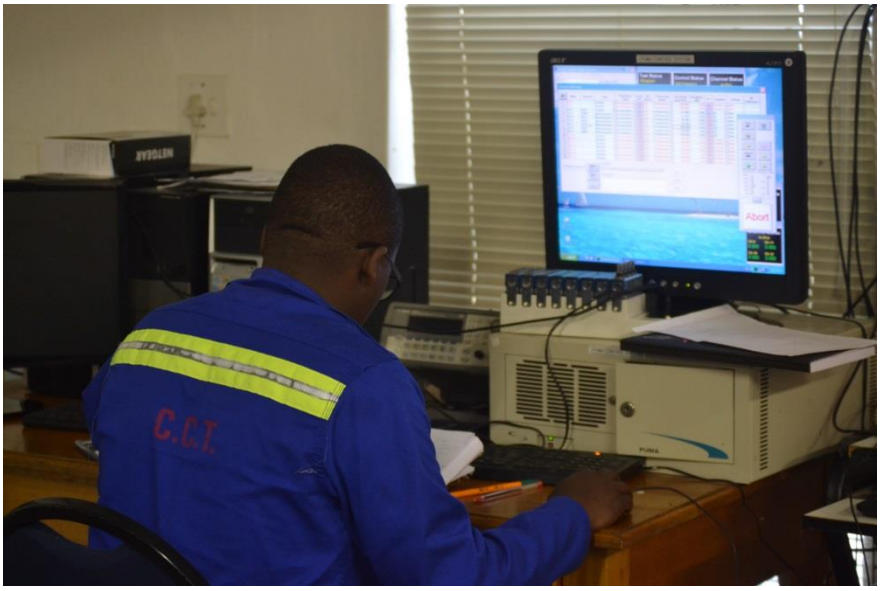

Figure 5.8: Recording Results on PUMA Control System

The data shown in Figure 5.9 was extracted from an accelerometer located at Flexi connection, which was located 1 metre from the fixed tension side. It shows the sweep test results plotted by the PUMA system's spectral dynamic viewer for a cable tension of 53.88 kN.

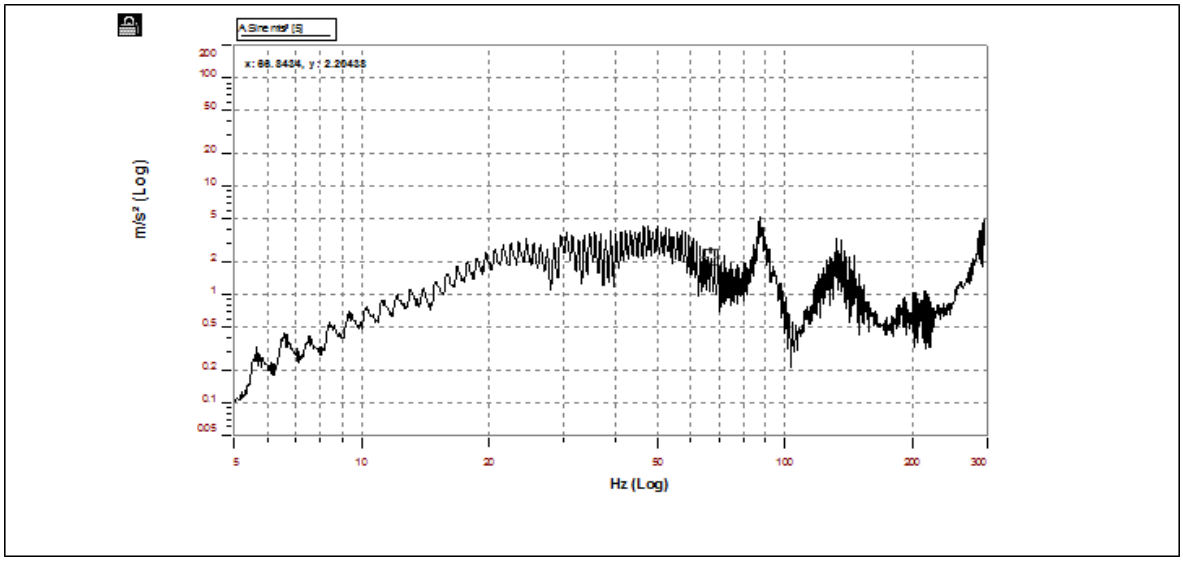

Figure 5.9: Results at 1m (Flexi connection), cable tension = 53.88 kN

Figure 4.13 shows how an accelerometer was positioned at the Flexi connector to produce the results that are shown in Figure 5.9

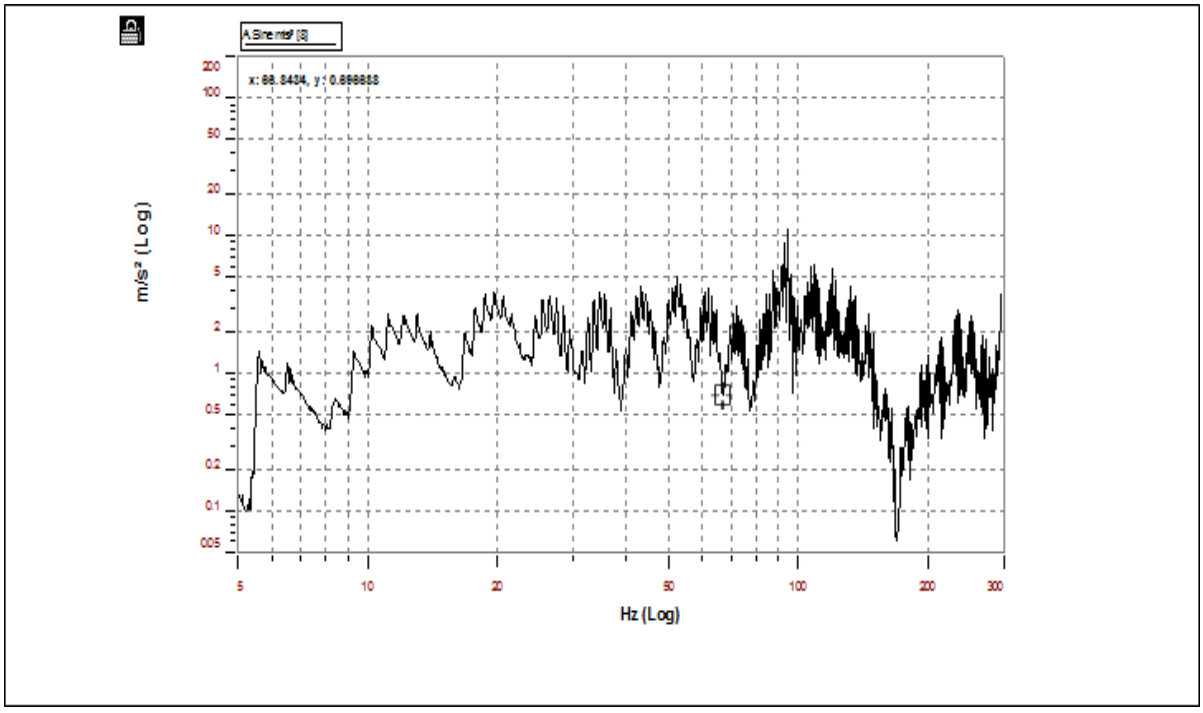

Figure 5.10: Results at 10.575 (accelerometer), cable tension = 53.88 kN

Figure 5.10 shows results of the sweep test captured by an accelerometer at 1/4 span of the conductor.

5.3 Free Vibration results for the Tern Conductor

As in the previous case, the researcher struck the conductor with a rubber hammer to initiate the free vibrations which were recorded by accelerometers linked to National Instrument Desk.

5.3.1 Accelerometer positioning and calibration for Tern conductors

Similarly, to Section 5.2, Mr Moodley, the UKZN technician responsible for the VRTC, calibrated the system and connected accelerometers to various acquisition systems' different channels, as shown in Table 5.5.

Table 5. 5: Accelerometer set-up and calibration for Tern conductor free vibration tests

Accelerometer	Channel Connection	Calibration Value/ Sensitivity	Serial Number	Distance from Tension side.
1	A0M1	97.565 mV/g	6526	2 m
2	A1M1	101.33 mV/g	6962	10.575 m
3	A2 M1	99.539 mV/g	6729	21.15 m
4	A3M1	102.369 mV/g	6959	28.2 m
5	A0M3	102.6296 mV/g	6961	42.3 m

TERN TEST 1

The set-up was tested using 26 KN tension for the conductor. After hammering the conductor, the results were recorded using all the accelerometer, as shown in Figure 5.11.

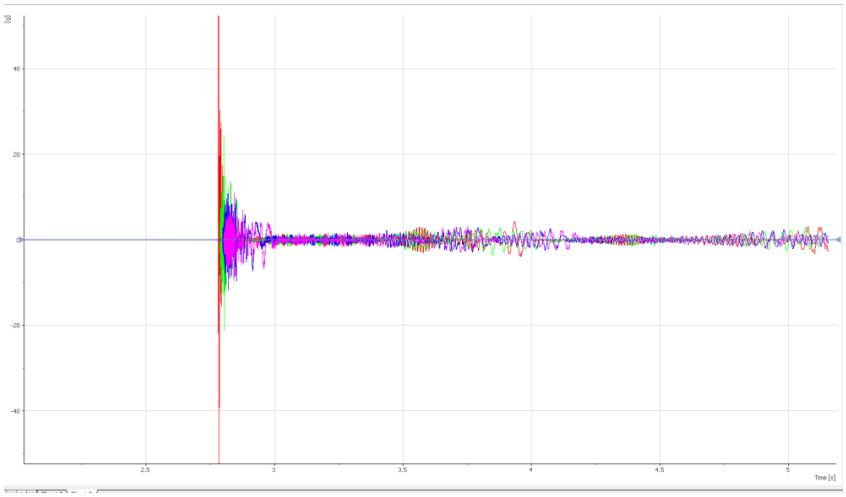

Figure 5.11: 26 kN All accelerometers

Figure 5.12 shows isolated results for 26kN tensioned conductor for accelerometer A0M1

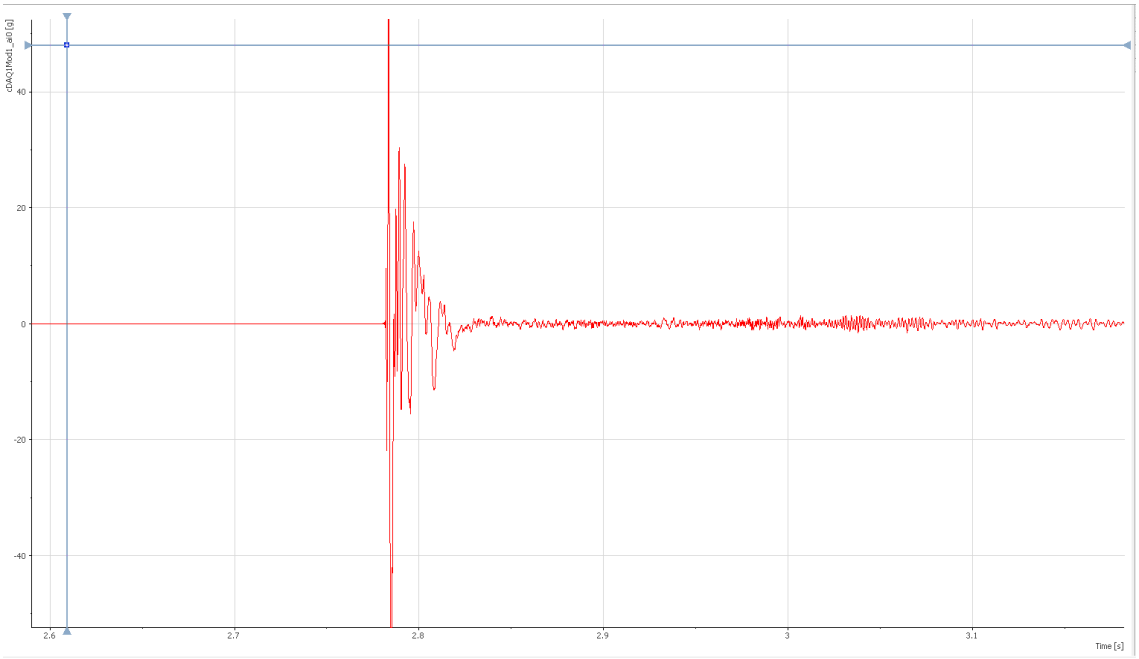

Figure 5.12: Results at 26 kN, Accelerometer AoM1 (National Instrument Desk)

Figure 5.12 presents a closer view of the results previously shown in Figure 5.11. The data used extracted from the PUMA system.

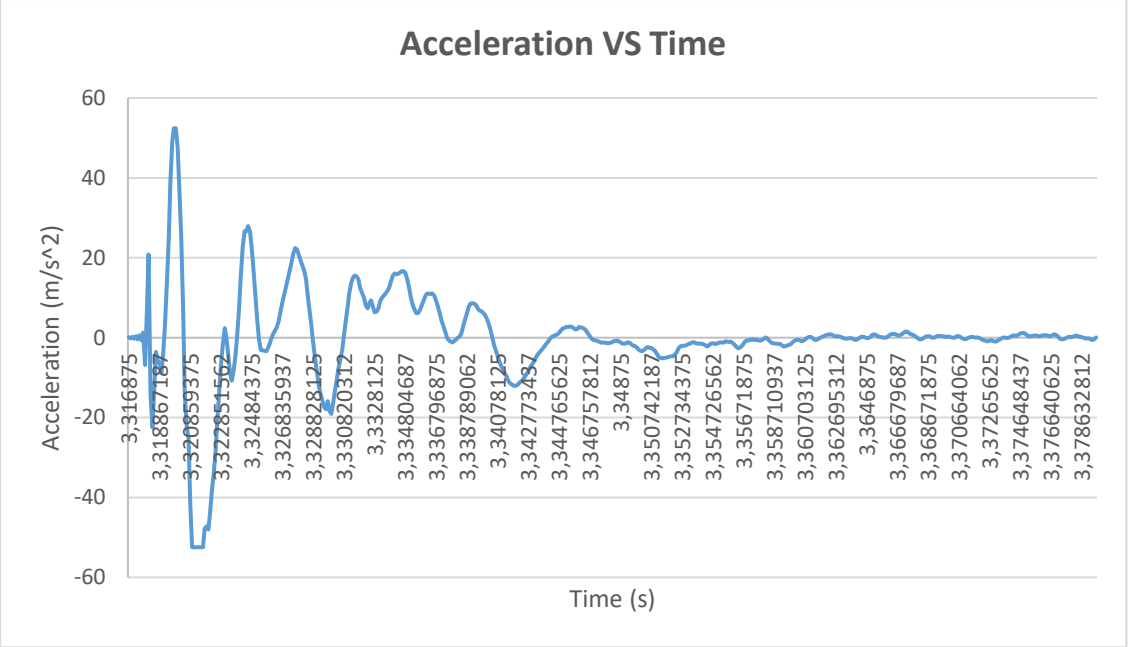

Figure 5.13: Results at 26 kN, Accelerometer AoM1 (Closer View)

The results presented in Figures 5.11 and 5.12 show that the vibration degenerated with time due to the conductor's self-damping. Similarly, Figure 5.13 above showed that the accelerometer next to the hitting point received high vibrations that decayed over time. Figure 5.13 was used to assess damping for the first decay region. Figure 5.14 shows isolated results for 26kN tensioned conductor for accelerometer A1M1.

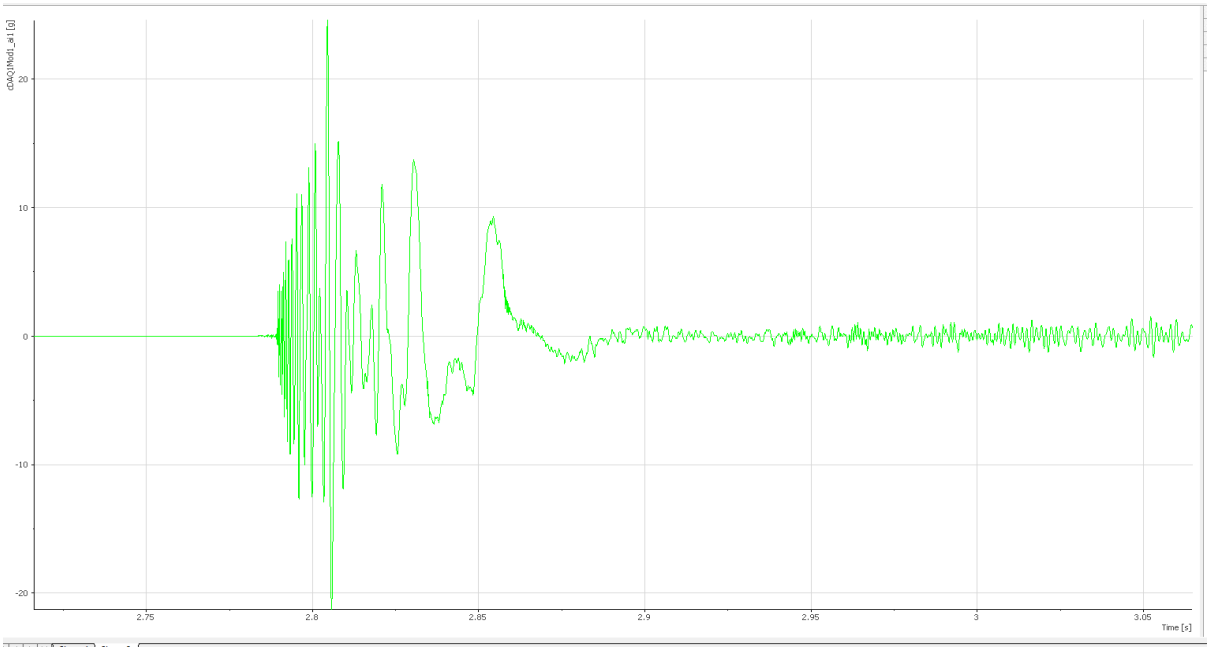

Figure 5.14: Results at 26 kN, Accelerometer A1M1 (National Instrument Desk)

Figure 5.15 presents a closer view of the results previously shown in Figure 5.14. The data used extracted from the PUMA system.

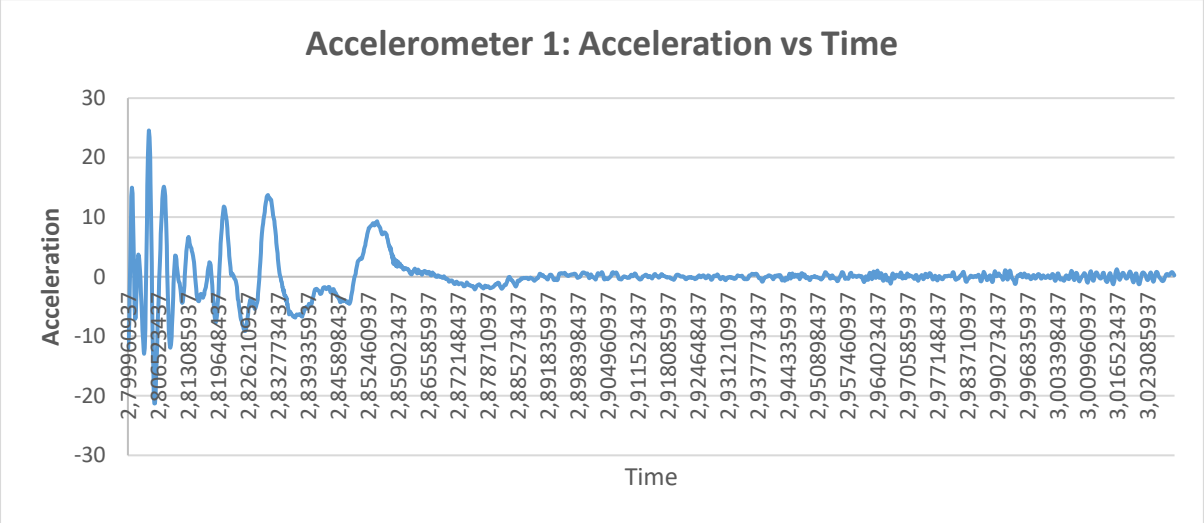

Figure 5.15: Results at 26 kN, Accelerometer A1M1 (Closer View)

The results presented in Figures 5.14 and 5.15 describe vibration degenerates with time due to the self-damping on the conductor. The changed time was used to find the frequency in-unit hertz, while the decaying quota of the wave was used to determine the variables (log decrement, damping coefficient, and frequency decaying oscillation).

In further testing, the Tern conductor's tension was changed from 26 kN to 33 kN and 39 kN to collaborate the results for 26 kN.

5.4 Forced vibration results for the Tern conductor

The Puma Controlled System was used to conduct the forced vibration tests to obtain vibration response when the conductor is subjected to a repetitive forcing function. The test used a sweep test from 5-150 Hz at 30 minutes intervals and constant speed of 0.05 m/s.

Figure 5.16 presents the vibration response recorded by the accelerometer located at Flexi connection, 1 meter from the fixed tension side. These results are for a cable tension of 39 kN.

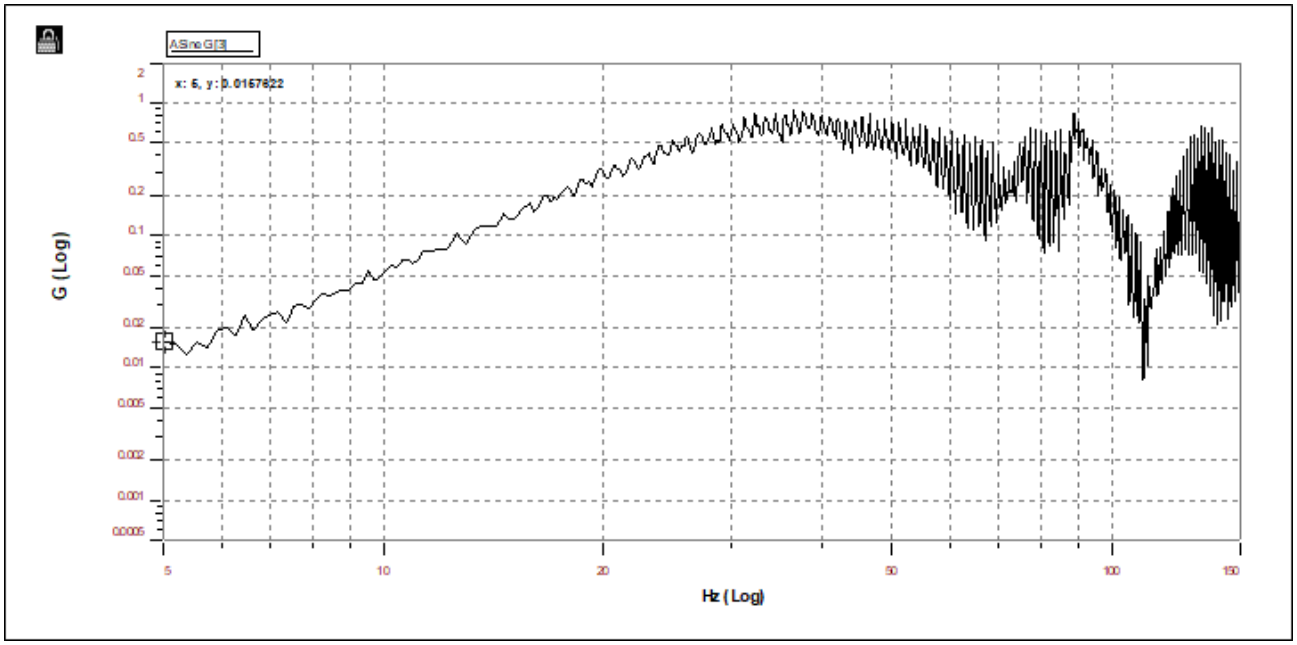

Figure 5.16: 39 kN sweep test, 1 m accelerometer

Figure 5.17 presents the vibration response recorded by the accelerometer located 1 meter from the fixed tension side. These results are for a cable tension of 39 kN.

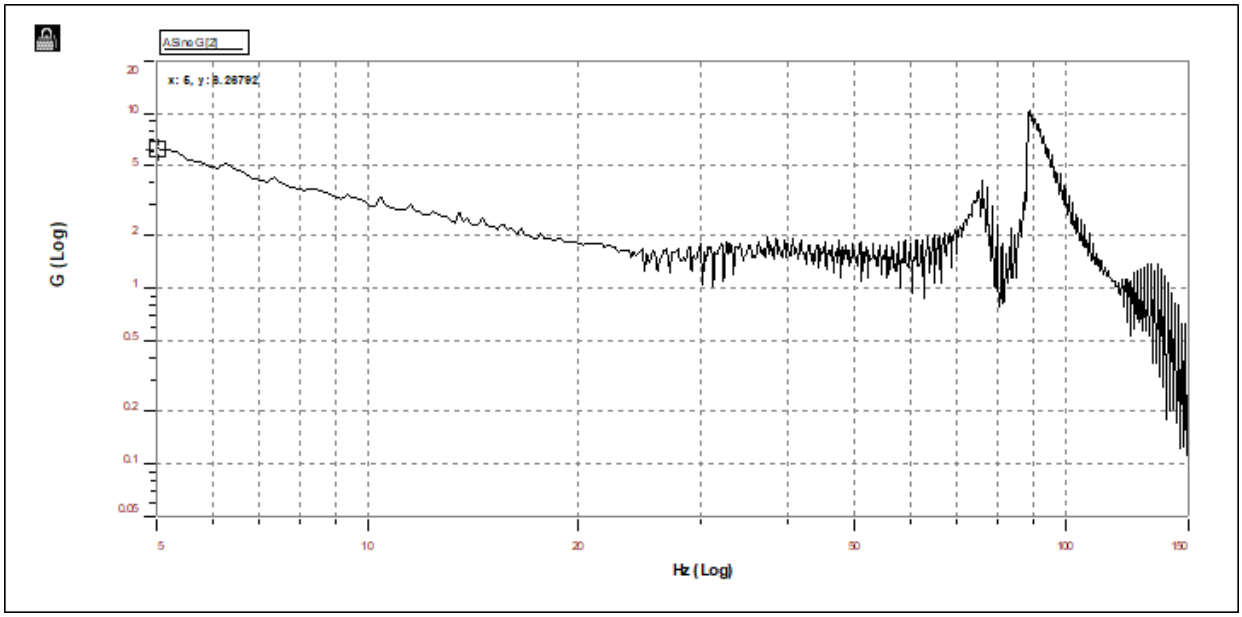

Figure 5.17: 39 kN sweep test, 1 m force transducer

Figure 5.18 presents the vibration response recorded by the accelerometer located 10.525 m from the fixed tension side. These results are for a cable tension of 39 kN. In this case, the sweep test was from 5 Hz to 150 Hz.

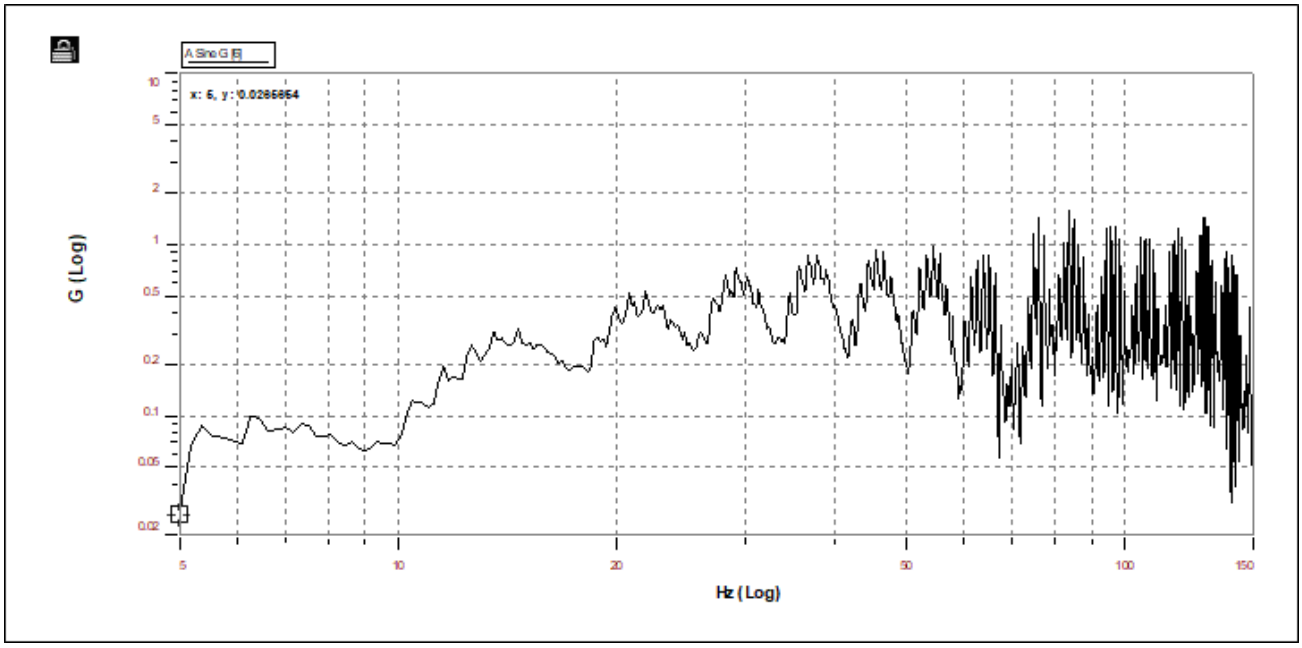

Figure 5.18: 39 kN sweep test, 10.525 m accelerometer

Figure 5.19 presents the vibration response recorded by the accelerometer located 42.3 m from the fixed tension side. These results are for a cable tension of 39 kN. In this case, the sweep test was from 5 Hz to 150 Hz.

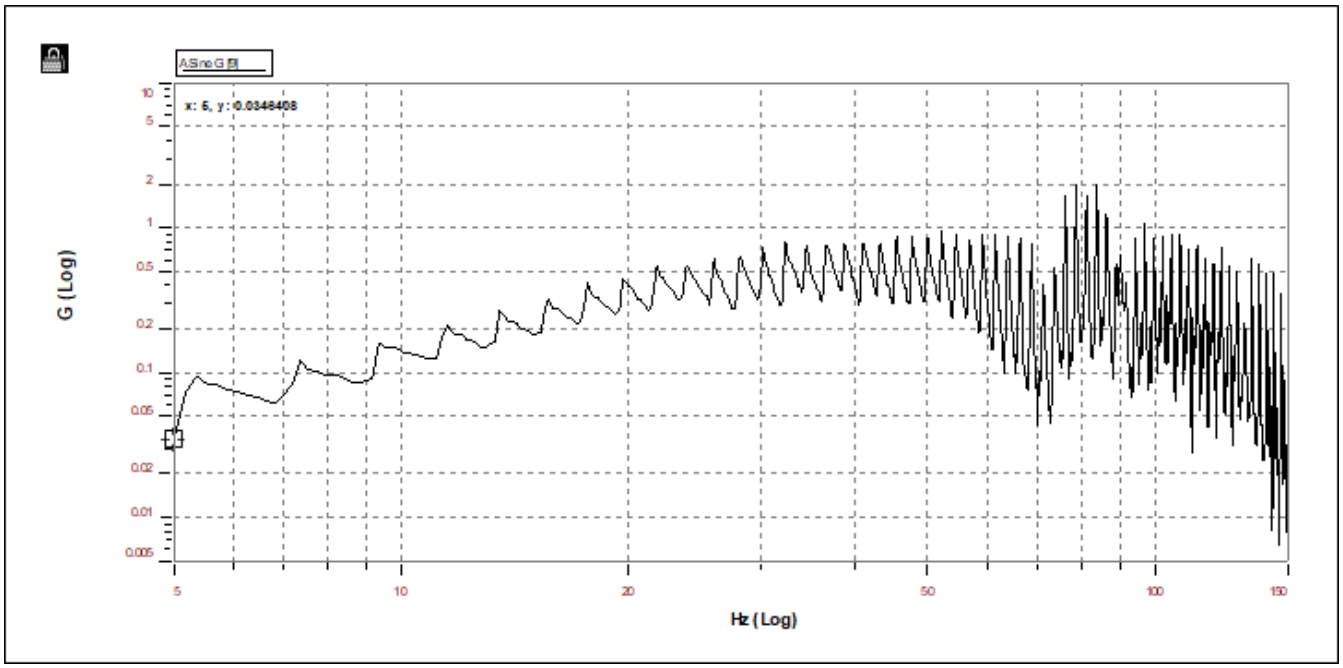

Figure 5.19: 39 kN sweep test, 42.3 m accelerometer

Further results for other accelerometer positions and tension are presented in the appendices. The appendices also present additional magnified graphs and the raw data extracted from the PUMA system as a Microsoft Excel spreadsheet.

5.5 Conclusion

Chapter 5 presented free vibration test results for both the ACSR Bersfort and Tern conductors. It also presented forced vibration test results for the two conductors, the ACSR Bersfort and Tern conductors.

CHAPTER 6
ANALYSIS OF THE FORCED VIBRATION RESULTS

6.1 Introduction

Chapter 6 presents the analysis of the results obtained during the forced vibration tests for ACSR Bersfort and Tern conductors. The objective of the analysis is to obtain self-damping characteristics of these two conductors.

6.2 Analysis of forced vibration results for the Tern conductor

As indicated in the previous chapter, resonance frequency, bandwidth, quality factor, Q and damping factor were identified for conductor tension of 26.15 kN, 32.69 kN and 39.23 kN. This section presents a sample of the analysis that was done to obtain the above praments. Detailed analysis for all the tensions are in Appendix II.

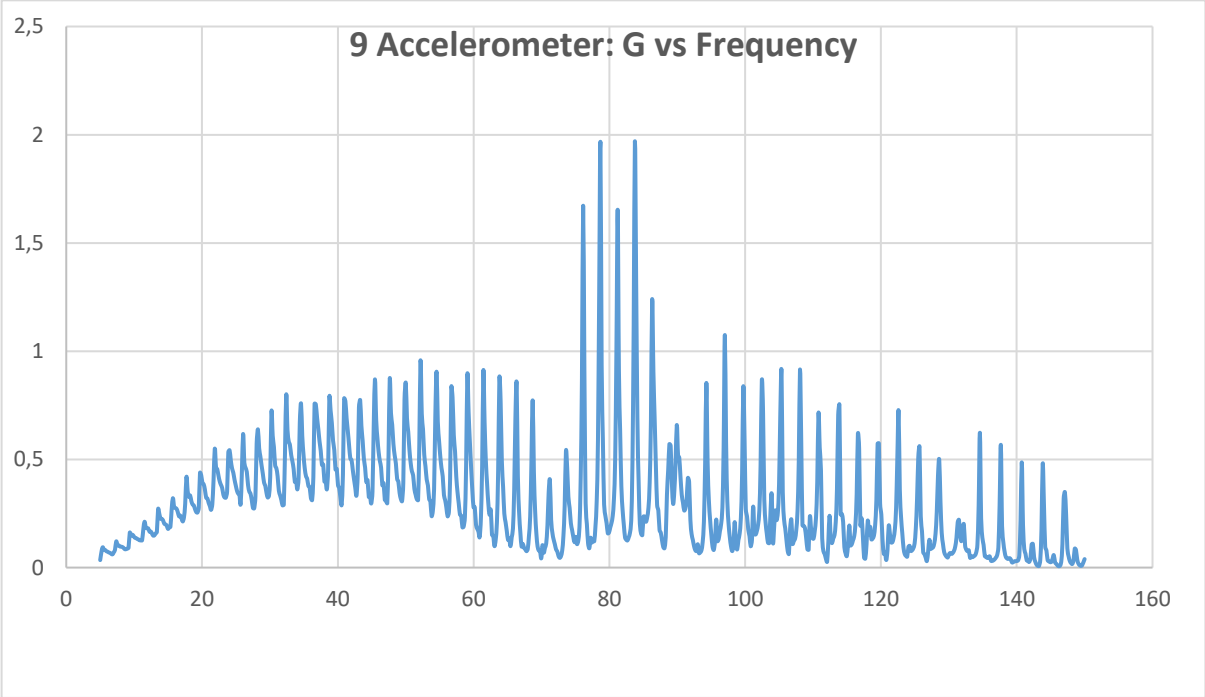

6.2.1 Calculations from an accelerometer positioned at mid-span (42.3 m) for conductor tension of 39.23 kN

Figure 6.1 present the mid-span results as a logarithmic graph of acceleration in G versus frequency in Hz. Figure 6.2 shows the same results on a non-logarithmic scale as such results were found more amenable to analysis.

Figure 6. 1: Acceleration (G) vs Frequency, channel 9, 39.23 kN (Test1)

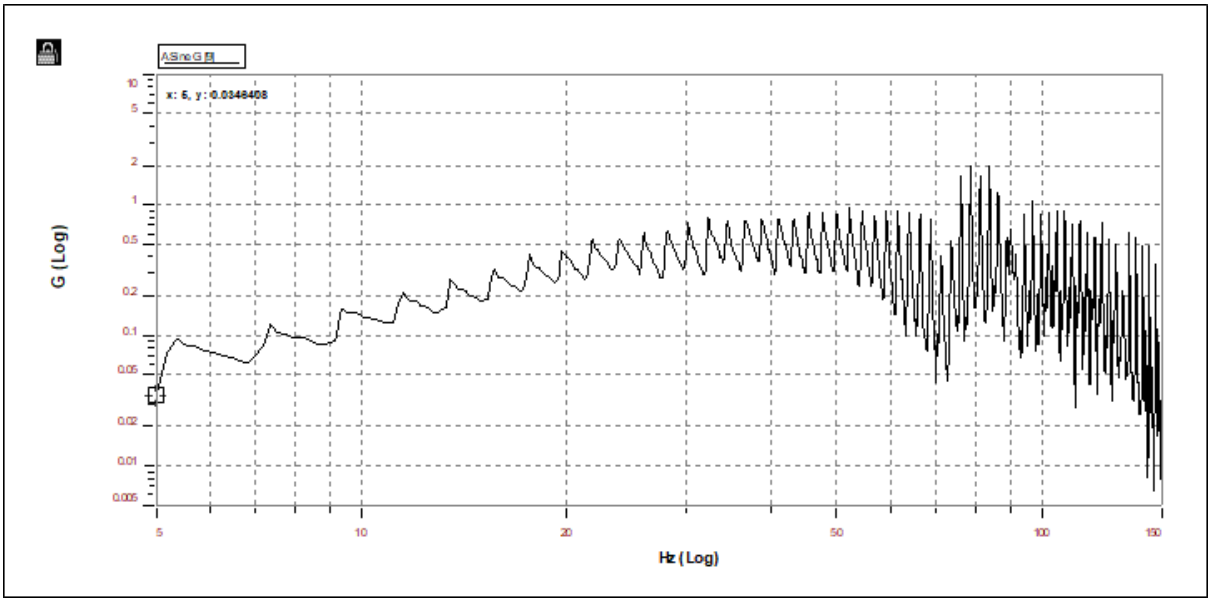

Figure 6. 2: Acceleration (G) vs Frequency, channel 9, 39.23 kN (Test1) Spectral Viewer

The Quality Factor and the damping factor were calculated from the results presented in Figure 6.1 follows:

- The parameter f_n was read from the graph as 52.183979 Hz
- The excitation frequencies f_1 and f_2 that correspond to a magnification factor were calculated as follows:

$$x = \frac{X_{peak}}{1.4142}$$

$$X_{peak} = 0.957837$$

where

X_{peak} is X identified on Fn value

Therefore:

$$x = \frac{0.957837}{1.4142}$$

$$x = 0.6773$$

- On 0.6773 a line was drawn towards the X axis and it touched the peak and both frequencies recorded.

f_1= 52.183979 (left side)

f_2= 52.546932 (right side)

- Thus,

$$Q = \frac{f_n}{f_2 - f_1}$$

$$Q = \frac{52.183979}{52.546932 - 52.183979}$$

$$Q = 149.2864889$$

- But

$$Q = \frac{1}{2\zeta}$$

- Therefore,

$$\zeta = \frac{1}{2 \times 149.2864889}$$

$$\zeta = 0.00669853$$

6.2.1.1 Additional Results for mid-span (42.3 m) for conductor tension of 39.23 kN

The calculations above were repeated for other peaks in the graph presented in Figure 6.1. Table 6.1 shows the results of these calculations. It is seen in Table 6.1 that the damping factor, ζ, ranges from 0.003741 to 0.006699. Thus, for 52.546932 Hz, the maximum damping factor was 0.006699.

In calculations for other tests at the tension of 39.23 kN, slightly different values of the damping factors were obtained. Further processing of these results suggests that for a conductor tension of 39.23 kN, the damping factor varies frequency, as indicated in Figure 6.1.

Table 6. 1: Data Collected on Figure 6.1

Peak	X peak	x1 and x2	f1	f2	Fn	Change F	Q	Zeta
	Read on Graph	Xp/1.4142	Read on Graph x1	Read on Graph x2	Read on Graph Xpeak	F2-F1	Fn/(F2-F1)	1/2Q
1	0.957837	0.6773	52.183979	52.546932	54.183979	0.362953	149.286489	0.006699
2	1.9675	1.391246	78.679596	79.042549	78.679596	0.362953	216.776266	0.004613
3	1.07466	0.759907	97.008759	97.371712	97.008759	0.362953	267.276366	0.003741

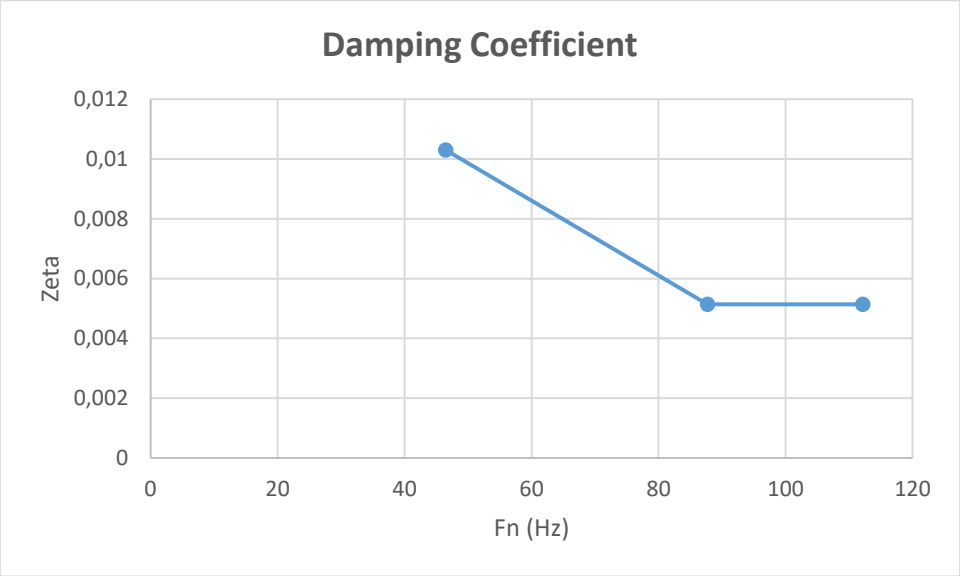

Figure 6. 3: Damping factor (Zeta) vs Fn (Hz)

6.2.2 Calculations from an accelerometer positioned at one-quarter span (21.15 m) for conductor tension of 39.23 kN

Figure 6.5 presents the quarter-span results as a logarithmic graph of acceleration in G versus frequency in Hz. Figure 6.4 shows the same results on a non-logarithmic scale as such results were found more amenable to analysis.

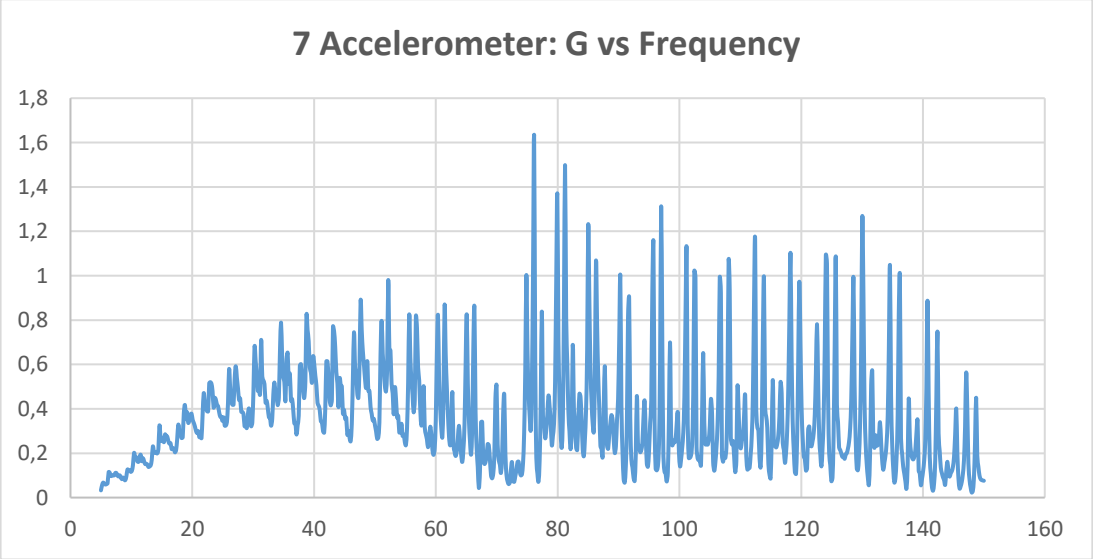

Figure 6. 4: Acceleration (G) vs Frequency, channel 7, 39.23 kN (Test1)

g

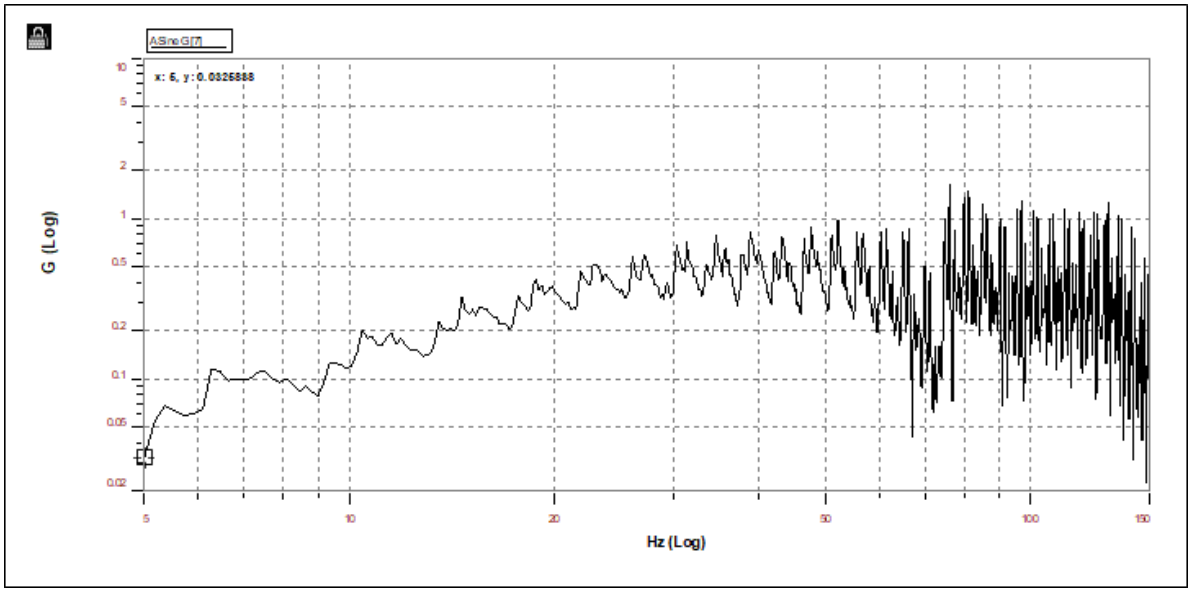

Figure 6. 5: Acceleration (G) vs Frequency, channel 7, 39.23 kN (Test1) Spectral Viewer

6.2.2.1 Additional results for mid-span (42.3 m) for conductor tension of 39.23 kN

The calculations above were repeated for other peaks in the graph presented in Figure 6.4. Table 6.2 shows the results of these calculations. It is seen in Table 6.2 that the damping factor, ζ, ranges from 0.004187 to 0.006655. Thus, for 52.546932 Hz, the maximum damping factor was 0.006655.

In calculations for other tests at the tension of 39.23 kN and on quarter-span, slightly different damping factors were obtained. Further processing of these results suggests that for a conductor tension of 39.23 kN, the damping factor varies frequency, as indicated in Figure 6.4.

Table 6. 2: Data Collected in Figure 6.4.

Peak	X peak	x1 and x2	f1	f2	Fn	Change F	Q	Zeta
	Read on Graph	Xp/1.4142	Read on Graph x1	Read on Graph x2	Read on Graph Xpeak	F2-F1	Fn/(F2-F1)	1/2Q
1	0.980764	0.693512	52.183979	52.546932	52.183979	0.362953	143.776134	0.006955
2	1.63541	1.156421	76.138924	76.501877	76.138924	0.362953	209.776263	0.004767
3	1.26941	0.897617	130.037537	130.58197	130.037537	0.544433	238.849476	0.004187

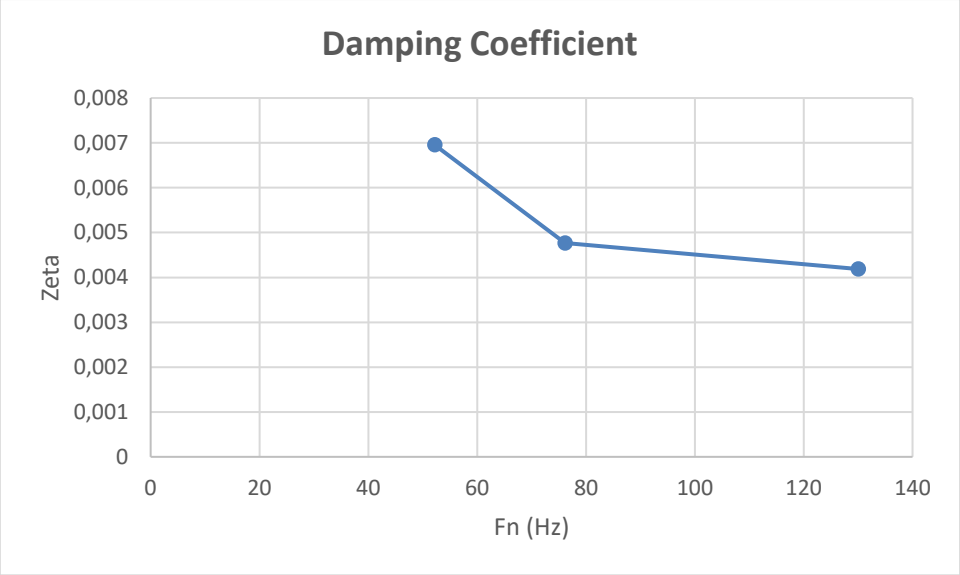

Figure 6. 6: Damping factor (Zeta) vs Fn (Hz)

6.2.3 Calculations from an accelerometer positioned at 1/3 span (28.2 m) for conductor tension of 39.23 kN

Figure 6.8 presents the 1/3 span results as a logarithmic graph of acceleration in G versus frequency in Hz. Figure 6.7shows the same results on a non-logarithmic scale as such results were found more amenable to analysis.

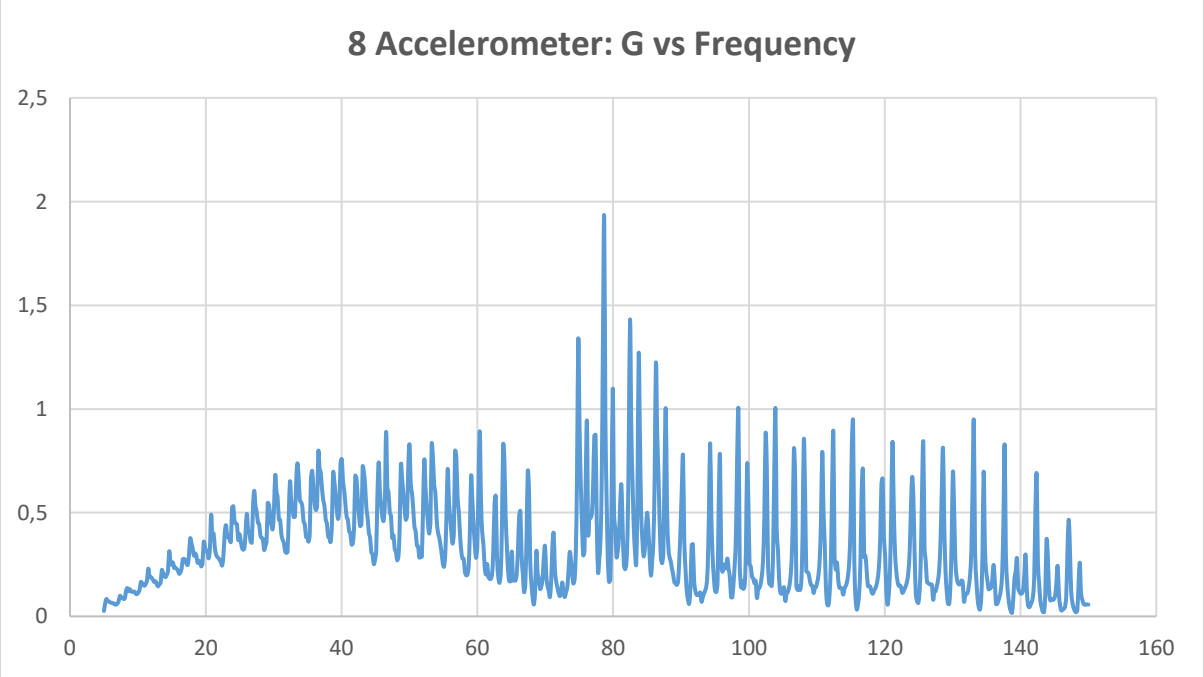

Figure 6. 7: Acceleration (G) vs Frequency, channel 8, 39.23 kN (Test1)

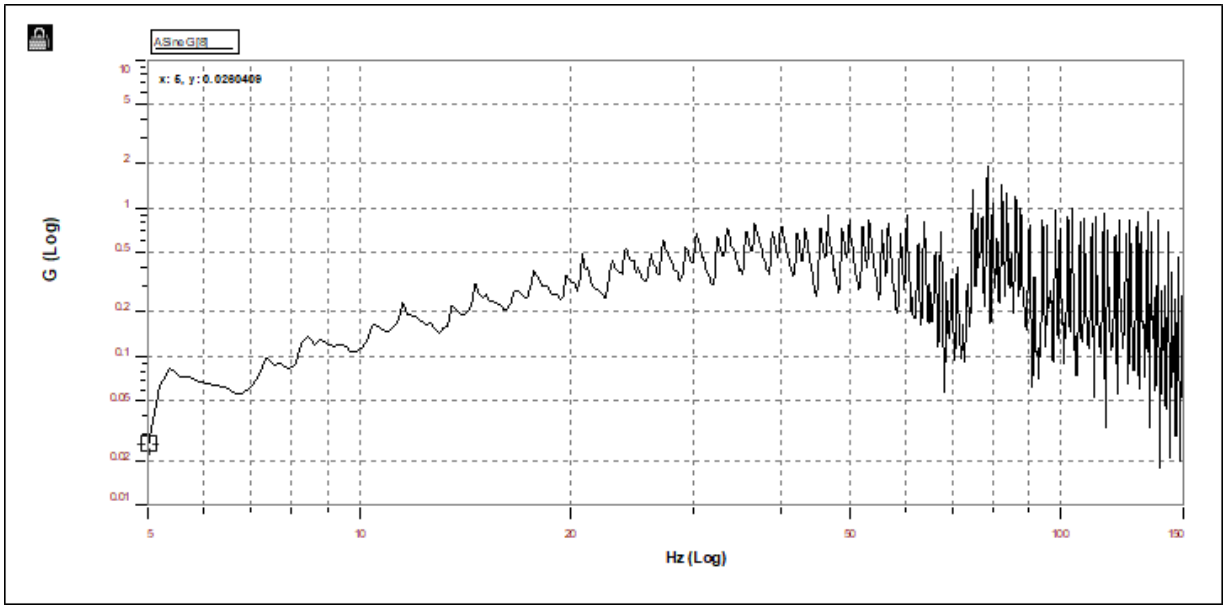

Figure 6. 8: Acceleration (G) vs Frequency, channel 8, 39.23 kN (Test1) Spectral Viewer

6.2.3.1 Additional results for one-third span (28.2 m) for conductor tension of 39.23 kN

The calculations above were repeated for other peaks in the graph presented in Figure 6.7. Table 6.3 shows the results of these calculations. It is seen in Table 6.3 that the damping factor, ζ, ranges from 0.00524 to 0.007796. Thus, for of 46.558197 Hz, the maximum damping factor was 0.007796.

In calculations for other tests at the tension of 39.23 kN and on 1/3 span, slightly different damping factors were obtained. Further processing of these results suggests that for a conductor tension of 39.23 kN, the damping factor varies frequency, as indicated in Figure 6.7.

Table 6. 3: Data Collected in Figure 6.7

Peak	X peak	x1 and x2	f1	f2	Fn	Change F	Q	Zeta
	Read on Graph	Xp/1.4142	Read on Graph x1	Read on Graph x2	Read on Graph Xpeak	F2-F1	Fn/(F2-F1)	1/2Q
1	0.889596	0.629045	46.558197	46.92115	46.558197	0.362953	128.276105	0.007796
2	1.92796	1.363287	78.679596	79.22403	78.679596	0.544434	144.516316	0.00692
3	0.999248	0.706582	103.904877	104.44931	103.904877	0.544433	190.849704	0.00524

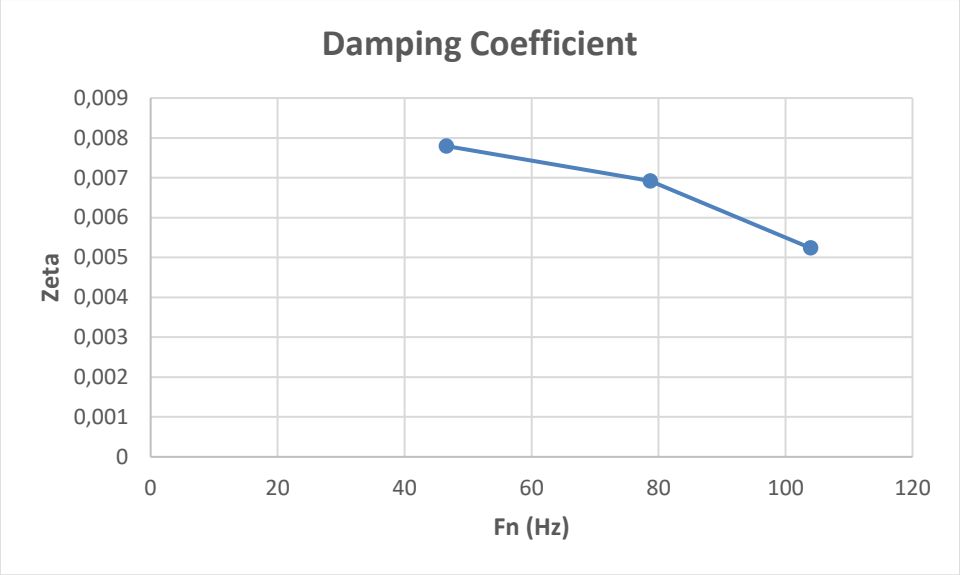

Figure 6. 9: Damping factor (Zeta) vs Fn (Hz)

6.2.4 Calculations from an accelerometer positioned at 1/8 span (10.525 m) for conductor tension of 39.23 kN

Figure 6.11 presents the 1/8 span results as a logarithmic graph of acceleration in G versus frequency in Hz. Figure 6.10 shows the same results on a non-logarithmic scale as such results were found more amenable to analysis.

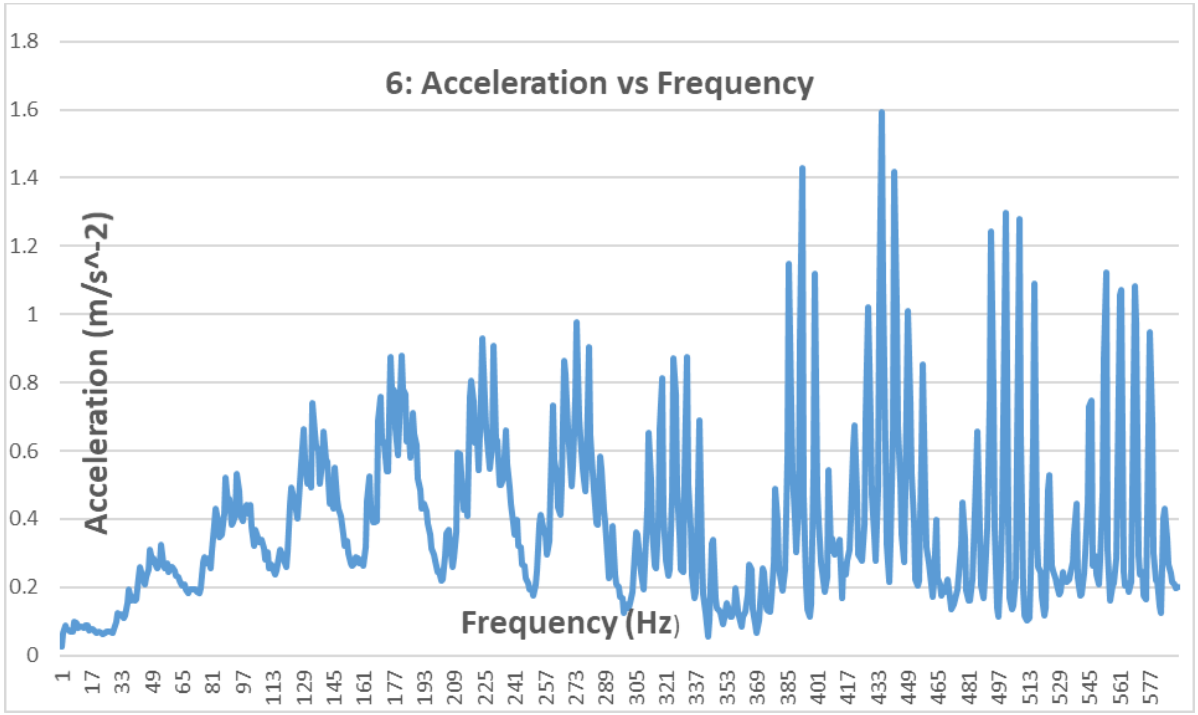

Figure 6. 10: Acceleration (G) vs Frequency, channel 6, 39.23 kN (Test1)

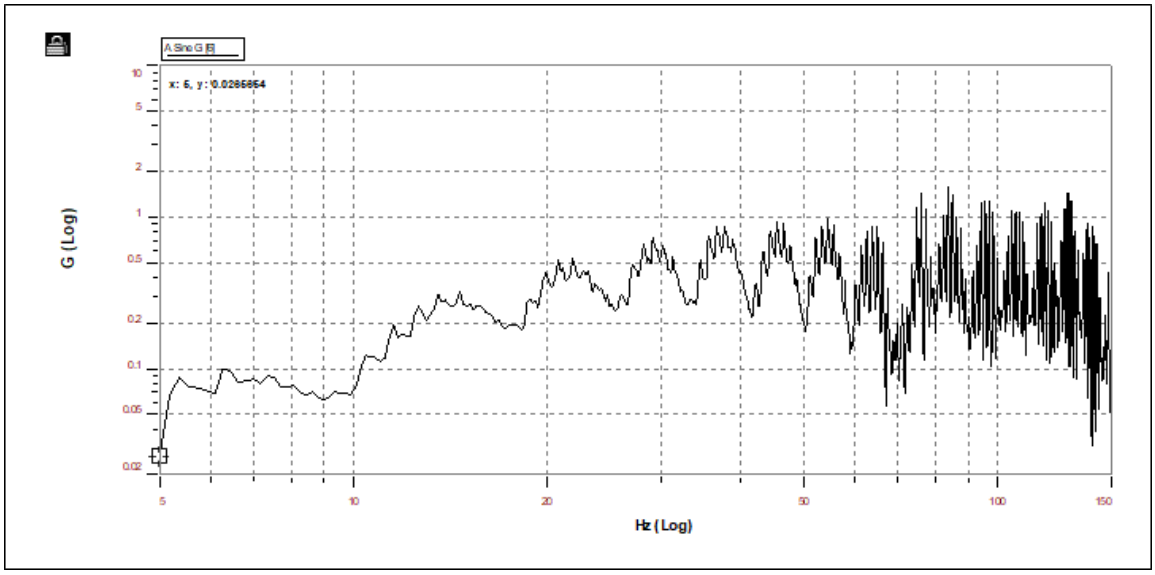

Figure 6. 11: Acceleration (G) vs Frequency, channel 6, 39.23 kN (Test1) Spectral Viewer

6.2.4.1 Additional results for 1/8 span (10.525 m) for conductor tension of 39.23 kN

The calculations above were repeated for other peaks in the graph presented in Figure 6.10. Table 6.4 shows the results of these calculations. It is seen in Table 6.4 that the damping factor, ζ, ranges from 0.002823 to 0.006654. Thus, for 54.9061320 Hz, the maximum damping factor was 0.006654.

In calculations for other tests at the tension of 39.23 kN and on 1/8 span, slightly different damping factors were obtained. Further processing of these results suggests that for a conductor tension of 39.23 kN, the damping factor varies frequency, as indicated in Figure 6.10.

Table 6. 4: Data Collected in Figure 6.10.

Peak	X peak	x1 and x2	f1	f2	Fn	Change F	Q	Zeta
	Read on Graph	Xp/1.4142	Read on Graph x1	Read on Graph x2	Read on Graph Xpeak	F2-F1	Fn/(F2-F1)	1/2Q
1	0.978401	0.691841	54.543179	54.906132	54.543179	0.362953	150.276149	0.006654
2	1.59422	1.127295	83.760948	84.123901	83.760948	0.362953	230.776293	0.004333
3	1.46044	1.032697	128.585724	128.948685	128.585724	0.362961	354.268707	0.002823

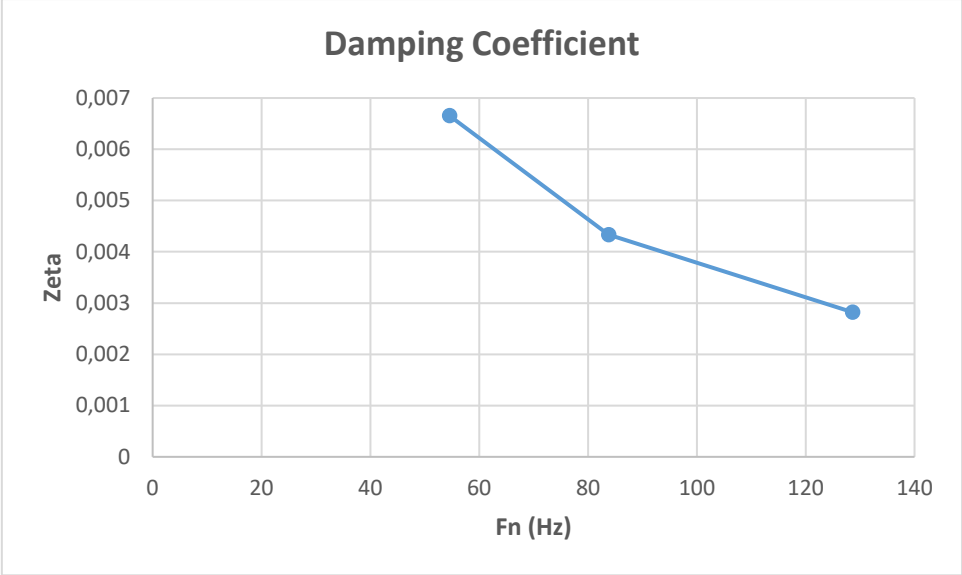

Figure 6. 12 : Damping factor (Zeta) vs Fn (Hz)

6.2.5 Calculations from an accelerometer positioned at 2m span for conductor tension of 39.23 kN

Figure 6.14 presents the 2m span results as a logarithmic graph of acceleration in G versus frequency in Hz. Figure 6.13 shows the same results on a non-logarithmic scale as such results were found more amenable to analysis.

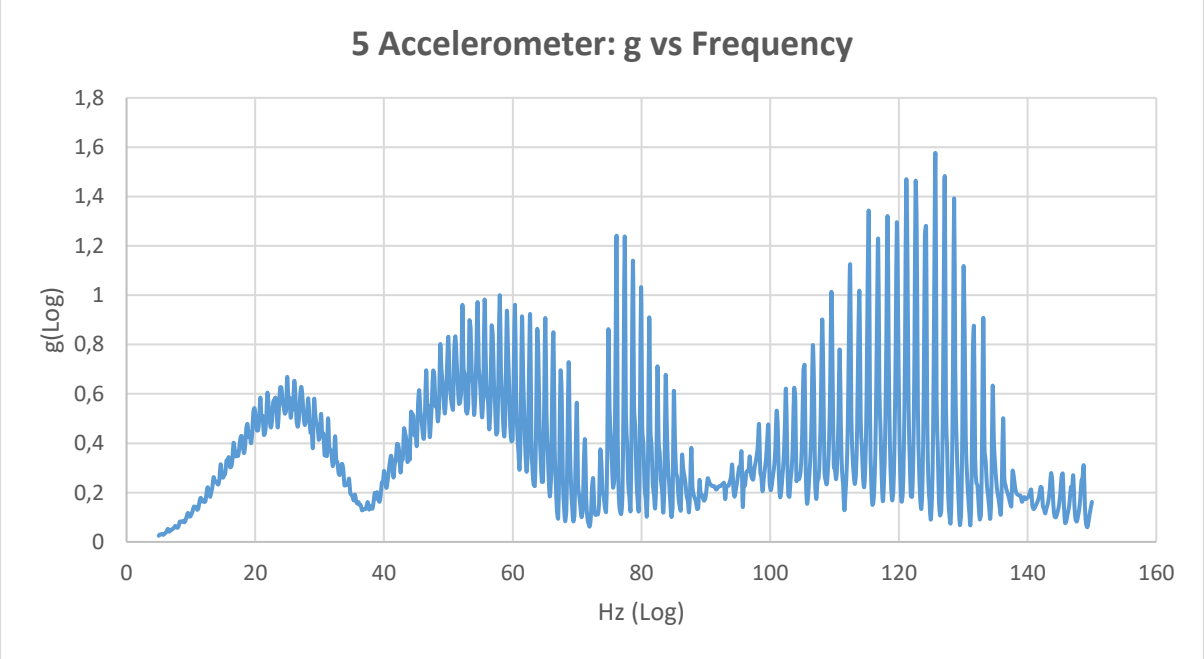

Figure 6. 13: Acceleration (g) vs Frequency, channel 6, 39.23 kN (Test1)

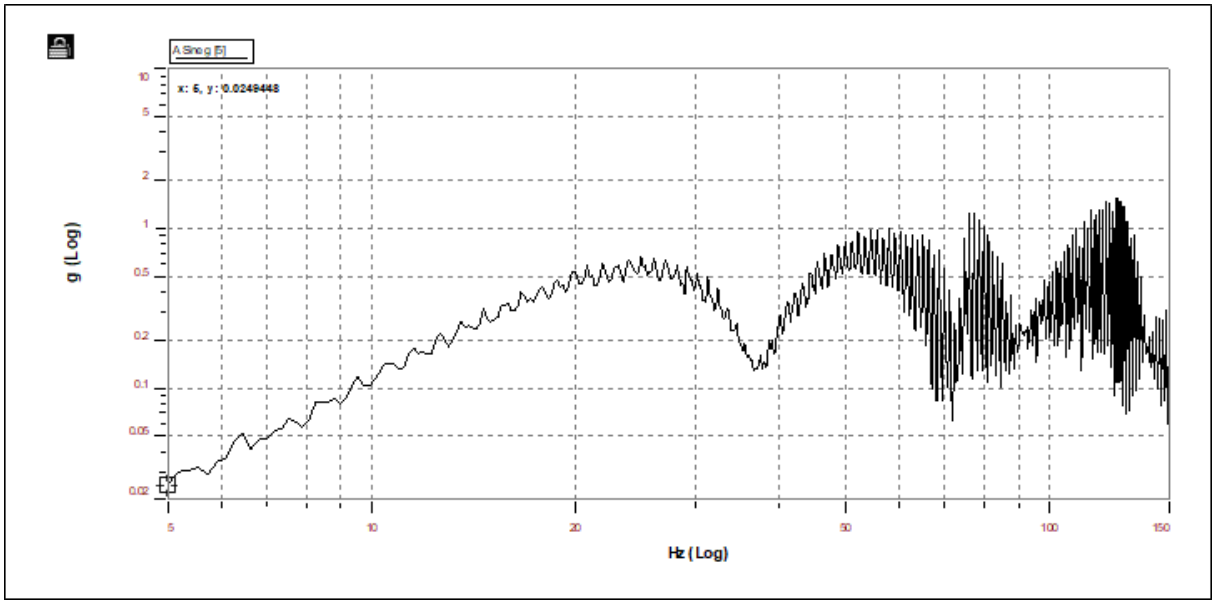

Figure 6. 14: Acceleration (g) vs Frequency, channel 5, 39.23 kN (Test1) Spectral Viewer

6.2.5.1 Additional results for 2 m span for conductor tension of 39.23 kN

The calculations above were repeated for other peaks in the graph presented in Figure 6.13. Table 6.5 shows the results of these calculations. It is seen in Table 6.5 that the damping factor, ζ, ranges from 0.002888 to 0.02181. Thus, for 24.9624 Hz, the maximum damping factor was 0.006259.

In calculations for other tests at the tension of 39.23 kN and on 2m span, slightly different damping factors were obtained. Further processing of these results suggests that for a conductor tension of 39.23 kN, the damping factor varies frequency, as indicated in Figure 6.13.

Table 6. 5: Data Collected in Figure 6.13.

Peak	X peak	x1 and x2	f1	f2	Fn	Change F	Q	Zeta
	Read on Graph	Xp/1.4142	Read on Graph x1	Read on Graph x2	Read on Graph Xpeak	F2-F1	Fn/(F2-F1)	1/2Q
1	0.669177	0.473184	24.962453	25.506884	24.962452	0.544431	45.8505339	0.02181
2	1.00012	0.707198	57.991238	58.354191	57.991238	0.362953	159.776164	0.006259
3	1.24137	0.87779	76.138924	76.501877	76.138924	0.362953	209.776263	0.004767
4	1.56676	1.107877	125.682098	126.045053	125.682098	0.362955	346.274602	0.002888

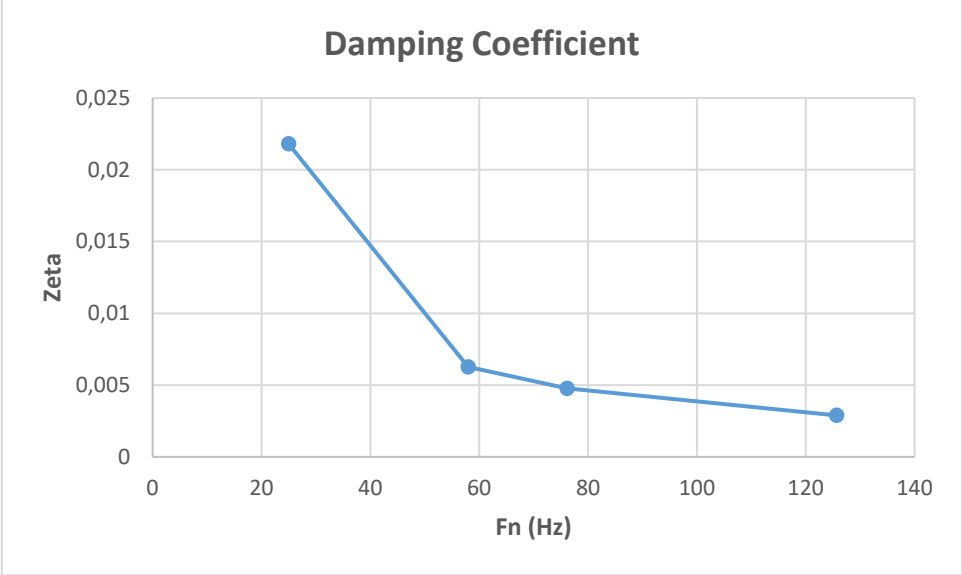

Figure 6. 15: Damping factor (Zeta) vs Fn (Hz)

6.2.6 Calculations from an accelerometer positioned at 1 m span for conductor tension of 39.23 kN

Figure 6.16 presents the 1m span results as a logarithmic graph of acceleration in G versus frequency in Hz. Figure 6.17 shows the same results on a non-logarithmic scale as such results were found more amenable to analysis.

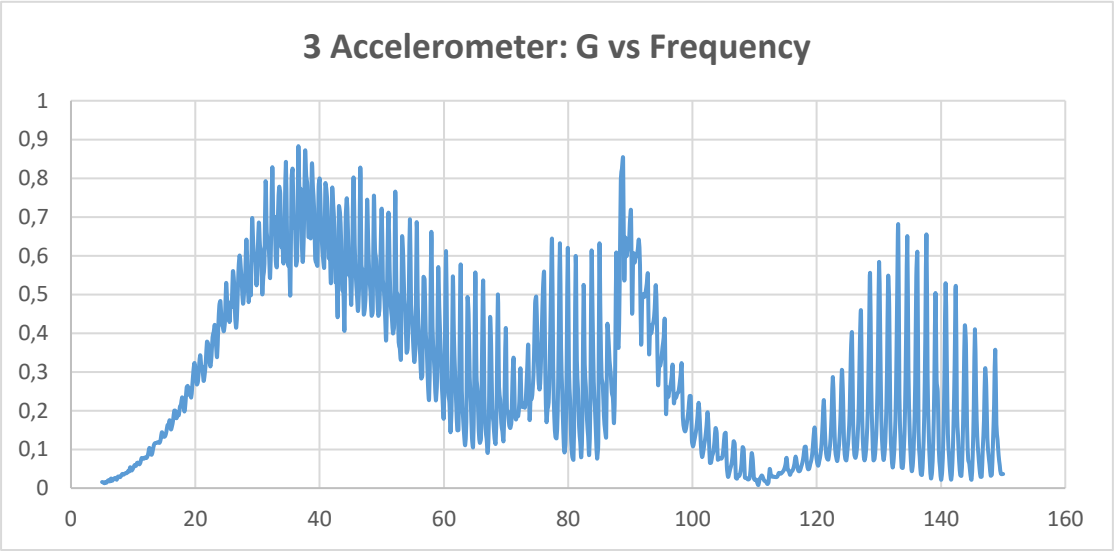

Figure 6. 16: Acceleration (G) vs Frequency, channel 6, 39.23 kN (Test1)

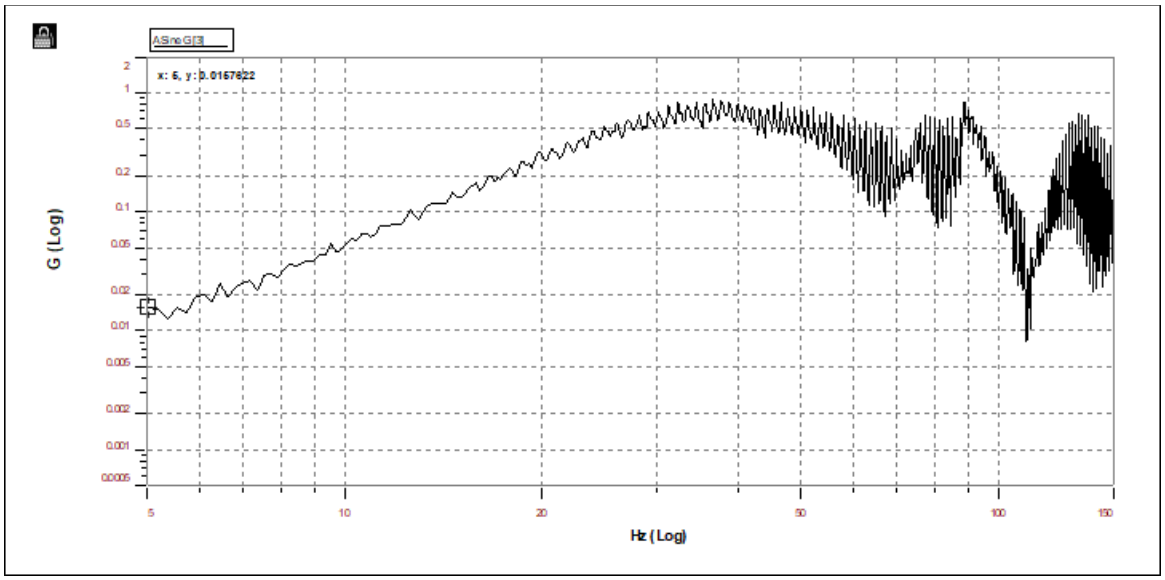

Figure 6. 17: Acceleration (G) vs Frequency, channel 3, 39.23 kN (Test1) Spectral Viewer

6.2.6.1 Additional results for 1 m span for conductor tension of 39.23 kN

The calculations above were repeated for other peaks in the graph presented in Figure 6.16. Table 6.6 shows the results of these calculations. It is seen in Table 6.6 that the damping factor, ζ, ranges from 0.001363 to 0.024807. Thus, for 36.576969 Hz, the maximum damping factor was 0.024807.

In calculations for other tests at the tension of 39.23 kN and on 1m span, slightly different damping factors were obtained. Further processing of these results suggests that for a conductor tension of 39.23 kN, the damping factor varies frequency, as indicated in Figure 1.Referring to Table 6.6 below, the damping factor was $0.001363 \leq 0.004689$ and the maximum damping factor was identified on the frequency of 36.576969 Hz as 0.024807.

Table 6. 6: Data Collected in Figure 6.16.

Peak	X peak	x1 and x2	f1	f2	Fn	Change F	Q	Zeta
	Read on Graph	Xp/1.4142	Read on Graph x1	Read on Graph x2	Read on Graph Xpeak	F2-F1	Fn/(F2-F1)	1/2Q
1	0.878525	0.621217	36.576969	37.484352	36.576969	0.907383	40.310397	0.024807
2	0.639915	0.452493	77.409256	77.772209	77.409256	0.362953	213.276253	0.004689
3	0.851603	0.60218	88.8423	89.023773	88.8423	0.181473	489.562084	0.002043
4	0.675579	0.477711	133.12265	133.304123	133.12265	0.181473	733.567252	0.001363

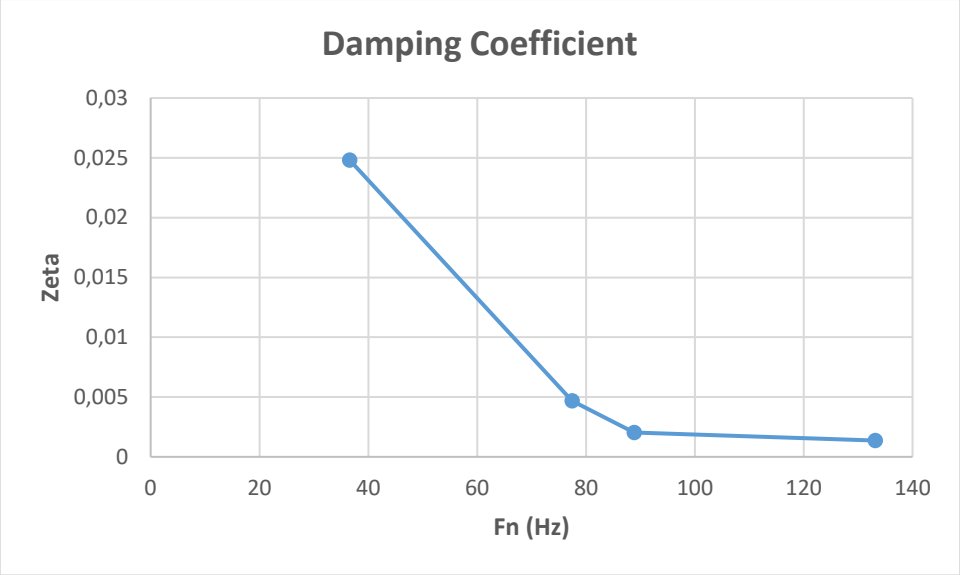

Figure 6. 18: Damping factor (Zeta) vs Fn (Hz)

6.3 Analysis of forced vibration results for the ACSR Bersfort

As indicated in the previous chapter, resonance frequency, bandwidth, quality factor, Q and damping factor were identified for conductor tension of 36 kN, 45 kN and 54 kN.. This section presents a sample of the analysis that was done to obtain the above praments. Detailed analysis for all the tensions in Appendix II.

6.3.1 Calculations from an accelerometer positioned at mid-span (42.3 m) for conductor tension of 54 kN

Figure 6.20 presents the mid-span results as a logarithmic graph of acceleration in G versus frequency in Hz. Figure 6.19 shows the same results on a non-logarithmic scale as such results were found more amenable to analysis.

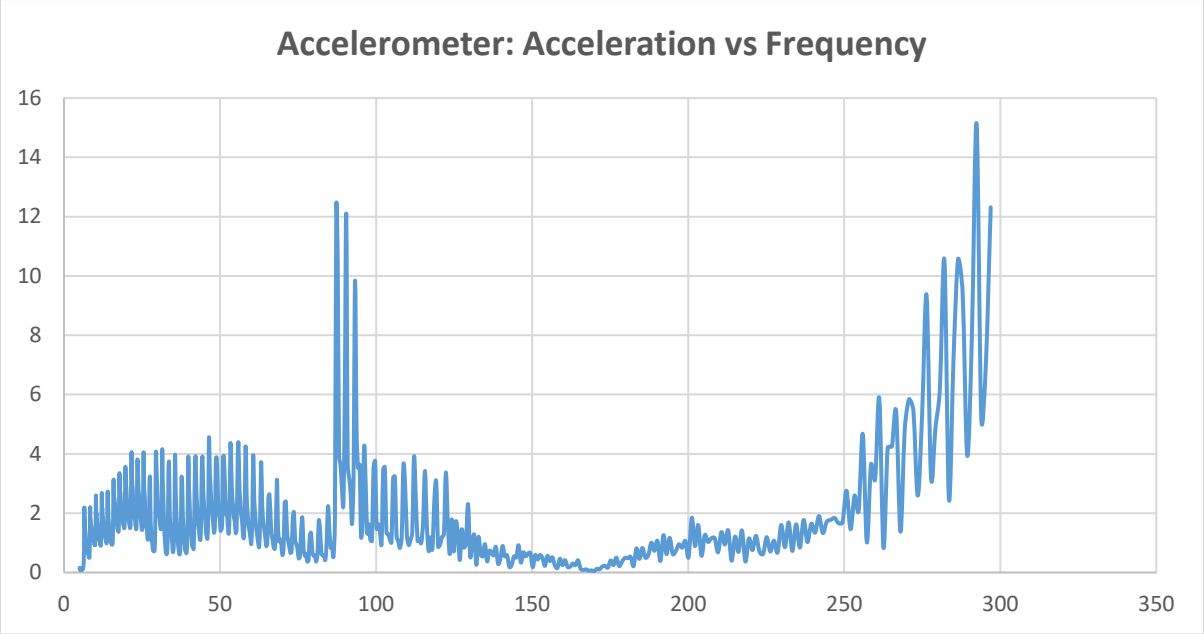

Figure 6. 19: Acceleration (m/s-2) vs Frequency, channel 6, 54 kN (Test1)

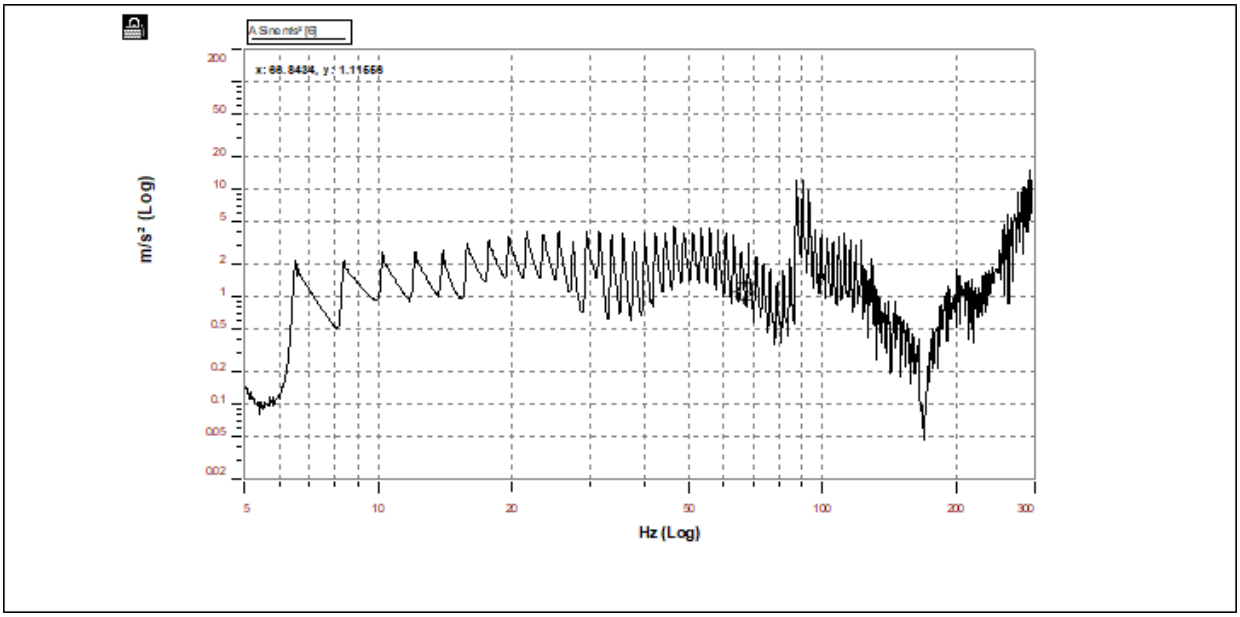

Figure 6. 20: Acceleration (m/s-2) vs Frequency, channel 6, 54 kN (Test1) Spectral ViewerAcceleration (m/s-2) vs Frequency, channel 6, 54 kN (Test1) Spectral Viewer

6.3.1.1 Additional results for mid-span for conductor tension of 54 kN

The calculations above were repeated for other peaks in the graph presented in Figure 6.19. Table 6.7 shows the results of these calculations. It is seen in Table 6.7 that the damping factor,

ζ, ranges from 0.005137 to 0.010301. Thus, for 46.456856 Hz, the maximum damping factor was 0.010301.

In calculations for other tests at the tension of 54 kN and on mid- span, slightly different damping factors were obtained. Further processing of these results suggests that for a conductor tension of 54 kN, the damping factor varies frequency, as indicated in Figure 6.19.

Table 6. 7: Data Collected in Figure 6.19.

Peak	X peak	x1 and x2	f1	f2	Fn	Change F	Q	Zeta
	Read on Graph	Xp/1.4142	Read on Graph x1	Read on Graph x2	Read on Graph Xpeak	F2-F1	Fn/(F2-F1)	1/2Q
1	4.52468	3.199463	46.456856	46.935425	46.456856	0.478569	97.0745201	0.010301
2	10.4855	7.414439	87.701736	88.152306	87.701736	0.45057	194.646195	0.005138
3	3.90485	2.761172	112.158142	112.734352	112.158142	0.57621	194.648031	0.005137

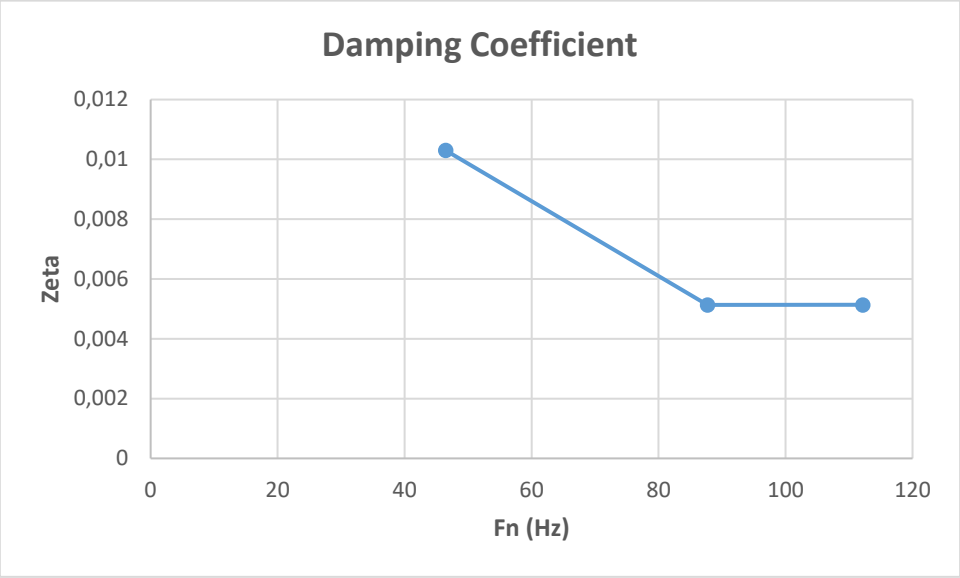

Figure 6. 21: Damping factor (Zeta) vs Fn (Hz)

6.3.2 Calculations from an accelerometer positioned at a quarter span (21.15 m) for conductor tension of 54 kN

Figure 6.23 presents the 1m span results as a logarithmic graph of acceleration in G versus frequency in Hz. Figure 6.22 shows the same results on a non-logarithmic scale as such results were found more amenable to analysis.

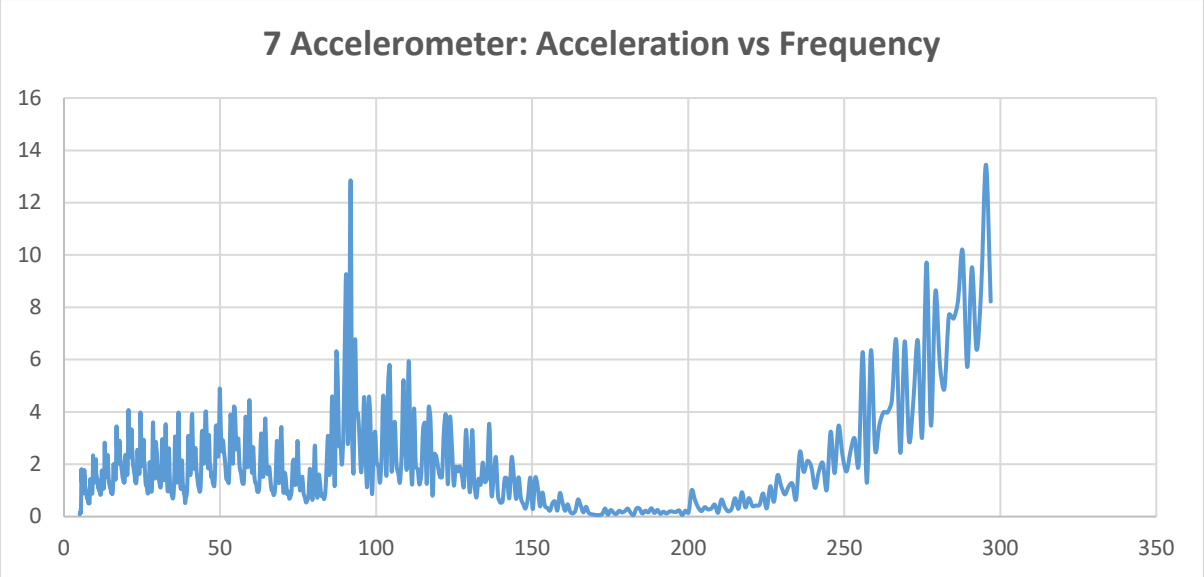

Figure 6. 22: Acceleration (m/s-2) vs Frequency, channel 7, 54 kN (Test1)

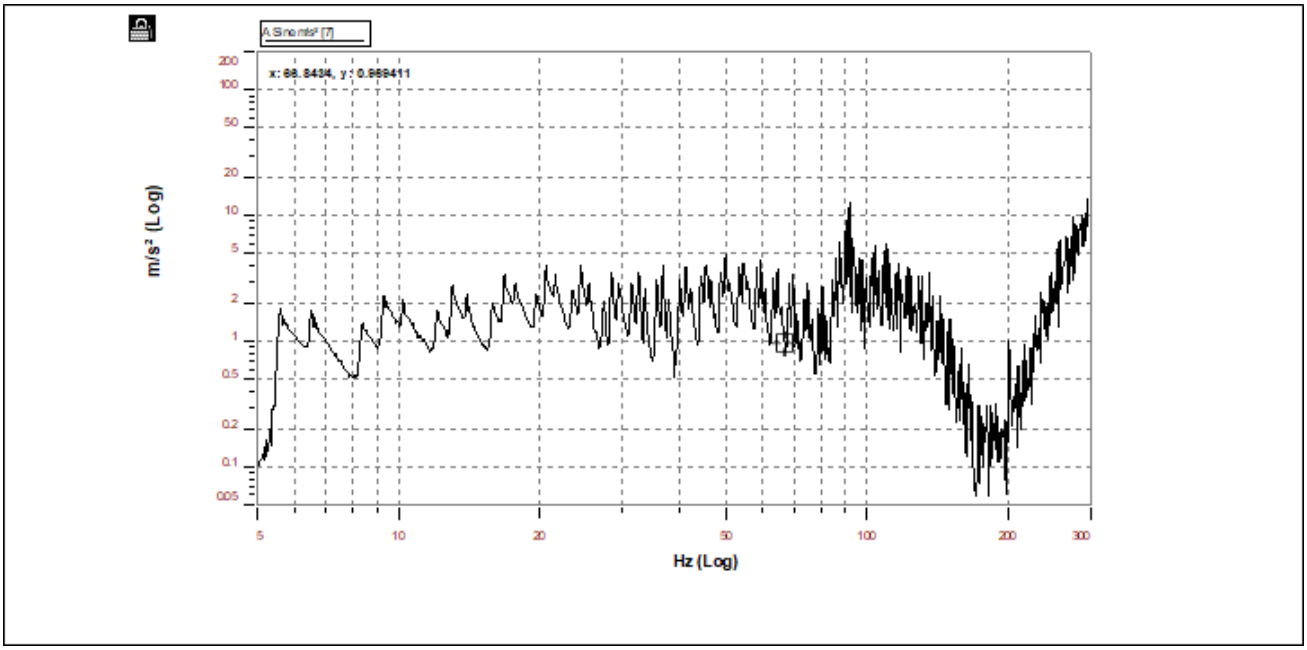

Figure 6. 23: Acceleration (m/s-2) vs Frequency, channel 7, 54 kN (Test1) Spectral Viewer

6.3.2.1 Additional results for quarter span for conductor tension of 54 kN

The calculations above were repeated for other peaks in the graph presented in Figure 6.22. Table 6.8 shows the results of these calculations. It is seen in Table 6.8 that the damping factor, ζ, ranges from 0.005137 to 0.010301. Thus, for 49.912163 Hz, the maximum damping factor was 0.010301.

In calculations for other tests at the tension of 54 kN and on quarter span, slightly different damping factors were obtained. Further processing of these results suggests that for a conductor tension of 54 kN, the damping factor varies frequency, as indicated in Figure 6.22.

Table 6. 8: Data Collected in Figure 6.22.

Peak	X peak	x1 and x2	f1	f2	Fn	Change F	Q	Zeta
	Read on Graph	Xp/1.4142	Read on Graph x1	Read on Graph x2	Read on Graph Xpeak	F2-F1	Fn/(F2-F1)	1/2Q
1	4.89912163	3.464235	49.912163	50.426327	49.912163	0.514164	97.0744023	0.010301
2	12.8529	9.08846	91.841179	92.313011	91.841179	0.471832	194.648051	0.005137
3	5.9431	4.202447	110.447121	111.014542	110.447121	0.567421	194.647574	0.005137

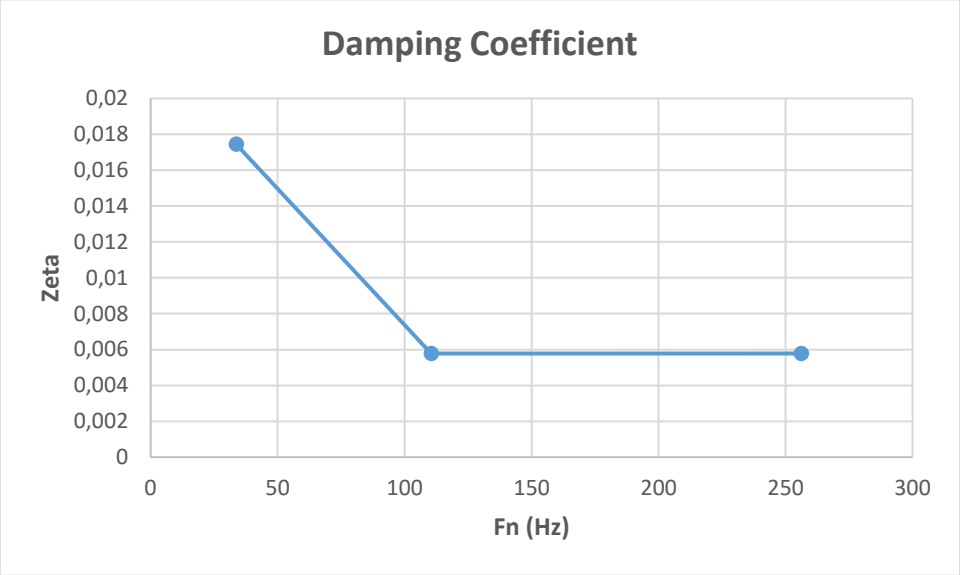

Figure 6. 24: Damping factor (Zeta) vs Fn (Hz)

6.3.3 Calculations from an accelerometer positioned at one-eighth span (10.525 m) for conductor tension of 54 kN

Figure 6.26 presents the one-eighth span results as a logarithmic graph of acceleration in G versus frequency in Hz. Figure 6.25 shows the same results on a non-logarithmic scale as such results were found more amenable to analysis.

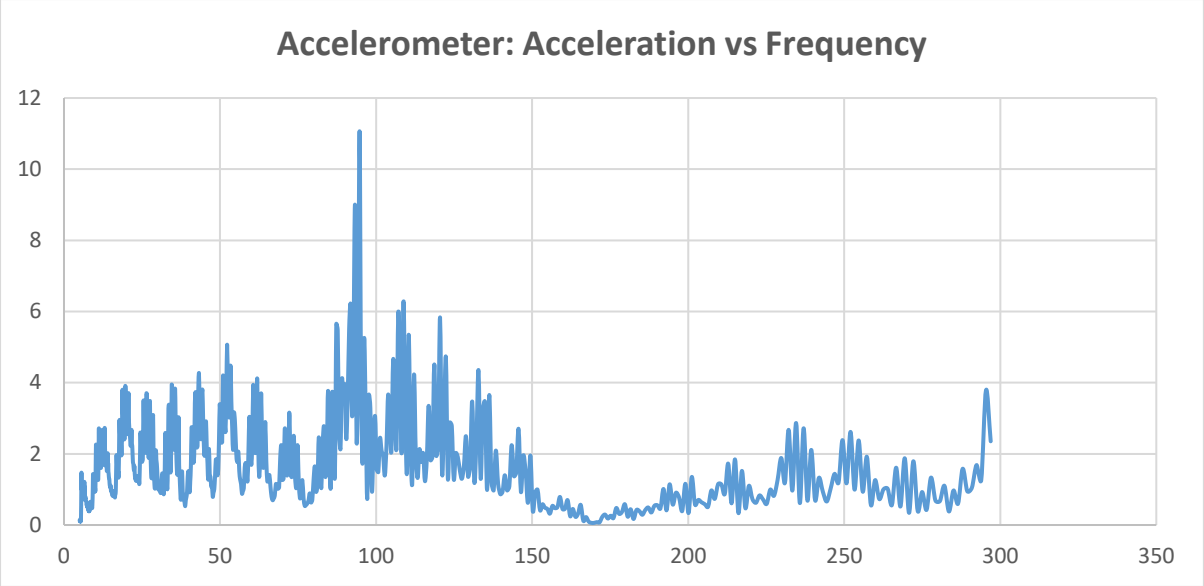

Figure 6. 25: Acceleration (m/s-2) vs Frequency, channel 8, 54 kN (Test1)

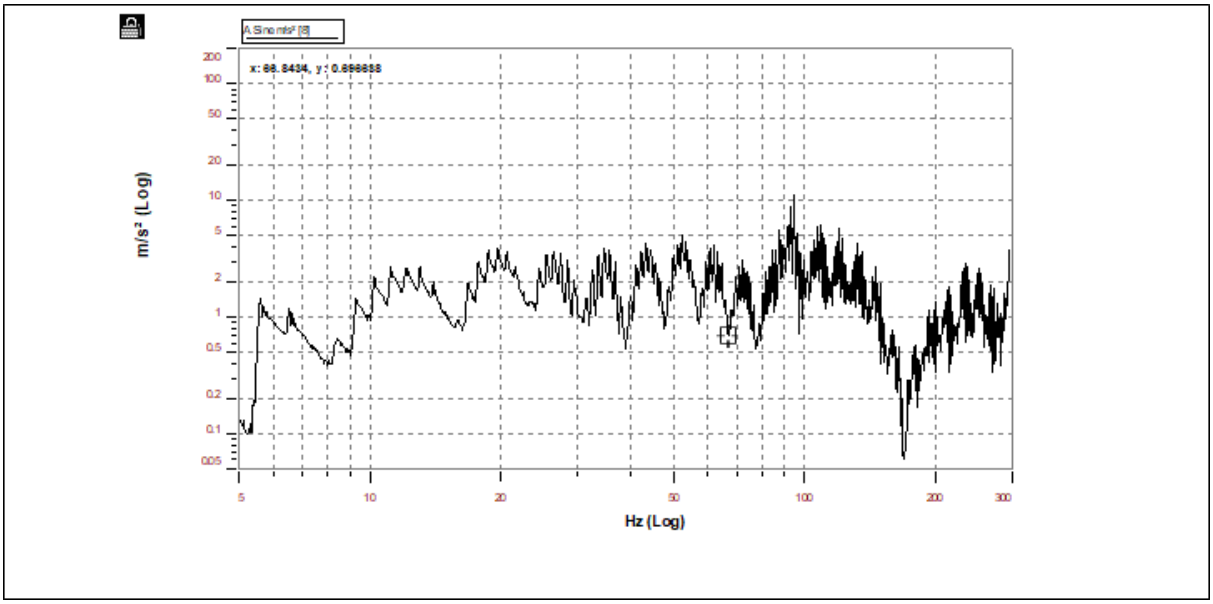

Figure 6. 26: Acceleration (m/s-2) vs Frequency, channel 8, 54 kN (Test1) Spectral Viewer

6.3.3.1 Additional results for one-eighth span for conductor tension of 54 kN

The calculations above were repeated for other peaks in the graph presented in Figure 6.25. Table 6.9 shows the results of these calculations. It is seen in Table 6.9 that the damping factor, ζ, ranges from 0.005137 to 0.010301. Thus, for 52.267971, the maximum damping factor was 0.010301.

In calculations for other tests at the tension of 54 kN and on 1/8 span, slightly different damping factors were obtained. Further processing of these results suggests that for a conductor tension of 54 kN, the damping factor varies with frequency, as indicated in Figure 6.25.

Table 6. 9: Data Collected in Figure 6.25.

Peak	X peak	x1 and x2	f1	f2	Fn	Change F	Q	Zeta
	Read on Graph	Xp/1.4142	Read on Graph x1	Read on Graph x2	Read on Graph Xpeak	F2-F1	Fn/(F2-F1)	1/2Q
1	5.067871	3.58356	52.267971	52.806404	52.267971	0.538433	97.0742339	0.010301
2	11.0656	7.824636	94.708786	95.195351	94.708786	0.486565	194.647757	0.005137
3	6.276451	4.438164	108.762199	109.320961	108.762199	0.558762	194.648525	0.005137
4	2.86704	2.027323	234.584122	235.789291	234.584122	1.205169	194.648321	0.005137

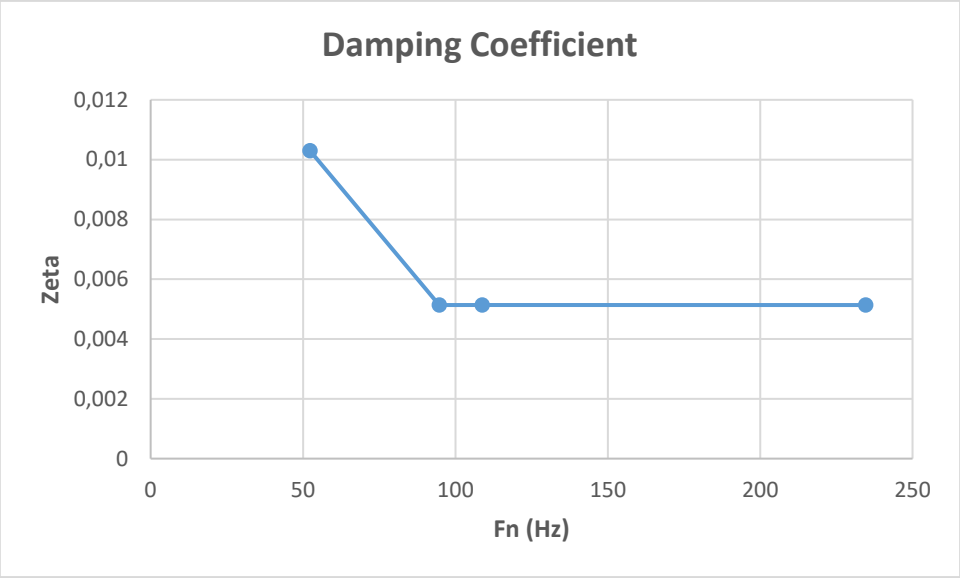

Figure 6. 27: Damping factor (Zeta) vs Fn (Hz)

6.3.4 Calculations from an accelerometer positioned at 2m span for conductor tension of 54 kN

Figure 6.29 presents the 1m span results as a logarithmic graph of acceleration in G versus frequency in Hz. Figure 6.28 shows the same results on a non-logarithmic scale as such results were found more amenable to analysis.

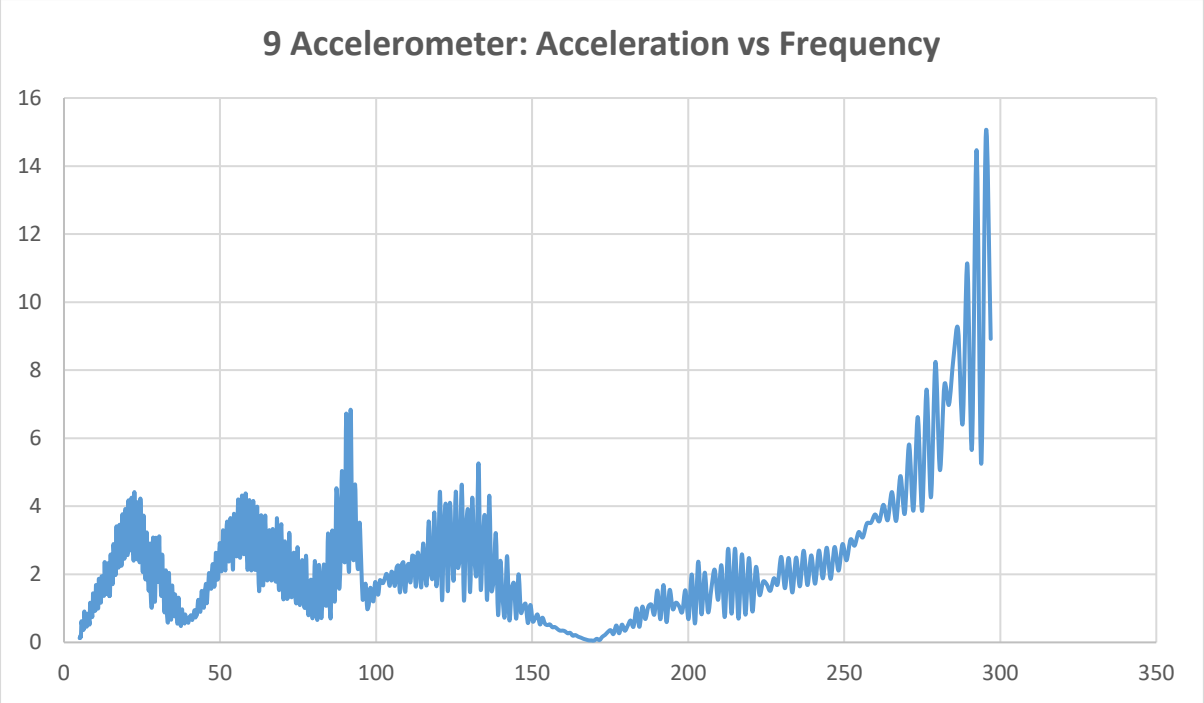

Figure 6. 28: Acceleration (m/s-2) vs Frequency, channel 9, 54 kN (Test1)

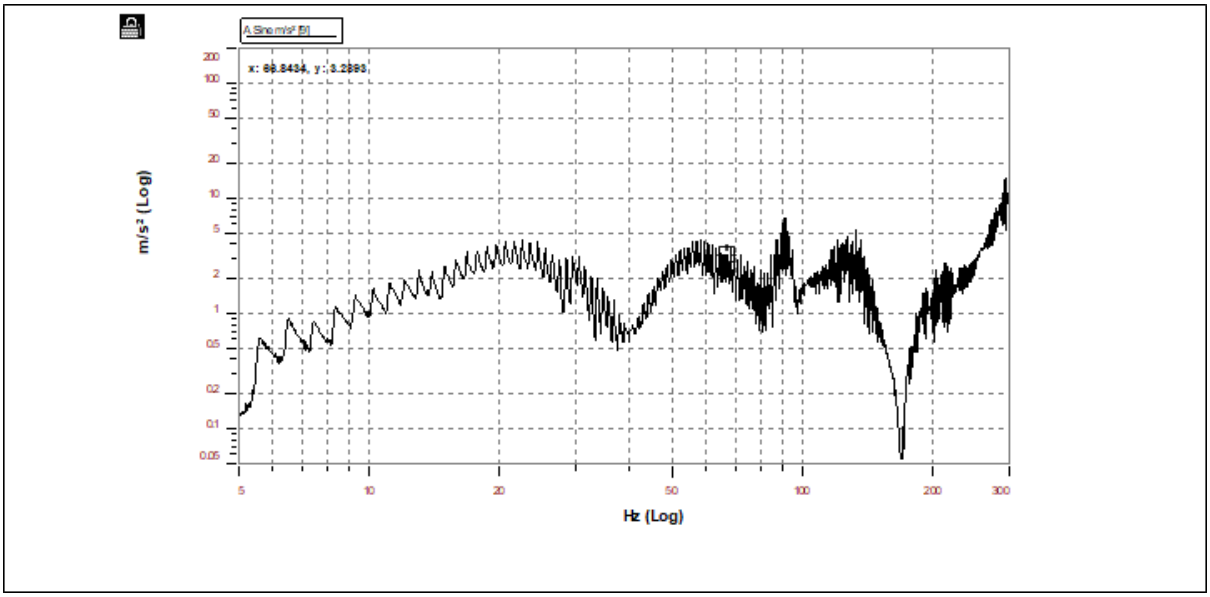

Figure 6. 29: Acceleration (m/s-2) vs Frequency, channel 9, 54 kN (Test1) Spectral Viewer

6.3.4.1 Additional results for 2 m span for conductor tension of 54 kN

The calculations above were repeated for other peaks in the graph presented in Figure 6.28. Table 6.10 shows the results of these calculations. It is seen in Table 6.10 that the damping

factor, ζ, ranges from 0.005137 to 0.020709. Thus, for 24.483074, the maximum damping factor was 0.020709.

In calculations for other tests at the tension of 54 kN and on 2m span, slightly different damping factors were obtained. Further processing of these results suggests that for a conductor tension of 54 kN, the damping factor varies frequency, as indicated in Figure 6.28.

Table 6. 10: Data Collected in Figure 6.28.

Peak	X peak	x1 and x2	f1	f2	Fn	Change F	Q	Zeta
	Read on Graph	Xp/1.4142	Read on Graph x1	Read on Graph x2	Read on Graph Xpeak	F2-F1	Fn/(F2-F1)	1/2Q
1	4.22834	2.989917	24.483074	24.990091	24.483074	0.507017	48.2884676	0.020709
2	4.37962	3.096889	58.206371	58.805977	58.206371	0.599606	97.0743638	0.010301
3	6.83929	4.836155	91.841179	92.313011	91.841179	0.471832	194.648051	0.005137
4	5.26187	3.72074	132.822403	133.504776	132.822403	0.682373	194.6478	0.005137

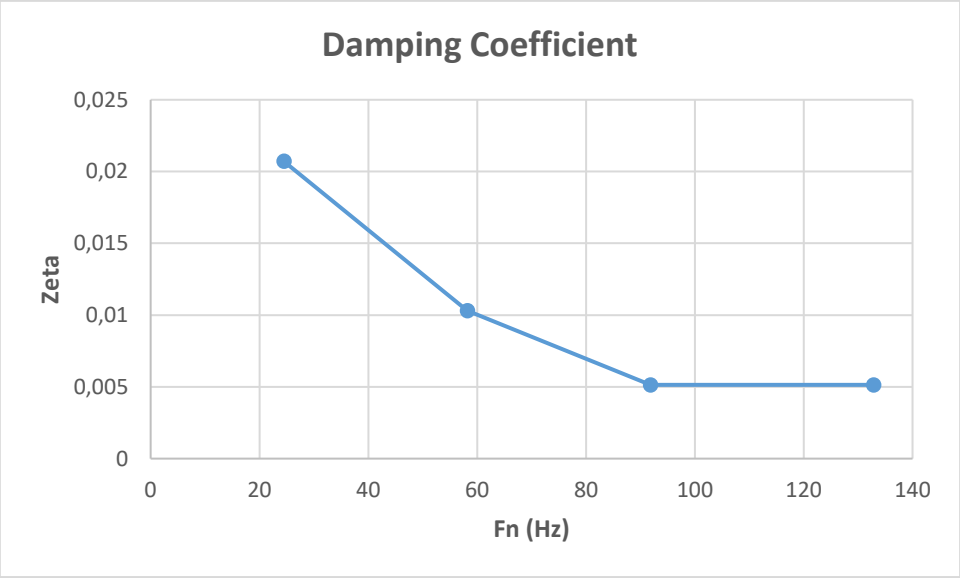

Figure 6. 30 Damping factor (Zeta) vs Fn (Hz)

6.3.5 Calculations from an accelerometer positioned at 1m span for conductor tension of 54 kN

Figure 6.31 presents the 1m span results as a logarithmic graph of acceleration in G versus frequency in Hz. Figure 6.30 shows the same results on a non-logarithmic scale as such results were found more amenable to analysis.

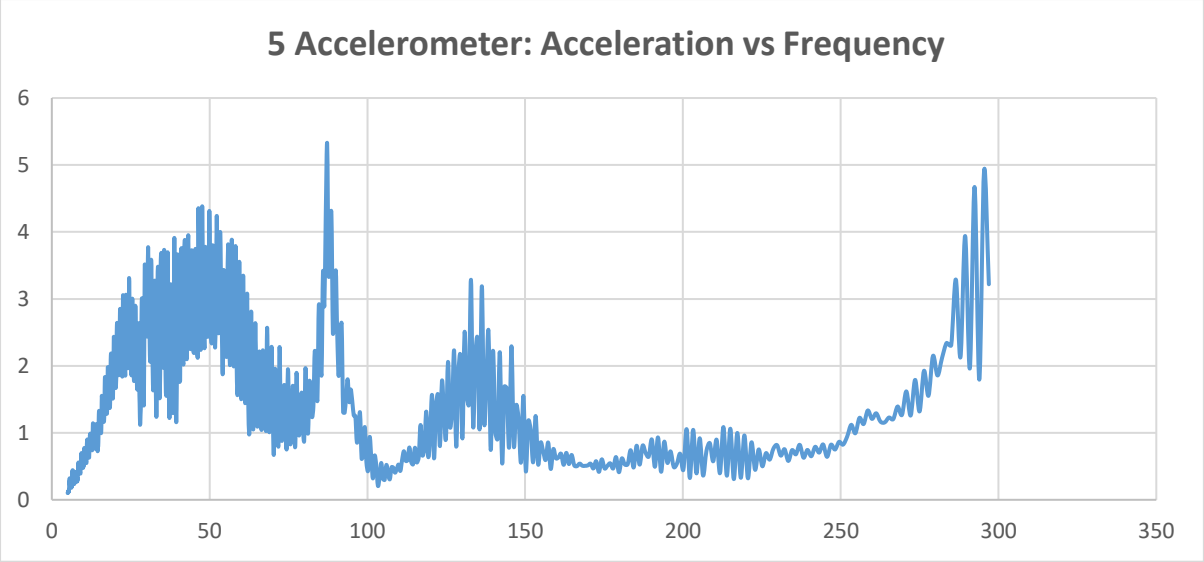

Figure 6. 31: Acceleration (m/s-2) vs Frequency, channel 5, 54 kN (Test1)

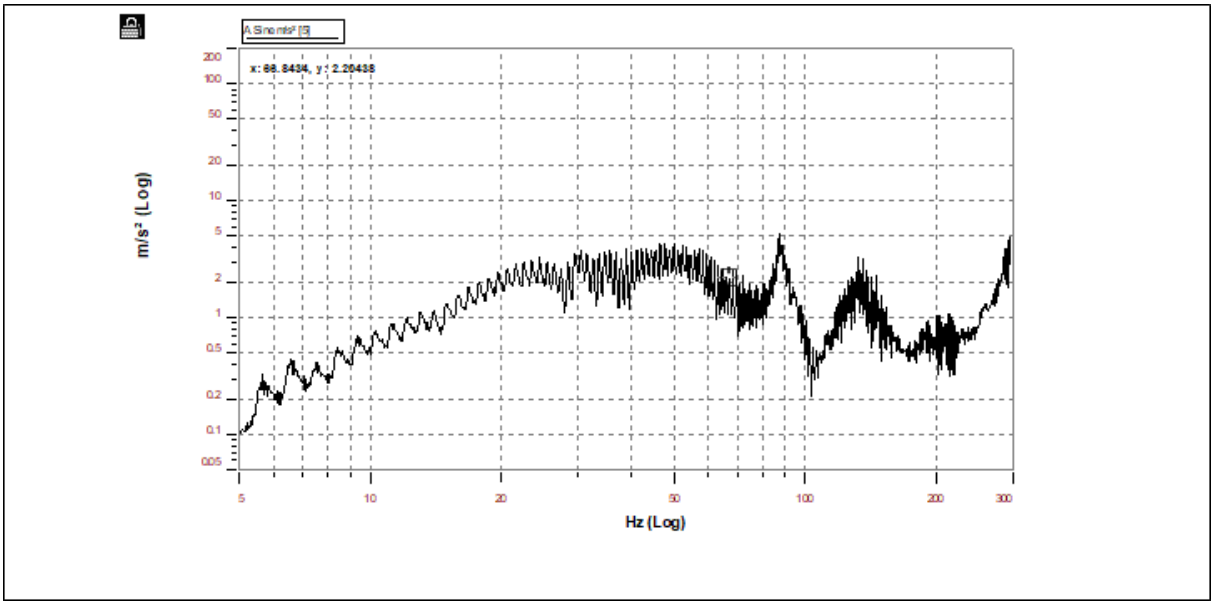

Figure 6. 32: Acceleration (m/s-2) vs Frequency, channel 5, 54 kN (Test1) Spectral Viewer

6.3.5.1 Additional results for 1m span for conductor tension of 54 kN

The calculations above were repeated for other peaks in the graph presented in Figure 6.30. Table 6.11 shows the results of these calculations. It is seen in Table 6.11 that the damping factor, ζ, ranges from 0.005137 to 0.010301. Thus, for 47.153526 Hz, the maximum damping factor was 0.010301.

In calculations for other tests at the tension of 54 kN and on 1m span, slightly different damping factors were obtained. Further processing of these results suggests that for a conductor tension of 54 kN, the damping factor varies frequency, as indicated in Figure 6.30.

Table 6. 11: Data Collected in Figure 6.30.

Peak	X peak	x1 and x2	f1	f2	Fn	Change F	Q	Zeta
	Read on Graph	Xp/1.4142	Read on Graph x1	Read on Graph x2	Read on Graph Xpeak	F2-F1	Fn/(F2-F1)	1/2Q
1	4.38333	3.099512	47.662537	48.153526	47.662537	0.490989	97.0745516	0.010301
2	5.31212	3.756272	87.253471	87.701736	87.253471	0.448265	194.647075	0.005138
3	3.28632	2.323801	132.822403	133.504776	132.822403	0.682373	194.6478	0.005137
4	1.06204	0.750983	215.013443	216.118073	215.013443	1.10463	194.647477	0.005137

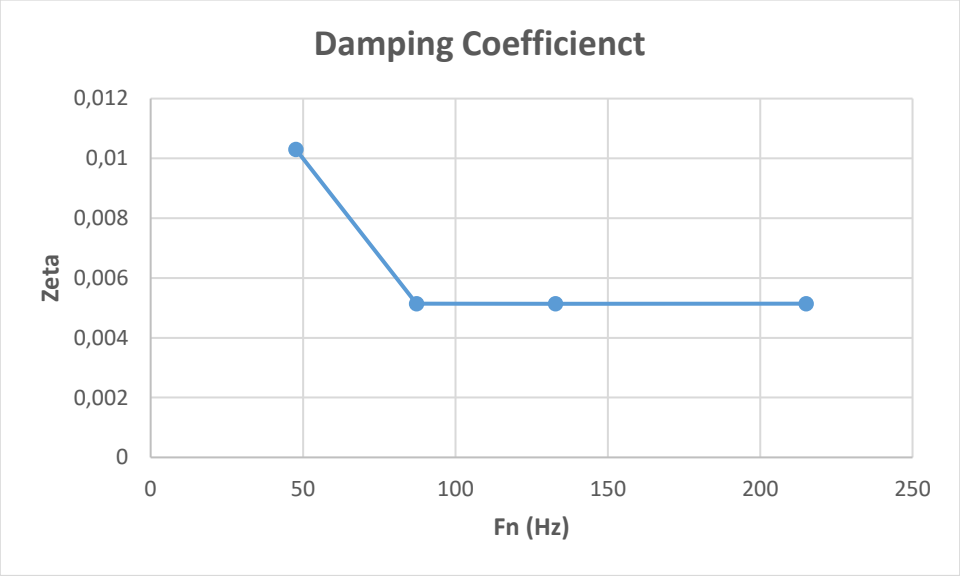

Figure 6. 33: Damping factor (Zeta) vs Fn (Hz)

6.4 Summary of the analysis of forced vibration results

6.4.1 ACSR Conductor

Table 6. 12: Forced Vibration ACSR Bersfort Results (Summary)

Tension (kN)	Damping Coefficient (Zeta)	Frequency (Fn) Hz	Table
36	0.020709	24.483074	6.10
	0.010301	58.206371	
	0.005137	91.841179	

	0.005137	132.822403	
45	0.011594	31.803459	**B8**
	0.00578	115.657883	
	0.00578	244.670715	
54	0.010301361	47.662537	**6.11**
	0.005137503	87.253471	
	0.005137484	132.822403	
	0.005137493	215.013443	

6.4.2 Tern Conductor.

Table 6. 13: Force Vibration Tern Results (Summary)

Tension (kN)	**Damping Coefficient (Zeta)**	**Frequency (Fn) Hz**	**Table**
39	0.030682	35.48811	**A7**
	0.002344	77.409256	
	0.006141	88.66082	
	0.002697	134.574463	
39	0.027865	26.051313	**A8**
	0.006143	59.080097	
	0.004767	76.138924	
	0.002961	122.596992	

6.4.3 Summary

The results for both conductors above demonstrated that the value of the damping coefficient depended on the top recurrence rate. The peaks at the beginning were usually smaller and had a higher damping coefficient, while the greater peaks had smaller damping coefficients.

CHAPTER 7
ANALYSIS OF FREE VIBRATION RESULTS

7.1 Introduction

Chapter 7 presents the analyses of the results obtained during the free vibration tests for ACSR Bersfort and Tern conductors. The objective of the analysis is to obtain self-damping characteristics of these two conductors.

7.2 Analysis of free vibration results for the Tern Conductor

The conductor tension impacted the characteristics of the conductor (the foremost prevailing resonance frequencies, bandwidth, quality factor, Q and the damping factor) as identified through varying conductor tension from 26 kN, 33 kN up to 39 kN which were 20% UTS, 25% UTS and 30% UTS.

The results of the free vibration on Tern, tension 26 kN, accelerometer on mode 1 were represented on the channel 0 diagram and analysed on the appendix. Different results for all tensions with compared channels showed up in Appendix II and a huge number of results were chosen upon to represent sensible factual information, including further magnified results stored in the National Instrument Desk.

7.2.1 Calculations arising from free vibrations captures by accelerometer 0, mode 1 for Tern conductor with a tension of 26 kN

Figure 7.1 presents the graph of acceleration (m/s^2) versus time (seconds) for all accelerometers in a Tern conductor test 1 experiment. Figure 7.2 shows the same results focusing on accelerometer 0, mode 1 located 2m away from the tension side. The graph was drawn to scale for analysis purposes.

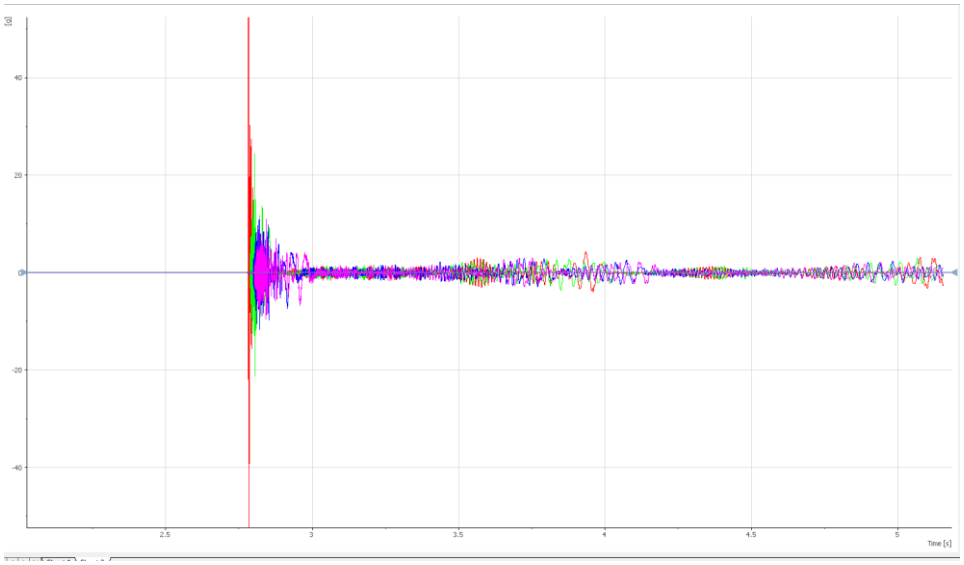

Figure 7. 1: Free Vibration, Accelerometer (all), 26 kN (Test1) National Instrument Desk

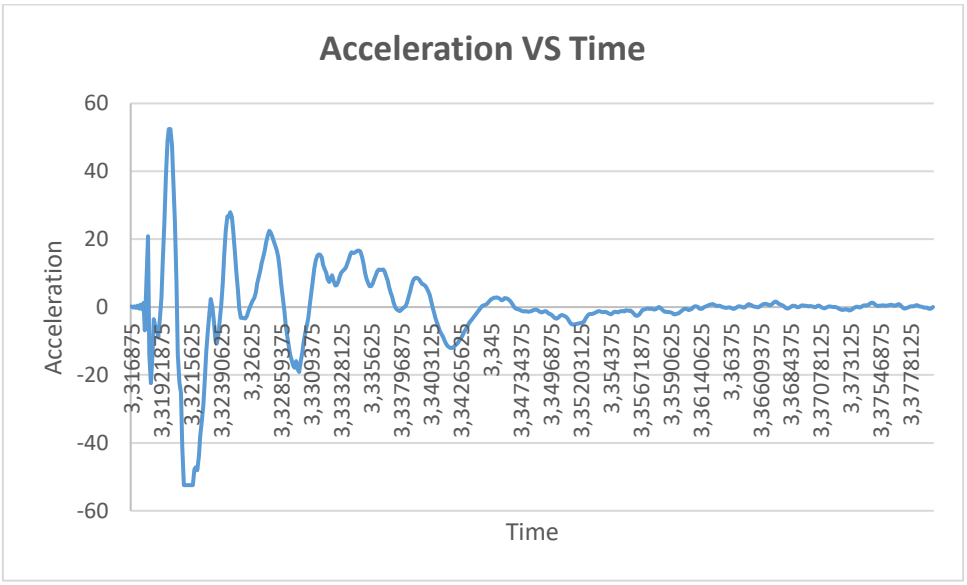

Figure 7. 2: Free Vibration, Accelerometer 0, Mode 1, 26 kN (Test 1)

The results in Table 7.1 below were calculated using results obtained from Figure 7.2 and were as follow:

The first row of in Table 7.1 below displayed the calculated results. Px was the time (ms) and Py was acceleration (m/s^-2) where both values were used to calculate the information of Table 7.1. The first loop was the least-square method, the log decrement was 1.5, the damping factor was 0.232, and the natural frequency identified as 1758.026 rad/s.

Table 7. 1: Calculated Data Collected on Figure 7.2

Px	Py	Period	Freq	In Py	Yj	In Py (Yj)	Yj^2	Zj	Log Dec	Zeta	Nat Freq	Nat Freq
s	m/s^2	s	Hz								rad/s	Hz
3,324609	27,9781386	0	0	3,331423	0	0	0	1,532727	1,5	0,232	1758,026	279,7985
3,327773	21,99133692	0,003164	316,0497	3,090649	1	3,090649	1	0,032727				
3,331758	14,52843409	0,003984	250,9802	2,676108	2	5,352215	4	-1,46727				
Sum	64,49790961			9,09818	3	12,09818	5					

Figure 7.3 to 7.6 in the X-value expanded and in the Y-value was diminished.

This means:

- The value of Xh was diminished as the time (Px) increased which subsequently implied Xh that was inversely proportional to the time (Px).

- The value of acceleration (Py) was decreased as the time (Px) increased which meant Py was inversely proportional to the time (Px).

The value of Acceleration (In Py) decreased as the time (Px) increased which meant In Py was inversely proportional to the time (Px).

The value of Zj decreased as the time (Px) increased which meant that Zj was inversely proportional to the time (Px).

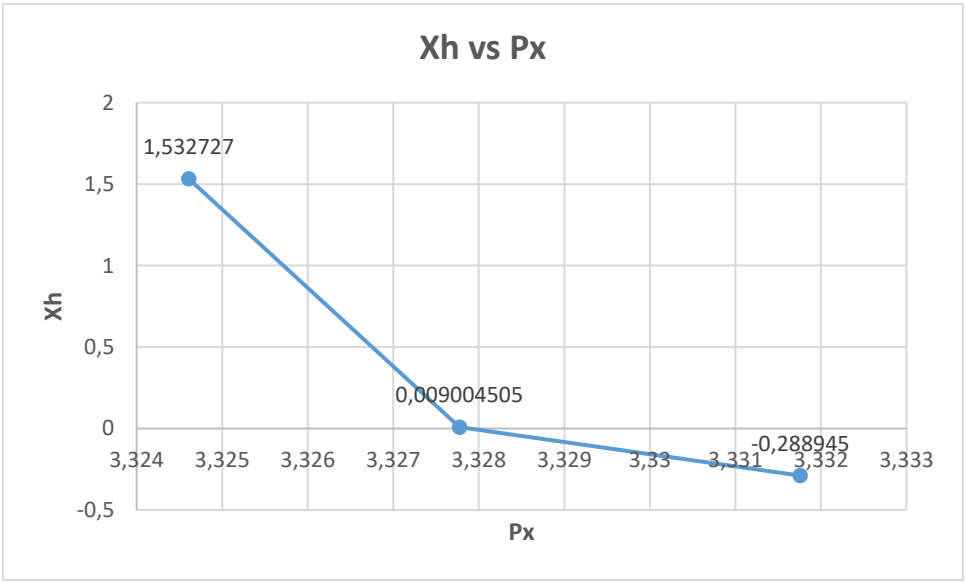

Figure 7. 3: (Xh) vs (Px)

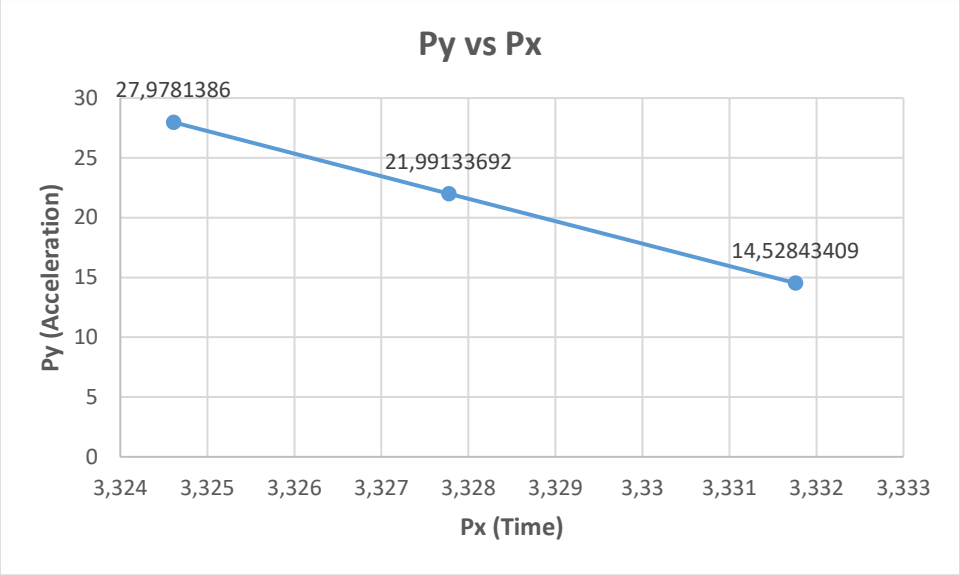

Figure 7. 4: (Py) vs (Px)

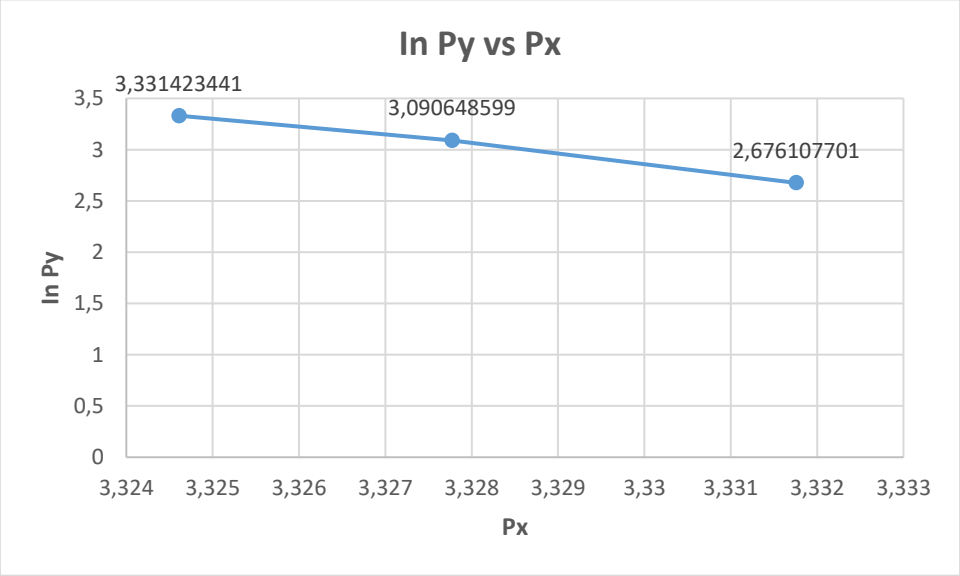

Figure 7. 5: (InPy) vs (Px)

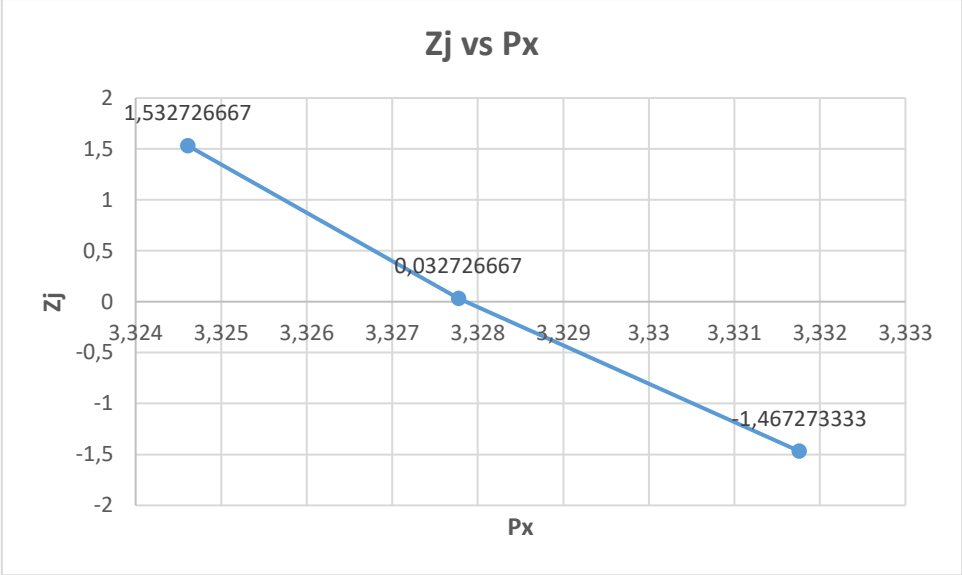

Figure 7. 6: (Zj) vs (Px)

7.2.1.2 Figure 7.7 presents the graph of acceleration (m/s^2) versus time (seconds) for accelerometer allocated at 1/8 span (10.575m) , away from the tension side in a Tern conductor tension. Figure 7.7 shows results from the National Instrument Desk program, while Figure 7.8 shows the same results on a non-logarithmic scale as such results were found more amenable to analysis.

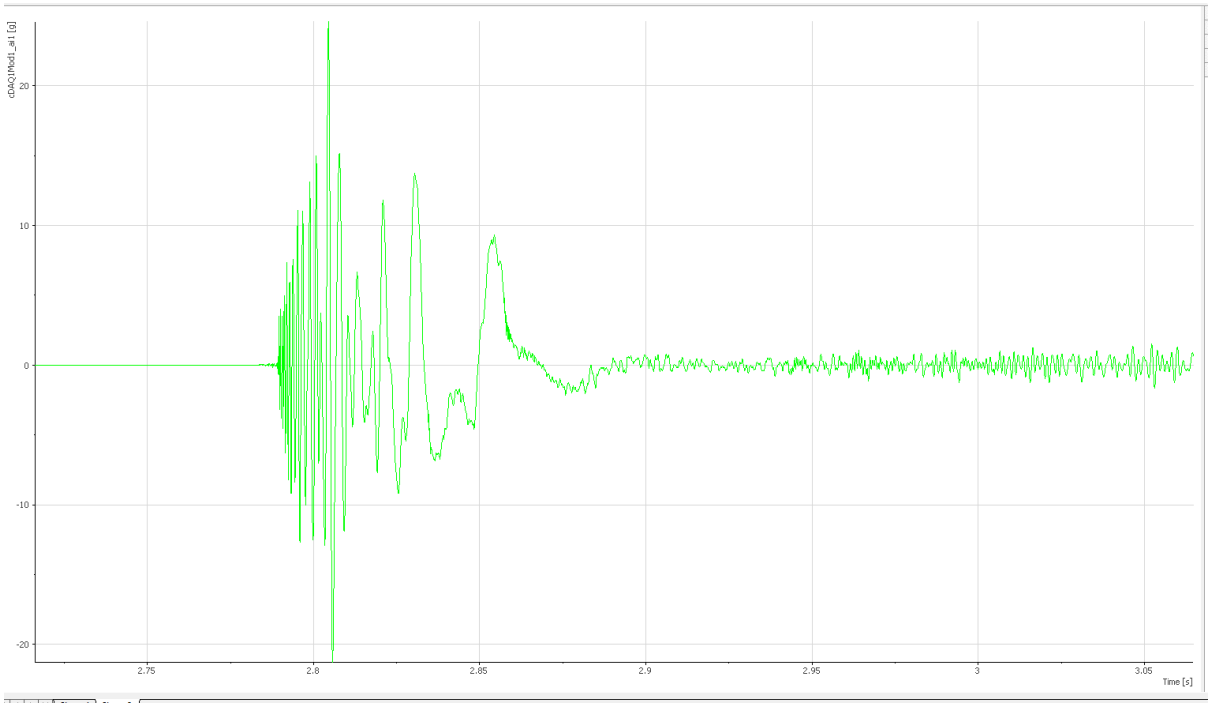

Figure 7. 7: Free Vibration, Accelerometer (1) Mode 1, 26 kN (Test1) National Instrument Desk

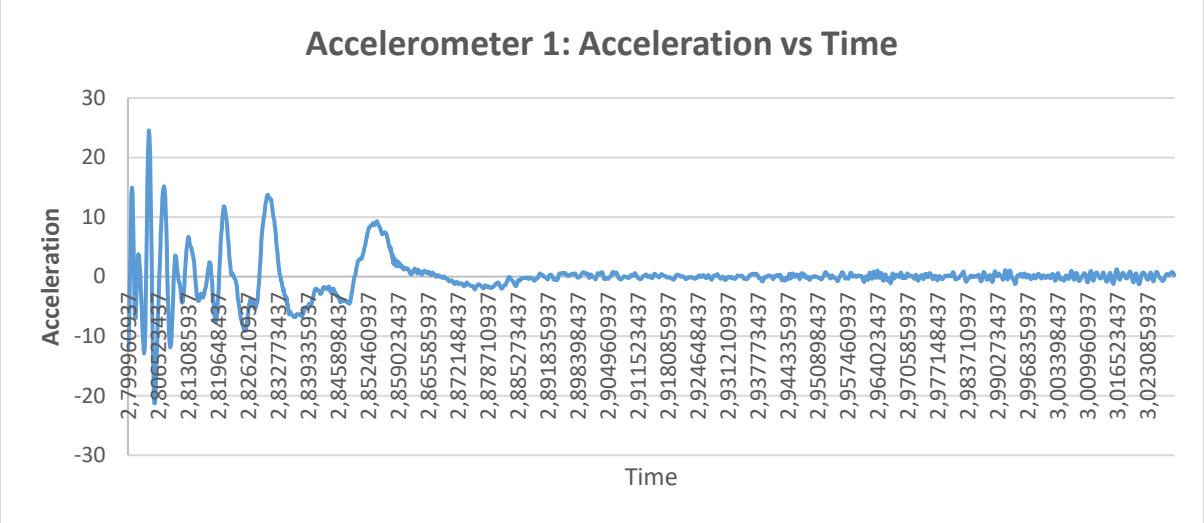

Figure 7. 8: Free Vibration, Accelerometer 1, 26 kN (Test 1)

The results in Table 7.2 below were calculated using results obtained from Figure 7.8 and were as follow:

The first row in Table 7.2 below displayed the calculated results. Px was the time (ms) and Py was the acceleration (m/s^-2) where both values were used to calculate the information of Table 7.2. The first loop used the least-squares method, the log decrement was 1.49999, the damping factor was 0.236, and the natural frequency was identified as 133.5995 rad/s.

Table 7. 2: Calculated Data Collected in Figure 7.8

Px s	Py m/s^2	Period s	Freq Hz	ln Py	Yj	ln Py (Yj)	Yj^2	Zj	Log Dec	Zeta	Nat Freq rad/s	Nat Freq Hz
2.804531	24.57095734	0	0	3.201565	0	0	0	0.853212	1.499999	0.236	133.5995	21.26302
2.80793	14.60791057	0.003398	294.2529	2.681563	1	2.681563	1	-0.64679				
2.898592	3.243014675	0.090662	11.02995	1.176503	2	2.353007	4	-2.14679				
Sum	42.42188259			7.059632	3	10.05963	5					

- Figure 7.9 to 7.10 in the X-value expanded and the Y-value diminished.
  This means:
- The value of Xh diminished as the time (Px) increased which subsequently implied Xh was inversely corresponding to the time (Px).
- The value of acceleration (Py) decreased as the time (Px) increased which meant Py was inversely proportional to the time (Px).
- The value of Acceleration (In Py) decreased as the time (Px) increased which meant In Py was inversely proportional to the time (Px).

- (Figures 7.9-7.12) obtained from the different results of the Tern conductor where the cable tension of 26 kN appeared to be a similar shape. The value of Zj decreased as the time (Px) increased which meant Zj was inversely proportional to the time (Px).

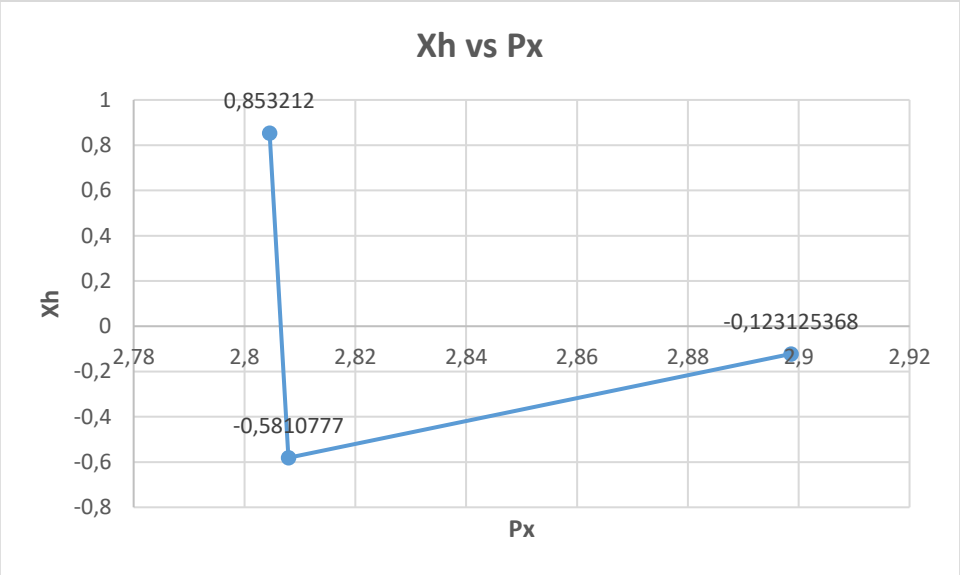

Figure 7. 9: (Xh) vs (Px)

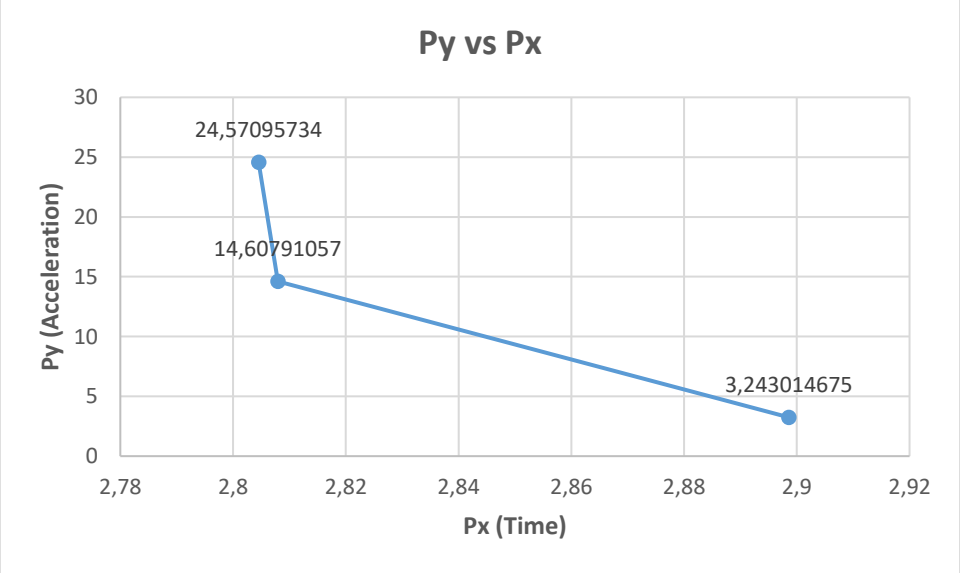

Figure 7. 10:(Py) vs (Px)

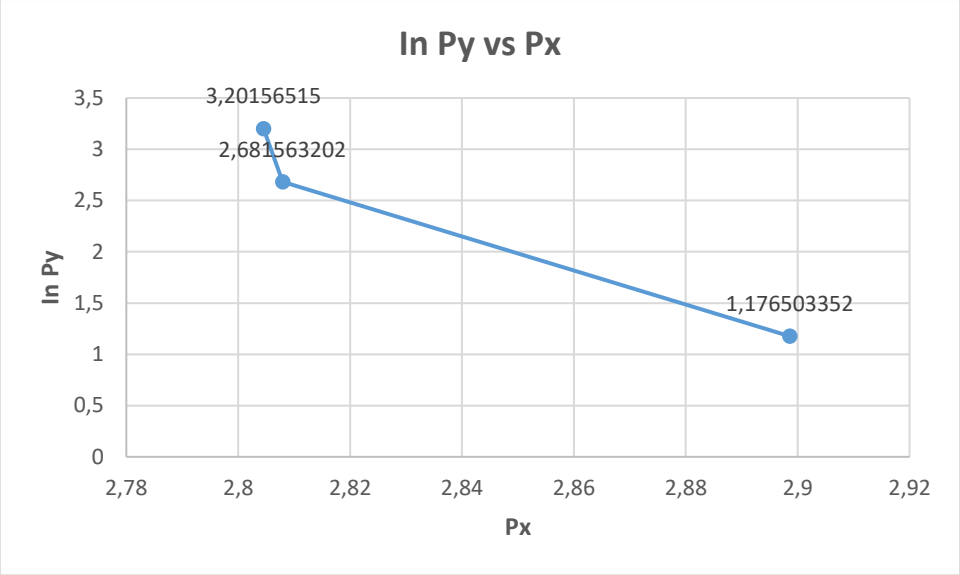

Figure 7. 11: (InPy) vs (Px)

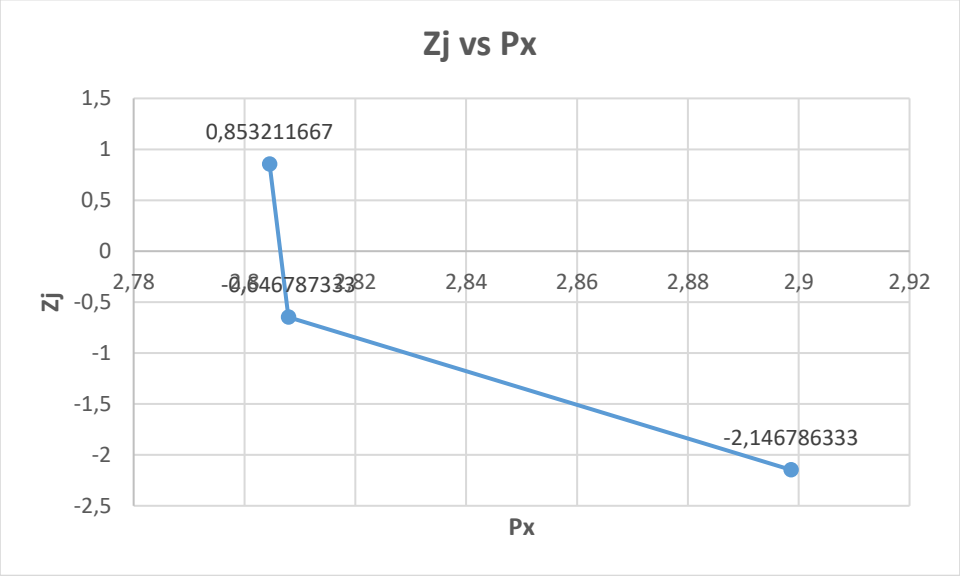

Figure 7. 12:(Zj) vs (Px)

7.2.1.3 Figures 7.11-7.12 presents the graph of acceleration (m/s^2) versus time (seconds) for accelerometer allocated at 1/4 span (21.15 m) , away from the tension side in a Tern conductor tension. Figure 7.13 shows results from the National Instrument Desk program, while Figure 7.12 shows the same results on a non-logarithmic scale as such results were found more amenable to analysis.

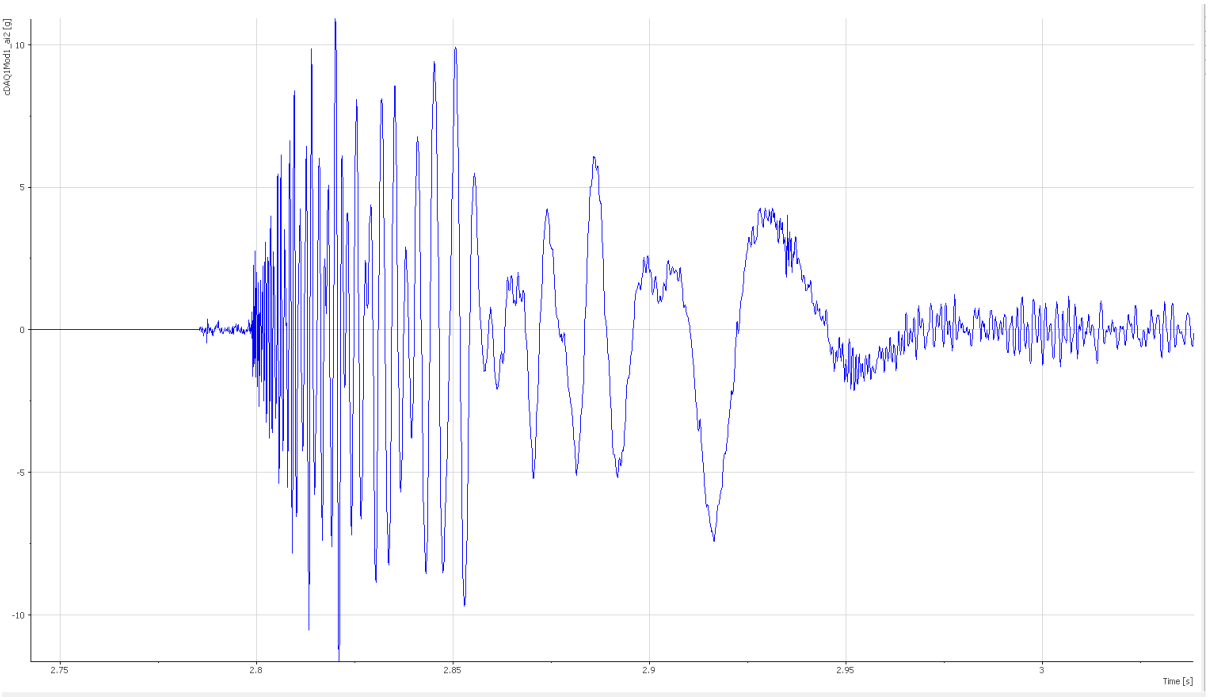

Figure 7. 13: Free Vibration, Accelerometer (2) Mode 1, 26 kN (Test1) National Instrument Desk

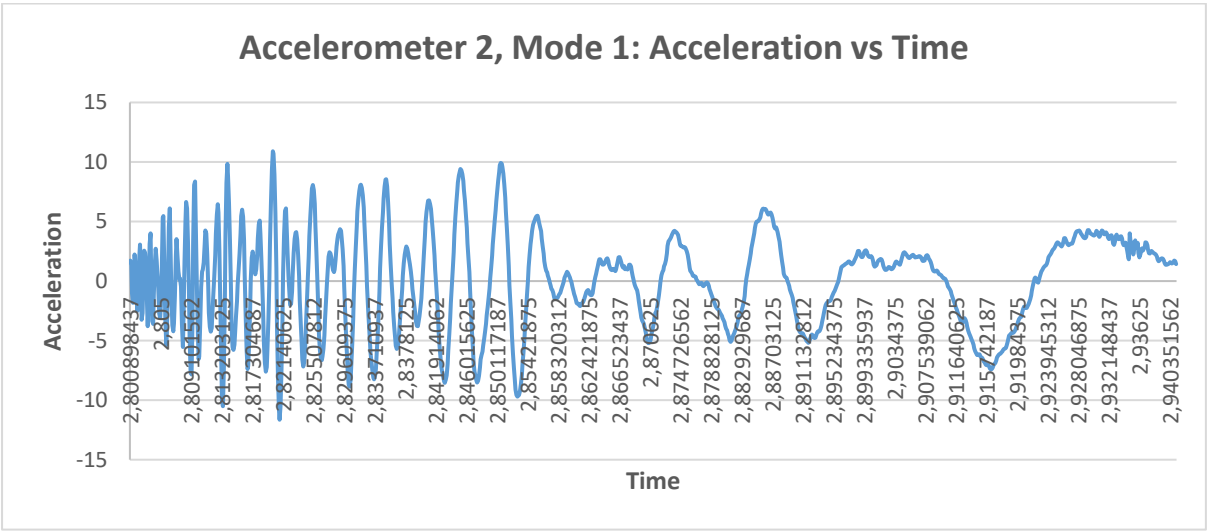

Figure 7. 14: Free Vibration, Accelerometer 2, Mode 1, 26 kN (Test 1)

The results in Table 7.3 below were calculated using results obtained from Figure 7.14 and were as follow:

The first row in Table 7.3 below displayed the calculated results. Px was the time (ms) and Py was the acceleration (m/s^-2) where both values were used to calculate the information of Table 7.3. The first loop used the least-squares method, the log decrement was 1.5, the damping factor was 0.232, and the natural frequency was identified as 3154.209 rad/s.

Table 7. 3 : Calculated Data Collected in Figure 7.14

Px s	Py m/s^2	Period s	Freq Hz	In Py	Yj	In Py (Yj)	Yj^2	Zj	Log Dec	Zeta	Nat Freq rad/s	Nat Freq Hz
2.813906	9.852180303	0	0	2.287693	0	0	0	0.066784	1.5	0.232	3154.209	500.5005
2.816016	5.39506308	0.002109	474.0741	1.685484	1	1.685484	1	-1.43322				
2.817891	2.069228745	0.001875	533.3333	0.727176	2	1.454352	4	-2.93322				
Sum	**17.31647213**			**4.700353**	**3**	**7.700353**	**5**					

- Figures 7.15 to 7.17 in the X-value expanded and the Y-value diminished.

  This means:

- The value of Xh diminished as the time (Px) increased which subsequently implied Xh was inversely corresponding to the time (Px).
- The value of the acceleration (Py) decreased as the time (Px) increased which meant Py was inversely proportional to the time (Px).
- The value of Acceleration (In Py) decreased as the time (Px) increased which meant In Py was inversely proportional to the time (Px).
- Figures 7.15-7.18 obtained from the different results of the Tern conductor where the cable tension of 26 kN appeared to be a similar shape. The value of Zj decreased the time (Px) increased which therefore means Zj is inversely proportional to the time (Px).

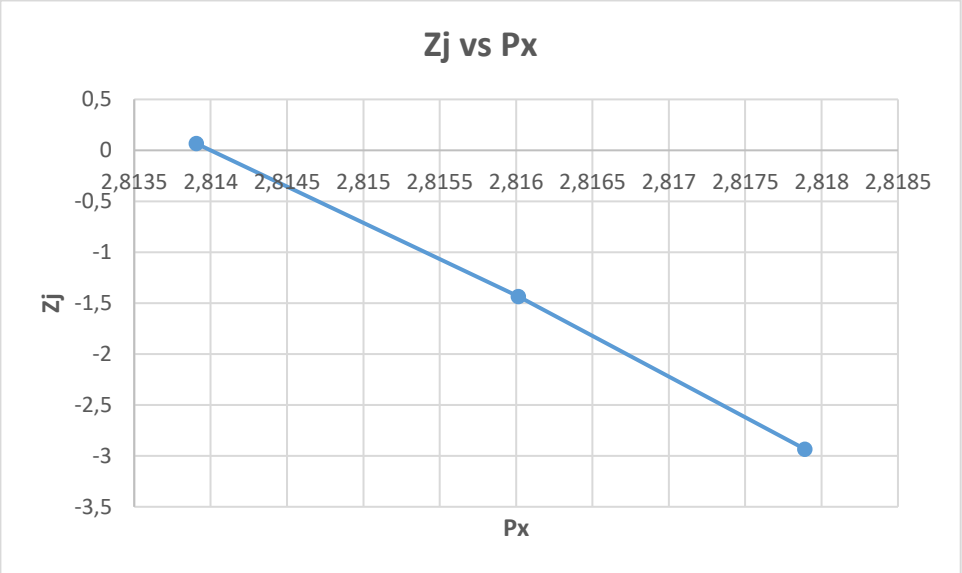

Figure 7. 15: (Zj) vs (Px)

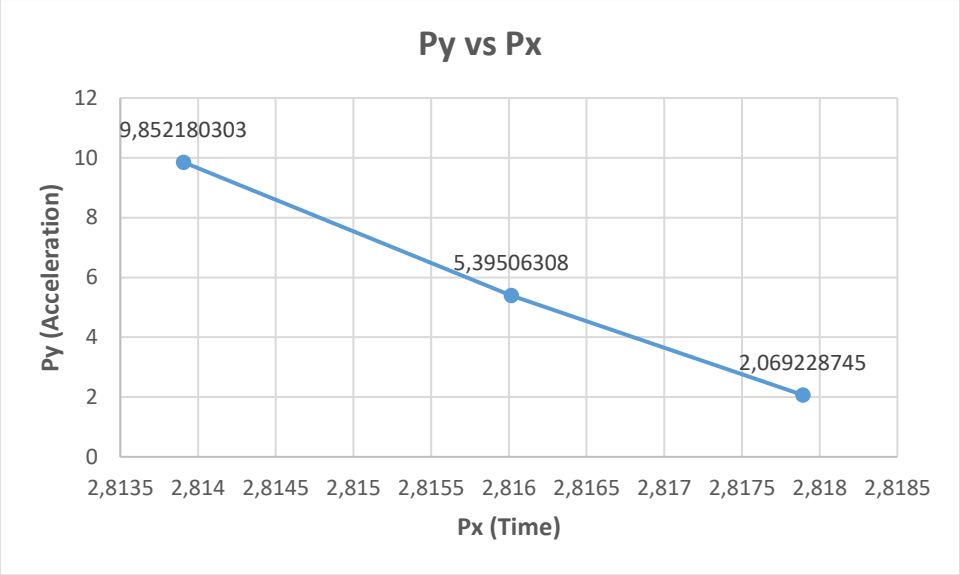

Figure 7. 16: (Py) vs (Px)

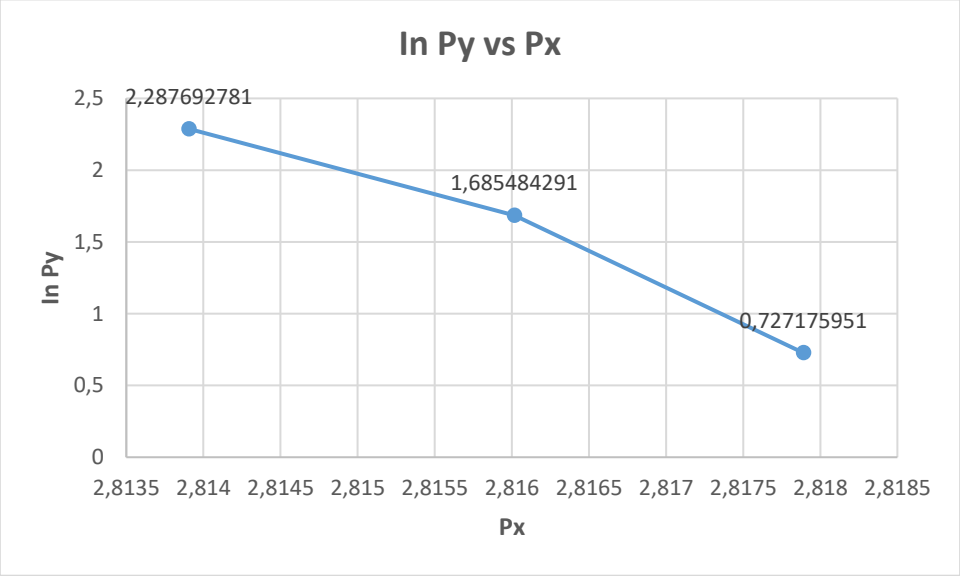

Figure 7. 17: (InPy) vs (Px)

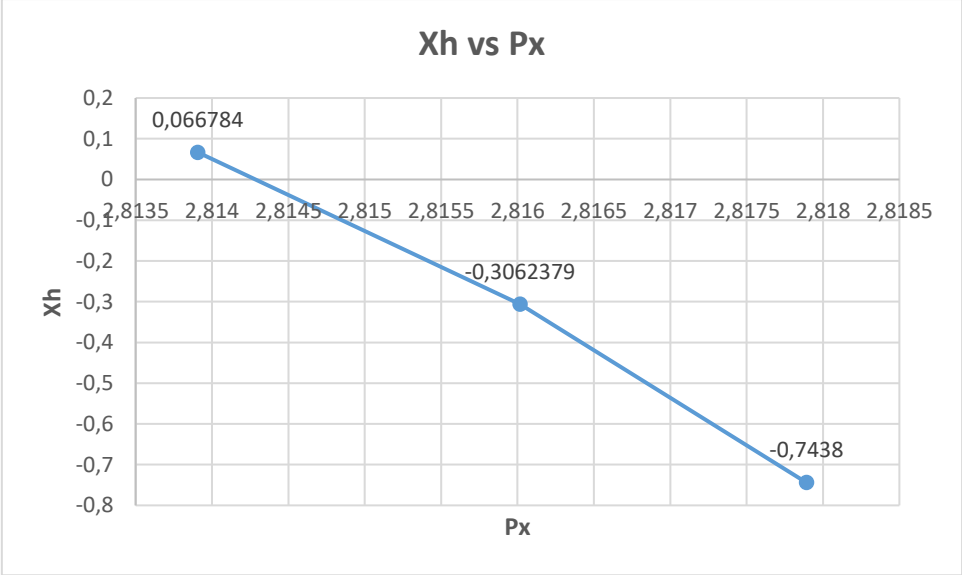

Figure 7. 18: (Xh) vs (Px)

7.2.1.4 Figures 7.19-7.20 presents the graph of acceleration (m/s^2) versus time (seconds) for accelerometer allocated at 1/3 span (28.2 m) , away from the tension side in a Tern conductor tension. Figure 7.19 shows results from the National Instrument Desk program, while Figure 7.20 shows the same results on a non-logarithmic scale as such results were found more amenable to analysis.

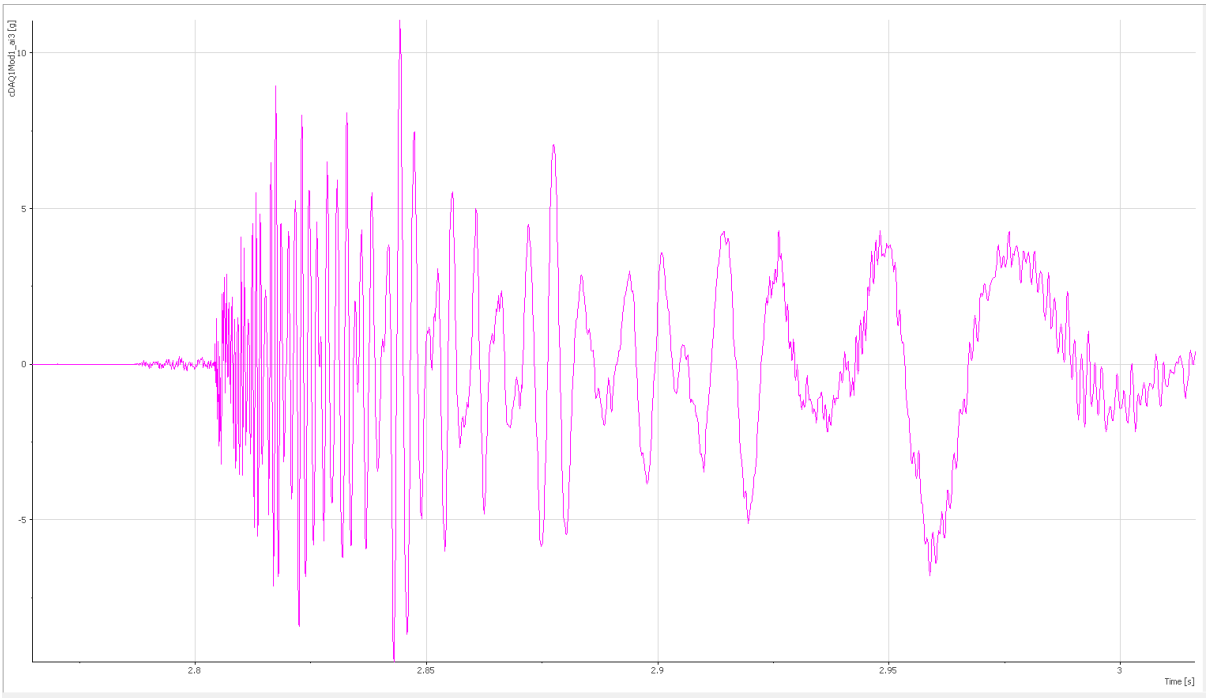

Figure 7. 19: Free Vibration, Accelerometer (3) Mode 1, 26 kN (Test1) National Instrument Desk

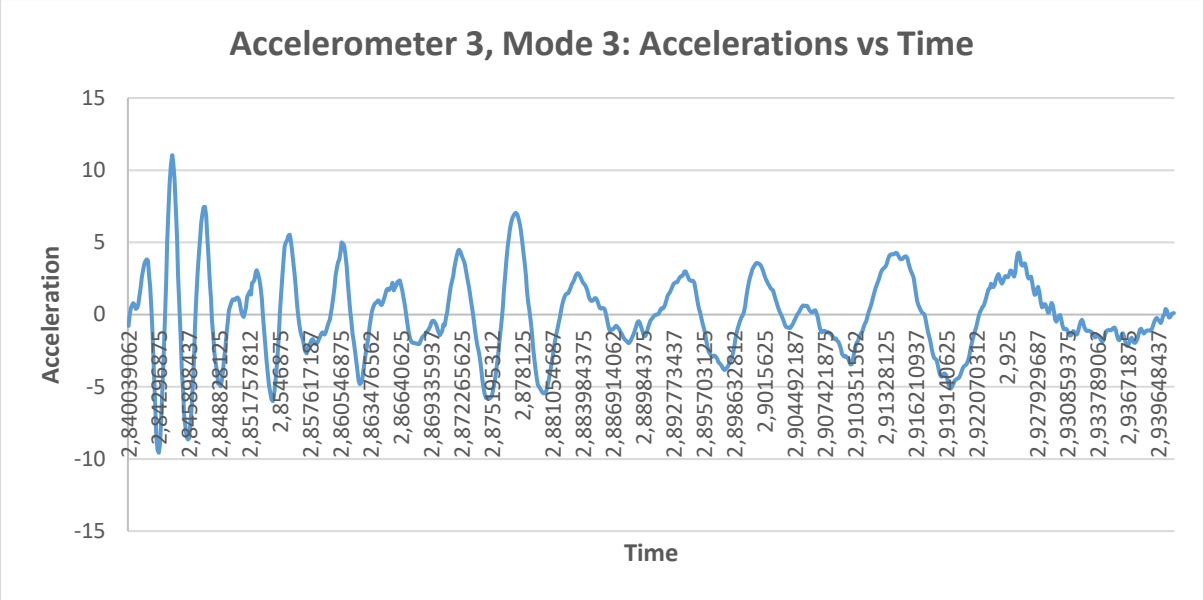

Figure 7. 20: Free Vibration, Accelerometer 3, Mode 1, 26 kN (Test 1)

The results in Table 7.4 below were calculated using results obtained from Figure 7.20 and were as follow:

The first row in Table 7.4 below displayed the calculated results. Px was the time (ms) and Py was the acceleration (m/s^-2) where both values were used to calculate the information of Table 7.4. The first loop was the least-squares method, the log decrement was 1.5, the damping factor was 0.232, and the natural frequency was identified as 1531.737 rad/s.

Table 7. 4: Calculated Data Collected in Figure 7.20

Px s	Py m/s^2	Period s	Freq Hz	ln Py	Yj	ln Py (Yj)	Yj^2	Zj	Log Dec	Zeta	Nat Freq rad/s	Nat Freq Hz	xh
2.844258	11.04374532	0	0	2.401864	0	0	0	0.344523	1.5	0.232	1531.737	243.8132	0.344523
2.847422	7.453829036	0.003164	316.0493	2.008728	1	2.008728	1	-1.15548					-0.5050885
2.852461	3.073989715	0.005039	198.4496	1.122976	2	2.245953	4	-2.65548					-0.39110428
Sum	**21.57156407**			**5.533568**	**3**	**8.533568**	**5**						

Figures 7.21 to 7.23 in the X-value expanded and in the Y-value diminished.

This therefore means:

- The value of Xh was diminished as the time (Px) increased which subsequently implied that Xh was inversely corresponding to the time (Px).

- The value of acceleration (Py) decreased as the time (Px) increases which meant Py was inversely proportional to the time (Px).
- The value of the acceleration (In Py) decreased as the time (Px) increased which meant In Py was inversely proportional to the time (Px).
- Figures 7.21-7.24 obtained from the different results of the Tern conductor and the cable tension of 26 kN appeared to be a similar shape. The value of Zj decreased as the time (Px) increased which meant Zj was inversely proportional to the time (Px).

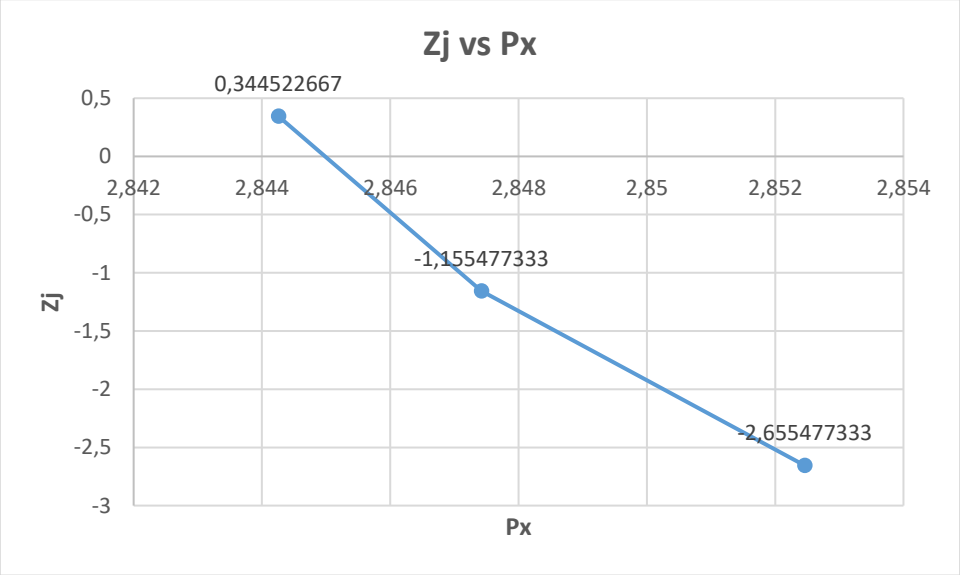

Figure 7. 21: (Zj) vs (Px)

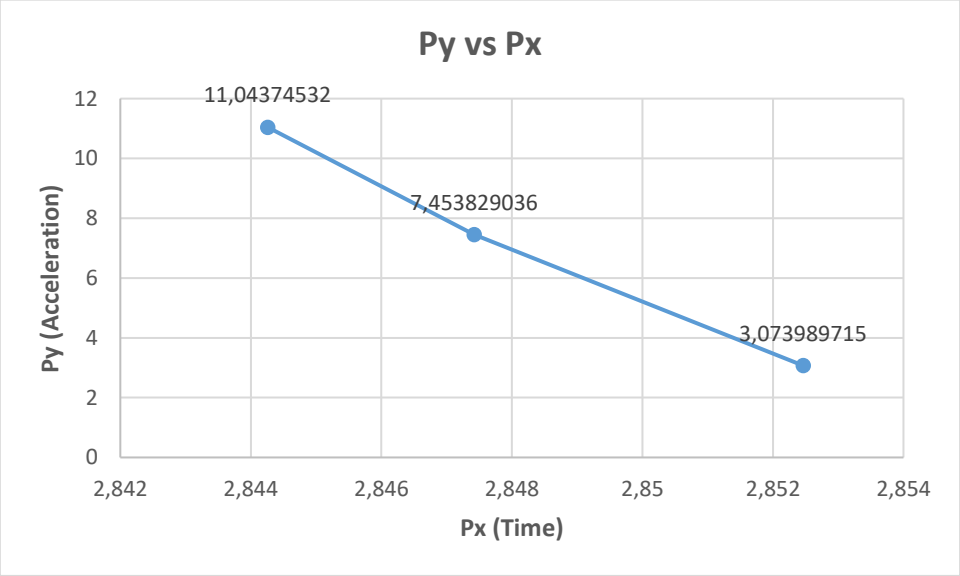

Figure 7. 22:(Py) vs (Px)

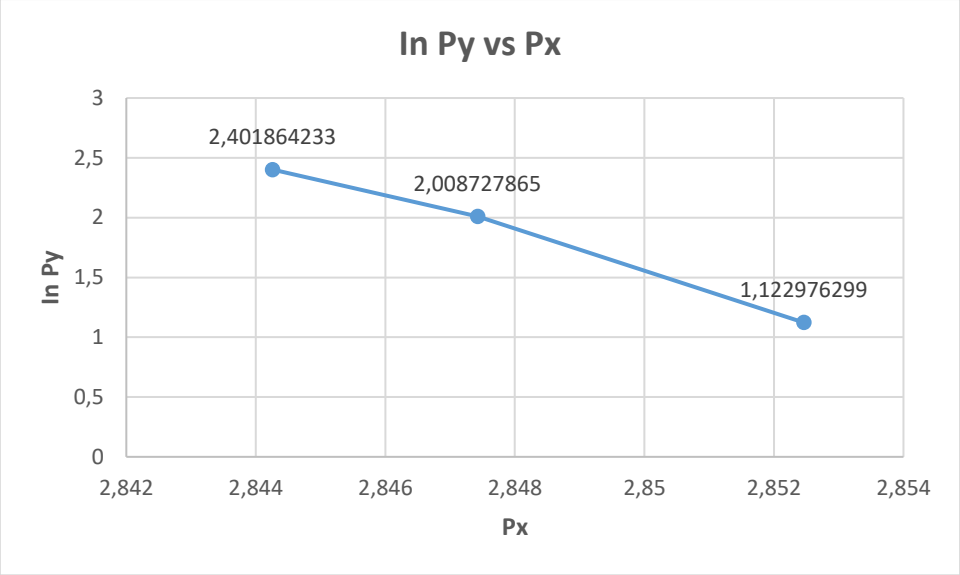

Figure 7. 23:(InPy) vs (Px)

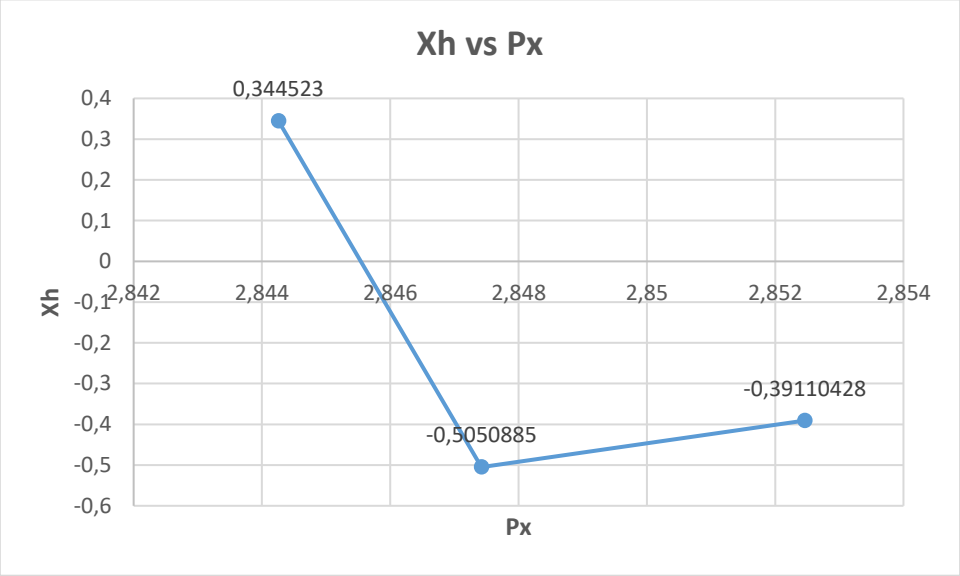

Figure 7. 24: (Xh) vs (Px)

7.2.1.5 Figures 7.25-7.26 presents the graph of acceleration (m/s^2) versus time (seconds) for accelerometer allocated at ½ span (42.3 m) , away from the tension side in a Tern conductor tension. Figure 7.25 shows results from the National Instrument Desk program, while Figure 7.26 shows the same results on a non-logarithmic scale as such results were found more amenable to analysis

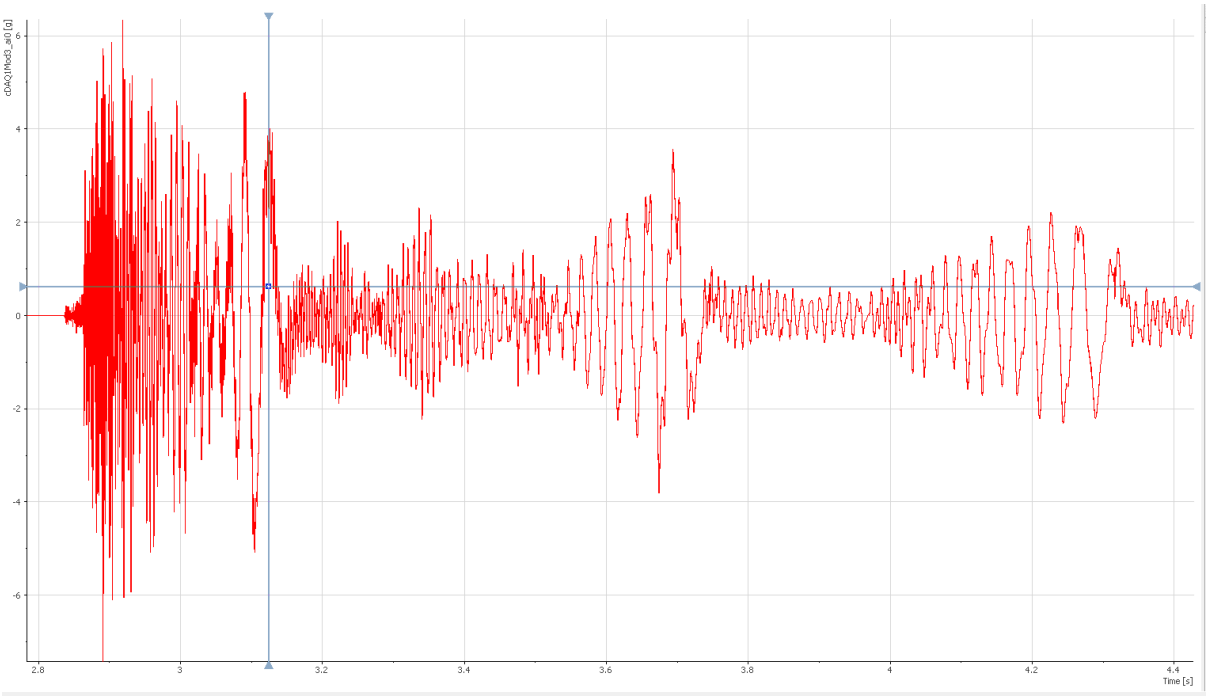

Figure 7. 25: Free Vibration, Accelerometer (0) Mode 3, 26 kN (Test1) National Instrument Desk

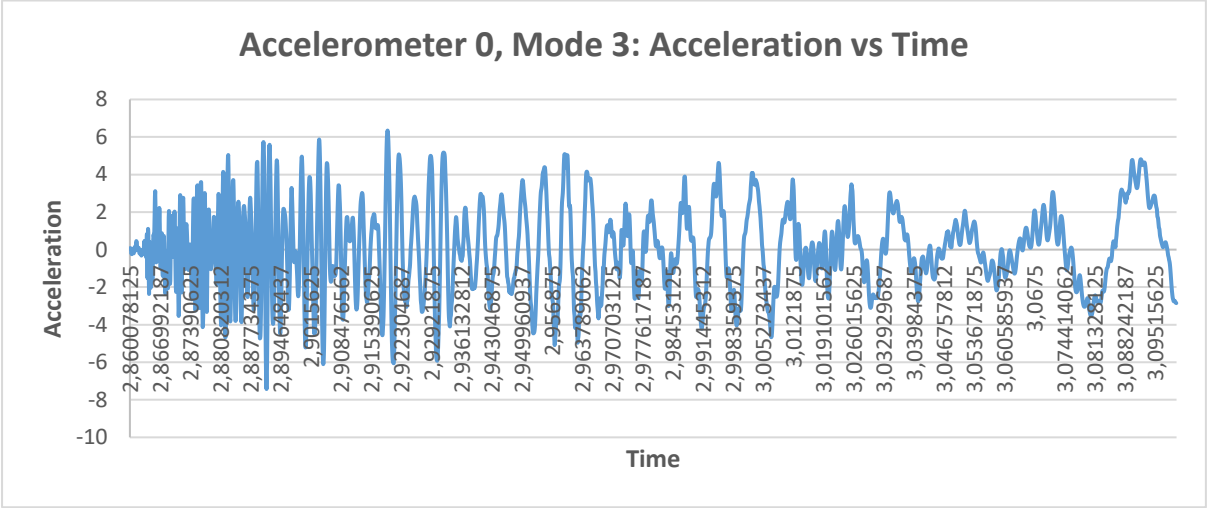

Figure 7. 26: Free Vibration, Accelerometer 0, Mode 3, 26 kN (Test 1)

The results in Table 7.5 below were calculated using results obtained from Figure 7.26 and were as follow:

The first row in Table 7.5 below display the calculated results. Px was the time (ms) and Py was the acceleration (m/s^-2) where both values were used to calculate the information of Table 7.5. The first loop used the least-squares method, the log decrement was 1.5, the damping factor was 0.232, and the natural frequency was identified as 1985.836 rad/s.

Table 7. 5: Calculated Data Collected on Figure 7.26.

Px s	Py m/s^2	Period s	Freq Hz	In Py	Yj	In Py (Yj)	Yj^2	Zj	Log Dec	Zeta	Nat Freq rad/s	Nat Freq Hz	xh
2.919141	6.343430247	0	0	1.84742	0	0	0	-0.00939	1.5	0.232	1985.836	316.0556	-9.39E-03
2.921719	5.074324817	0.002578	387.8788	1.624193	1	1.624193	1	-1.50937					-0.46023
2.925469	2.718701602	0.00375	266.6667	1.000154	2	2.000309	4	-3.00935					-0.53475
Sum	**14.13645667**			**4.471768**	**3**	**7.471768**	**5**						

Figures 7.27 to 7.29 appeared in the X-value expanded and in the Y-value diminished. This means:

- The value of Xh was diminised as the time (Px) increased which subsequently implied that Xh was inversely corresponding to the time (Px).
- The value of the acceleration (Py) decreased as the time (Px) increased which meant Py was inversely proportional to the time (Px).
- The value of acceleration (In Py) decreased as the time (Px) increased which meant In Py was inversely proportional to the time (Px).
- Figures 7.27-7.28 obtained from the different results of the Tern conductor and the cable tension of 26 kN appeared to be a similar shape. The value of Zj decreased as the time (Px) increased which meant Zj was inversely proportional to the time (Px).

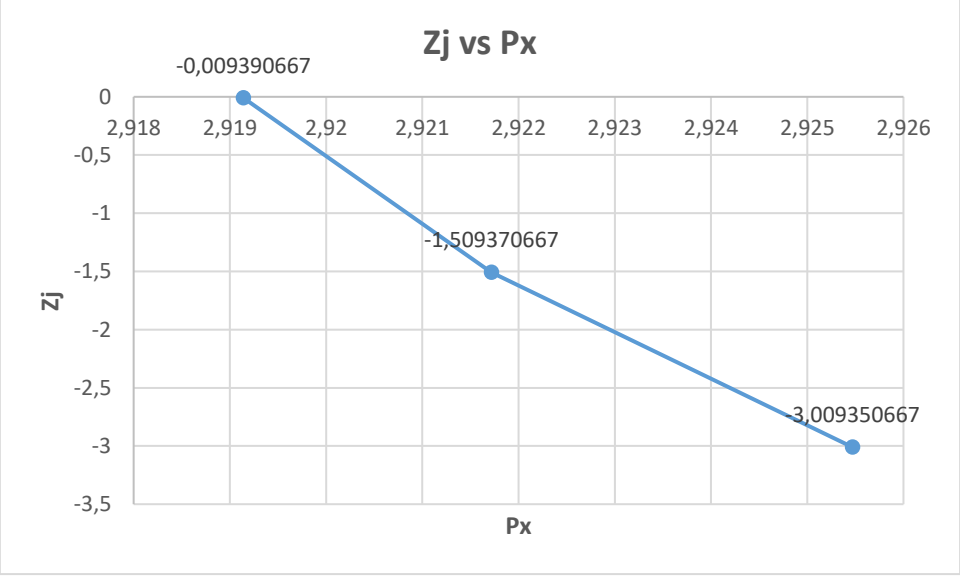

Figure 7. 27: (Zj) vs (Px)

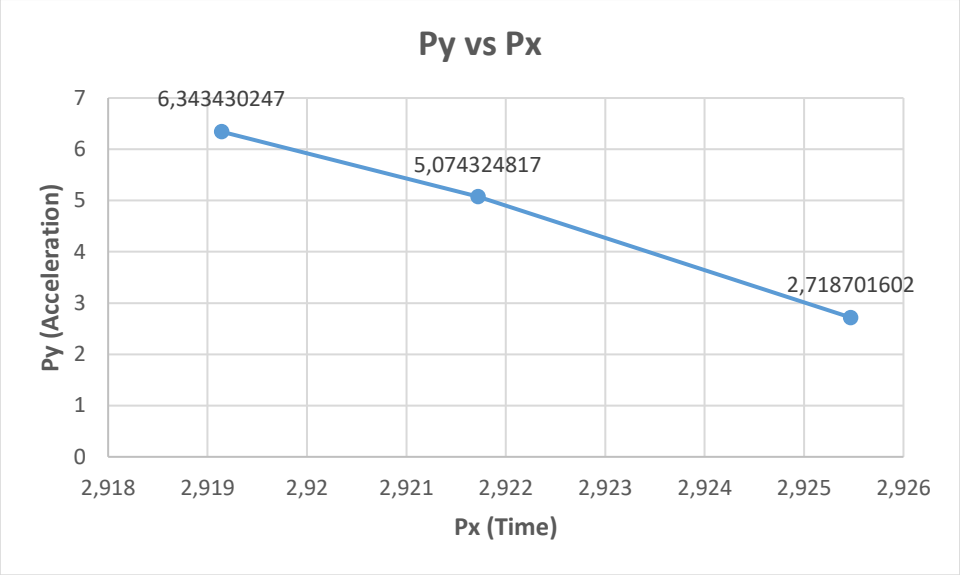

Figure 7. 28: (Py) vs (Px)

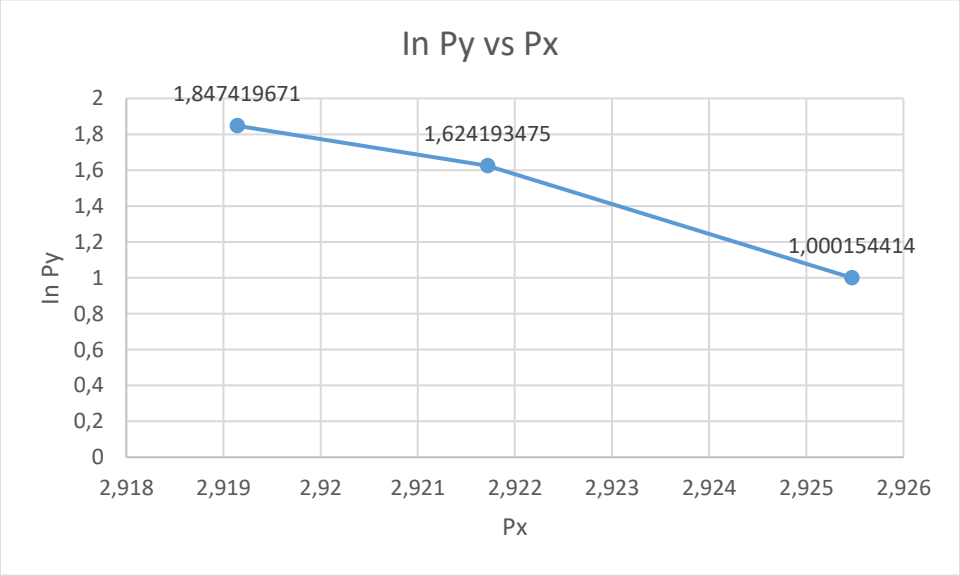

Figure 7. 29: (Py) vs (Px)

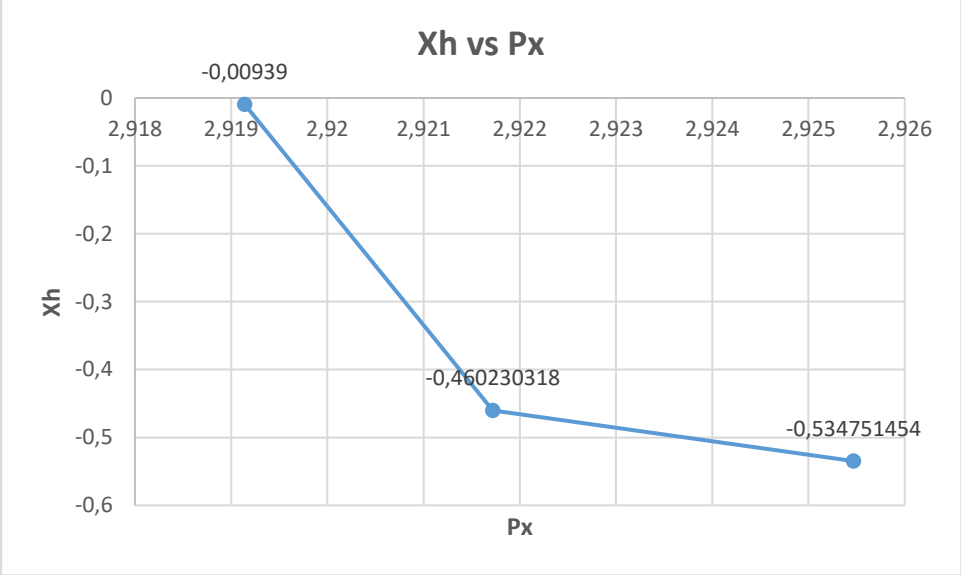

Figure 7. 30: (Py) vs (Px)

7.2.2 Analysis of free vibration results for the ACSR Bersfort Conductor

The ACSR Bersfort conductor's damping characteristics influence its resonance frequencies, bandwidth, quality factor, and damping factor. This section presents the analysis of results presented for conductor tensions of 36 kN, 45 kN and 54 kN.

7.2.2.1 Figures 7.31-7.32 presents the graph of acceleration (m/s^2) versus time (seconds) for accelerometer allocated at 1/8 span (10.575 m) PEAK 1 , away from the tension side in a ACSR Bersfort conductor tension. Figure 7.31 shows results from the National Instrument

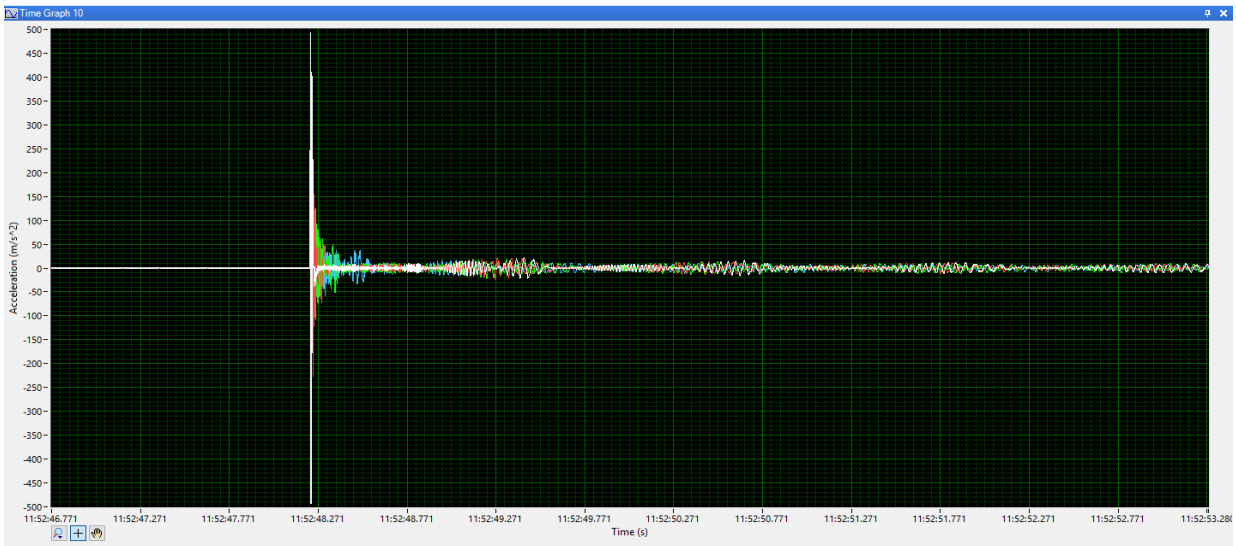

Figure 7. 31: Free Vibration, Accelerometer (all), 36 kN (Test2) National Instrument Desk

Desk program, while Figure 7.32 shows the same results on a non-logarithmic scale as such results were found more amenable to analysis.

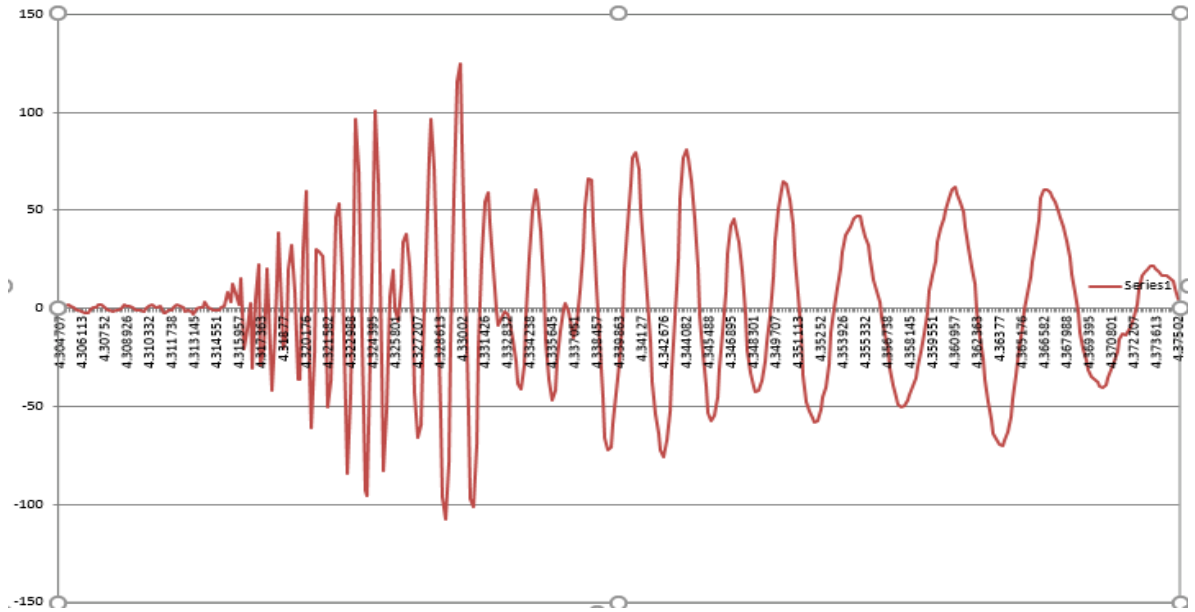

Figure 7. 32: Free Vibration, Accelerometer 2, 36 kN (Test 2)

The results in Table 7.6 were calculated using results from Figure 7.32 and indicated as follows:

The first row in Table 7.6 below displayed the calculated results. Px was the time (ms) and Py was the acceleration (m/s^-2), both values were used to calculate the information of Table 7.6. In the first loop, using the least-squares method, the log decrement was 1.5, the damping factor was 0.232, and the natural frequency identified was 71.4 rad/s.

Table 7. 6: Calculated Data Collected in Figure 7.32)

Px	Py	Period	Freq	ln Py	Yj	ln Py (Yj)	Yj^2	Zj	Log Dec	Zeta	Nat Freq	Nat Freq
ms	x10^-3 m/s^2	ms	Hz								rad/s	Hz
0	209.407	0	0	5.34428	0	0	0	3.377893	1.5	0.232	71.4	11.36
0.176	106.243	0.176	5.681818	4.665729	1	4.665729	1	1.877893				
0.352	101.867	0.176	5.681818	4.623668	2	9.247336	4	0.377893				
Sum	417.517			14.63368	3	17.63368	5					

Figures 7.33 to 7.35 in the X-value expanded and Y-value diminished. This means:

- The value of Xh diminished as the time (Px) increased which subsequently implied that Xh was inversely corresponding to the time (Px).

- The value of acceleration (Py) decreased as the time (Px) increased which therefore meant Py was inversely proportional to the time (Px).

The value of Acceleration (In Py) decreased as the time (Px) increased which meant that In Py was inversely proportional to the time (Px).

The value of Zj was decreased as the time (Px) increased which meant Zj was inversely proportional to the time (Px). The difference in Figure 7.33 to 7.35 and Figure 7.36 was the shape of the graph. Figure 7.33 to 7.35 were in hyperbolic shape and Figure 7.36 was a decreased straight line.

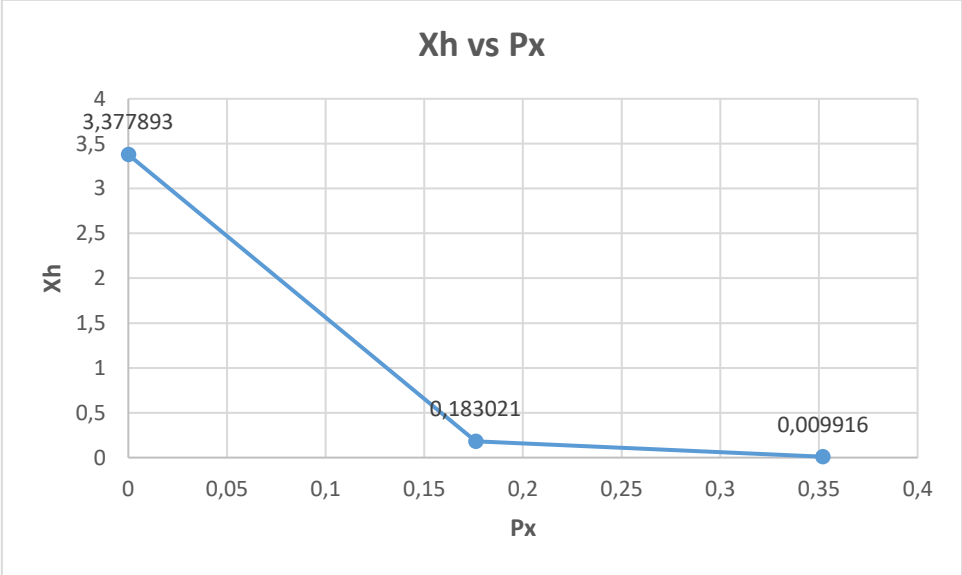

Figure 7. 33: (Xh) vs (Px)

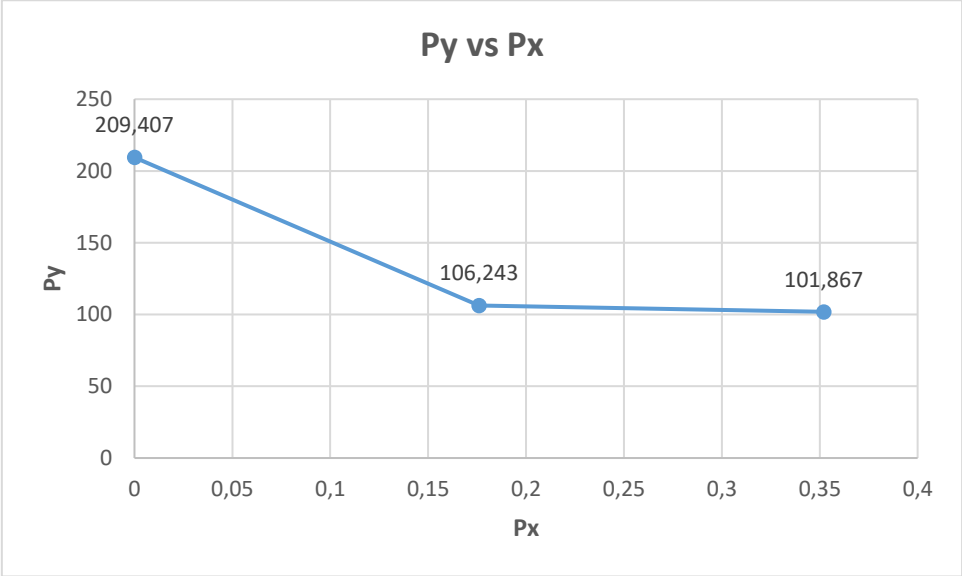

Figure 7. 34: (Py) vs (Px)

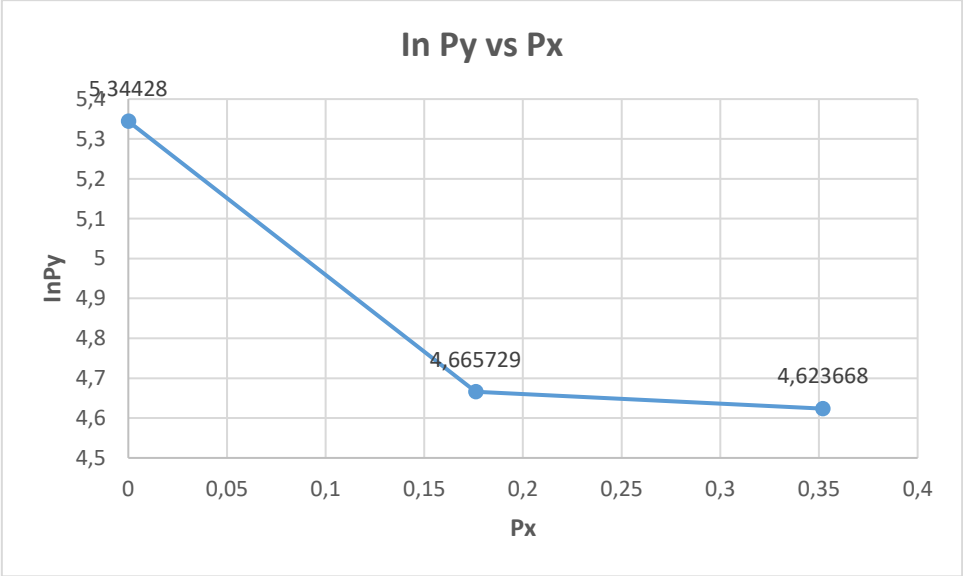

Figure 7. 35: (In Py) vs (Px)

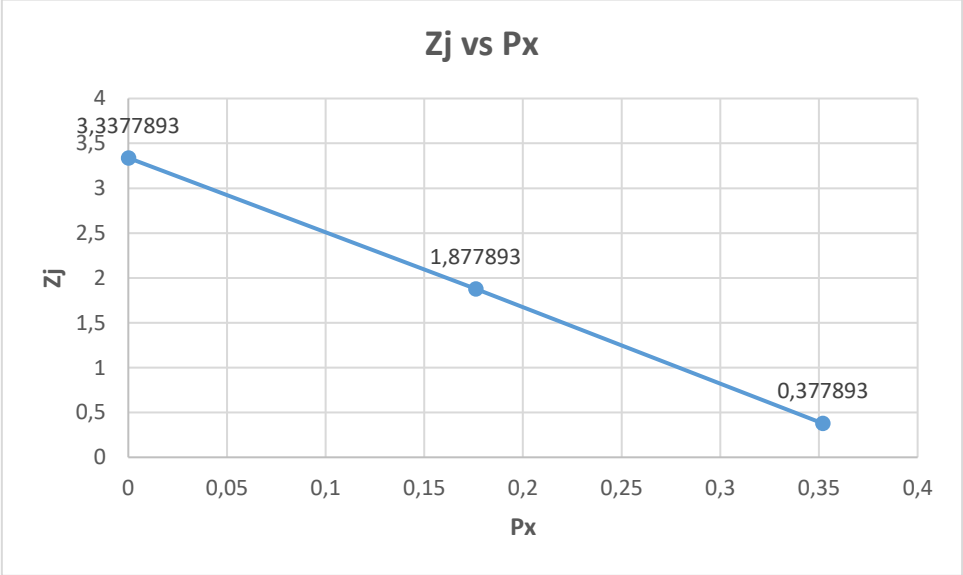

Figure 7. 36: (Zj) vs (Px)

To verify Figure 7.33, the time was adjusted from 0.01-1 to monitor how Xh decreased in the following results:

Table 7. 7: New Px Values (0.01-1)

Px (new)	**Xh (new)**
0.01	2.862307
0.02	2.455552
0.03	2.05578
0.04	1.742783
0.05	1.477896
0.06	1.253752
0.07	1.064095
0.08	0.903615
0.09	0.76781
0.1	0.652867
0.2	0.136239
0.3	0.033076
0.4	0.010028
0.5	0.004052
0.6	0.00231
0.7	0.001951
0.8	0.002537
0.9	0.00521
1	0.001714

Figure 7.37: The value of Xh (new) was decreased as the time (Px) new increases, which therefore means Xh is inversely proportional to the time (Px) and both graphs are in hyperbolic shape.

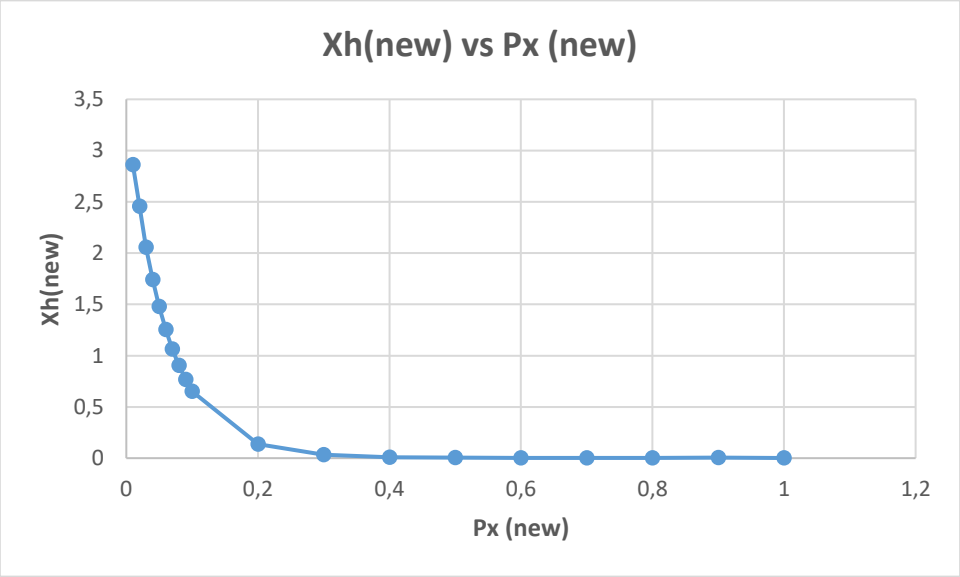

Figure 7. 37: (Xh) new vs (Px) new

7.2.2.2 Additional Results for Figures 7.31-7.32 graph, using (peak 2) allocated at 1/8 spam (10.575m) for conductor tension of 36 kN. The results on Table 7.8 below were as follows: The first row of in Table 7.8 below displayed the calculated results. Px was the time (ms) and Py was the acceleration (m/s^-2) where both values were used to calculate the information of Table 7.8. In the first loop it used the least-square method, the log decrement was 3.383047, the damping factor was 0.232, and the natural frequency was identified as 71.4 rad/s.

Table 7. 8: Calculated Data Collected in Figure 7.32, peak 2

Period	Freq	ln Py	Yj	ln Py (Yj)	Yj^2	Zj	Log Dec	Zeta	Nat Freq	Nat Freq
ms	Hz								rad/s	Hz
0	0	5.027728	0	0	0	3.383047	1.5	0.232	71.4	11.36
0.176	5.681818	4.834033	1	4.834033	1	1.883047				
0.176	5.681818	4.787375	2	9.57475	4	0.383047				
		14.64914	3	17.64914	5					

Figures 7.38 to 7.40 in the X-value expanded and in the Y-value diminished. This means:

- The value of Xh diminished as the time (Px) increased which subsequently implied Xh was inversely corresponding to the time (Px).

- The value of the acceleration (Py) decreased as the time (Px) increased which meant that Py was inversely proportional to the time (Px).

-The value of Acceleration (In Py) decreased as the time (Px) increased which meant In Py was inversely proportional to the time (Px).

The value of Zj decreased as the time (Px) increased which meant Zj was inversely proportional to the time (Px). The difference in Figures 7.38 to 7.40 and Figure 7.41 was the shape of the graph. Figures 7.38 to 7.40 was in hyperbolic shape and Figure 7.41 was a decreased straight line.

The value of Zj decreased as the time (Px) increased which therefore meant that Zj was inversely proportional to the time (Px). The difference in Figures 7.38 to 7.40 and Figure 7.41 was the shape of the graph. Figure 7.38 to 7.40 was in hyperbolic shape and Figure 7.41 was a decreased straight line.

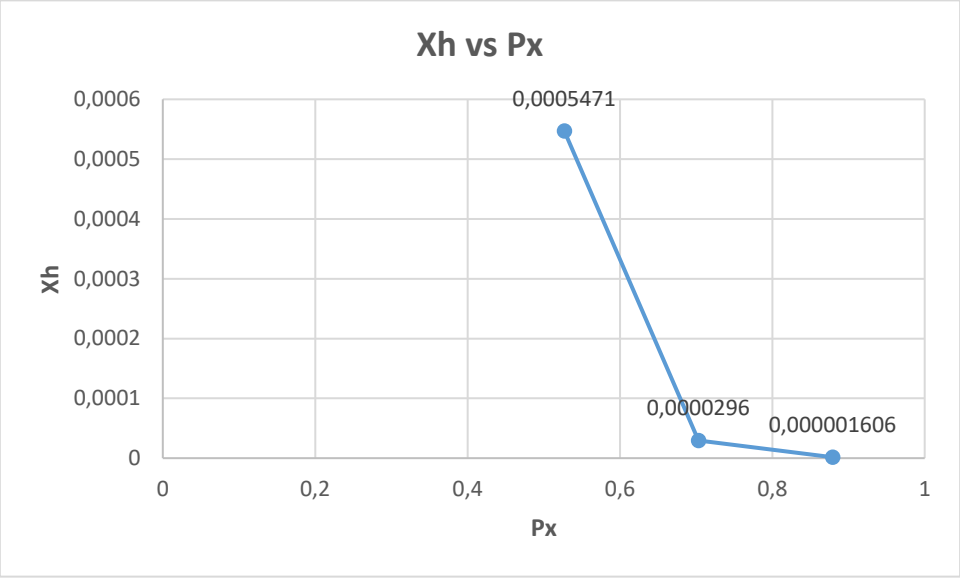

Figure 7. 38:(Xh) vs (Px)

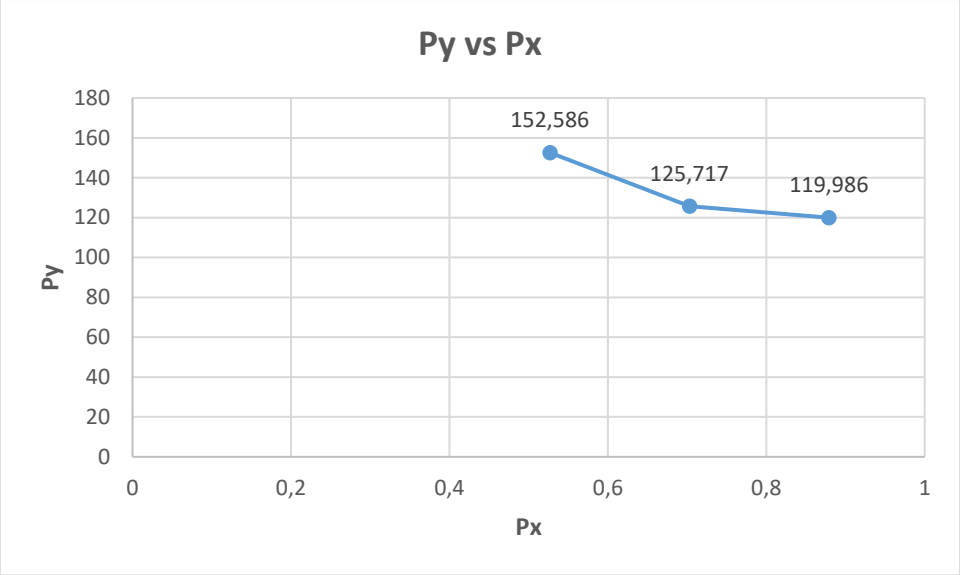

Figure 7. 39: (Py) vs (Px)

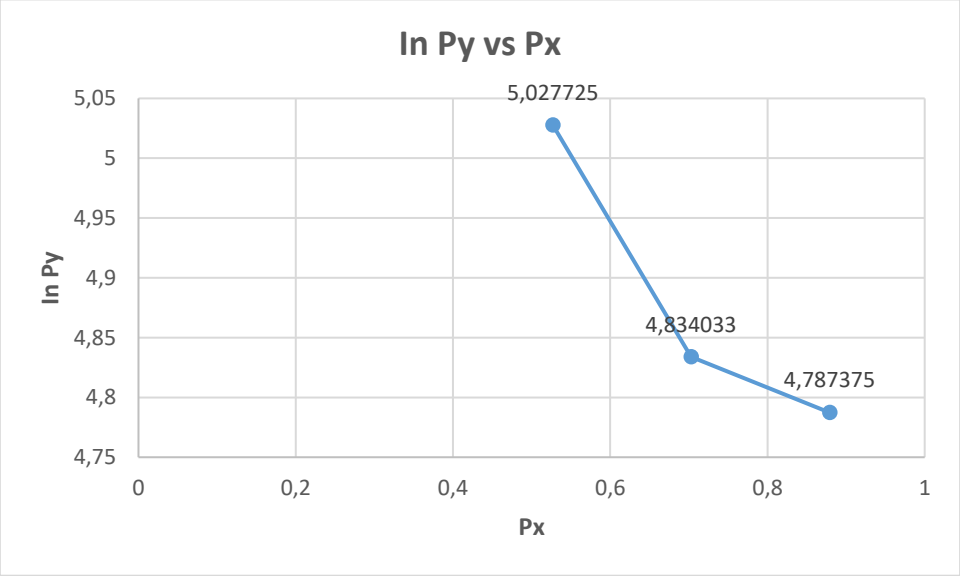

Figure 7. 40:(In Py) vs (Px)

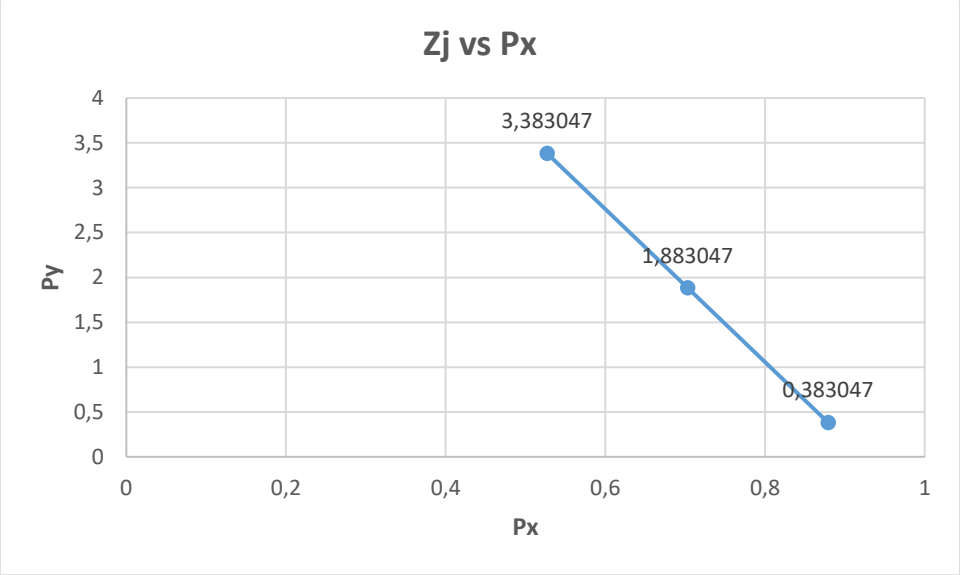

*Figure 7. 41: **(Zj) vs (Px)***

7.3 Summary of the analysis of free vibration results

7.3.1 Tern Conductor

Table 7.9 below show that the Log Dec and Damping coefficient were constant while the natural frequency differed in all cases. This might be caused by the different locations of accelerometers which meant that the natural frequency value depended on the period that we get through the initial time (Px).

Table 7. 9: Free Vibration Tern Results (Summary)

Tension (kN)	**Log Dec**	**Damping Coefficient (Zeta)**	**Natural Frequency (Hz)**	**Table**
26	1.5	0.232	279.7985	7.1
	1.5	0.232	500.5005	7.3
	1.499999	0.236	133.5995	7.2
33	**1.5**	**0.232**	**270.9293**	**C1**
	1.5	**0.232**	**741.8398**	**C4**

39	**1.5**	**0.232**	**424.0882**	**C10**
	1.5	**0.232**	**406.3389**	**C11**

7.3.2 ACSR Conductor

Table 7.10 below show the Log Dec and Damping coefficient were constant. This might have caused the different locations in the accelerometers which meant that the natural frequency value depended on the period gotten through the initial time (Px).

Table 7. 10: Free Vibration ACSR Bersfort Results (Summary)

Tension (kN)	**Log Dec**	**Damping Coefficient (Zeta)**	**Natural Frequency (Hz)**	**Table**
36	1.5	0.232	11.36	6.5
	1.5	0.232	11.36	6.7
45	**1.5**	**0.232**	**11.36**	**D3**
	1.5	**0.232**	**11.36**	**D4**
54	**1.5**	**0.232**	**11.36**	**D5**

7.3.3 Conclusion

Results for free vibration were analysed using Log Decrement and the value for zeta for both conductors was less than 1. More calculations were done (see annexures) and they also confirmed that zeta is less than 1.

CHAPTER 8
DISCUSSION OF RESULTS

8.1 Introduction

This chapter will present an overview of results for the free and forced vibrations experiments conducted on an ACSR BERSFORT DISSCAAY5 / BS215 / IEC61089 transmission conductor and Tern conductor that was used at the UKZN VRTC at Westville campus.

In this chapter the summary of results will be divided into three sections which are:

Section 8.2 Results (Tern and Bersfort)

Section 8.2.1 Tern conductor (Free and Forced vibration)

Section 8.2.2 Discussion of free and forced vibration of ACSR Bersfort conductor method

Section 8.2.3 Comparison of results of Tern and ACSR Bersfort

Section 8.3 Comparison between Mokeretla

8.2 Results (Tern and Bersfort)

8.2.1 Tern conductor (Free and Forced Vibrations)

A procedure for self-damping characteristics developed by Mokeretla (2011) was used to experiment free and forced vibration. Upon using the experiment, the damping factor, zeta, for the free vibration was between $0.232 \leq \zeta \leq 0.236$ for all tension ranging between 29 kN-39 kN as shown Chapter 7, Section 7.2.1 from Table 7.1 to 7.5). Zeta and Log Dec were observed to be constant while the natural frequency was changing based on the location of the accelerometers. The function of acceleration (Py) vs time (Px) decays with time indicating the presence of damping. The results for the forced vibration has shown that on a smaller peak, the damping factor was higher and on a higher peak, the damping factor was reduced or small as shown from (Section 6.2, Tables 6.1 to 6.6) . The statement indicates the damping factor decreases with frequency.

For free vibration, the damping factor varies from 0.232 to 0.236 due to the cable tensioning, as the higher tension the cable behaves as if it were a solid, thereby losing the damping effect arising from rubbing of the strands of cables. When the tension is lower, the friction becomes

higher and this contributes to increase of the damping effect, thereby increasing the damping factor. The findings for forced vibration confirm those of free vibration, higher tension produces lower damping than lower tension.

In practice the choice between high conductor tension, low friction, and low conductor tension, high friction. This is because if the tension is lowered, the sag of the cable become high and this therefore means the towers will need to be high for the conductor not to be close to the buildings. If the tension is high the conductor might not sag but have friction lesser.

8.2.2 Discussion Results for ACSR Bersfort Conductor Subject to Free and Forced Vibrations

The experimental procedure for self-damping characteristics was used for ACSR Bersfort experiment for free and forced vibration for tension ranging between 36-54 kN. Zeta and Log Dec were observed to be constant while the natural frequency was changing based on the location of the accelerometers. The damping factor for free vibration was found to be 0.232 (Section 7, on 7.3.2 Table 7.6-7.8), while for the force vibration was between 0.005137 and 0.024807 as shown (Section 6, on 6.6 Table 6.7-6.11). The function of acceleration (Py) vs time (Px) decays with time indicating the presence of damping.

The results for the forced vibration have shown that on a smaller peak, the damping factor was higher and on a higher peak, the damping factor was reduced or small. The statement indicates the damping factor decreases with frequency.

8.2.3 Comparison of Tern and ACSR Bersfort

The Table 8.1 below indicates the characteristics for the different conductors used for the study and the results obtained. The tension for the Bersfort conductor was higher than the Tern conductor and when the tension is lower, the friction becomes higher and this contributes to increase of the damping effect, thereby increasing the damping factor. The results obtained from both conductors, agrees with Mokeretla's findings that both cables cannot be able to supress Aeolian vibration.

Table 8. 1: Comparison between ACSR Bersfort Results and Tern Results

Item	Characteristics	Tern	ACSR Bersfort
1.	Tension Range	26-39 kN	36-54 kN
2.	Total Area (mm squared)	430.71	746.9
3.	Ultimate Tensile Strength (kN)	98.7	180
4.	Diameter (Overall) mm	27	35.56
5.	Diameter of steel wire (mm)	2.25	3.32
6.	Diameter of aluminium wire (mm)	3.38	4.27
7.	Number of strands (i) Steel (ii) Aluminium	 (i) 6-1 (ii) 21-15-9	 (i) 6-1 (ii) 22-16-9
8.	Linear Mass (kg/m)	1.334	2.386
9.	Flexural Rigidity (Newton meter squared)	21.60	62.76
10.	Free Vibration Damping Factor	Between 0.232 to 0.236	0.232
11.	Forced vibration Damping Factor	Between 0.001363 to 0.02181	Between 0.005137 to 0.024807

The damping factor obtained in both conductors was not sufficient to suppress Aeolian vibration, even though the characteristics varied for both conductors the damping factor for the free vibration was closer and varied on forced vibration.

8.3 Comparison of results with the results presented in Mokeretla (2011)

Table 8.2 below show the comparison between the experiment conducted, the damping factor was found to be different in both studies with rage not exceeding 0.2 from Mokeretla and

0.236 from the current study. On the current study high tensions were used, while on Mokeretla's study lower tensions where used. This therefore will contribute in the results the lower tension will result in higher conductor sag. The study conducted by (Mokeretla, 2011) included mass absorbers, while this study only focused on the conductors.

Table 8. 2: Comparison of results with the results presented in Mokeretla (2011))

Item	Malwande	Mokeretla
Tension Tern ACSR Bersfort Aero	 Range from 26-39 kN Range from 36-54 kN Not used	 Range from 20-29 kN Not used Range from 20-29 kN
Program(s) used.	Free (National Instrument Desk) Force (Puma)	Free (Fluke Scope Meter) Forced (Puma)
Damping Factor Tern (free vibration)	 Range between 0 to 0.236	 Range between 0 to 0.213 (Mokeretla,2011) Table 32
Damping Factor Tern (forced vibration)	Range between 0 to 0.02181	Range between 0 to 0.093 (Mokeretla,2011) Table 33
ACSR Bersfort vs Aero Damping Factor (free)		

ACSR Bersfort Aero	Range between 0 to 0.232 N/A	N/A Range between 0 to 0.105 (Mokeretla,2011) Table 34
ACSR Bersfort vs Aero Damping Factor (forced) ACSR Bersfort Aero	Range between 0 to 0.024807 N/A	N/A Range between 0 to 0.626 (Mokeretla,2011) Table 35

Even though the characteristics of Tern conductor used by Mokeretla was not known, the damping factor obtained for Tern conductors where at a closer range.

CHAPTER 9
CONCLUSIONS

The procedure developed by Mokeretla (2011) was used to determine the self-damping characteristics of the Tern and Bersfort conductors. The damping coefficient was found to be $\leq$ 0.236 for both Tern and ACSR Bersfort conductors. The damping factor for forced vibration on the Tern conductor was $\leq$ **0.02181** and for the Tern free vibration was **0.236.** While the damping factor for the ACSR Bersfort (forced vibration) was found to be **$\leq$0.024807** and for the ACSR Bersfort (free vibration) was found to be **$\leq$ 0.232.** The study has shown that the internal damping factor of a conductor is dependent on the characteristics of a conductor, hence the internal damping factor for the ACSR was higher than the Tern conductor.

The natural vibration damping behavior was discovered to be insufficient to suppress the wind induced Aeolian vibration The damping factors obtained in both conductor-tests were not sufficient to suppress Aeolian vibrations. Results obtained by Mokeretla (2011) that the internal self-damping of TERN transmission lines could not suppress Aeolian vibrations have been confirmed, due to the damping values being much less than critical damping ($\zeta \ll 1$).

CHAPTER 10
RECOMMENDATIONS

In this research, the method on self-damping characteristics of transmission line conductors subjected to free and forced vibrations was done. It is recommendable that for the free vibration, a hammer used must be connected to the program used to measure the force applied and further studies need to be conducted using external dampers in different locations.

REFERENCES

Alderton, T., Chaganti, M., Chisholm, B., Dimnik, C., Dolan, M., Freimark, B., Fulk, N., Garrels, M., Goch, W., Goodwin, T., Harvard, D., Havel, J., Hopkins, R., Jagtiani, A., McCoy, R., Pon, C., Roughan, J., Smith, R., Snider, K., Springer, P., Varner, J., Whapham, B. & Wortmann, K. 2015. An Introductory Discussion on Aeolian Vibration of Single Conductors. Available[Online] : https://resourcecenter.ieee-pes.org/publications/technical-reports/PESTR17.html Accessed on [Accessed 13 Sep. 2018].

Barry, O.R.2014.Vibration and analysis of single conductor with Stockbridge damper, Department of Mechanical and Industrial Engineering: University of Toronto.

Bukhari, M., Barry, O & Tanbour, E. 2018. PLP (Preformed Line Products). 2008. Aeolian vibration basics. Cleveland, Ohio: SAGE Journals: Your gateway to world-class journalresearch.Journals.sagepub.com.Available[Online]http://journals.sagepub.com/doi/pdf/10.1177/1077546317719194 [Accessed 20 September 2018].

Chan, J., Havard, D., Rawlins, C. & Weisel, J. 2006. EPRI Transmission Line Reference Book-Wind Induced Conductor Motion. 2nd ed. California: Electric Power Research Institute.

Darmasaputra, A. 2016. Vortex Induced Vibration on Pipeline. Available[online]: http://ardyansyah30.blogspot.com/2016/02/vortex-induced-vibration-on-pipeline.html. Accessed 08 September 2018.

De Silva, C., 2007. *Vibration Damping, Control, and Design*. 1st ed. Boca Raton: CRC Press.: Available [Online] https://www.taylorfrancis.com/books/mono/10.1201/9781420053227/vibration-damping-control-design-clarence-de-silva [Accessed 20 June 2019]

Diana, G. & Milano, P. 2018. Some basic principles. Available[Online]: http://www.tdee.ulg.ac.be/doc-26.html . Accessed 8 September 2018.

Diana, G., Falco, M., Cigada, A. and Manenti, A.2000. *On the Measurement of Over Head Transmission Lines Conductor Self-Damping*. Available[Online]: https://www.researchgate.net/publication/3273870_On_the_Measurement_of_Over_Head_Transmission_Lines_Conductor_Self-Damping. [Accessed on 17 May 2018]

Doucy et al, E. S. 1979. Wind induced conductor motion, transmission line reference book.

Electrical Power Research Institute.

Eshiemogie, O. 2011. Dynamic Characteristics of Bare Conductors. Available[Online]: https://researchspace.ukzn.ac.za/bitstream/handle/10413/5826/Eshiemogie_Ojo_Evans_2011.pdf;sequence=1 . [Accessed on 17 May 2018]

Fletcher, M., Svatora, L., Weyer, D., Pon, C. & Rizzetto, A. 2018. Managing Aeolian Powerline Vibrations: *The Basics. Transmission & Distribution World*. Available[Online] : http://www.tdworld.com/white-papers/managing-aeolian-powerline-vibrations-basics [Accessed 17 May 2018].

Irvine, T. 2006. Welcome to vibration date. Vibrationdata.com.Available[Online]: http://www.vibrationdata.com/Newsletters/May2006_NL.pdf8, .[Accessed on 17 September 2018.]

Koh, C.G. & Rong, Y. 2004. Dynamic analysis of large displacement cable motion with experimental verification. Available[Online]: https://www.sciencedirect.com/science/article/abs/pii/S0022460X03003262 . Accessed on [15 Feb 2019]

Kubelwa, Y., Loubser, R. & Moodley, P. 2018. *Experimental investigation of bending stresses of ACSR conductors due to Aeolian Vibration. Experimental investigations of bending stresses of ACSR conductors due to aeolian vibrations: 17*. Available[Online] : https://www.researchgate.net/publication/320858011_Experimental_investigations_of_bending_stresses_of_ACSR_conductors_due_to_aeolian_vibrations. [Accessed 8 September 2018.]

Maurya, P., Sharma, S., and Khan, S., 2020. How To Define Damping? What Is Damping Factor?. Available[Online]: https://www.indiastudychannel.com/experts/36574-How-to-define-damping-What-is-damping-factor . [Accessed 11 June 2020.]

Meirovitch, L., 2008. Fundamentals Of Vibrations. Available[Online}: https://www.academia.edu/4052607/Fundamentals_of_Vibrations_Leonard_Meirovitch . [Accessed on 11 June 2020]

Mogilevsky, A., Wrathall, N., Dimnik, C., Lotho, K. & Tsimberg, Y. 2014. *Determining Transmission Line Conductor*.. Available[Online]: https://www.researchgate.net/publication/269211707_Determining_transmission_line_conductor_condition_and_remaining_life . [Accessed on 11 June 2020]

Mokeretla, M. 2011. Self-Damping Characteristics Of Transmission Line Conductors Subjected To Free And Forced Vibration. Available[Online]: http://ir.cut.ac.za/bitstream/handle/11462/15/Mokeretla%20Molungoa%20Samuel.pdf?sequence=4&isAllowed=y . [Accessed on 17 May 2018]

Moodley, P. 2018. STIP | VRTC. Available[Online]: http://stip.ukzn.ac.za/VRTC.aspx . [Accessed on 17 May 2018.]

Munaswamy, K. and Haldar, A. 2000.Self-Damping Measurements of Conductors with Circular and Trapezoidal Wires. Available[Online]: https://ieeexplore.ieee.org/document/852992 .[Accessed on 17 May 2018]

Munaswamy, K. and Haldar, A. (2000). IEEE TRANSACTIONS ON POWER DELIVERY. Self-Damping Measurements of Conductors with Circular and Trapezoidal Wires, 15(2), pp.604-609.

Line Products). 2008. Aeolian vibration basics. Cleveland, Ohio: SAGE Journals: Your gateway to world-class journalresearch.Journals.sagepub.com.Available[Online]http://journals.sagepub.com/doi/pdf/10.1177/1077546317719194 [Accessed 20 September 2018].

Nigol, O. & Barrett, J. 1981. Characteristics of ACSR Conductors at High Temperatures and Stresses. IEEE Transactions on Power Apparatus and Systems, PAS-100(2): 485-493.

Panth, D. 2014. International Journal of Electrical, Electronics and Data Communication. Available[Online]: http://www.iraj.in/journal/journal_file/journal_pdf/1-35-139099330601-04.pdf [Accessed 8 September 2018].

Rawlins, C. (2008). Flexural self-damping in overhead electrical transmission conductors. Available[Online]t: https://ac.els-cdn.com/S0022460X08010080/1-s2.0-

S0022460X08010080-main.pdf?_tid=d464dfa9-6b72-40ce-9ed7-02e9023a1d43&acdnat=1536857109_f3bb5767c96e0227c46f818126fc4e77. [Accessed 19

Thomson, W. 1986. *Theory of vibration with the application*. 2nd ed. London: G. Allen & Unwin. [Available online] http://docshare01.docshare.tips/files/27874/278745641.pdf [Accessed 17 August 2020]

Wayer, D. 2016. Material Evaluation: Self Damping Wire. Thesis.Available[Online]: https://digitalcommons.unl.edu/mechengdiss/102/ .[Accessed on 20 May 2018]

Wolf, H., Adum, B., Semenski, D. And Pustaić, D.2008. Using the Energy Balance Method in Estimation of Overhead Transmission Line Aeolian Vibrations. Available[Online]:https://r.search.yahoo.com/_ylt=AwrE18_pz31gKsYAFzVXNyoA;_ylu=Y29sbwNiZjEEcG9zAzEEdnRpZANBMDU5OV8xBHNlYwNzcg--/RV=2/RE=1618886761/RO=10/RU=https%3a%2f%2fhrcak.srce.hr%2ffile%2f63700/RK=2/RS=dCITomZ22ms6rVArADWJxKq0n8s . [Accessed on 17 May 2018]

Rawlins, C. (2008). Flexural self-damping in overhead electrical transmission conductors. Available[Online]t: https://ac.els-cdn.com/S0022460X08010080/1-s2.0-S0022460X08010080-main.pdf?_tid=d464dfa9-6b72-40ce-9ed7-02e9023a1d43&acdnat=1536857109_f3bb5767c96e0227c46f818126fc4e77 [accessed on 17 May 2018]

Thomson, W. 1986. Theory of vibration with the application. 2nd ed. London: G. Allen & Unwin.

APPENDICES

APPENDIX I

RESULTS FOR FORCED VIBRATION METHOD ON TERN CONDUCTOR

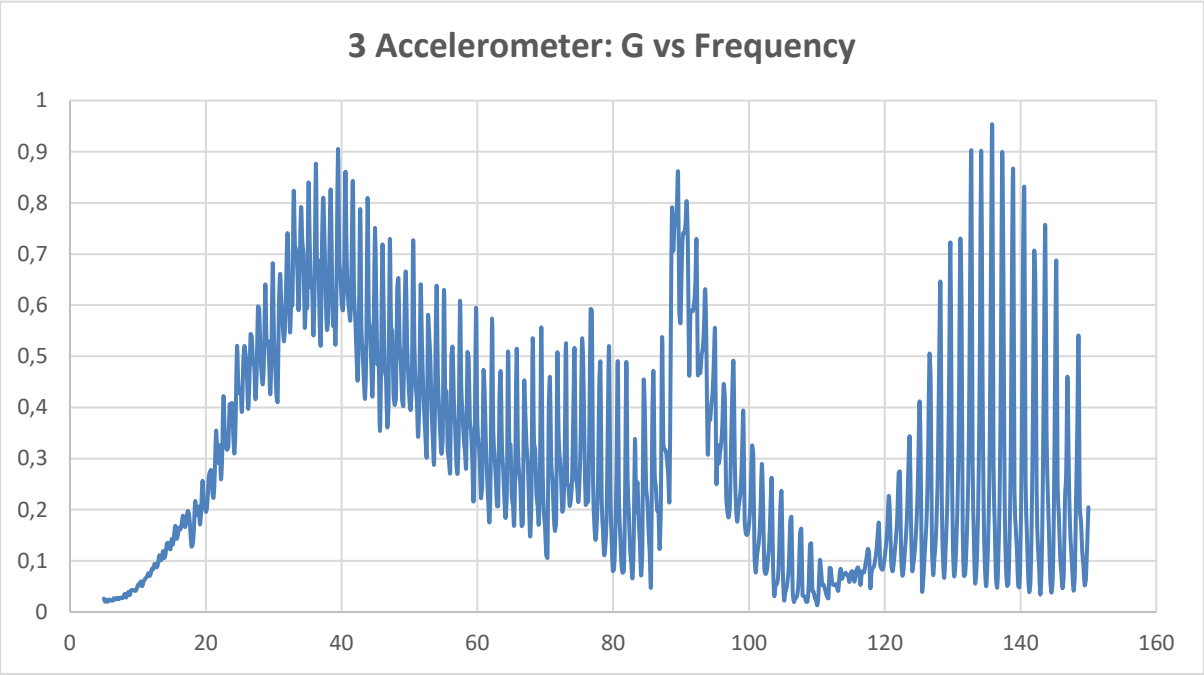

Figure A1: Acceleration (G) vs Frequency, channel 3, 39.23 kN (Test2)

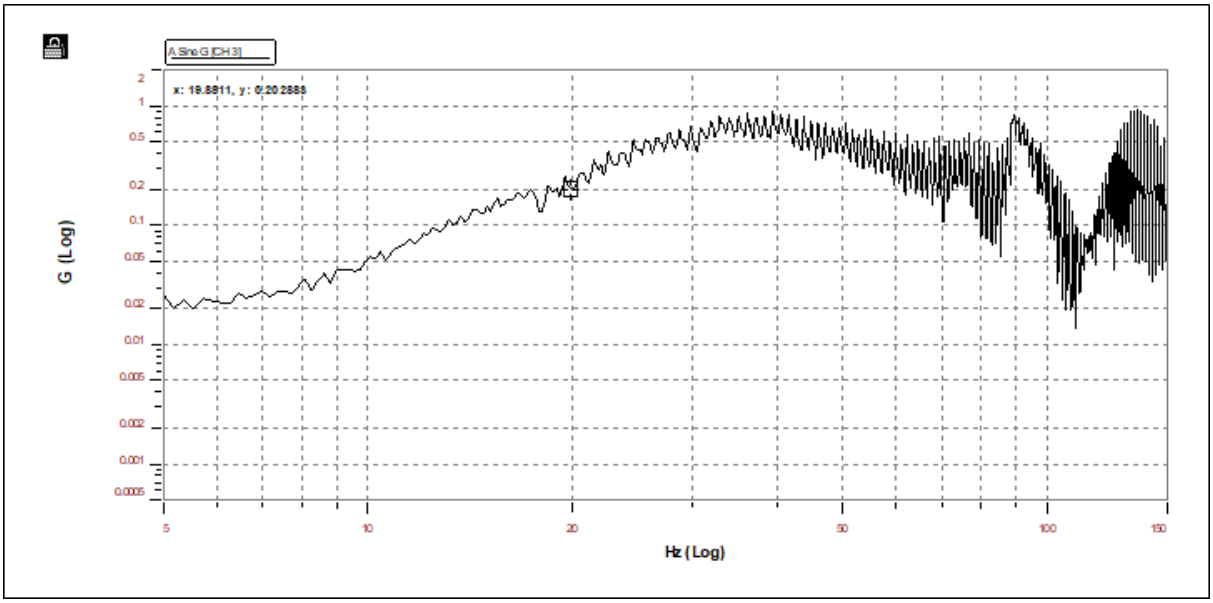

Figure A2: Acceleration (G) vs Frequency, channel 3, 39.23 kN (Test 2) Spectral Viewer

Table A1: Data Collected on Figure A1

Peak	X peak	x1 and x2	f1	f2	Fn	Change F	Q	Zeta
	Read on Graph	Xp/1.4142	Read on Graph x1	Read on Graph x2	Read on Graph Xpeak	F2-F1	Fn/(F2-F1)	1/2Q
1	0.90537	0.640199	39.480598	40.025028	39.480598	0.54443	72.517308	0.01379
2	0.854672	0.60435	89.568207	90.11264	89.568207	0.544433	164.516491	0.006078
3	0.941001	0.665395	135.844803	136.389236	135.844803	0.544433	249.516108	0.004008

It is seen in Table A1 that the damping factor, ζ, ranges from 0.004008 to 0.01372. Thus, for 72.517308 Hz, the maximum damping factor was 0.01379.

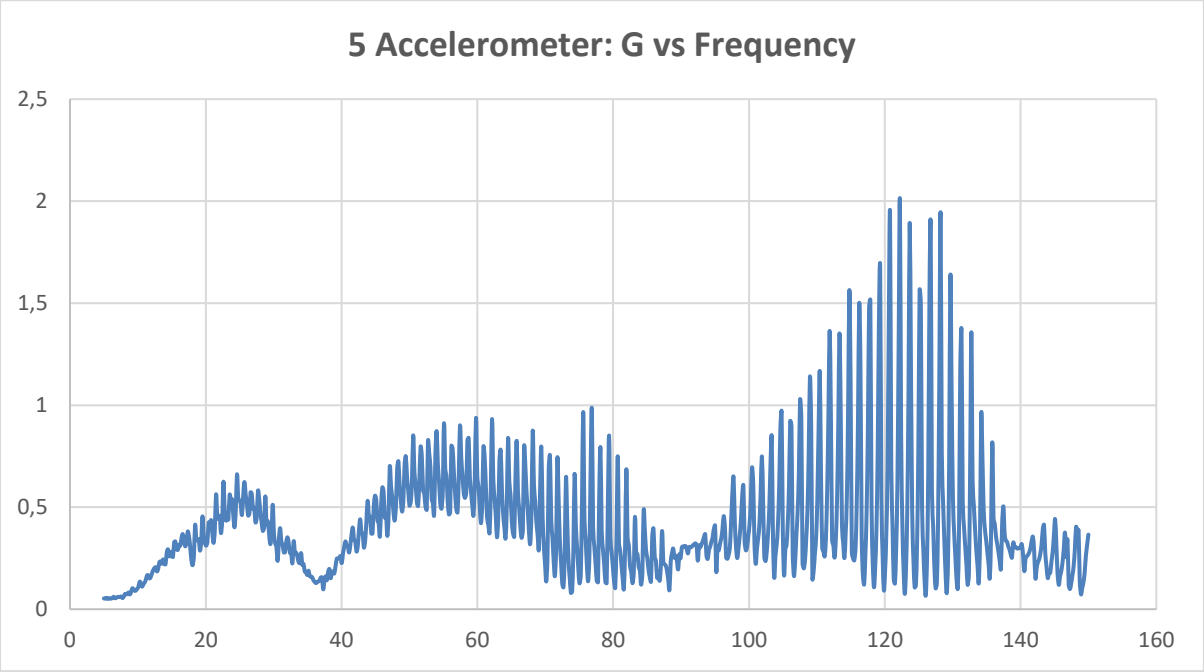

Figure A3: Acceleration (G) vs Frequency, channel 5, 39.23 kN (Test2)

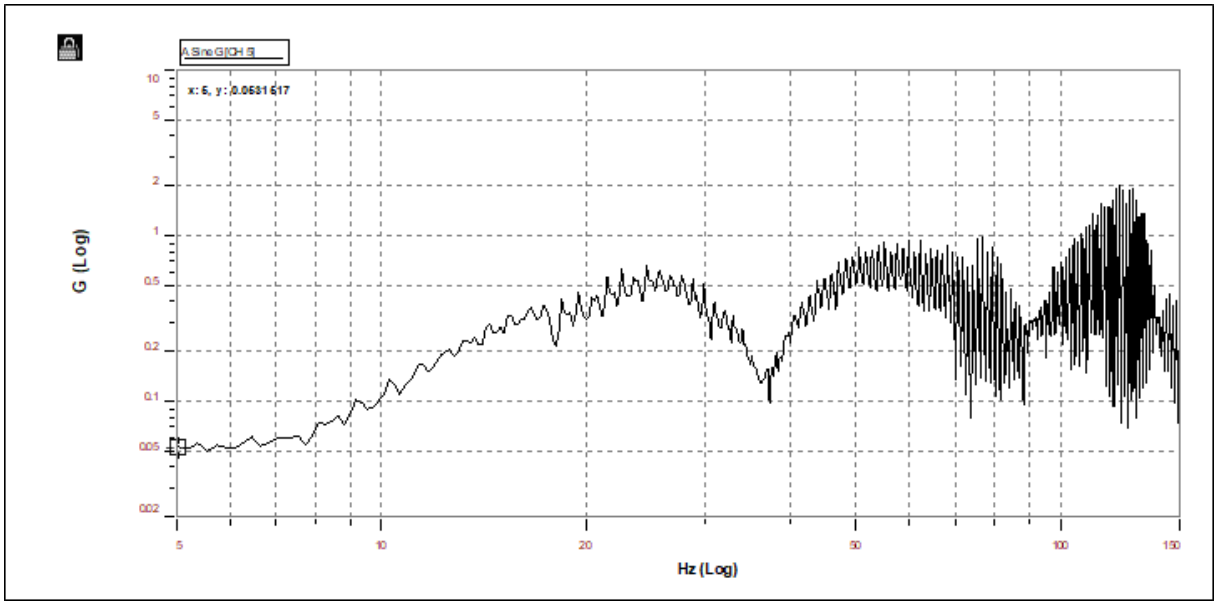

Figure A4: Acceleration (G) vs Frequency, channel 5, 39.23 kN (Test 2) Spectral Viewer

Table A2: Data Collected on Figure A3

Peak	X peak	x1 and x2	f1	f2	Fn	Change F	Q	Zeta
	Read on Graph	Xp/1.4142	Read on Graph x1	Read on Graph x2	Read on Graph Xpeak	F2-F1	Fn/(F2-F1)	1/2Q
1	0.66158	0.467812	24.599499	25.506884	24.962452	0.907385	27.5103203	0.03635
2	0.938131	0.663365	59.806007	60.168961	59.806007	0.362954	164.775721	0.006069
3	2.01515	1.42494	122.234039	122.596992	122.234039	0.362953	336.776494	0.002969

It is seen in Table A2 that the damping factor, ζ, ranges from 0.002969 to 0.03635. Thus, for 24.962452 Hz, the maximum damping factor was 0.03635.

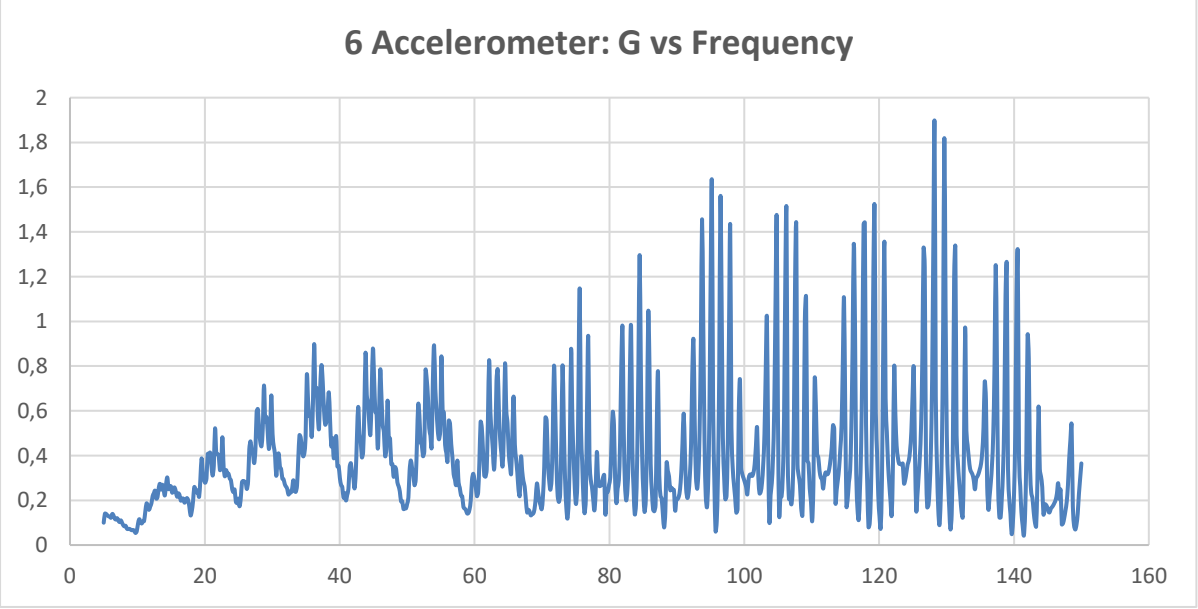

Figure A5: Acceleration (G) vs Frequency, channel 6, 39.23 kN (Test2)

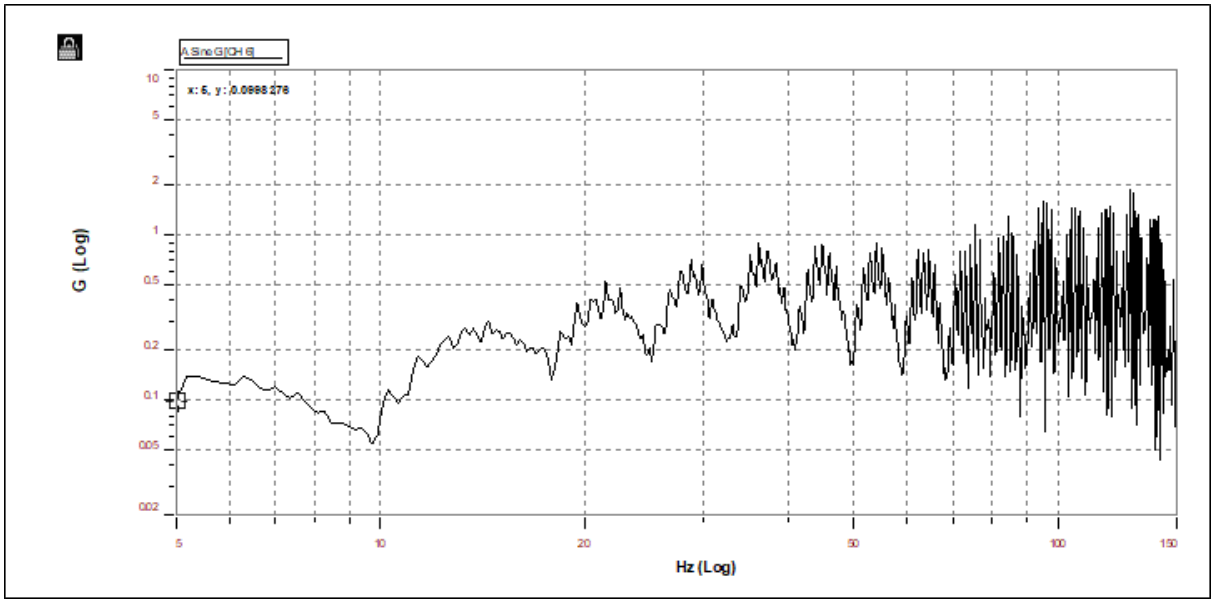

Figure A6: Acceleration (G) vs Frequency, channel 6, 39.23 kN (Test 2) Spectral Viewer

Table A3: Data Collected on Figure 131

Peak	X peak	x1 and x2	f1	f2	Fn	Change F	Q	Zeta
	Read on Graph	Xp/1.4142	Read on Graph x1	Read on Graph x2	Read on Graph Xpeak	F2-F1	Fn/(F2-F1)	1/2Q
1	0.898558	0.635383	36.214016	36.939922	36.214016	0.725906	49.8880241	0.020045
2	1.62184	1.146825	95.193993	95.556946	95.193993	0.362953	262.276364	0.003813
3	1.88127	1.330272	128.222778	128.585724	128.222778	0.362946	353.283348	0.002831

It is seen in Table A3 that the damping factor, ζ, ranges from 0.002831 to 0.020045. Thus, for 36.939922 Hz, the maximum damping factor was 0.020045.

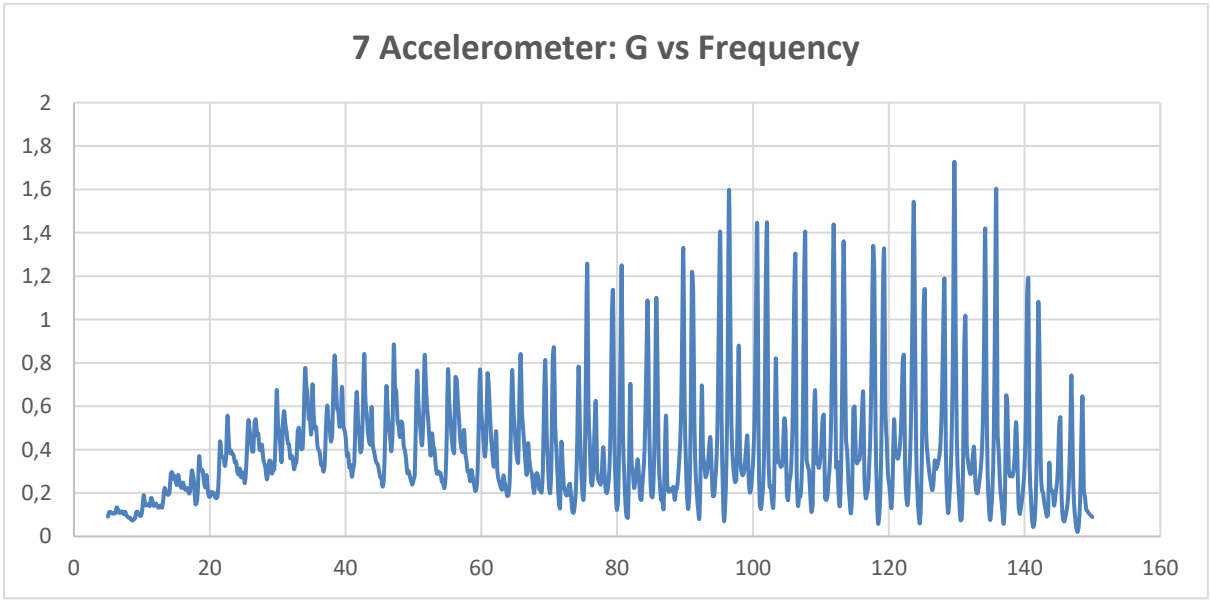

Figure A7: Acceleration (G) vs Frequency, channel 7, 39.23 kN (Test2)

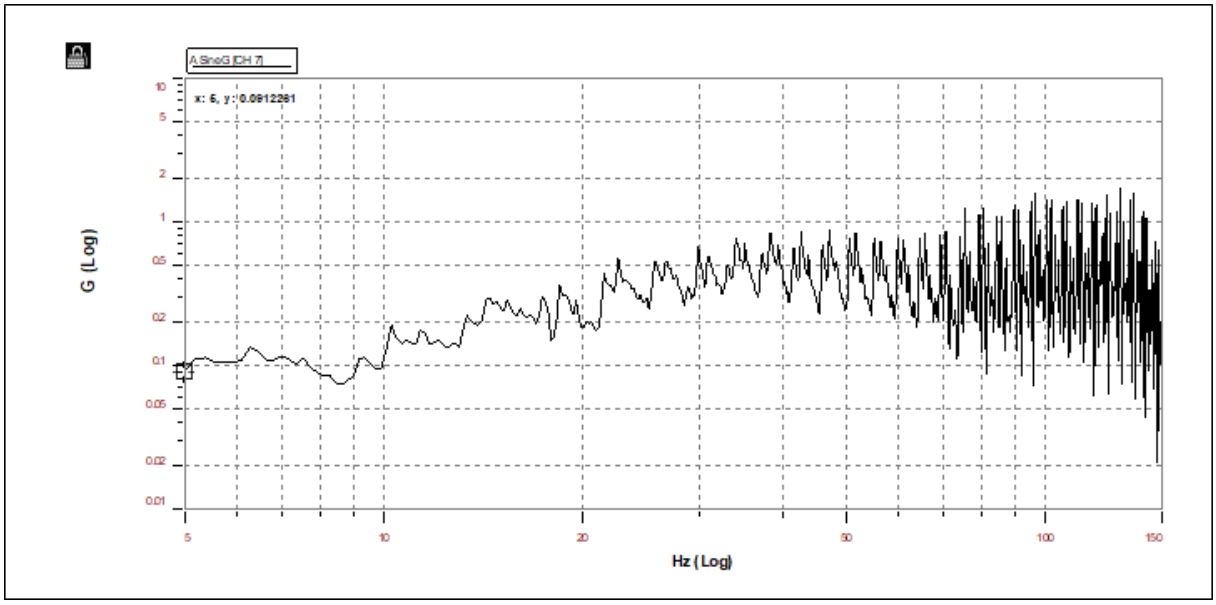

Figure A8: Acceleration (G) vs Frequency, channel 7, 39.23 kN (Test 2) Spectral Viewer

Table A4: Data Collected on Figure A7

Peak	X peak	x1 and x2	f1	f2	Fn	Change F	Q	Zeta
	Read on Graph	Xp/1.4142	Read on Graph x1	Read on Graph x2	Read on Graph Xpeak	F2-F1	Fn/(F2-F1)	1/2Q
1	0.881002	0.622968	47.102627	47.647057	47.102627	0.54443	86.5173245	0.011558
2	1.59086	1.124919	96.464325	96.827278	96.464325	0.362953	265.776354	0.003763
3	1.72717	1.221305	129.674591	130.037537	129.674591	0.362946	357.283428	0.002799

It is seen in Table 36 that the damping factor, ζ, ranges from 0.002799 to 0.011588. Thus, for 47.647057 Hz, the maximum damping factor was 0.011558.

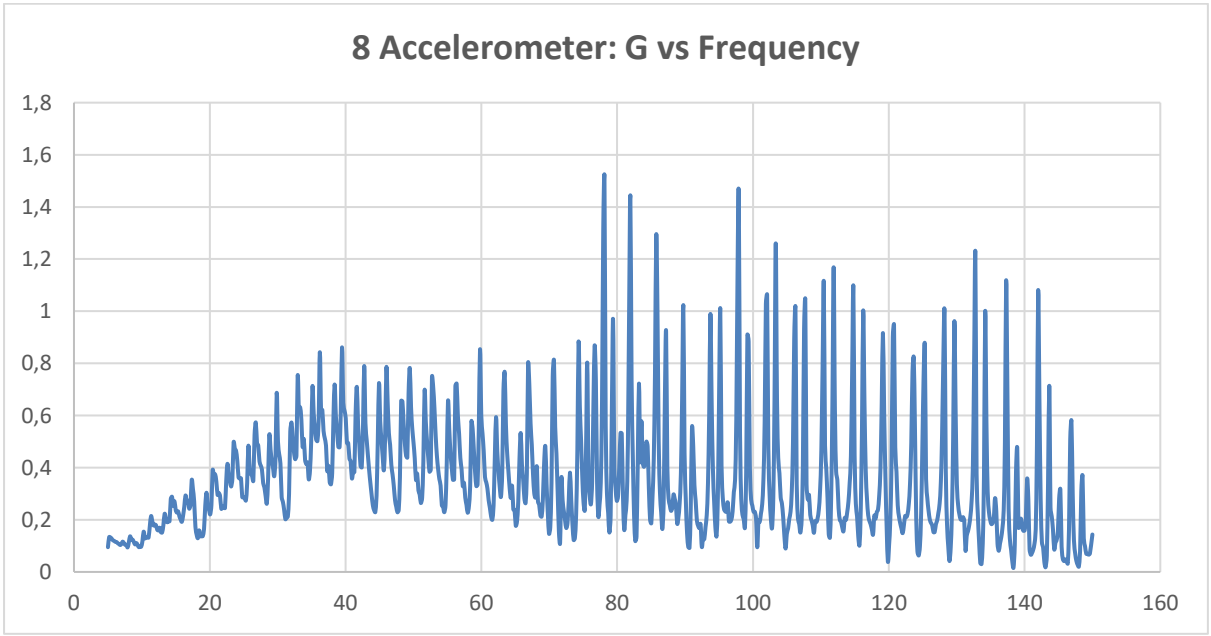

Figure A9: Acceleration (G) vs Frequency, channel 8, 39.23 kN (Test2)

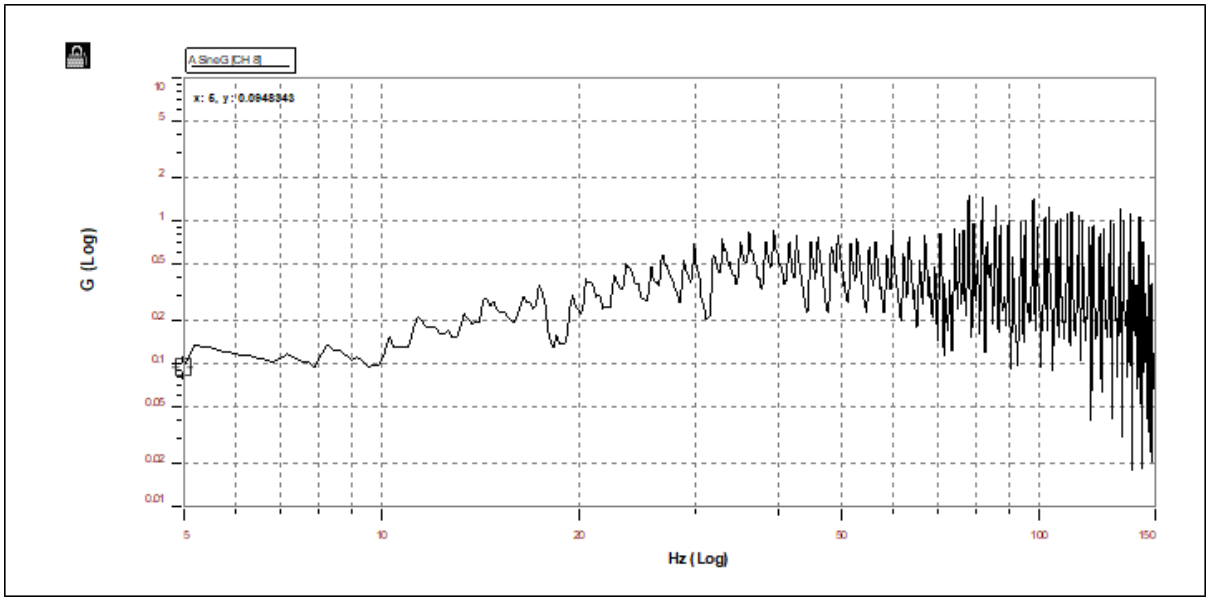

Figure A10: Acceleration (G) vs Frequency, channel 8, 39.23 kN (Test 2) Spectral Viewer

Table A5: Data Collected on Figure A9

Peak	X peak	x1 and x2	f1	f2	Fn	Change F	Q	Zeta
	Read on Graph	Xp/1.4142	Read on Graph x1	Read on Graph x2	Read on Graph Xpeak	F2-F1	Fn/(F2-F1)	1/2Q
1	0.861475	0.609161	39.480598	40.025028	39.480598	0.54443	72.517308	0.01379
2	1.5021	1.062155	78.135162	78.498116	78.135162	0.362954	215.27566	0.004645
3	1.22227	0.864284	132.759689	133.304123	132.759689	0.544434	243.849005	0.004101

It is seen in Table A5 that the damping factor, ζ, ranges from 0.004101 to 0.01379. Thus, for 40.025028 Hz, the maximum damping factor was 0.01379.

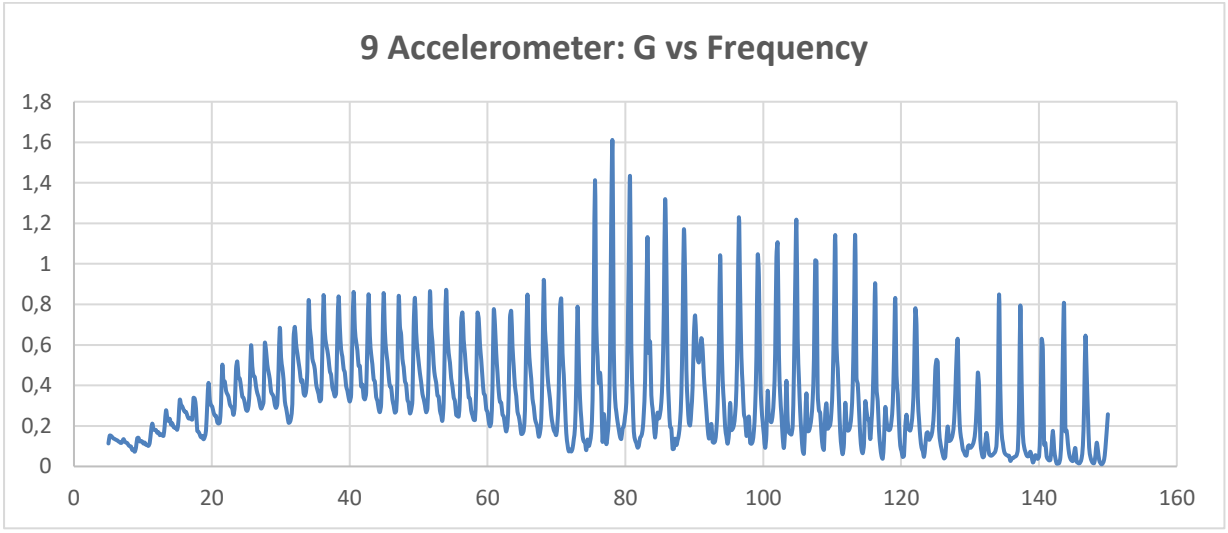

Figure A11: Acceleration (G) vs Frequency, channel 9, 39.23 kN (Test2)

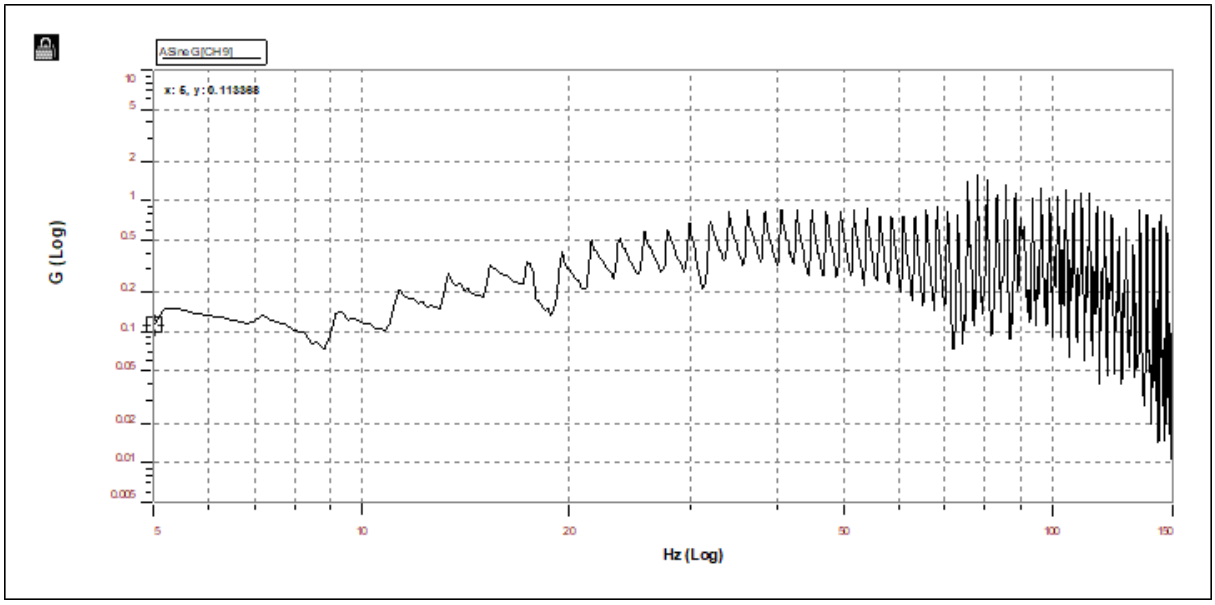

Figure A12: Acceleration (G) vs Frequency, channel 9, 39.23 kN (Test 2) Spectral Viewer

Table A6: Data Collected on Figure A11

Peak	X peak	x1 and x2	f1	f2	Fn	Change F	Q	Zeta
	Read on Graph	Xp/1.4142	Read on Graph x1	Read on Graph x2	Read on Graph Xpeak	F2-F1	Fn/(F2-F1)	1/2Q
1	0.872073	0.616655	53.998745	54.543179	53.998745	0.544434	99.1832711	0.010082
2	1.58626	1.121666	78.135162	78.498116	78.135162	0.362954	215.27566	0.004645
3	1.21251	0.857382	104.812263	105.356689	104.812263	0.544426	192.518842	0.005194

It is seen in Table A6 that the damping factor, ζ, ranges from 0.004645 to 0.010082. Thus, for 54.543179 Hz, the maximum damping factor was 0.010082.

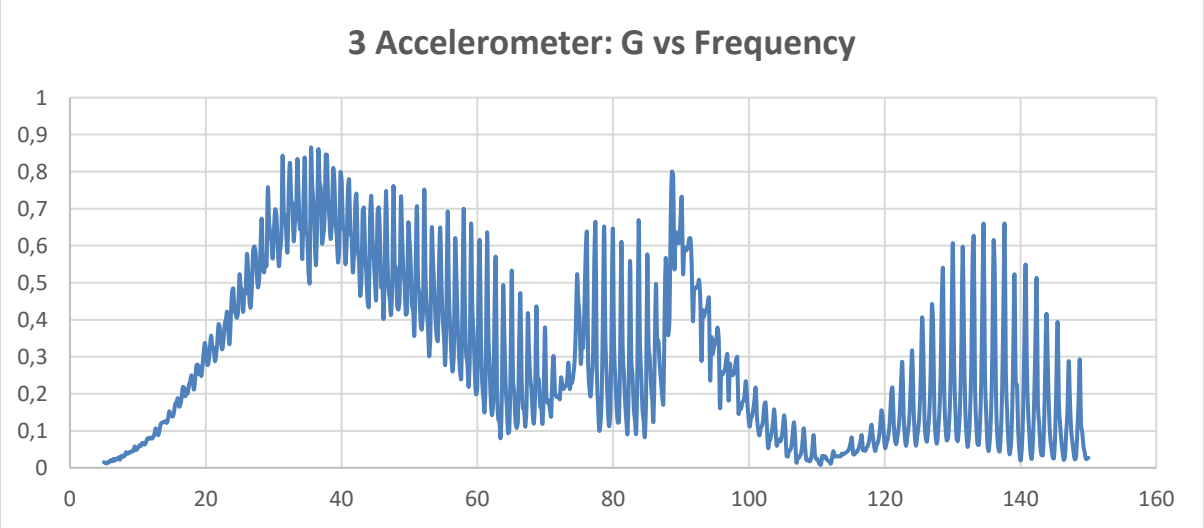

Figure A13: Acceleration (G) vs Frequency, channel 3, 39.23 kN (Test 3)

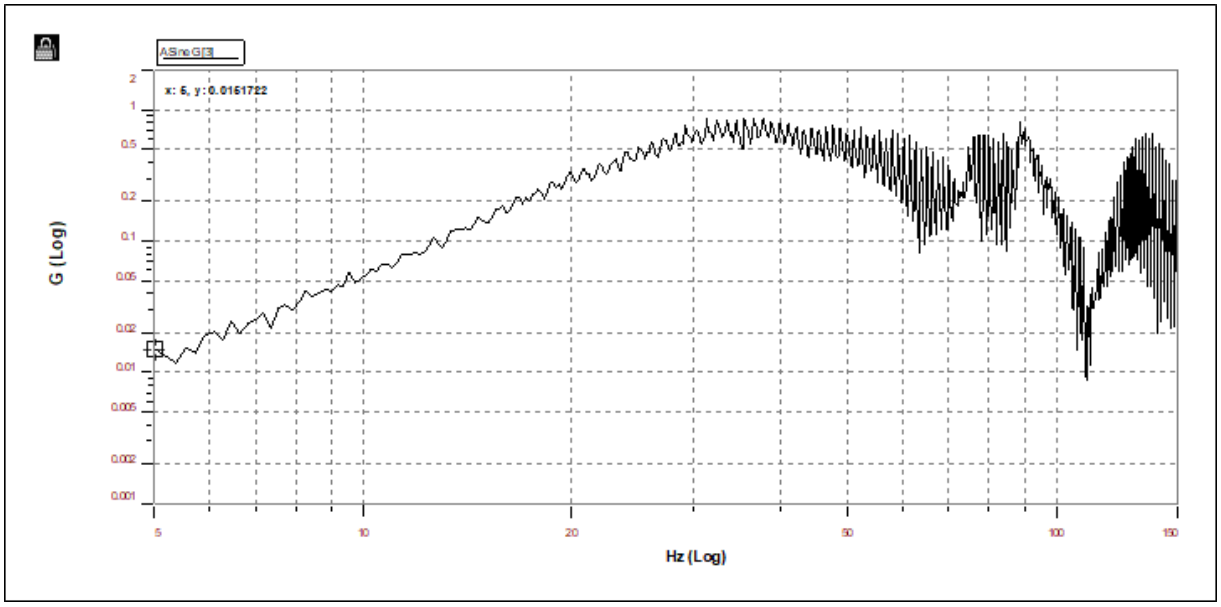

Figure A14: Acceleration (G) vs Frequency, channel 3, 39.23 kN (Test 3) Spectral Viewer

Table A 7: Data Collected on Figure A13

Peak	X peak	x1 and x2	f1	f2	Fn	Change F	Q	Zeta
	Read on Graph	Xp/1.4142	Read on Graph x1	Read on Graph x2	Read on Graph Xpeak	F2-F1	Fn/(F2-F1)	1/2Q
1	0.855283	0.604782	35.48811	36.576969	35.48811	1.088859	32.592016	0.030682
2	0.653773	0.462292	77.409256	77.590736	77.409256	0.18148	426.54428	0.002344
3	0.800121	0.565776	88.66082	89.205254	88.66082	0.544434	162.849528	0.006141
4	0.654878	0.463073	134.574463	134.937408	134.574463	0.362945	370.784728	0.002697

It is seen in Table A7 that the damping factor, ζ, ranges from 0.002397 to 0.030682. Thus, for 36.576969 Hz, the maximum damping factor was 0.030682.

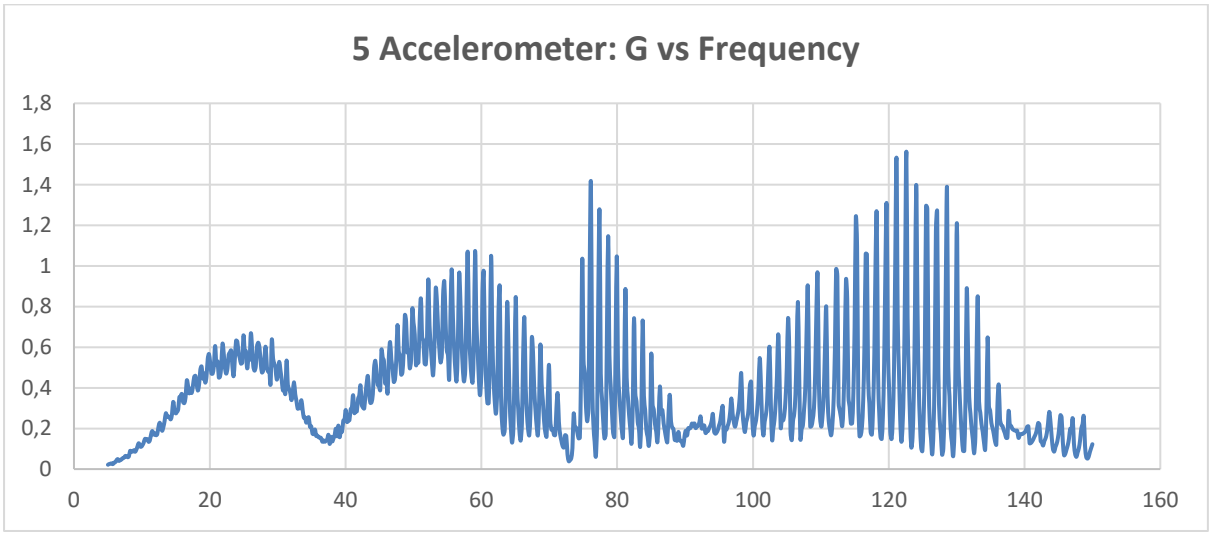

Figure A15: Acceleration (G) vs Frequency, channel 5, 39.23 kN (Test 3)

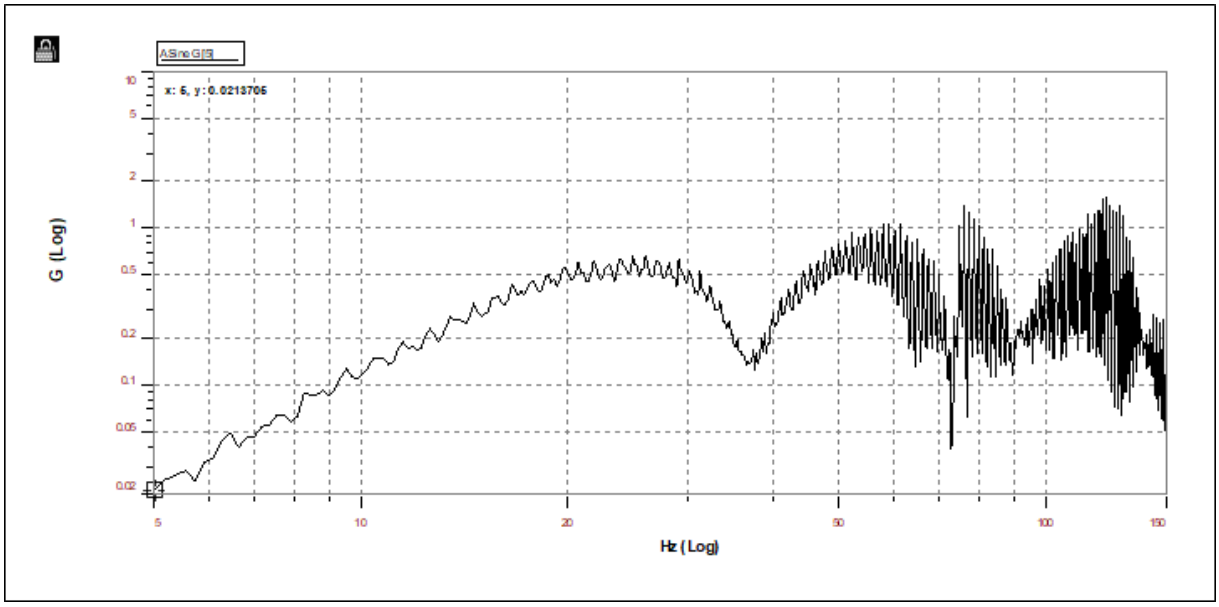

Figure A16: Acceleration (G) vs Frequency, channel 5, 39.23 kN (Test 3) Spectral Viewer

Table A8: Data Collected on Figure A15

Peak	X peak	x1 and x2	f1	f2	Fn	Change F	Q	Zeta
	Read on Graph	Xp/1.4142	Read on Graph x1	Read on Graph x2	Read on Graph Xpeak	F2-F1	Fn/(F2-F1)	1/2Q
1	0.667688	0.472131	26.051313	26.77722	26.051313	0.725907	35.8879485	0.027865
2	1.07364	0.759185	59.080097	59.44305	59.080097	0.362953	162.776164	0.006143
3	1.40477	0.993332	76.138924	76.501877	76.138924	0.362953	209.776263	0.004767
4	1.5622	1.104653	122.596992	122.959946	122.596992	0.362954	337.775564	0.002961

It is seen in Table A8 that the damping factor, ζ, ranges from 0.002961 to 0.027865. Thus, for 26.77722 Hz, the maximum damping factor was 0.027865.

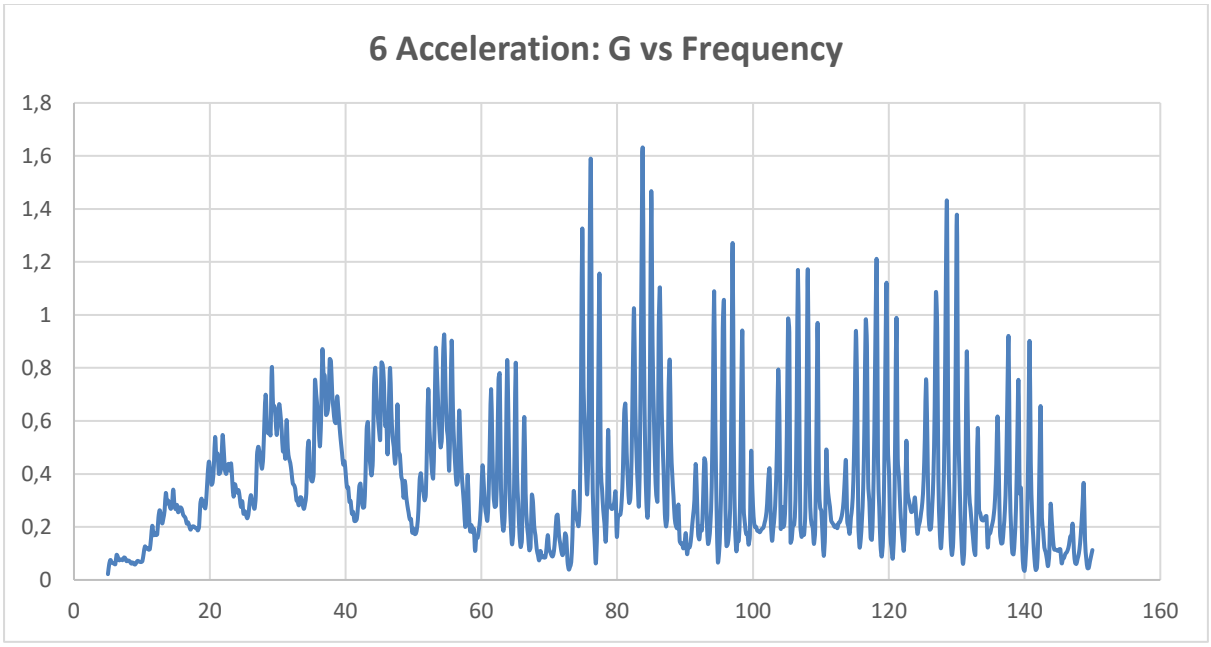

Figure A17: Acceleration (G) vs Frequency, channel 6, 39.23 kN (Test 3)

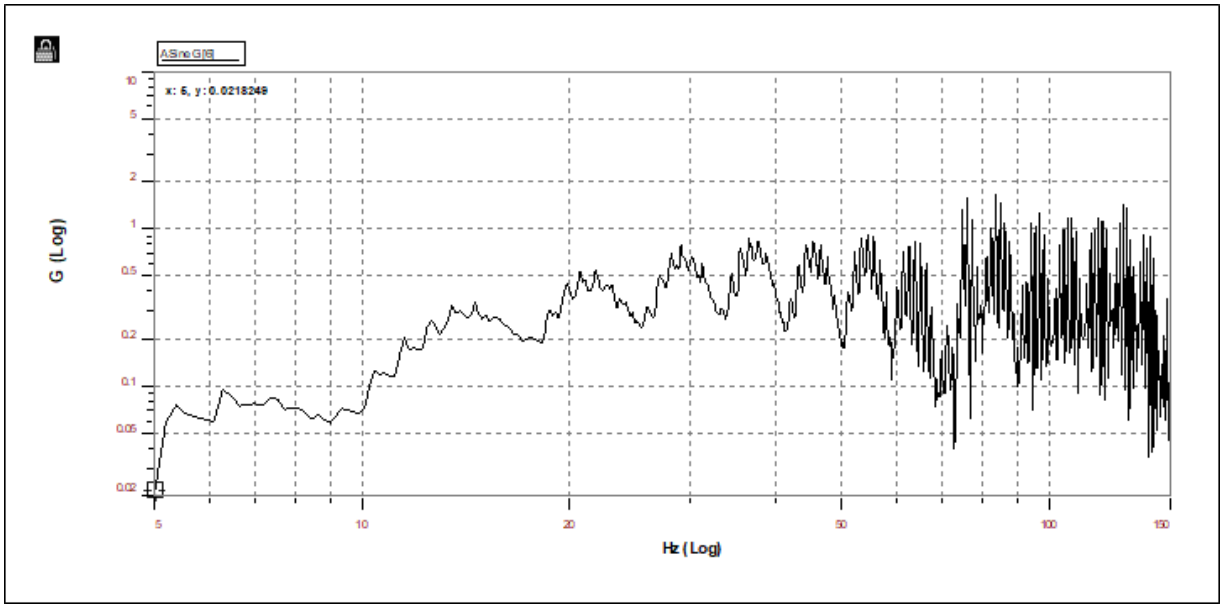

Figure A18: Acceleration (G) vs Frequency, channel 6, 39.23 kN (Test 3) Spectral Viewer

Table A9: Data Collected on Figure A17

Peak	X peak	x1 and x2	f1	f2	Fn	Change F	Q	Zeta
	Read on Graph	Xp/1.4142	Read on Graph x1	Read on Graph x2	Read on Graph Xpeak	F2-F1	Fn/(F2-F1)	1/2Q
1	0.924682	0.653855	54.543179	55.087608	54.543179	0.544429	100.184191	0.009982
2	1.63216	1.154122	83.760948	84.123901	83.760948	0.362953	230.776293	0.004333
3	1.41537	1.000827	128.585724	128.948685	128.585724	0.362961	354.268707	0.002823

It is seen in Table A9 that the damping factor, ζ, ranges from 0.002823 to 0.009982. Thus, for 55.543179 Hz, the maximum damping factor was 0.009982.

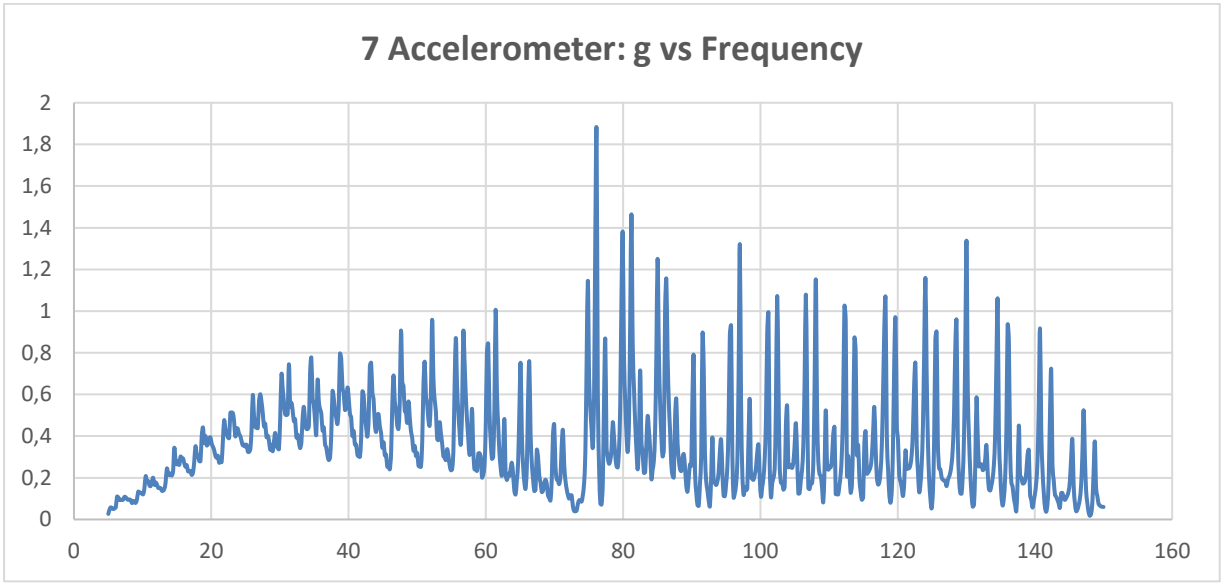

Figure A19: Acceleration (g) vs Frequency, channel 7, 39.23 kN (Test 3)

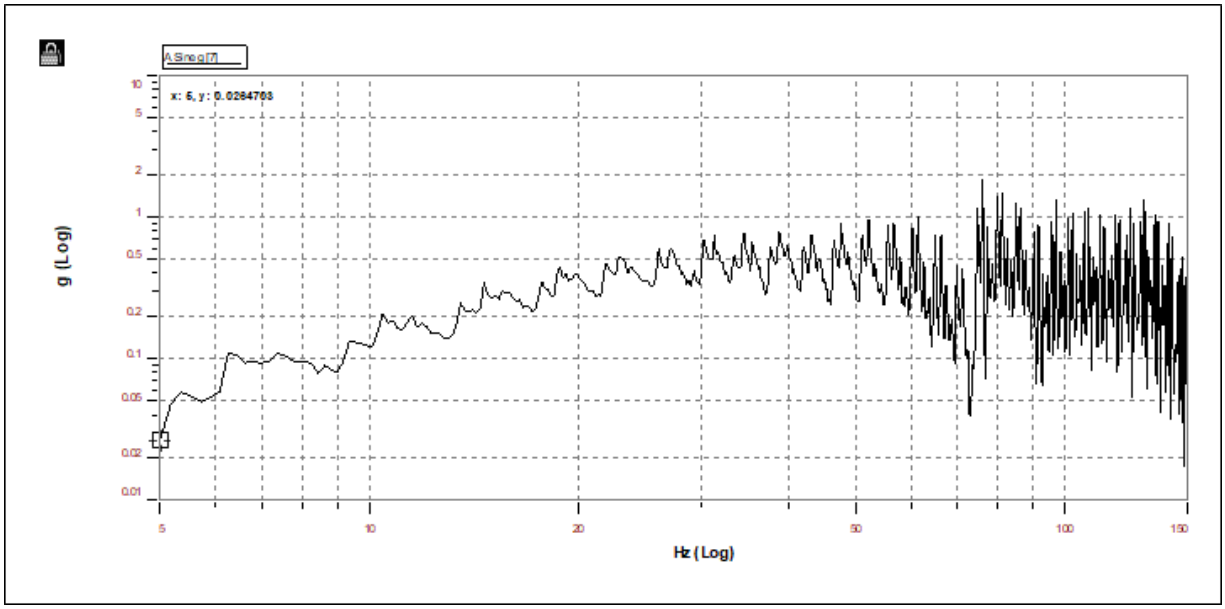

Figure A20: Acceleration (g) vs Frequency, channel 7, 39.23 kN (Test 3) Spectral Viewer

Table A10: Data Collected on Figure A19

Peak	X peak	x1 and x2	f1	f2	Fn	Change F	Q	Zeta
	Read on Graph	Xp/1.4142	Read on Graph x1	Read on Graph x2	Read on Graph Xpeak	F2-F1	Fn/(F2-F1)	1/2Q
1	1.00631	0.711575	61.439297	61.983727	61.439297	0.54443	112.850682	0.008861
2	1.86192	1.316589	76.138924	76.501877	76.138924	0.362953	209.776263	0.004767
3	1.33805	0.946153	130.037537	130.58197	130.037537	0.544433	238.849476	0.004187

It is seen in Table A10 that the damping factor, ζ, ranges from 0.004187 to 0.008861. Thus, for 61.983727 Hz, the maximum damping factor was 0.008861.

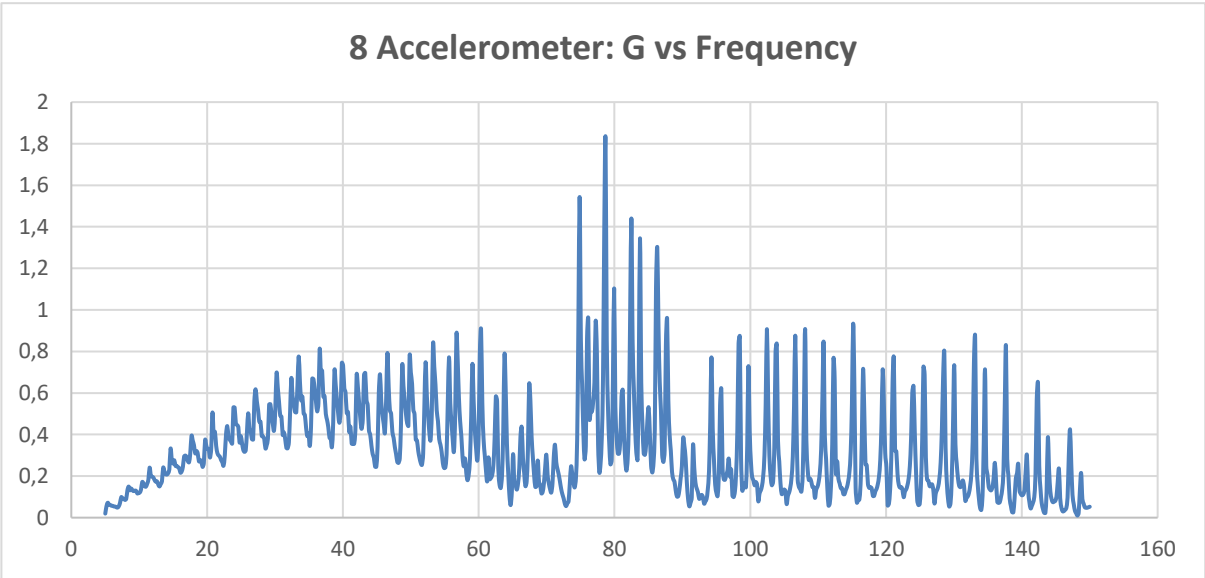

Figure A21: Acceleration (G) vs Frequency, channel 8, 39.23 kN (Test 3)

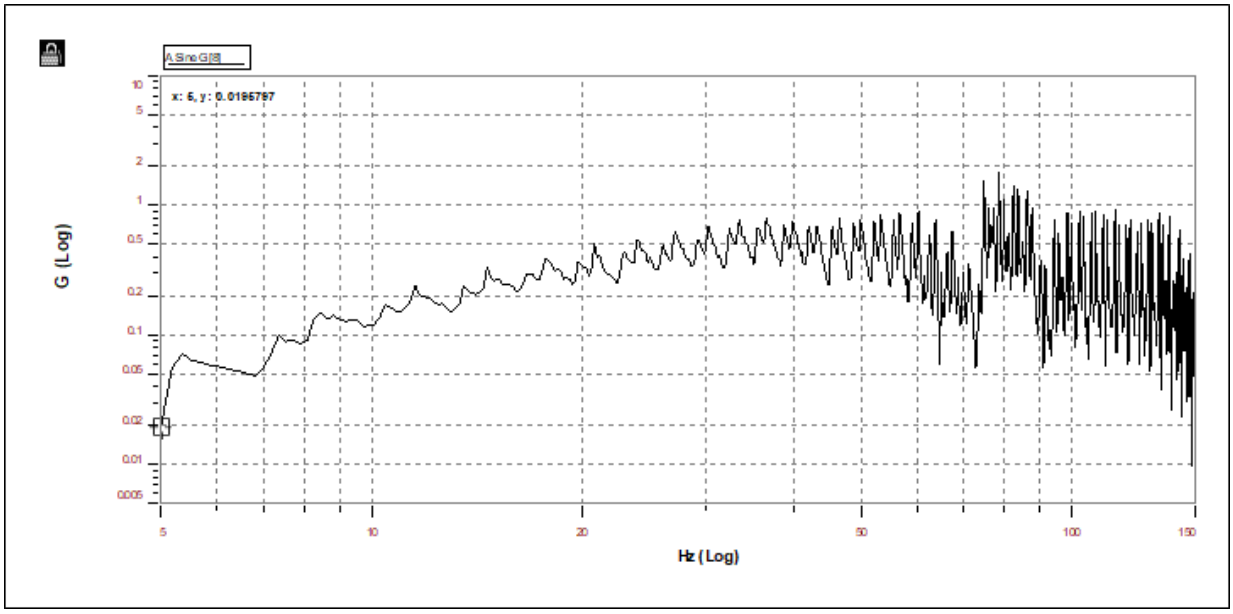

Figure A22: Acceleration (G) vs Frequency, channel 8, 39.23 kN (Test 3) Spectral Viewer

Table A11: Data Collected on Figure A21

Peak	X peak	x1 and x2	f1	f2	Fn	Change F	Q	Zeta
	Read on Graph	Xp/1.4142	Read on Graph x1	Read on Graph x2	Read on Graph Xpeak	F2-F1	Fn/(F2-F1)	1/2Q
1	0.906695	0.641136	60.350437	60.894867	60.350437	0.54443	110.850682	0.009021
2	1.82273	1.288877	78.679596	79.042549	78.679596	0.362953	216.776266	0.004613
3	0.933981	0.660431	115.156441	115.519394	115.156441	0.362953	317.276455	0.003152

It is seen in Table A11 that the damping factor, ζ, ranges from 0.003152 to 0.009021. Thus, for 60.894867 Hz, the maximum damping factor was 0.009021.

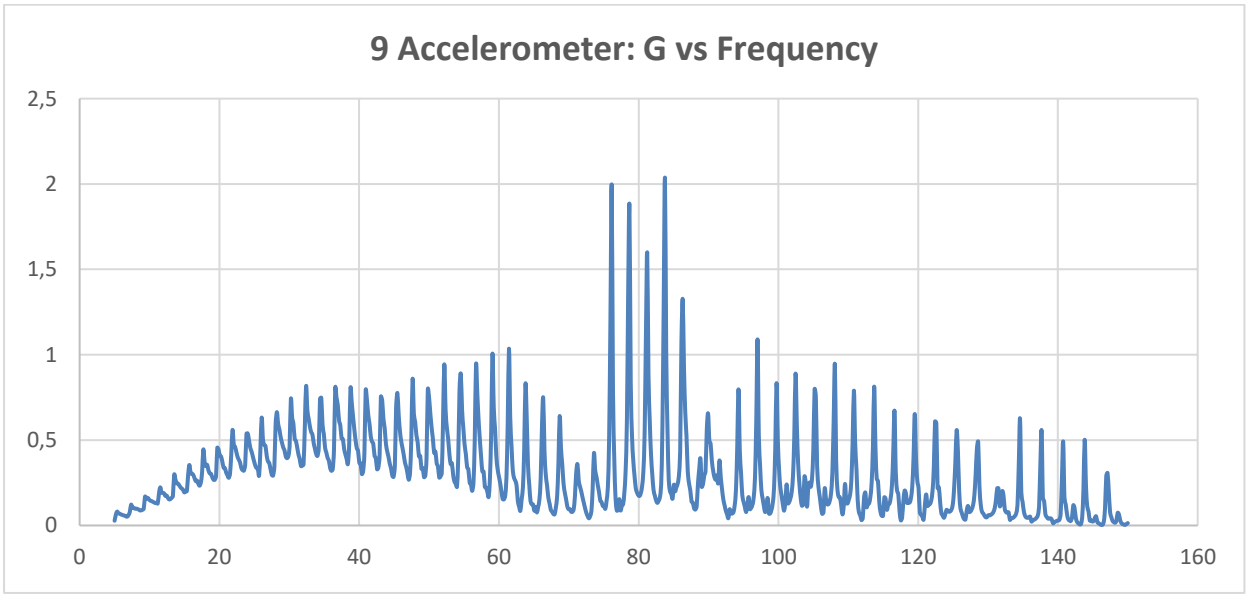

Figure A23: Acceleration (G) vs Frequency, channel 9, 39.23 kN (Test 3)

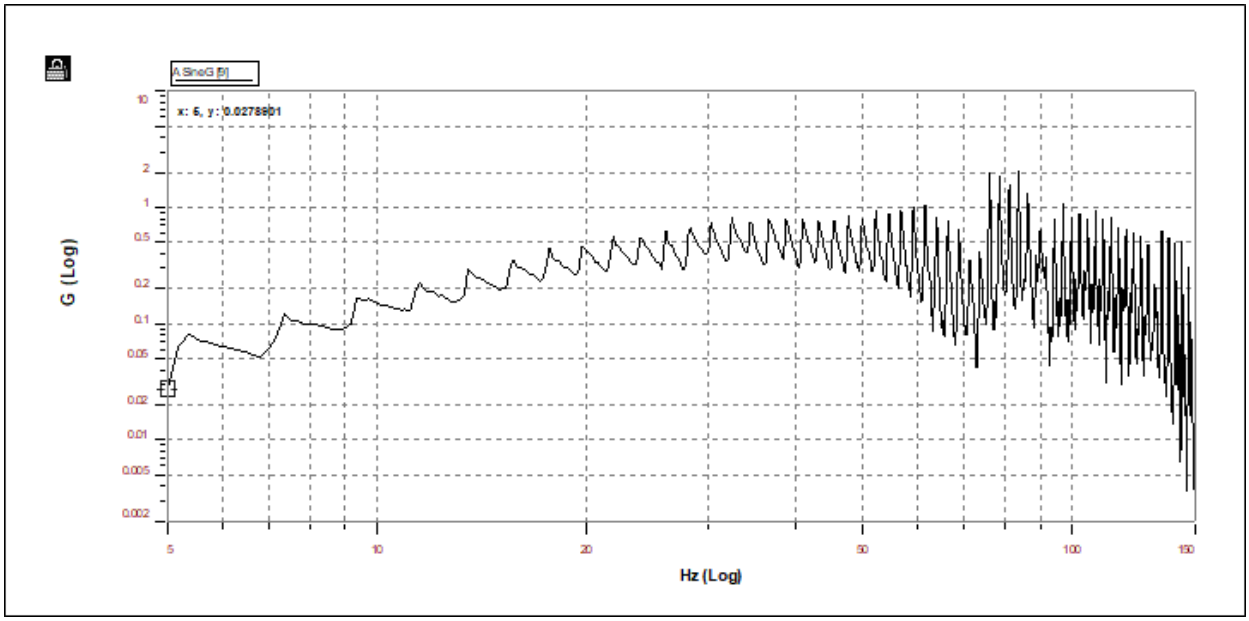

Figure A24: Acceleration (G) vs Frequency, channel 9, 39.23 kN (Test 3) Spectral Viewer

Table A12: Data Collected on Figure A23

Peak	X peak	x1 and x2	f1	f2	Fn	Change F	Q	Zeta
	Read on Graph	Xp/1.4142	Read on Graph x1	Read on Graph x2	Read on Graph Xpeak	F2-F1	Fn/(F2-F1)	1/2Q
1	1.03578	0.732414	61.439297	61.80225	61.439297	0.362953	169.276179	0.005908
2	2.03782	1.44097	83.760948	84.123901	83.760948	0.362953	230.776293	0.004333
3	1.09003	0.770775	97.00879	97.371712	97.008759	0.362922	267.299197	0.003741

It is seen in Table A12 that the damping factor, ζ, ranges from 0.003741 to 0.005908. Thus, for 61.439297 Hz, the maximum damping factor was 0.005908.

APPENDIX II

RESULTS FOR FORCED VIBRATION METHOD ON ACSR BERSFORT CONDUCTOR

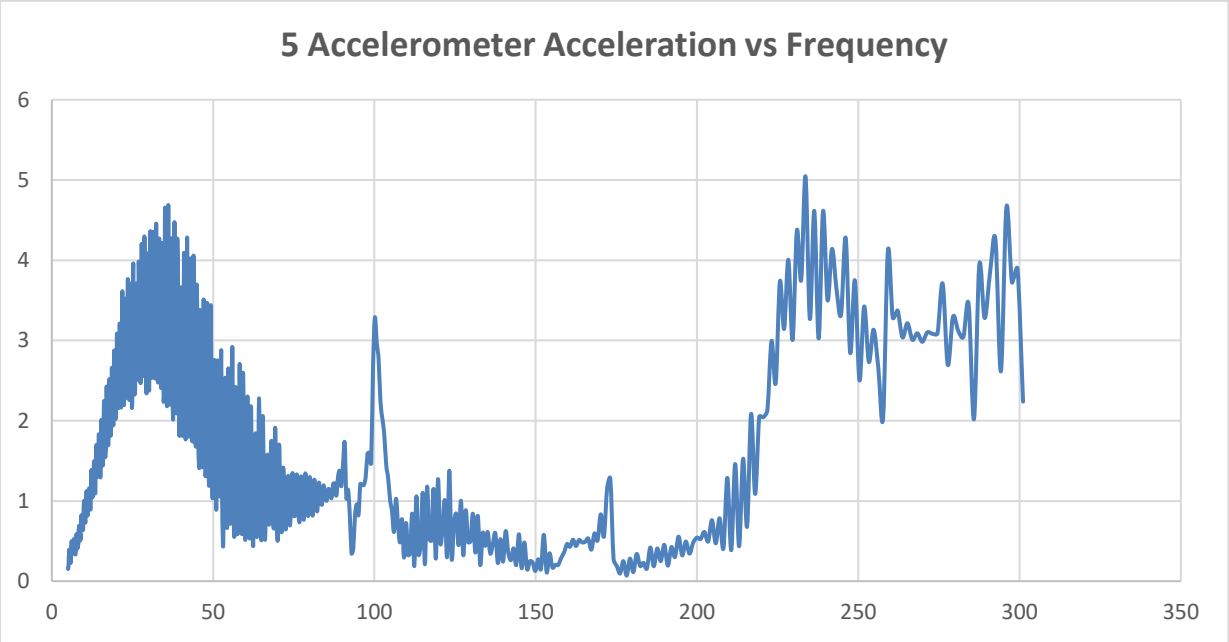

Figure B1: Acceleration (m/s^2) vs Frequency, channel 5, 35.93 kN (Test 1)

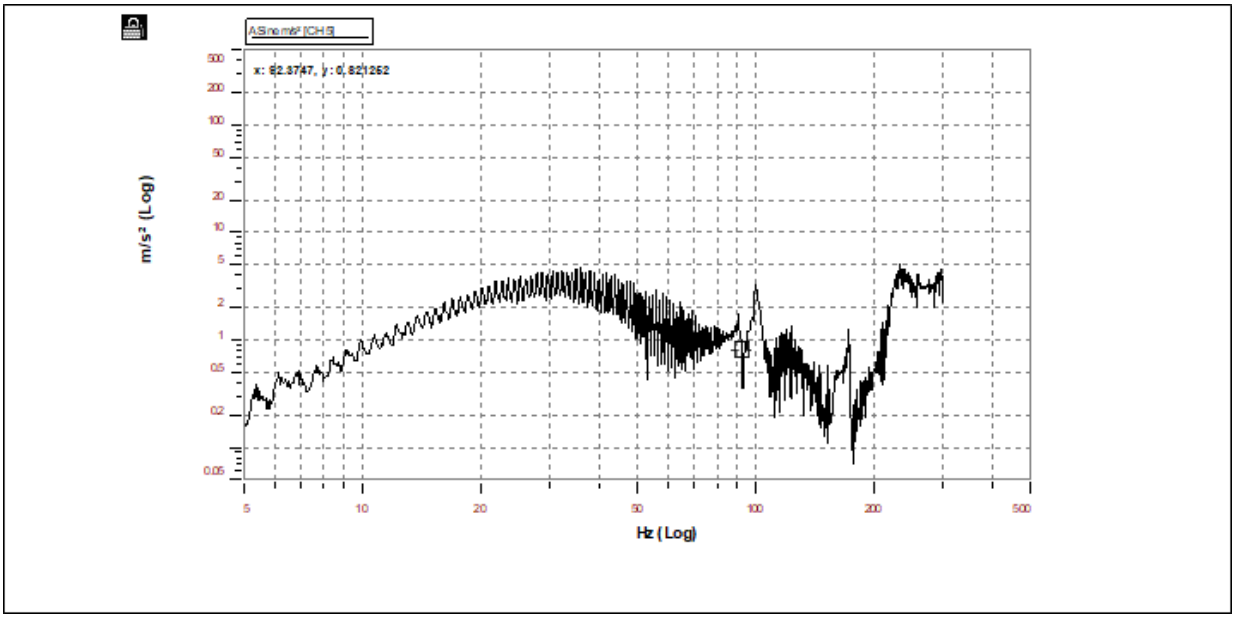

Figure B2: Acceleration (m/s^2) vs Frequency, channel 5, 35.93 kN (Test 1) Spectral Viewer

Table B1: Data Collected on Figure B1

Peak	X peak	x1 and x2	f1	f2	Fn	Change F	Q	Zeta
	Read on Graph	Xp/1.4142	Read on Graph x1	Read on Graph x2	Read on Graph Xpeak	F2-F1	Fn/(F2-F1)	1/2Q
1	4.68845	3.315267	36.102993	36.521572	36.102993	0.418579	86.2513241	0.011594
2	1.37708	0.973752	123.228073	123.940369	123.228073	0.712296	173.001214	0.00578
3	1.27581	0.902143	173.138733	174.139542	173.139733	1.000809	172.999776	0.00578
4	5.04415	3.566787	233.645248	234.995789	233.645248	1.350541	173.001225	0.00578

It is seen in Table B1 that the damping factor, ζ, ranges from 0.00578 to 0.011594. Thus, for 36.521572 Hz, the maximum damping factor was 0.011594.

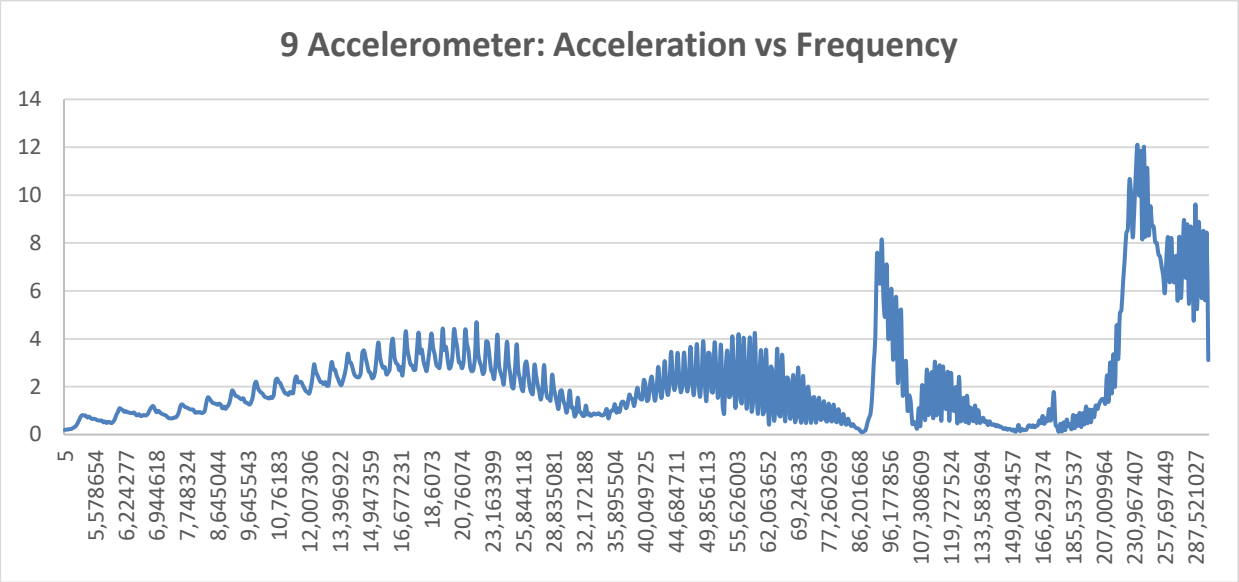

Figure B3: Acceleration (m/s^2) vs Frequency, channel 9, 35.93 kN (Test 1)

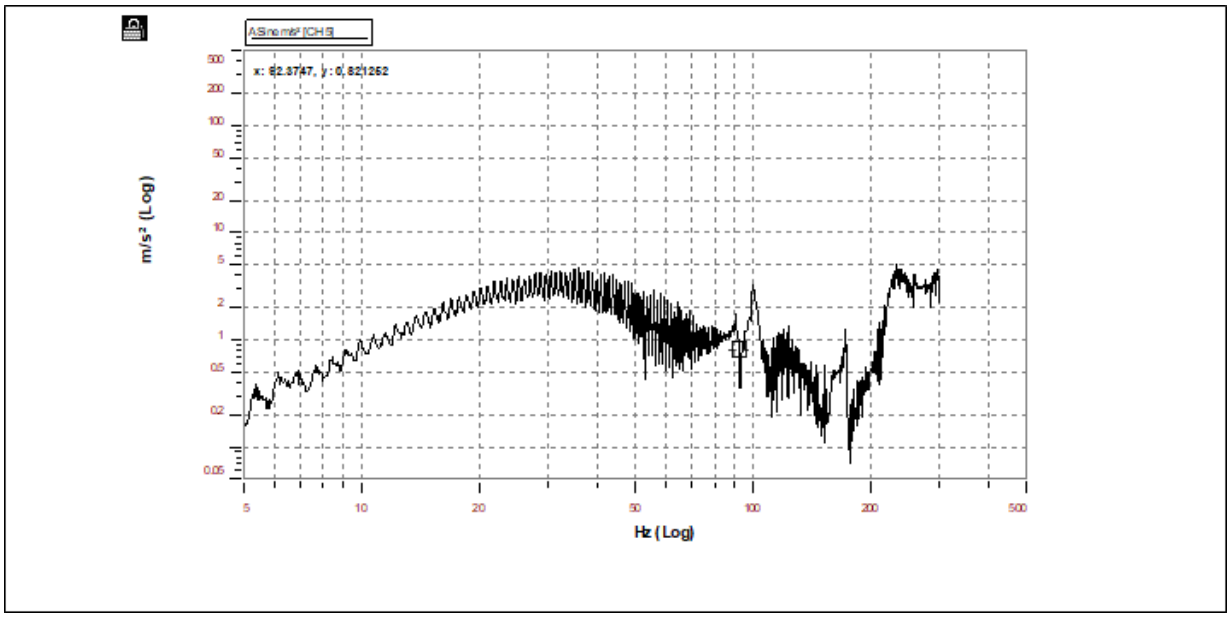

Figure B4: Acceleration (m/s^2) vs Frequency, channel 9, 35.93 kN (Test 1) Spectral Viewer

Table B2: Data Collected on Figure B3

Peak	X peak	x1 and x2	f1	f2	Fn	Change F	Q	Zeta
	Read on Graph	Xp/1.4142	Read on Graph x1	Read on Graph x2	Read on Graph Xpeak	F2-F1	Fn/(F2-F1)	1/2Q
1	4.69377	3.319028	21.866083	22.247458	21.866083	0.381375	57.334862	0.017441
2	4.24708	3.003168	59.266911	59.609489	59.266711	0.342578	173.002093	0.00578
3	6.07814	4.297935	96.733795	97.292946	96.733795	0.559151	173.001202	0.00578
4	3.04802	2.155296	113.021927	113.67232	113.021927	0.650393	173.774821	0.005755

It is seen in Table B2 that the damping factor, ζ, ranges from 0.005755 to 0.017441. Thus, for 22.247458 Hz, the maximum damping factor was 0.017441.

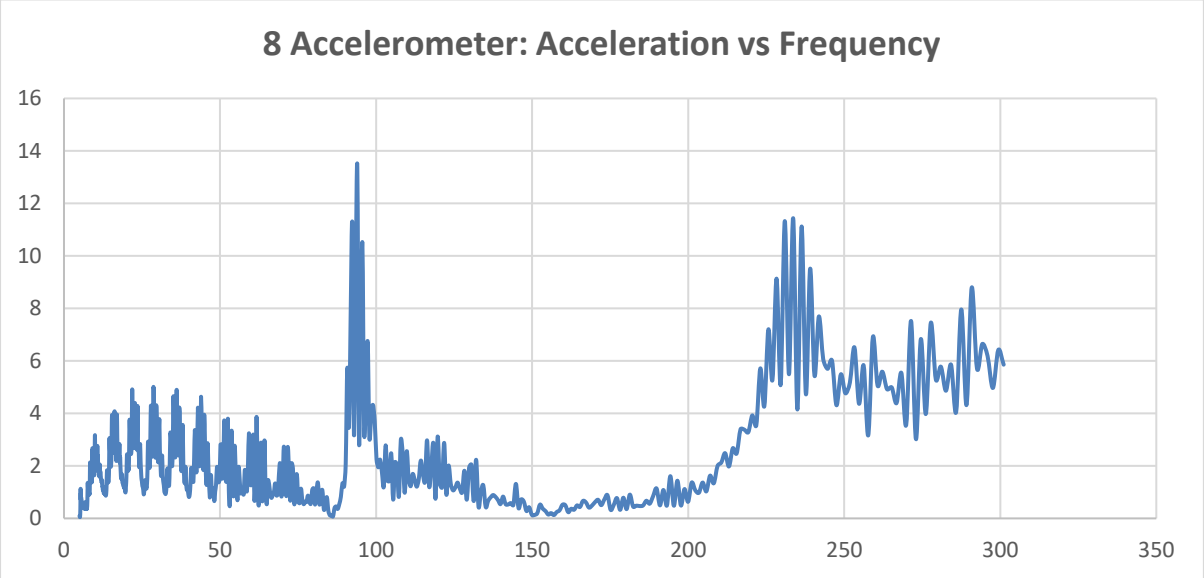

Figure B5: Acceleration (m/s^2) vs Frequency, channel 8, 35.93 kN (Test 1)

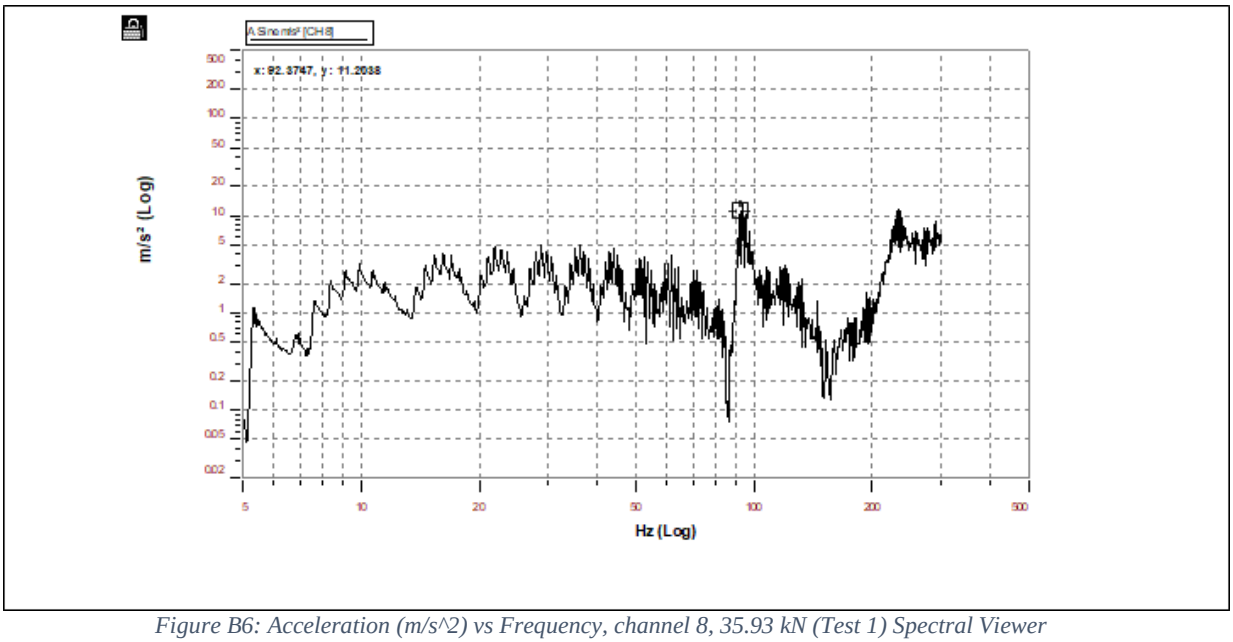

Figure B6: Acceleration (m/s^2) vs Frequency, channel 8, 35.93 kN (Test 1) Spectral Viewer

Table B3: Data Collected on Figure B5

Peak	X peak	x1 and x2	f1	f2	Fn	Change F	Q	Zeta
	Read on Graph	Xp/1.4142	Read on Graph x1	Read on Graph x2	Read on Graph Xpeak	F2-F1	Fn/(F2-F1)	1/2Q
1	4.89982	3.464729	36.102993	36.521572	36.102993	0.418579	86.2513241	0.011594
2	13.3809	9.461816	93.985878	94.529144	93.985878	0.543266	173.001583	0.00578
3	3.12068	2.206675	119.727524	120.419586	119.727524	0.692062	173.001153	0.00578
4	11.4388	8.088531	233.645248	234.995789	234.645248	1.350541	173.741669	0.005756

It is seen in Table B3 that the damping factor, ζ, ranges from 0.005756 to 0.011594. Thus, for 36.521572 Hz, the maximum damping factor was 0.011594.

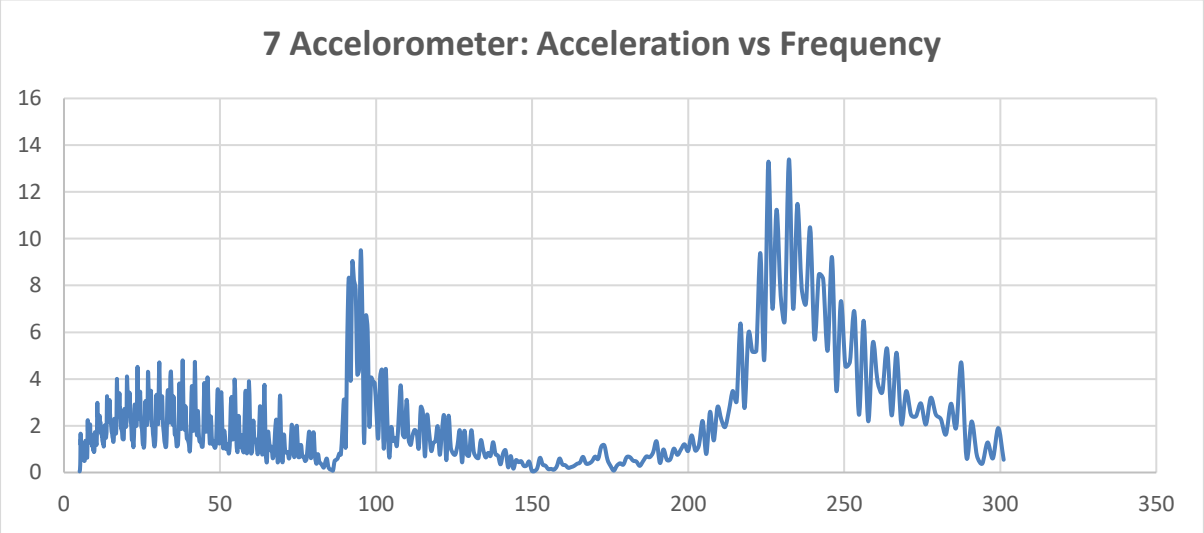

Figure B7: Acceleration (m/s^2) vs Frequency, channel 7, 35.93 kN (Test 1)

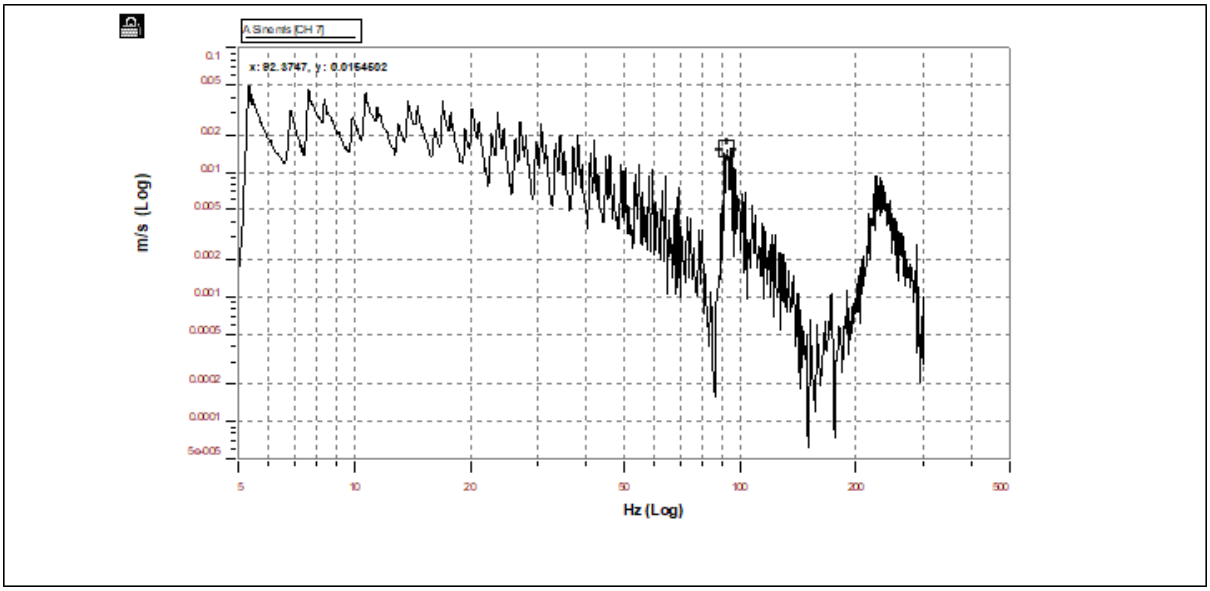

Figure B8: Acceleration (m/s^2) vs Frequency, channel 7, 35.93 kN (Test 1) Spectral Viewer

Table B4: Data Collected on Figure B7

Peak	X peak	x1 and x2	f1	f2	Fn	Change F	Q	Zeta
	Read on Graph	Xp/1.4142	Read on Graph x1	Read on Graph x2	Read on Graph Xpeak	F2-F1	Fn/(F2-F1)	1/2Q
1	4.79656	3.391713	38.025188	38.466053	38.025188	0.440865	86.2513196	0.011594
2	9.4558	6.686324	95.075554	96.177856	95.075554	1.102302	86.2518203	0.011594
3	13.3932	9.470513	232.302475	233.645248	232.302475	1.342773	173.002045	0.00578

It is seen in Table B4 that the damping factor, ζ, ranges from 0.00578 to 0.011594. Thus, for 38.466053Hz, the maximum damping factor was 0.011594.

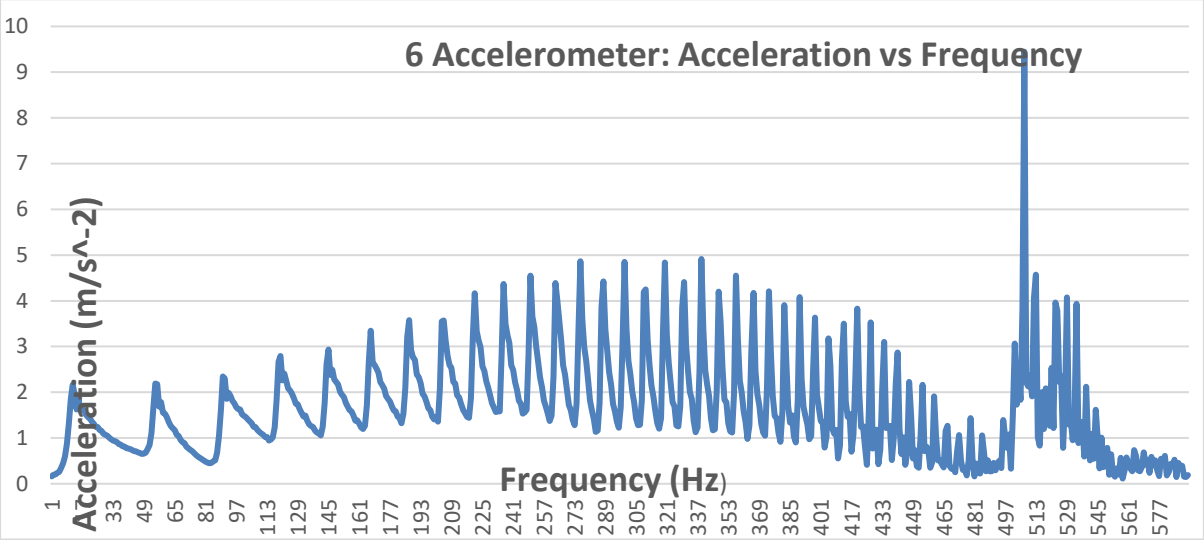

Figure B9: Acceleration (m/s^2) vs Frequency, channel 6, 35.93 kN (Test 1)

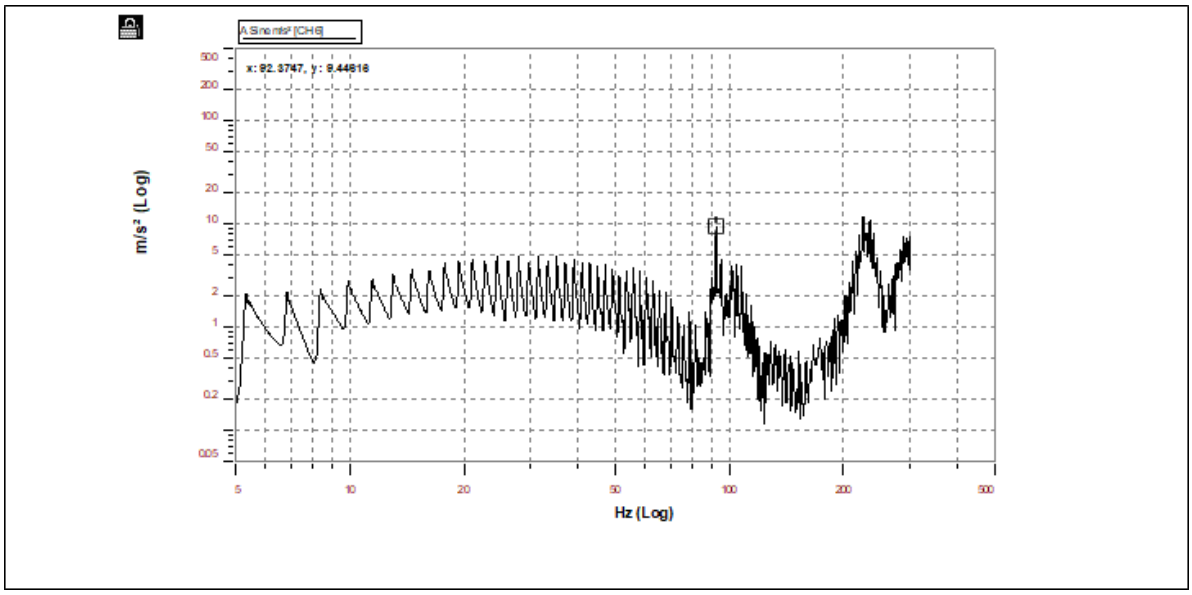

Figure B10: Acceleration (m/s^2) vs Frequency, channel 6, 35.93 kN (Test 1) Spectral Viewer

Table B5: Data Collected on Figure B9

Peak	X peak	x1 and x2	f1	f2	Fn	Change F	Q	Zeta
	Read on Graph	Xp/1.4142	Read on Graph x1	Read on Graph x2	Read on Graph Xpeak	F2-F1	Fn/(F2-F1)	1/2Q
1	4.91188	3.473257	35.077412	35.28017	35.077412	0.202758	173.001371	0.00578
2	9.44616	6.679508	92.374733	92.908691	92.374733	0.533958	172.999998	0.00578
3	11.8487	8.378376	225.703445	227.008087	225.703445	1.304642	173.000291	0.00578

It is seen in Table B5 that the damping factor, $\zeta$was 0.00578.

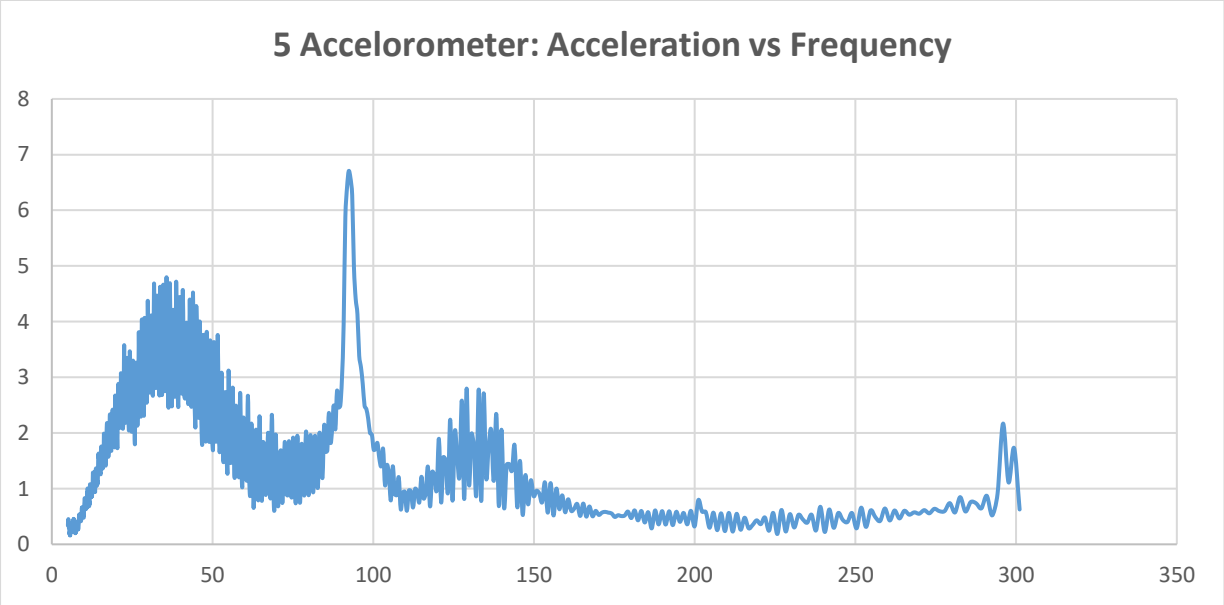

Figure B11: Acceleration (m/s^2) vs Frequency, channel 5, 45 kN (Test 1)

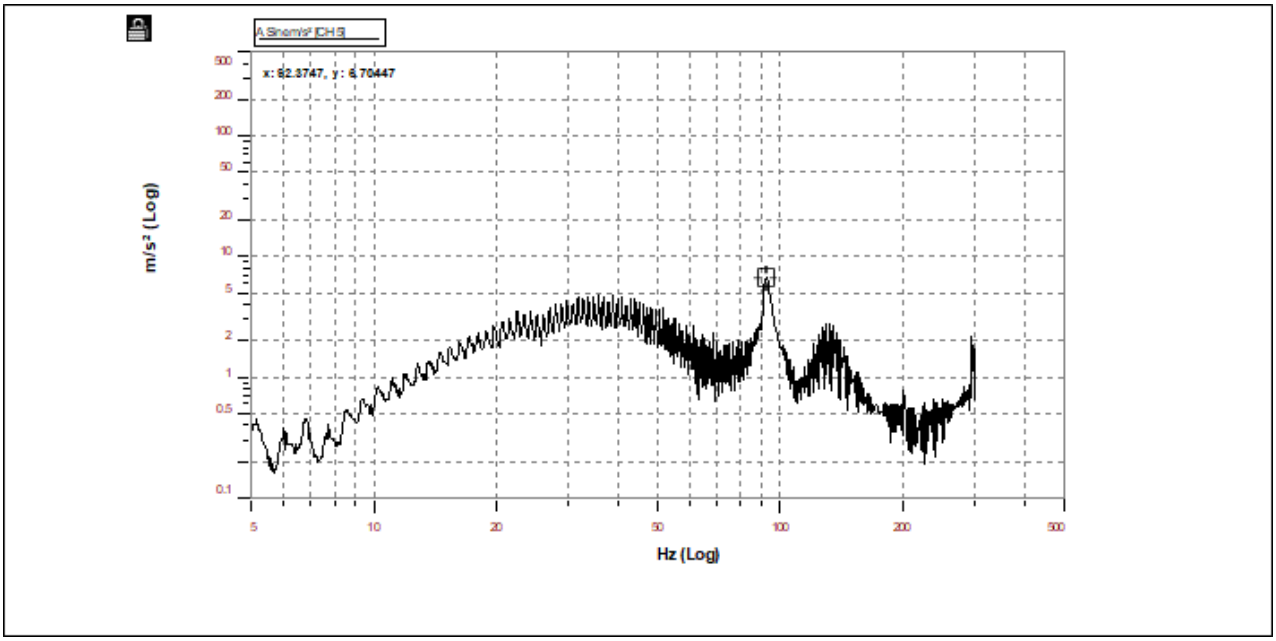

Figure B12: Acceleration (m/s^2) vs Frequency, channel 5, 45 kN (Test 1) Spectral Viewer

Table B6: Data Collected on Figure B11

Peak	X peak	x1 and x2	f1	f2	Fn	Change F	Q	Zeta
	Read on Graph	Xp/1.4142	Read on Graph x1	Read on Graph x2	Read on Graph Xpeak	F2-F1	Fn/(F2-F1)	1/2Q
1	4.79752	3.392391	35.689209	36.31168	35.689209	0.622471	57.3347337	0.017441
2	6.5801	4.652878	91.843849	94.529144	92.908691	2.685295	34.599063	0.028903
3	2.79811	1.978582	129.04306	129.788971	129.04306	0.745911	173.000613	0.00578

It is seen in Table B6 that the damping factor, ζ, ranges from 0.00578 to 0.017441. Thus, for 36.31168 Hz, the maximum damping factor was 0.017441.

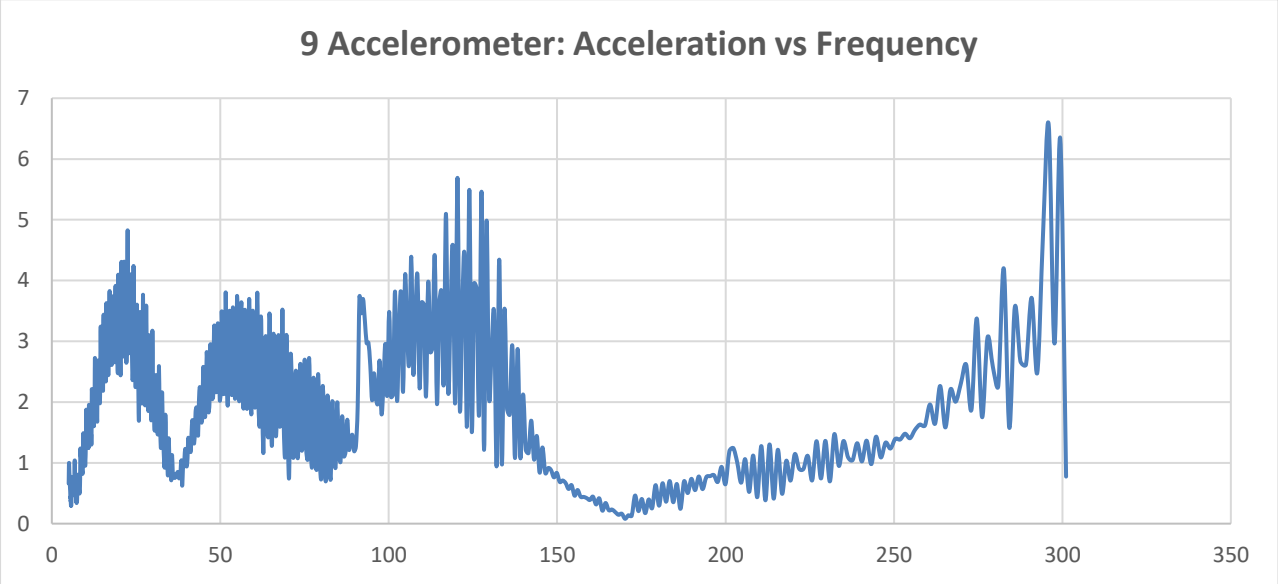

Figure B13: Acceleration (m/s^2) vs Frequency, channel 9, 45 kN (Test 1)

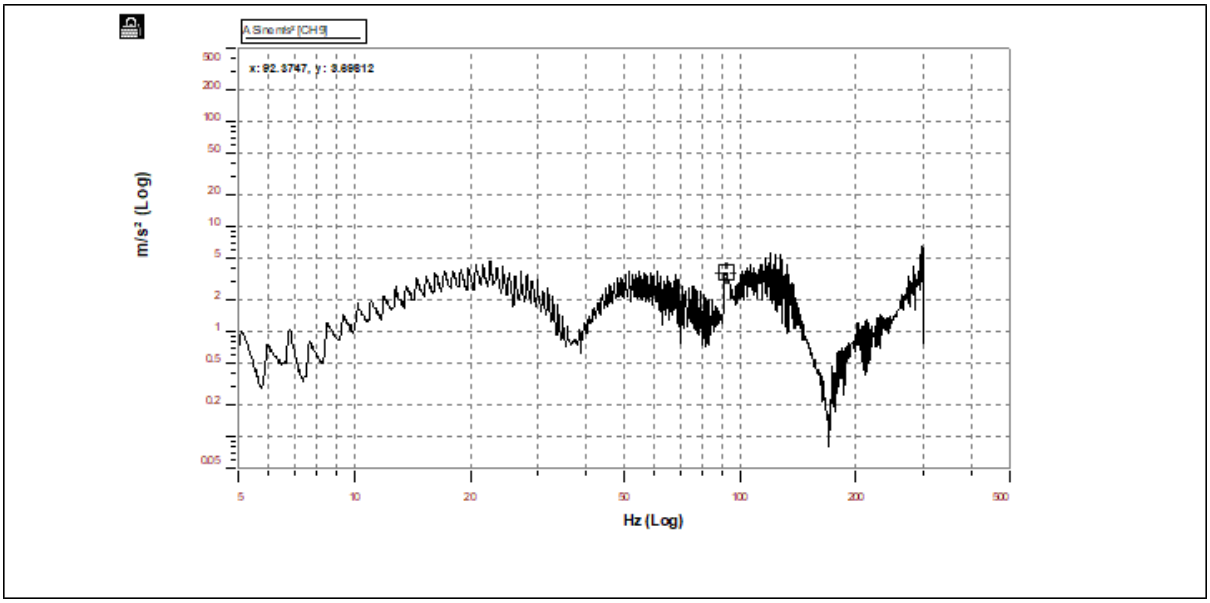

Figure B14: Acceleration (m/s^2) vs Frequency, channel 9, 45 kN (Test 1) Spectral Viewer

Table B7: Data Collected on Figure B13

Peak	X peak	x1 and x2	f1	f2	Fn	Change F	Q	Zeta
	Read on Graph	Xp/1.4142	Read on Graph x1	Read on Graph x2	Read on Graph Xpeak	F2-F1	Fn/(F2-F1)	1/2Q
1	4.82677	3.413075	22.505394	22.897919	22.505394	0.392525	57.3349315	0.017441
2	3.80597	2.691253	51.610397	51.908758	51.610397	0.298361	172.979702	0.005781
3	5.69016	4.023589	120.419586	121.115654	120.419586	0.696068	172.999744	0.00578

It is seen in Table B7 that the damping factor, ζ, ranges from 0.00578 to 0.017441. Thus, for 22.897919 Hz, the maximum damping factor was 0.017441.

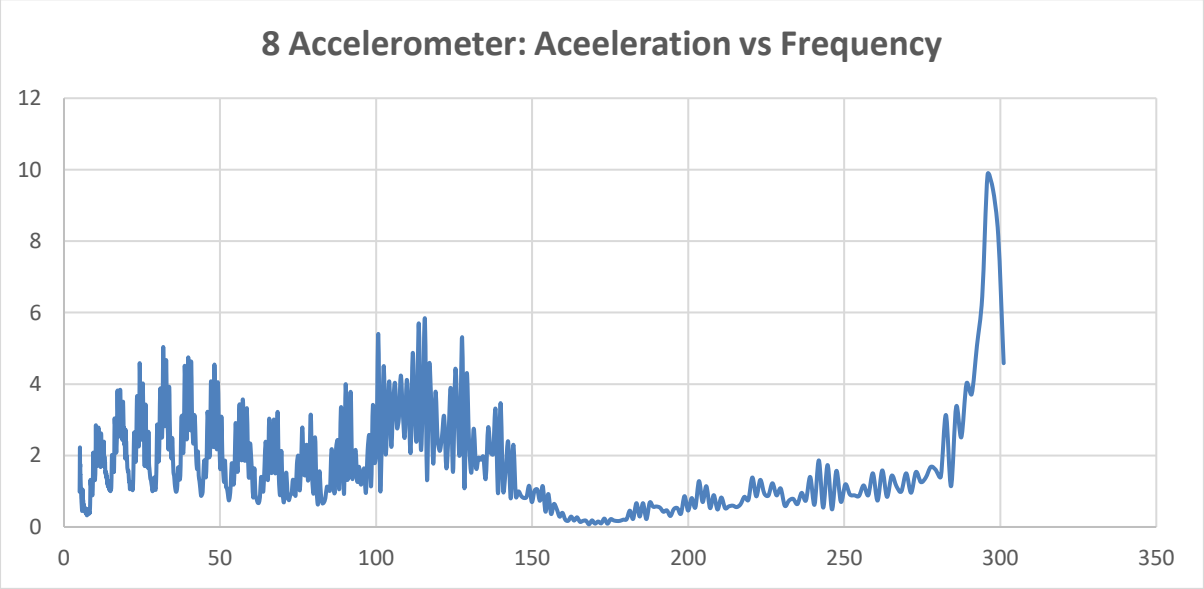

Figure B15: Acceleration (m/s^2) vs Frequency, channel 8, 45 kN (Test 1)

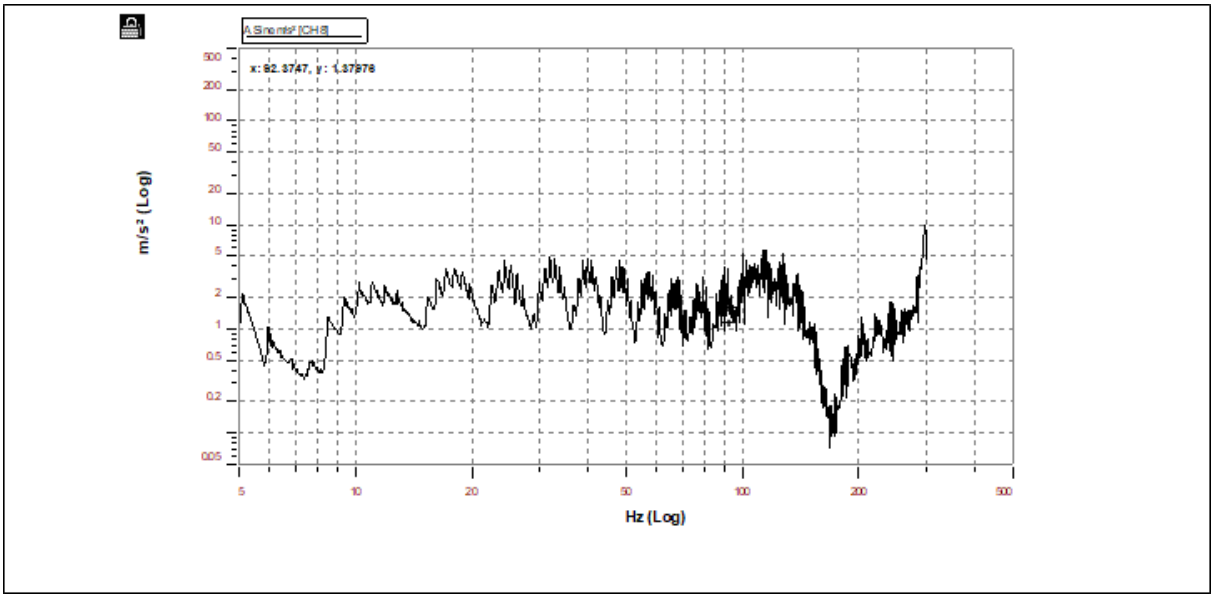

Figure B16: Acceleration (m/s^2) vs Frequency, channel 8, 45 kN (Test 1) Spectral Viewer

Table B8: Data Collected on Figure B15

Peak	X peak	x1 and x2	f1	f2	Fn	Change F	Q	Zeta
	Read on Graph	Xp/1.4142	Read on Graph x1	Read on Graph x2	Read on Graph Xpeak	F2-F1	Fn/(F2-F1)	1/2Q
1	5.03828	3.562636	31.803459	32.172188	31.803459	0.368729	86.2515804	0.011594
2	5.79352	4.096677	115.657883	116.326424	115.657883	0.668541	173.000434	0.00578
3	1.7345	1.226488	244.670715	246.084991	244.670715	1.414276	173.000684	0.00578

It is seen in Table B8 that the damping factor, ζ, ranges from 0.00578 to 0.011594. Thus, for 31.172188Hz, the maximum damping factor was 0.011594.

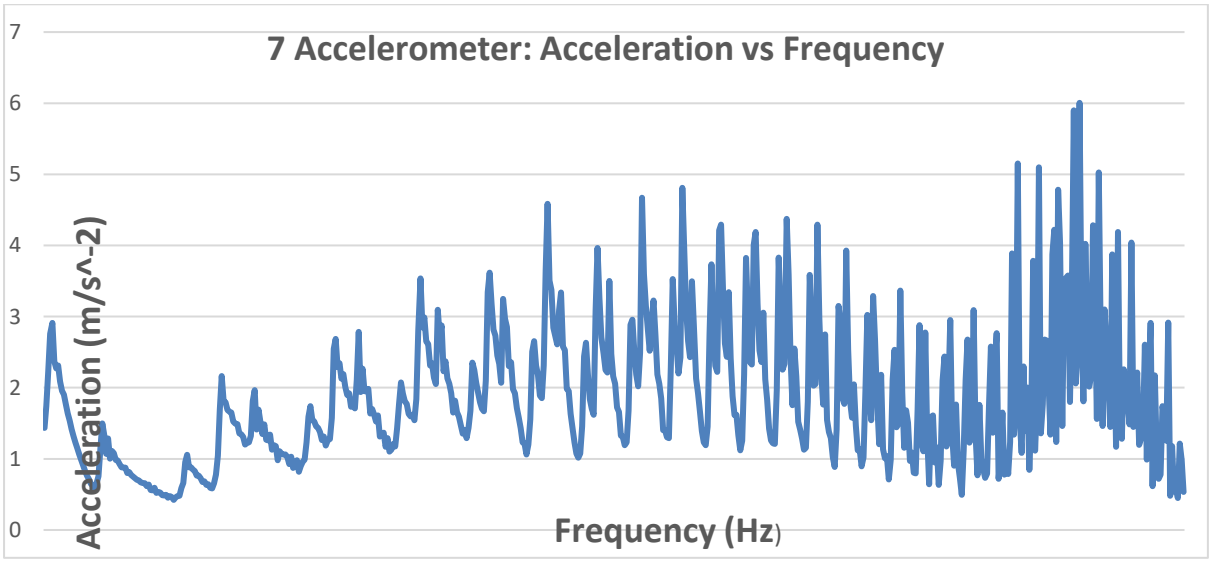

Figure B17: Acceleration (m/s^2) vs Frequency, channel 7, 45 kN (Test 1)

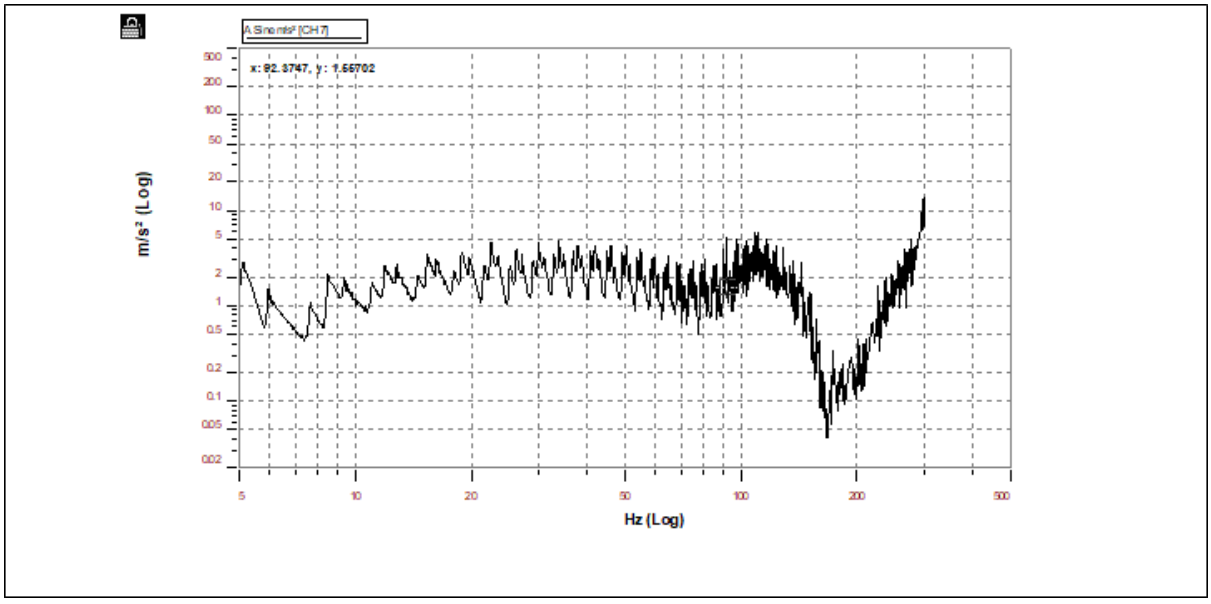

Figure B18: Acceleration (m/s^2) vs Frequency, channel 7, 45 kN (Test 1) Spectral Viewer

Table B9: Data Collected on Figure B17

Peak	X peak	x1 and x2	f1	f2	Fn	Change F	Q	Zeta
	Read on Graph	Xp/1.4142	Read on Graph x1	Read on Graph x2	Read on Graph Xpeak	F2-F1	Fn/(F2-F1)	1/2Q
1	4.81205	3.402666	33.690361	34.277966	33.690361	0.587605	57.3350482	0.017441
2	6.00509	4.246281	110.446053	111.084465	110.446053	0.638412	173.001217	0.00578
3	13.3932	9.470513	256.216461	257.697449	256.216461	1.480988	173.003739	0.00578

It is seen in Table B9 that the damping factor, ζ, ranges from 0.00578 to 0.017441. Thus, for 34.277966 Hz, the maximum damping factor was 0.017441.

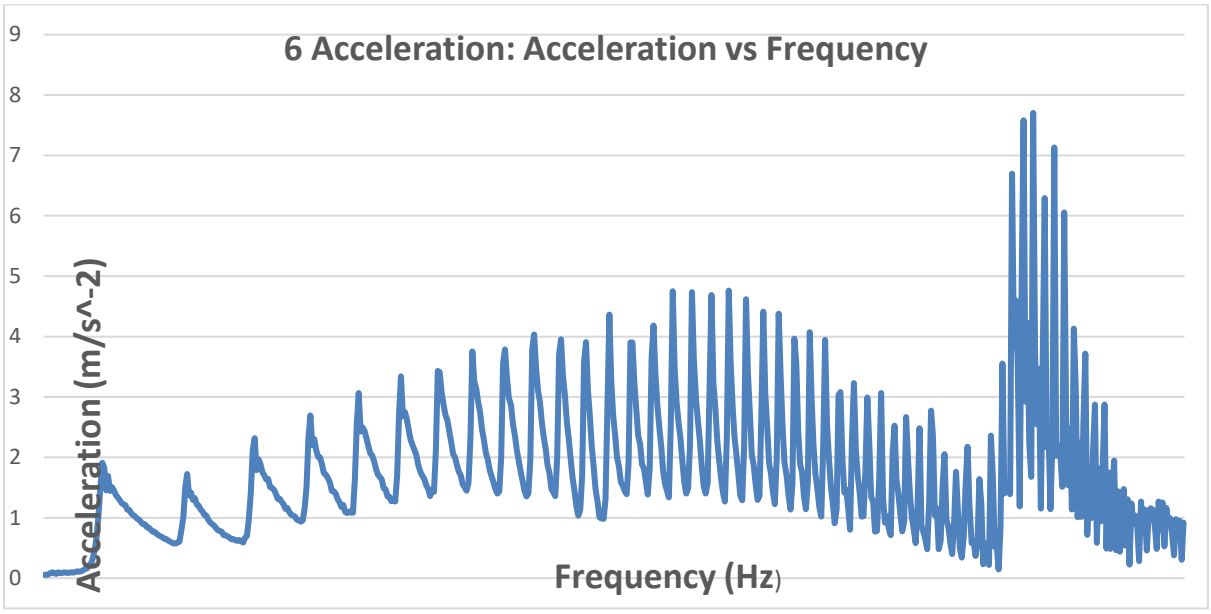

Figure B19: Acceleration (m/s^2) vs Frequency, channel 6, 45 kN (Test 1)

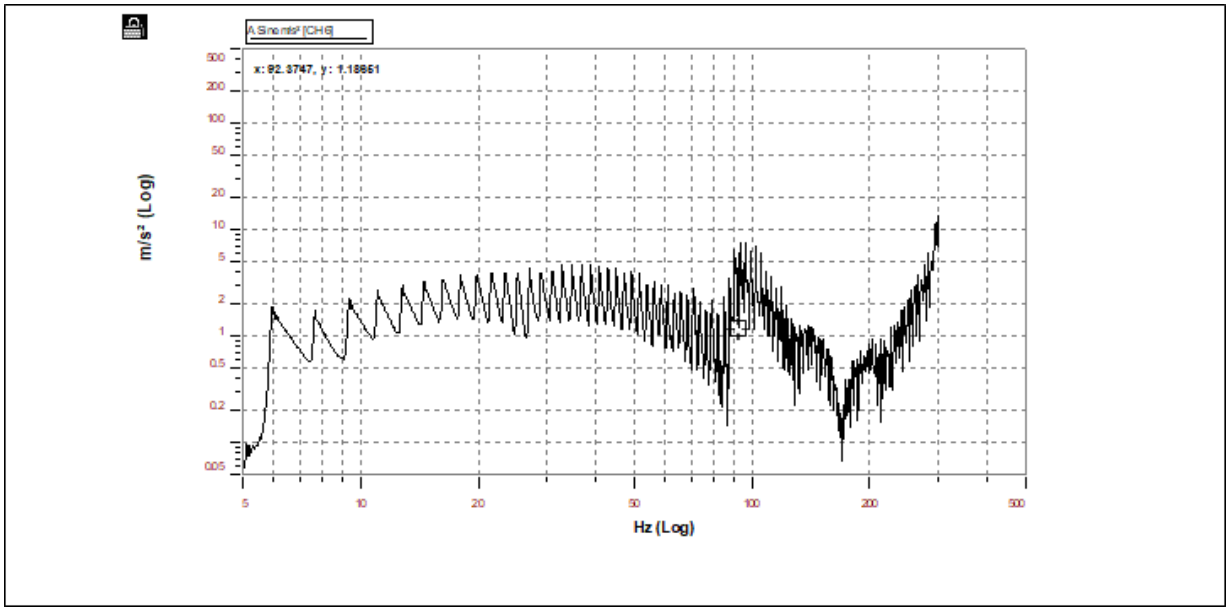

Figure B20: Acceleration (m/s^2) vs Frequency, channel 6, 45 kN (Test 1) Spectral Viewer

Table B10: Data Collected on Figure B19

Peak	X peak	x1 and x2	f1	f2	Fn	Change F	Q	Zeta
	Read on Graph	Xp/1.4142	Read on Graph x1	Read on Graph x2	Read on Graph Xpeak	F2-F1	Fn/(F2-F1)	1/2Q
1	4.76103	3.366589	38.688396	39.363174	38.688396	0.674778	57.3349991	0.017441
2	7.70349	5.447242	96.177856	96.733795	96.177856	0.555939	173.000736	0.00578
3	0.948563	0.670742	203.461319	204.63739	203.461319	1.176071	173.000881	0.00578

It is seen in Table 10 that the damping factor, ζ, ranges from 0.00578 to 0.017441. Thus, for 39.363174 Hz, the maximum damping factor was 0.017441.

\

APPENDIX III

RESULTS FOR FREE VIBRATION METHOD ON TERN CONDUCTOR

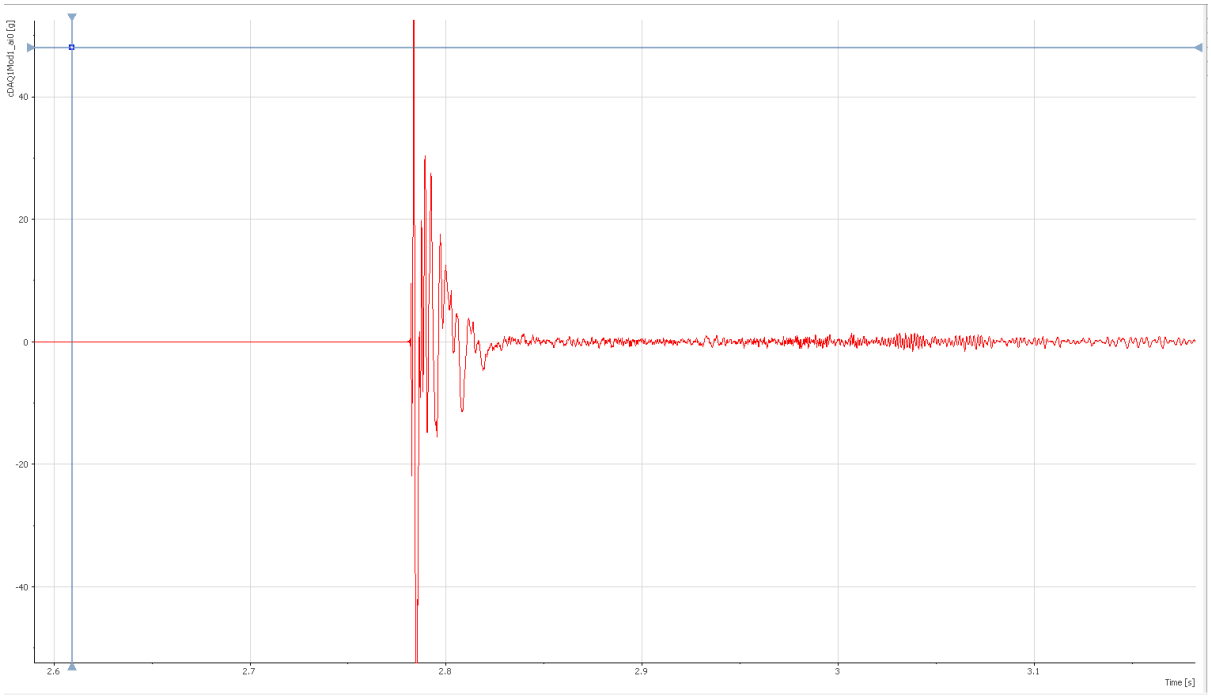

Figure C1: Free Vibration, Accelerometer (0) Mode 1, 33 kN (Test1) National Instrument Desk

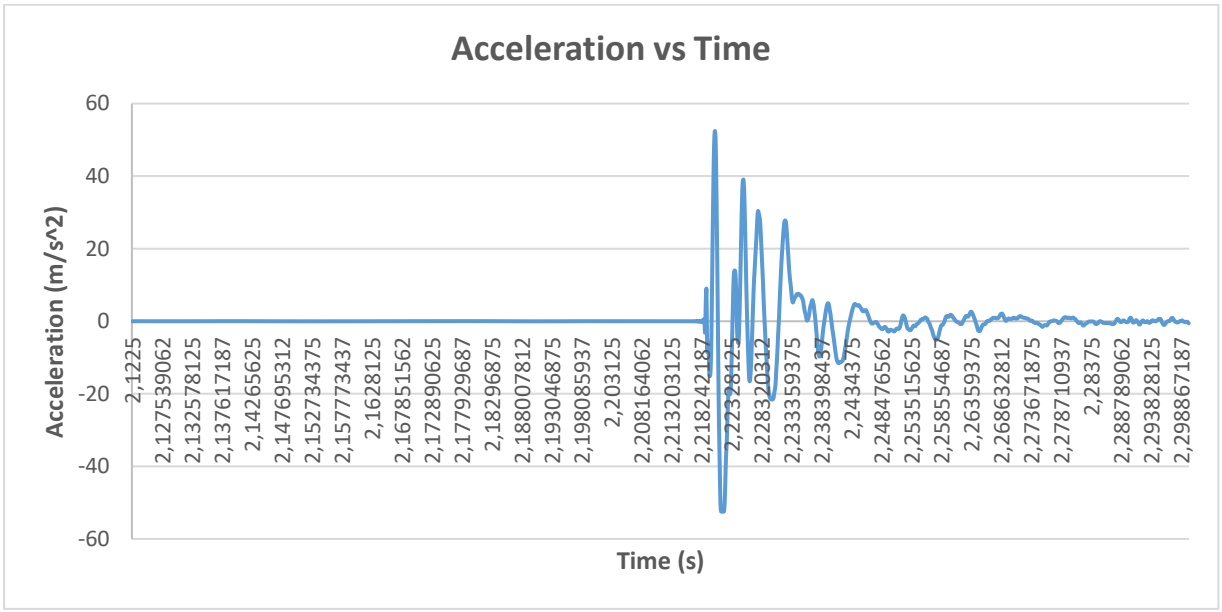

Figure C2: Free Vibration, Accelerometer 0, 33 kN (Test 1)

The results in Table C1 below were calculated using results obtained from Figure C2 and were as follow:

The first row in Table C1 below displayed the calculated results. Px was the time (ms) and Py was the acceleration (m/s^-2) where both values were used to calculate the information of Table C1. The first loop used the least-squares method, the log decrement was 1.5, the damping factor was 0.232, and the natural frequency was identified as 170.298 rad/s.

Table C1: Calculated Data Collected in Figure C2

Px	Py	Period	Freq	In Py	Yj	In Py (Yj)	Yj^2	Zj	Log Dec	Zeta	Nat Freq	Nat Freq
s	m/s^2	s	Hz								rad/s	Hz
2.220586	50.68298077	0	0	3.92559	0	0	0	2.151487	1.5	0.232	1702.298	270.9293
2.225273	39.07219587	0.004687	213.3333	3.665411	1	3.665411	1	0.651487				
2.227969	28.8889892	0.002695	371.0144	3.363461	2	6.726921	4	-0.84851				
Sum	118.6441658			10.95446	3	13.95446	5					

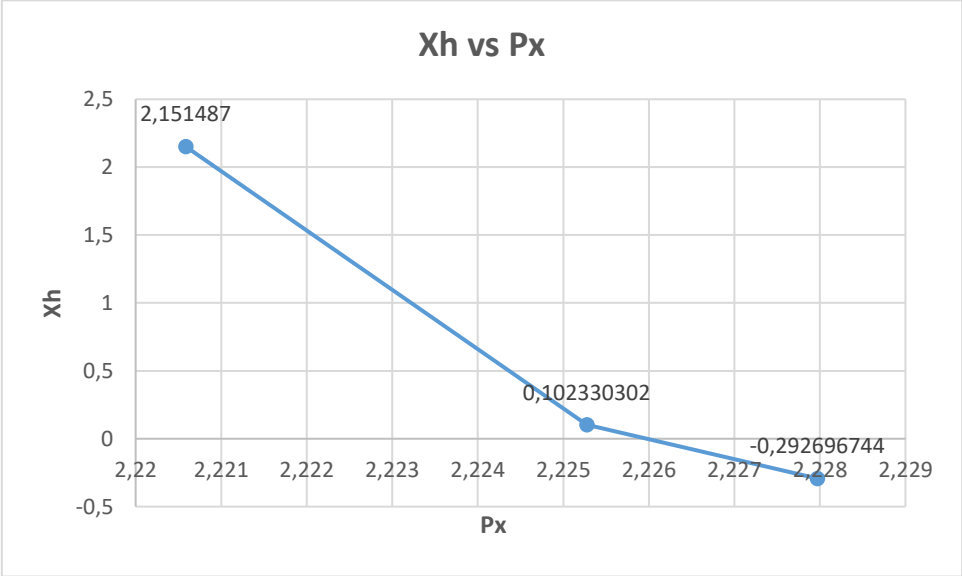

Figure C3: (Xh) vs (Px)

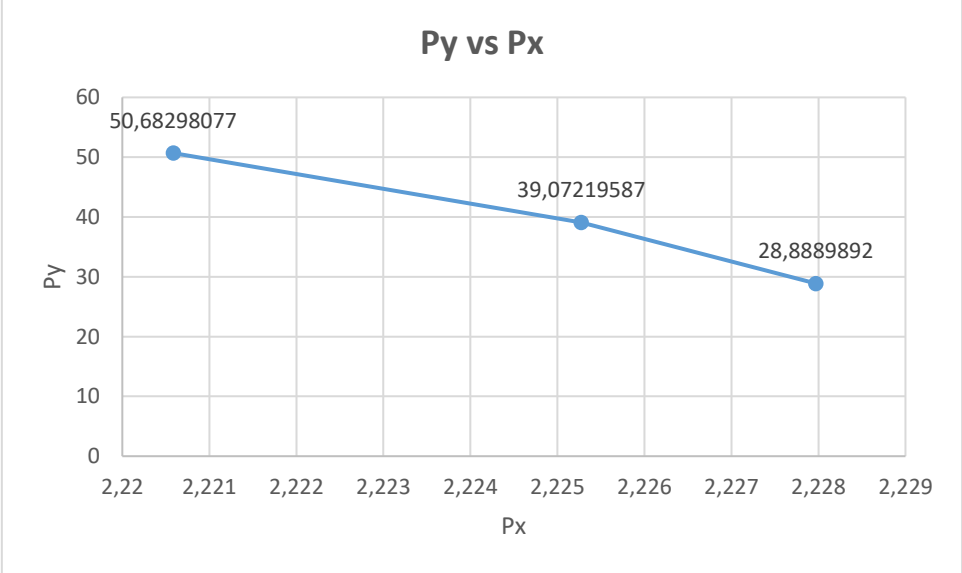

Figure C4:(Py) vs (Px)

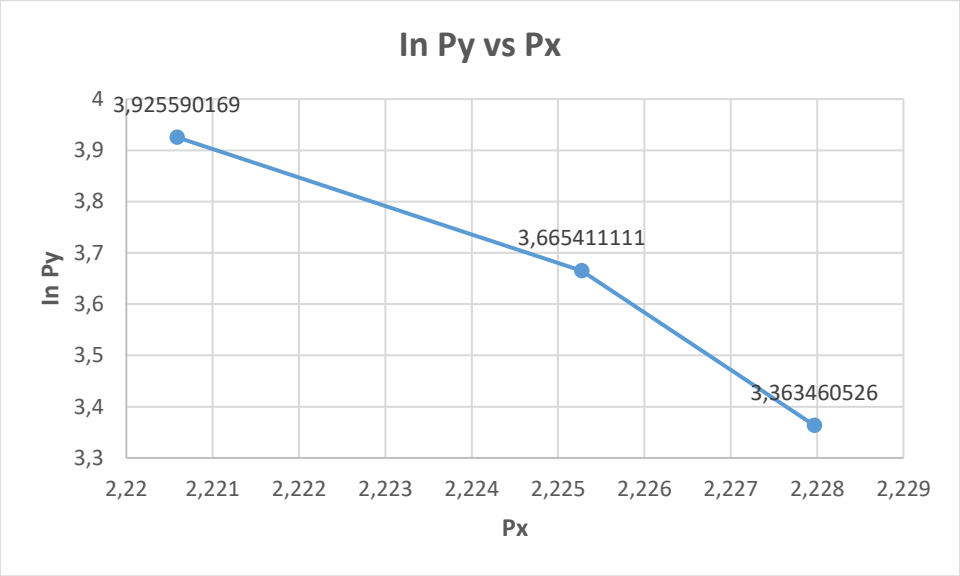

Figure C5: (InPy) vs (Px)

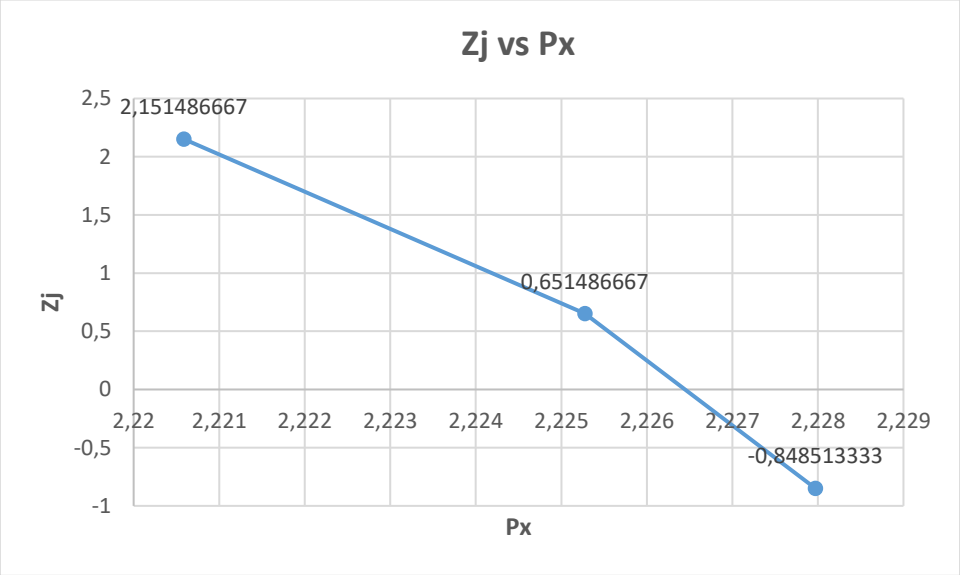

Figure C6:(Zj) vs (Px)

- Figure C3 to C5 in the X-value expanded and the Y-value diminished.

  This means:
- The value of Xh diminished as the time (Px) increased which subsequently implied Xh was inversely corresponding to the time (Px).
- The value of acceleration (Py) decreased as the time (Px) increased which meant Py was inversely proportional to the time (Px).

- The value of Acceleration (In Py) decreased as the time (Px) increased which meant In Py was inversely proportional to the time (Px).

- (Figure C3-C6) obtained from the different results of the Tern conductor where the cable tension of 33 kN appeared to be a similar shape. The value of Zj decreased as the time (Px) increased which meant Zj was inversely proportional to the time (Px).

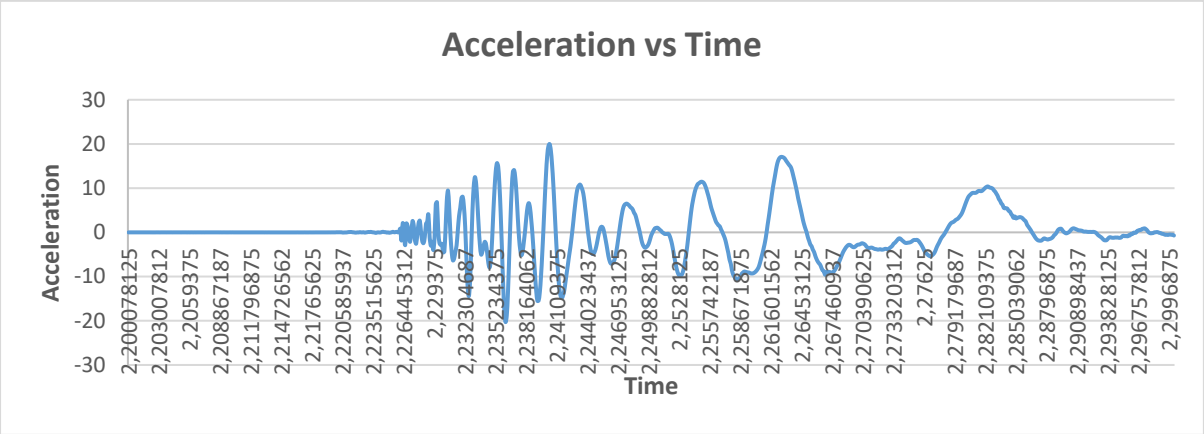

Figure C7: Free Vibration, Accelerometer 1, 33 kN (Test 1)

The results in Table C2 below were calculated using results obtained from Figure 177 and were as follow:

The first row in Table C2 below displayed the calculated results. Px was the time (ms) and Py was the acceleration (m/s^-2) where both values were used to calculate the information of Table C2. The first loop used the least-squares method, the log decrement was 1.5, the damping factor was 0.232, and the natural frequency was identified as 4288.864 rad/s.

Table C2: Calculated Data Collected in Figure C7

Px	Py	Period	Freq	In Py	Yj	In Py (Yj)	Yj^2	Zj	Log Dec	Zeta	Nat Freq	Nat Freq
s	m/s^2	s	Hz								rad/s	Hz
2.235469	14.8414327	0	0	2.697423	0	0	0	0.902037	1.5	0.232	4288.864	682.5939
2.236875	13.709906	0.001406	711.1111	2.618119	1	2.618119	1	-0.59796				
2.238398	6.623092563	0.001523	656.4105	1.890562	2	3.781125	4	-2.09796				
Sum	35.17443126			7.206104	3	10.2061	5					

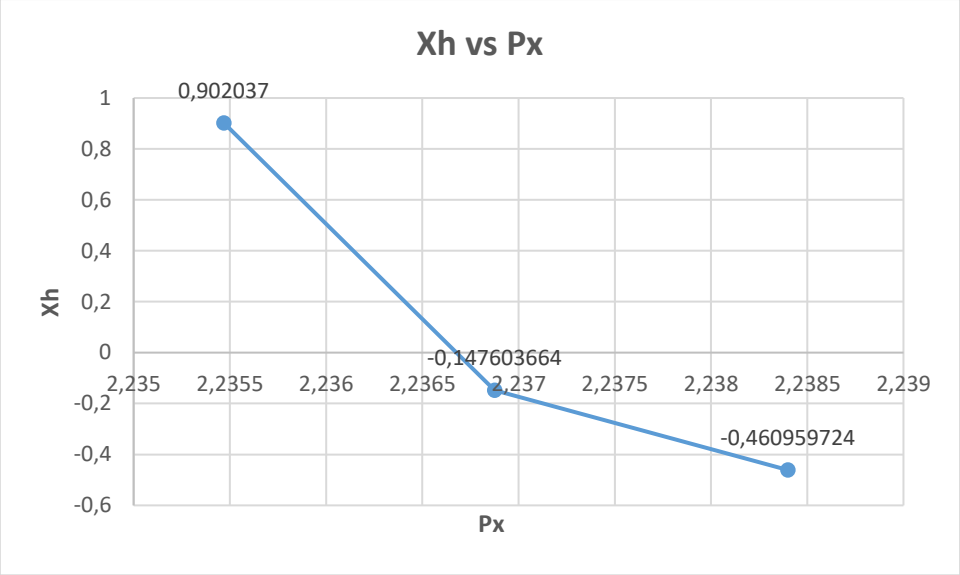

Figure C8: (Xh) vs (Px)

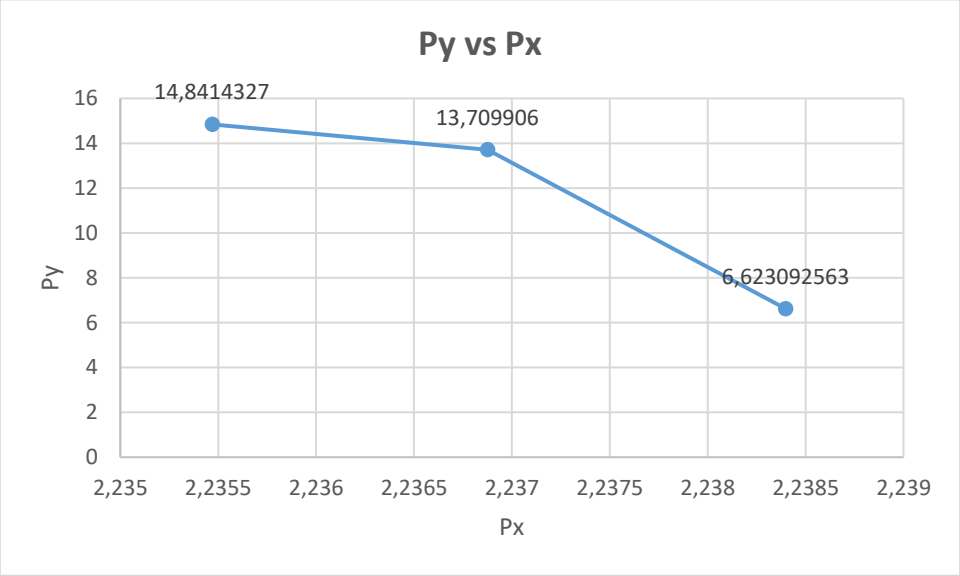

Figure C9: (Py) vs (Px)

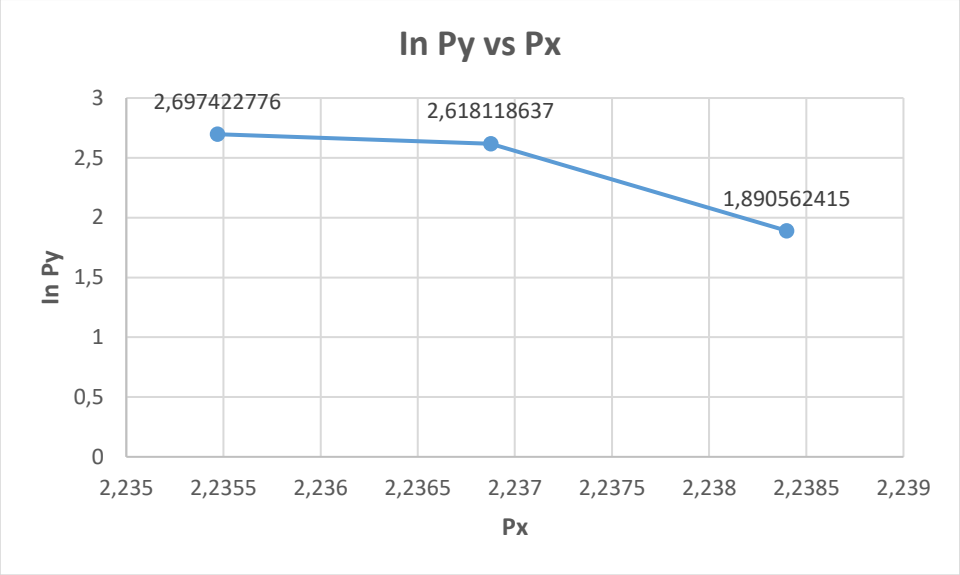

Figure C10: (InPy) vs (Px)

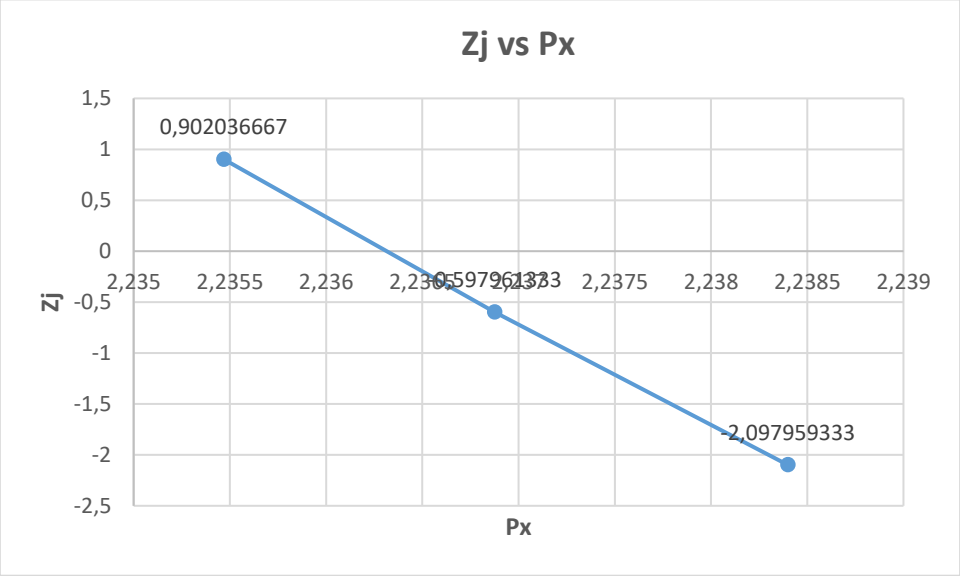

Figure C11: (Zj) vs (Px)

- Figure C8 to C10 in the X-value expanded and the Y-value diminished.
  This means:
- The value of Xh diminished as the time (Px) increased which subsequently implied Xh was inversely corresponding to the time (Px).
- The value of acceleration (Py) decreased as the time (Px) increased which meant Py was inversely proportional to the time (Px).

- The value of Acceleration (In Py) decreased as the time (Px) increased which meant In Py was inversely proportional to the time (Px).
- (Figure C8-C11) obtained from the different results of the Tern conductor where the cable tension of 33 kN appeared to be a similar shape. The value of Zj decreased as the time (Px) increased which meant Zj was inversely proportional to the time (Px).

Results for Free Vibration, Accelerometer 1, Mode 1, (Test 1), 33kN Peak 2

The results in Table C3 below were calculated using results obtained from Figure 177 and were as follow:

The first row in Table C3 below displayed the calculated results. Px was the time (ms) and Py was the acceleration (m/s^-2) where both values were used to calculate the information of Table C3. The first loop used the least-squares method, the log decrement was 1.5, the damping factor was 0.232, and the natural frequency was identified as 2493.328 rad/s.

Table C3: Calculated Data Collected in Figure C11

Px	Py	Period	Freq	In Py	Yj	In Py (Yj)	Yj^2	Zj	Log Dec	Zeta	Nat Freq	Nat Freq
s	m/s^2	s	Hz								rad/s	Hz
2.240391	19.98736551	0	0	2.9951	0	0	0	0.339507	1.5	0.232	2493.328	396.8254
2.243438	10.20082537	0.003047	328.2051	2.322469	1	2.322469	1	-1.16049				
2.24543	1.222567601	0.001992	501.9609	0.200953	2	0.401906	4	-2.66049				
Sum	31.41075848			5.518522	3	8.518522	5					

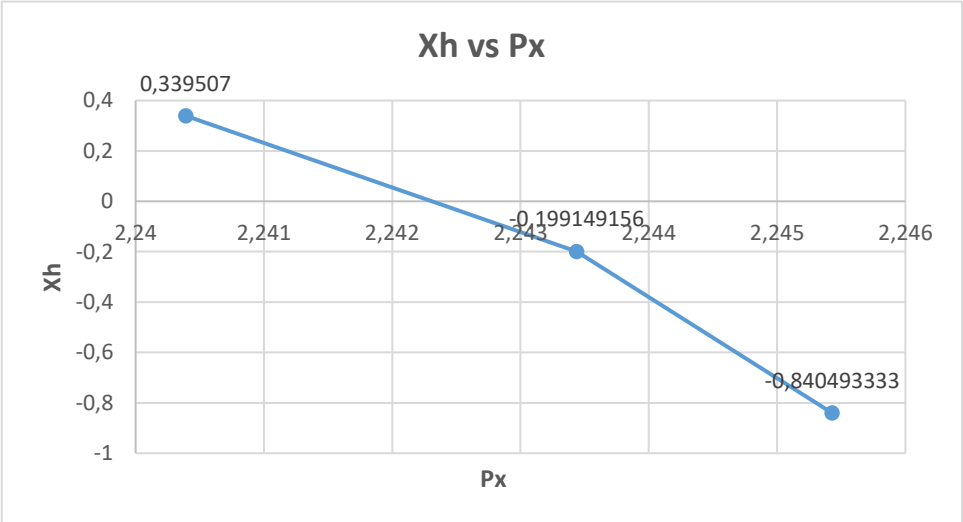

Figure C12: (Xh) vs (Px)

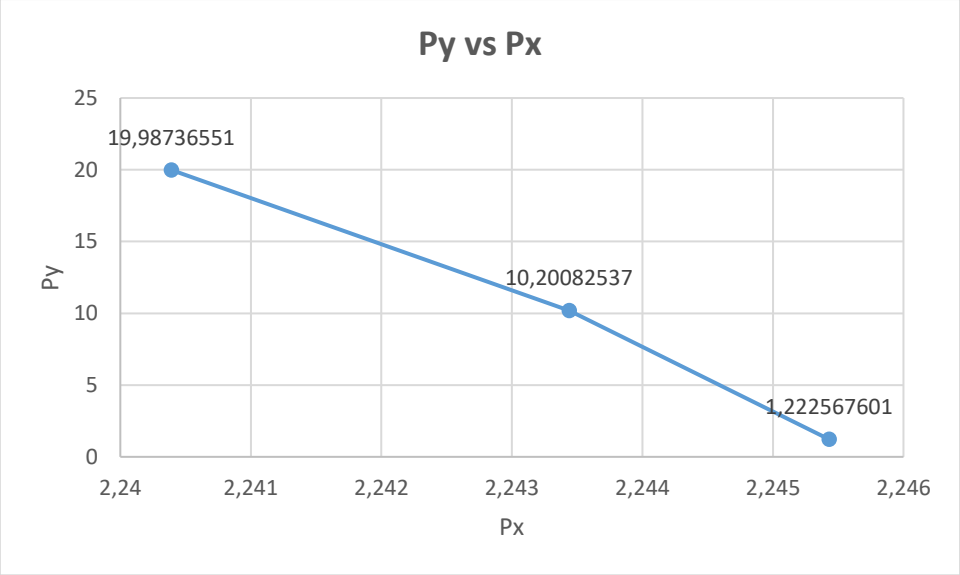

Figure C13: (Py) vs (Px)

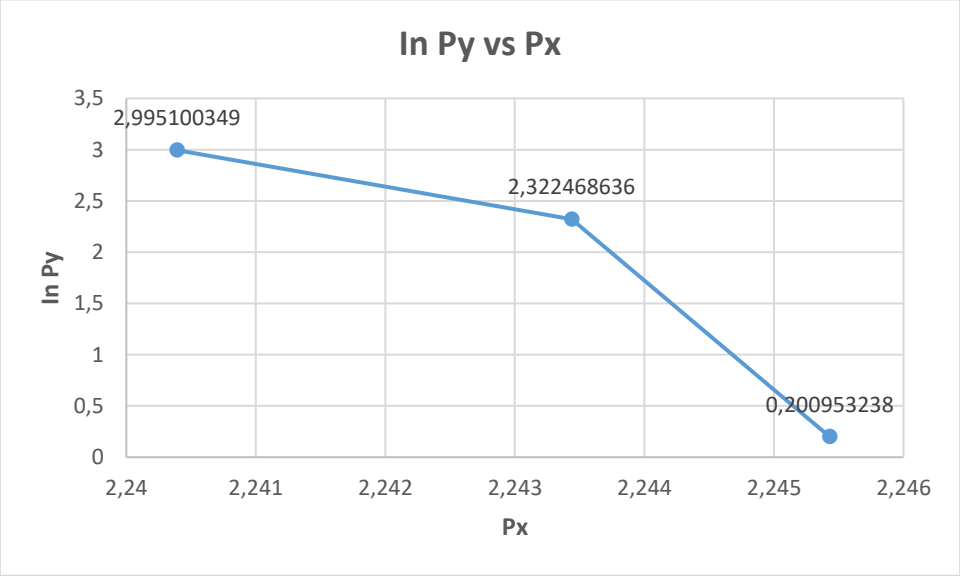

Figure C14: (In Py) vs (Px)

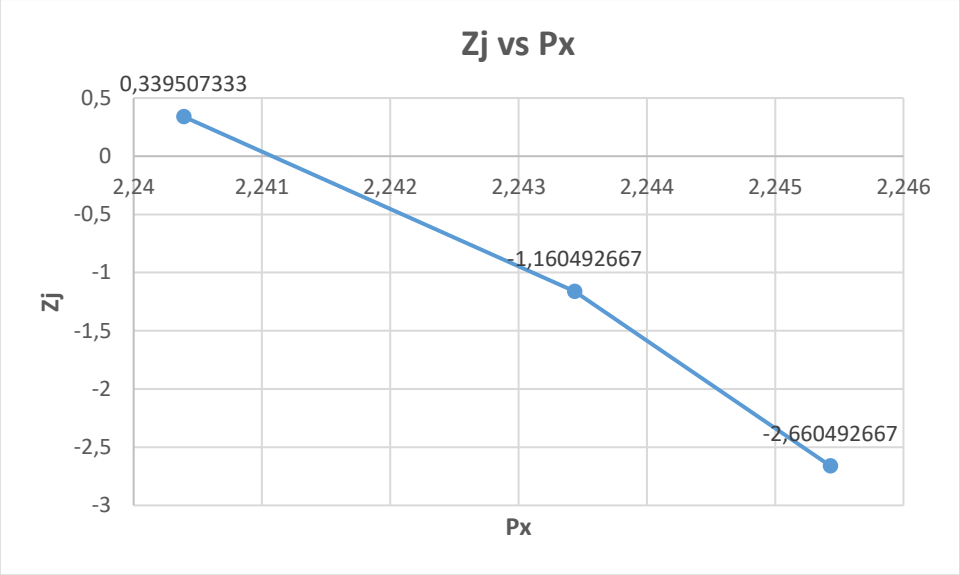

Figure C15: (Zj) vs (Px)

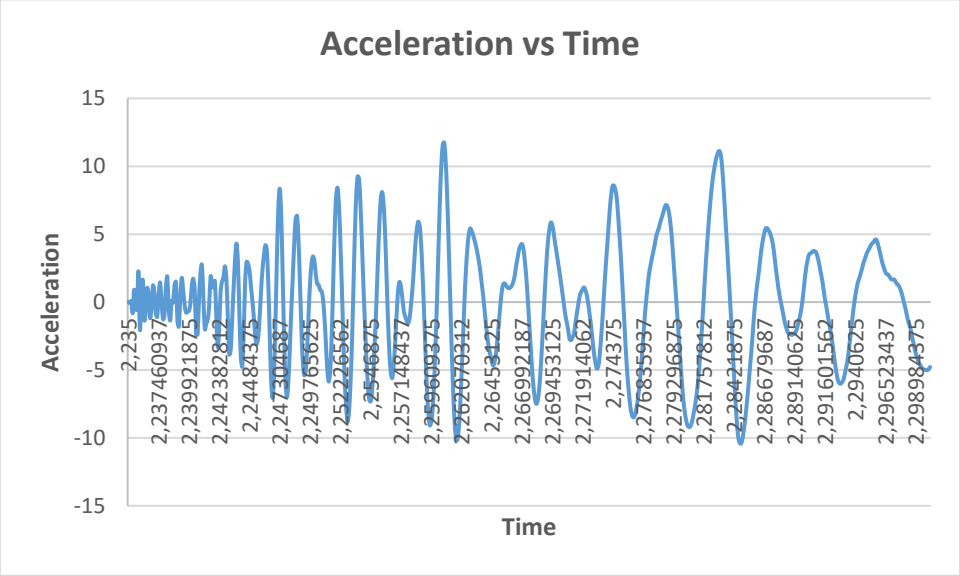

Figure C16: Free Vibration, Accelerometer 2, Mode 1, 33 kN (Test 1) Peak 1

The results in Table C4 below were calculated using results obtained from Figure 186 and were as follow:

The first row in Table C4 below displayed the calculated results. Px was the time (ms) and Py was the acceleration (m/s^-2) where both values were used to calculate the information of Table C4. The first loop used the least-squares method, the log decrement was 1.5, the damping factor was 0.232, and the natural frequency was identified as 4661.117 rad/s.

Table C4: Calculated Data Collected in Figure C16

Px	Py	Period	Freq	In Py	Yj	In Py (Yj)	Yj^2	Zj	Log Dec	Zeta	Nat Freq	Nat Freq
s	m/s^2	s	Hz								rad/s	Hz
2.247305	8.357127007	0	0	2.123115	0	0	0	0.228153	1.5	0.232	4661.117	741.8398
2.248711	6.338833241	0.001406	711.1111	1.846695	1	1.846695	1	-1.27185				
2.25	3.369110732	0.001289	775.7573	1.214649	2	2.429298	4	-2.77185				
Sum	18.06507098			5.184458	3	8.184458	5					

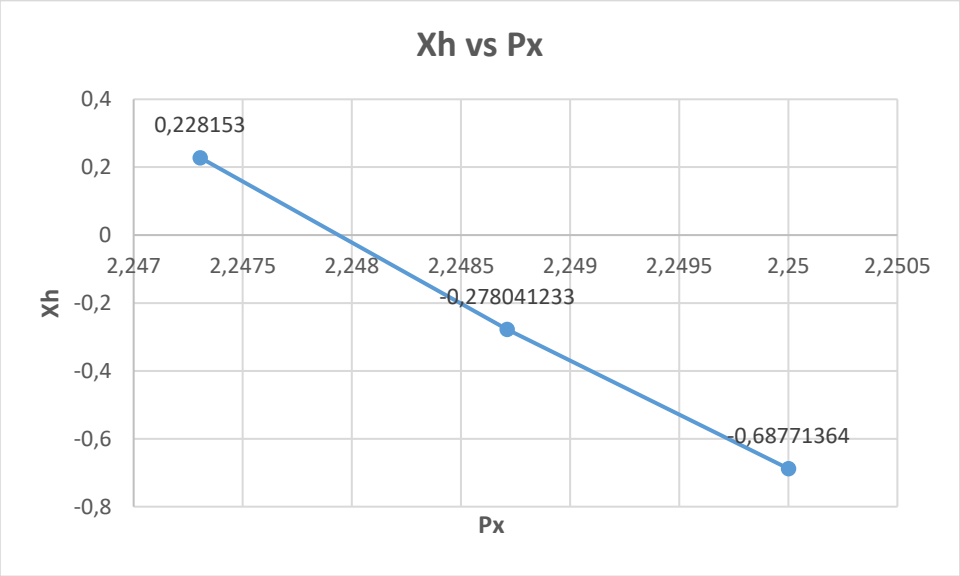

Figure C17: (Xh) vs (Px)

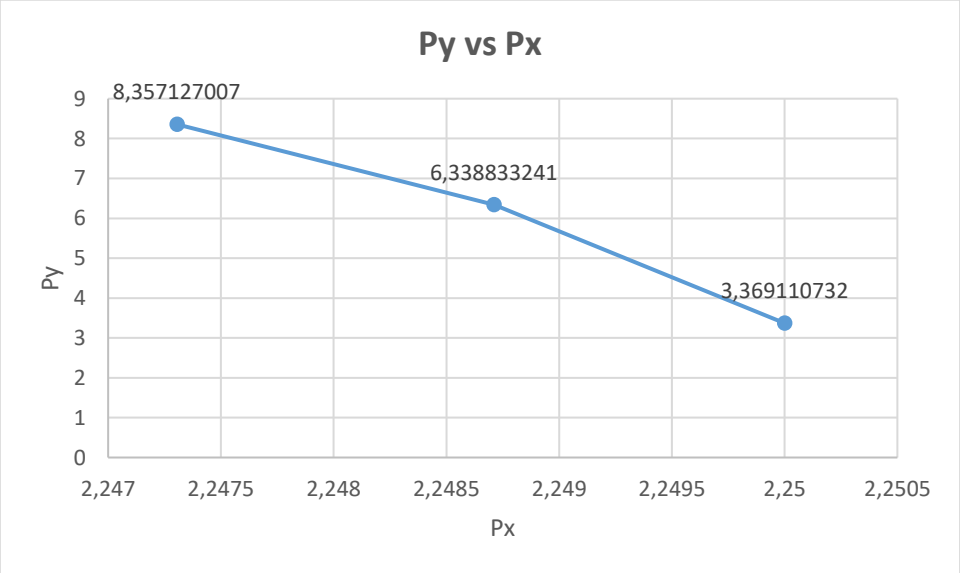

Figure C18: (Py) vs (Px)

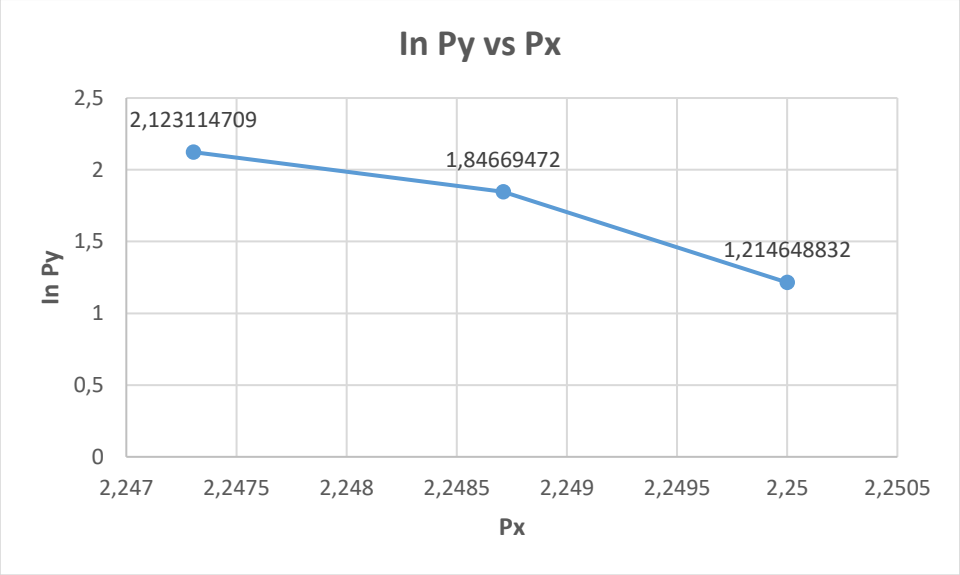

Figure C19: (In Py) vs (Px)

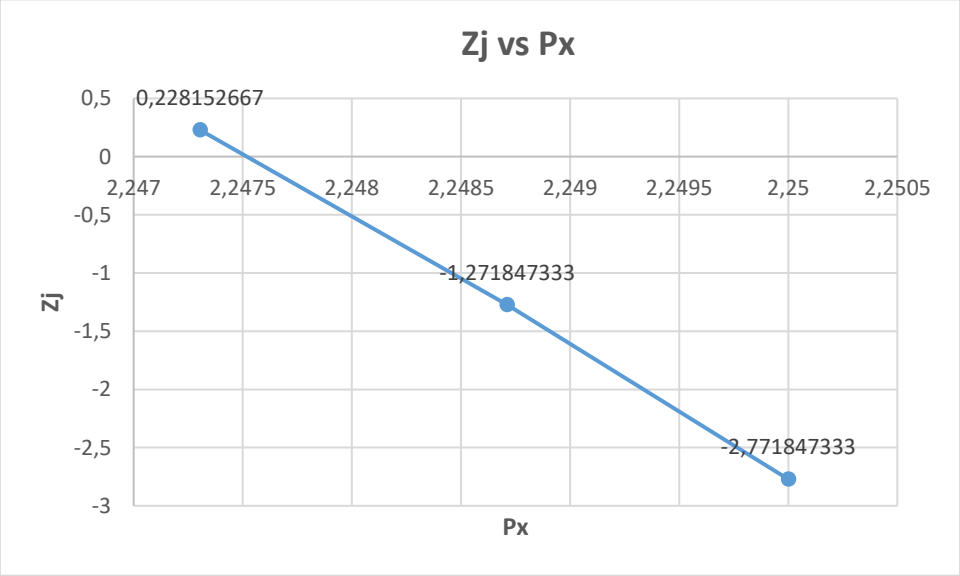

Figure C20: (Zj) vs (Px)

- Figure C17 to C19 in the X-value expanded and the Y-value diminished.
  This means:
- The value of Xh diminished as the time (Px) increased which subsequently implied Xh was inversely corresponding to the time (Px).
- The value of acceleration (Py) decreased as the time (Px) increased which meant Py was inversely proportional to the time (Px).

- The value of Acceleration (In Py) decreased as the time (Px) increased which meant In Py was inversely proportional to the time (Px).
- (Figure C17) obtained from the different results of the Tern conductor where the cable tension of 33 kN appeared to be a similar shape. The value of Zj decreased as the time (Px) increased which meant Zj was inversely proportional to the time (Px).

Results for Free Vibration, Accelerometer 2, Mode 1, (Test 1), 33kN Peak 2

The results in Table C5 below were calculated using results obtained from Figure 177 and were as follow:

The first row in Table C5 below displayed the calculated results. Px was the time (ms) and Py was the acceleration (m/s^-2) where both values were used to calculate the information of Table C5. The first loop used the least-squares method, the log decrement was 1.5, the damping factor was 0.232, and the natural frequency was identified as 1948.483 rad/s.

Table C5: Calculated Data Collected in Figure C16

Px	Py	Period	Freq	ln Py	Yj	ln Py (Yj)	Yj^2	Zj	Log Dec	Zeta	Nat Freq	Nat Freq
s	m/s^2	s	Hz								rad/s	Hz
2.260664	11.7458046	0	0	2.463496	0	0	0	0.328449	1.5	0.232	1948.483	310.2699
2.262891	5.243129061	0.002227	449.1227	1.656918	1	1.656918	1	-1.17155				
2.267109	3.915455613	0.004219	237.037	1.364932	2	2.729863	4	-2.67155				
Sum	20.90438927			5.485346	3	8.485346	5					

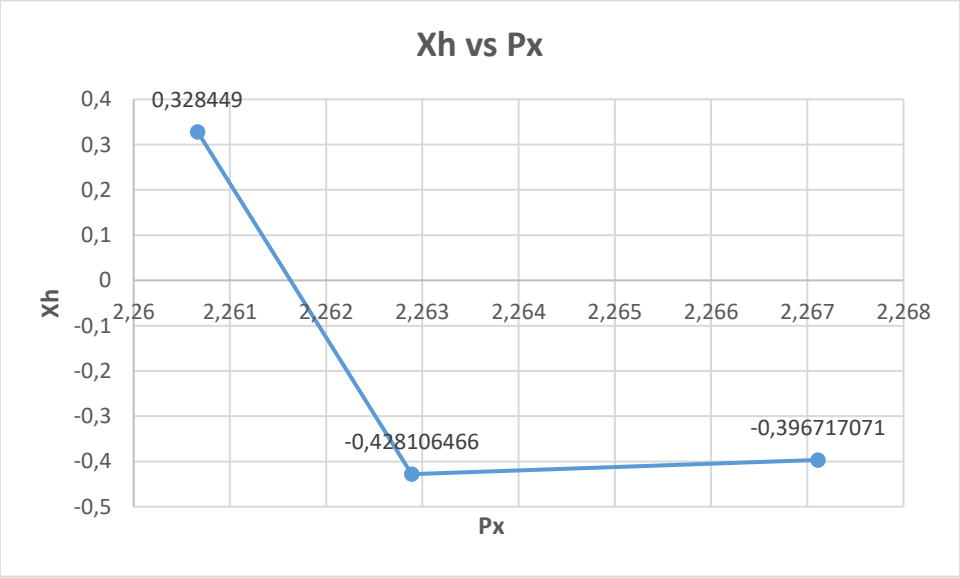

Figure C21: (Xh) vs (Px)

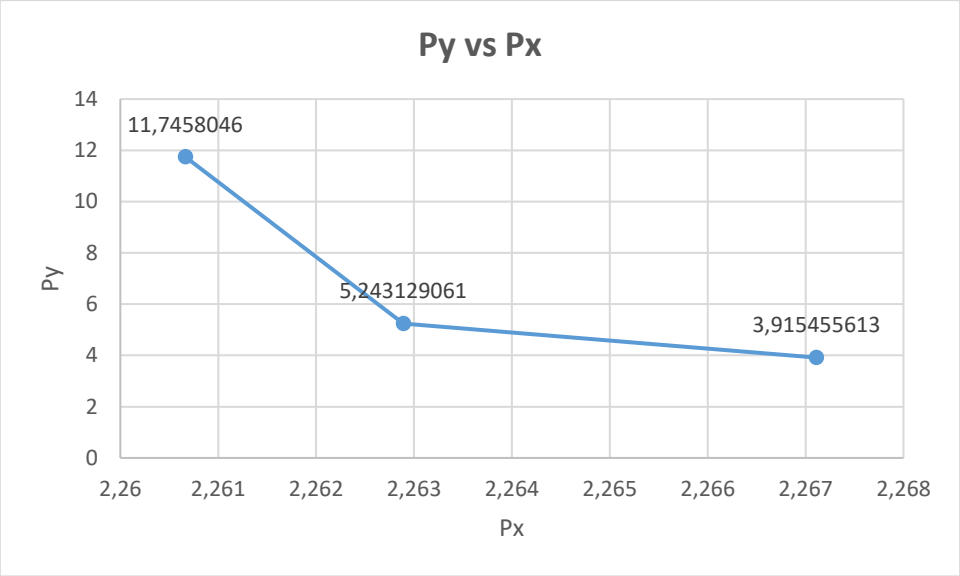

Figure C22: (Py) vs (Px)

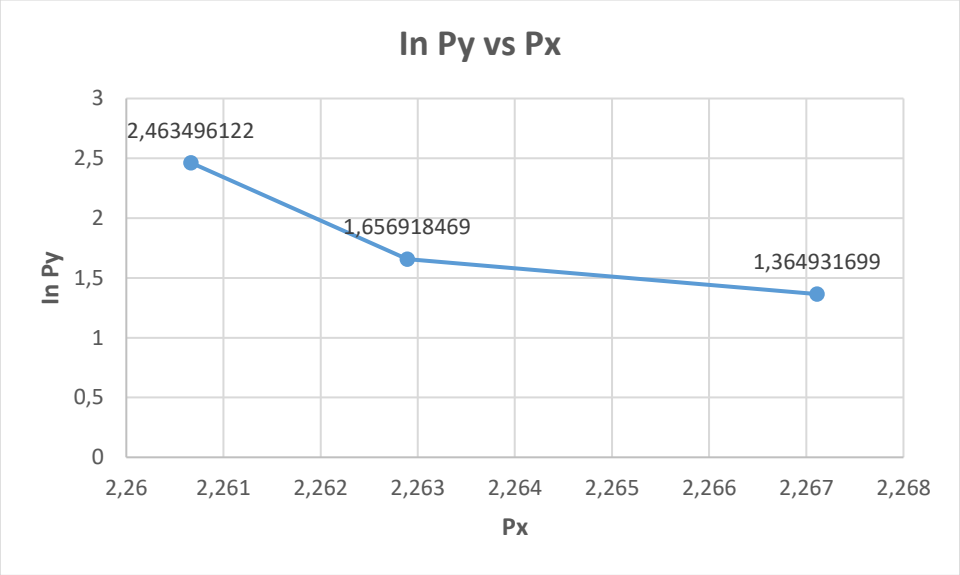

Figure C23: (In Py) vs (Px)

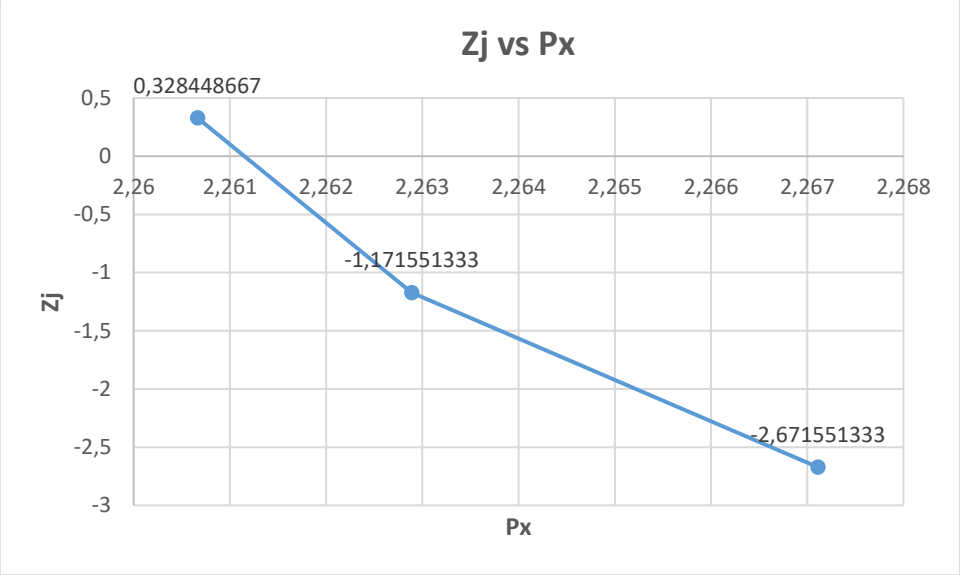

Figure C24: (Zj) vs (Px)

- Figure C21 to C23 in the X-value expanded and the Y-value diminished.
  This means:
- The value of Xh diminished as the time (Px) increased which subsequently implied Xh was inversely corresponding to the time (Px).
- The value of acceleration (Py) decreased as the time (Px) increased which meant Py was inversely proportional to the time (Px).
- The value of Acceleration (In Py) decreased as the time (Px) increased which meant In Py was inversely proportional to the time (Px).

- (Figure C21-C24) obtained from the different results of the Tern conductor where the cable tension of 33 kN appeared to be a similar shape. The value of Zj decreased as the time (Px) increased which meant Zj was inversely proportional to the time (Px).

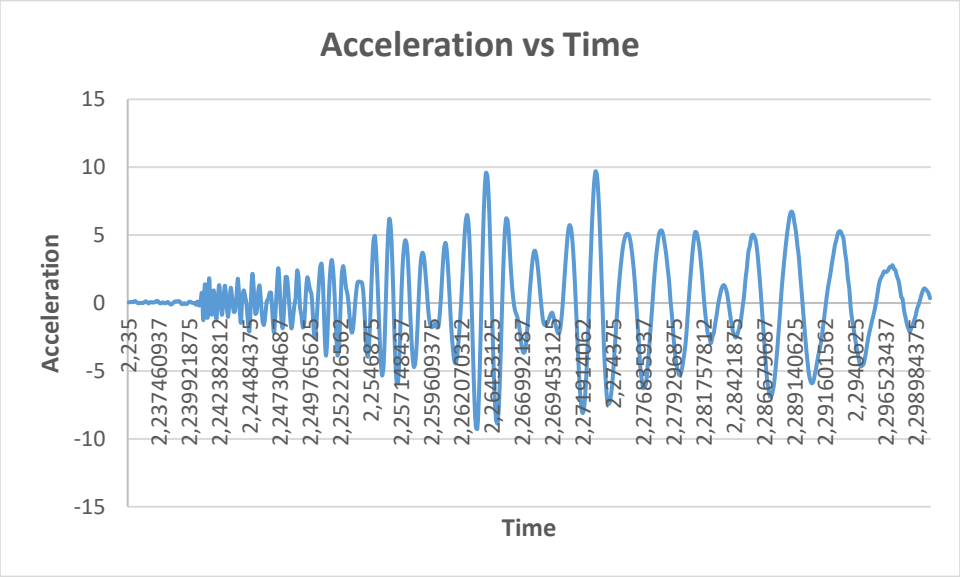

Figure C25: Free Vibration, Accelerometer 3, Mode 1, 33 kN (Test 1) Peak 1

The results in Table C6 below were calculated using results obtained from Figure 195 and were as follow:

The first row in Table C6 below displayed the calculated results. Px was the time (ms) and Py was the acceleration (m/s^-2) where both values were used to calculate the information of Table C6. The first loop used the least-squares method, the log decrement was 1.5, the damping factor was 0.232, and the natural frequency was identified as 4468.837 rad/s.

Table C6: Calculated Data Collected in Figure C25

Px	Py	Period	Freq	ln Py	Yj	ln Py (Yj)	Yj^2	Zj	Log Dec	Zeta	Nat Freq	Nat Freq
s	m/s^2	s	Hz								rad/s	Hz
2.256211	6.201297227	0	0	1.824759	0	0	0	0.002163	1.5	0.232	4468.837	711.2376
2.257617	4.337532897	0.001406	711.1111	1.467306	1	1.467306	1	-1.49784				
2.259023	3.368359239	0.001406	711.1111	1.214426	2	2.428852	4	-2.99784				
Sum	13.90718936			4.50649	3	7.50649	5					

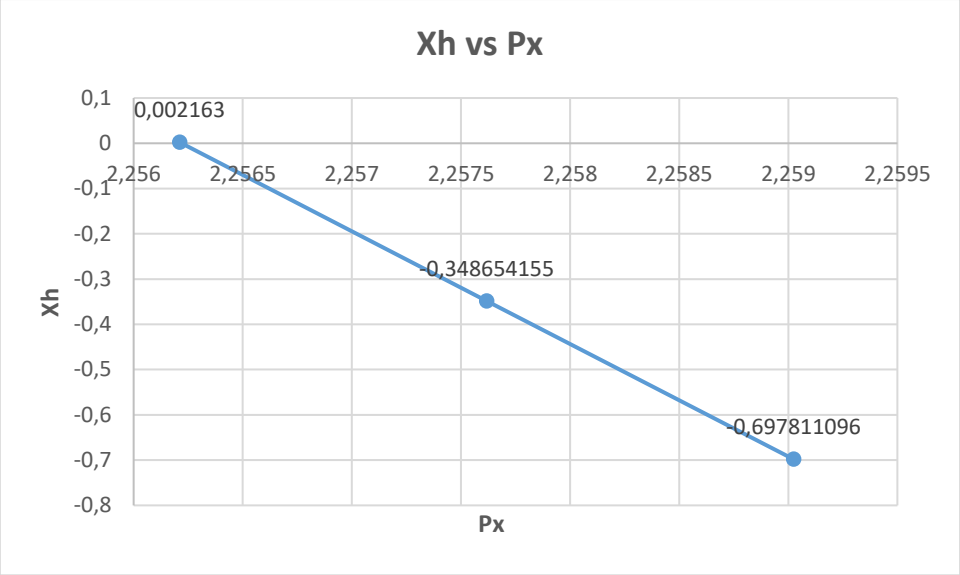

Figure C26: (Xh) vs (Px)

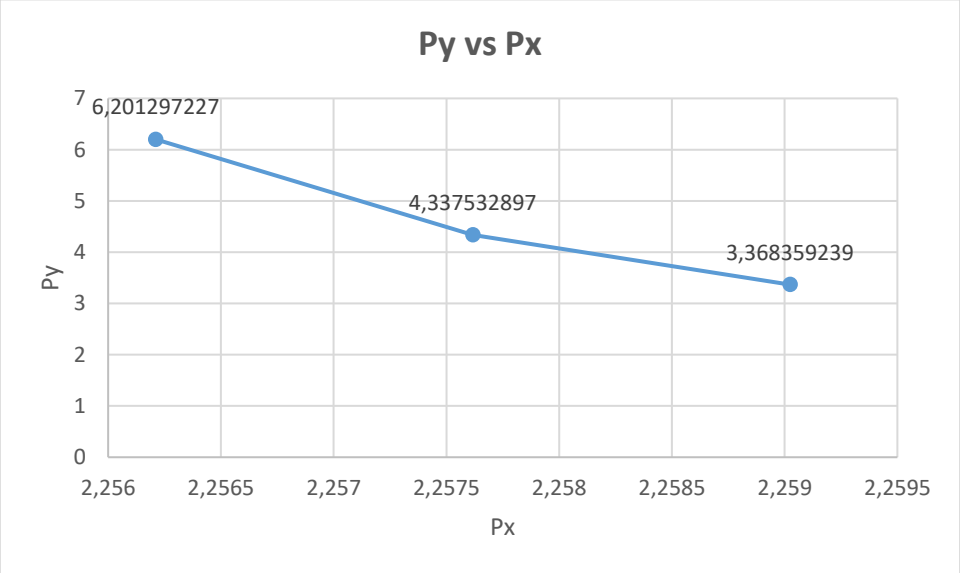

Figure C27: (Py) vs (Px)

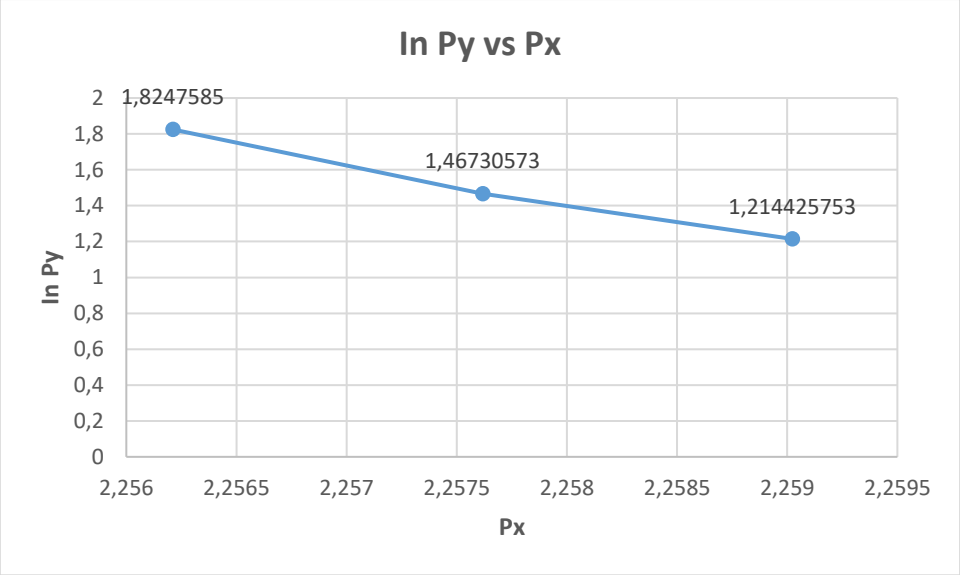

Figure C28: (In Py) vs (Px)

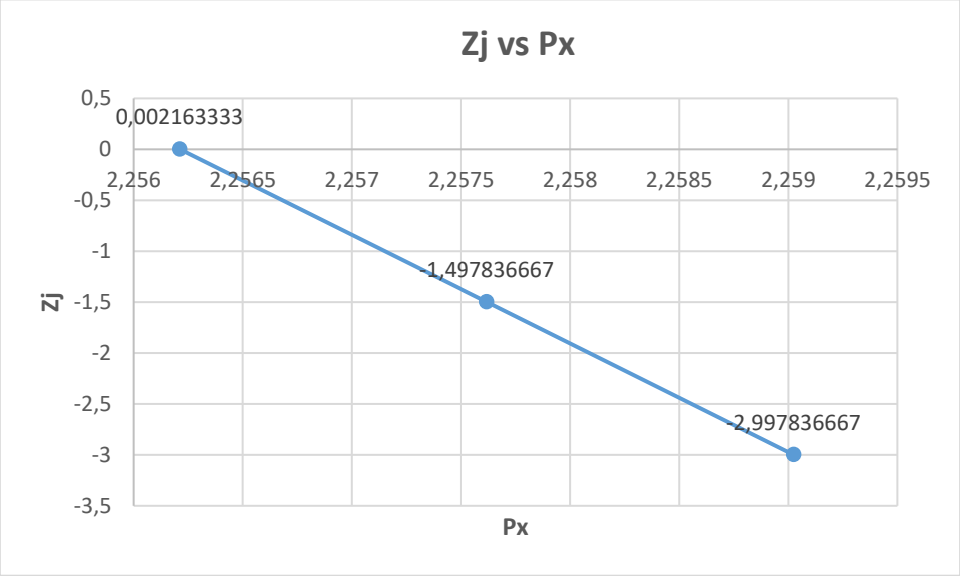

Figure C29: (Zj) vs (Px)

- Figure C26 to C28 in the X-value expanded and the Y-value diminished.
  This means:
- The value of Xh diminished as the time (Px) increased which subsequently implied Xh was inversely corresponding to the time (Px).
- The value of acceleration (Py) decreased as the time (Px) increased which meant Py was inversely proportional to the time (Px).

- The value of Acceleration (In Py) decreased as the time (Px) increased which meant In Py was inversely proportional to the time (Px).
- (Figure C26-C29) the value of Zj decreased as the time (Px) increased which meant Zj was inversely proportional to the time (Px).

Results for Free Vibration, Accelerometer 3, Mode 1, (Test 1), 33kN Peak 2

The results in Table C7 below were calculated using results obtained from Figure 186 and were as follow:

The first row in Table 61 below displayed the calculated results. Px was the time (ms) and Py was the acceleration (m/s^-2) where both values were used to calculate the information of Table 61. The first loop used the least-squares method, the log decrement was 1.5, the damping factor was 0.232, and the natural frequency was identified as 3154.209 rad/s.

Table C7: Calculated Data Collected in Figure C25

Px	Py	Period	Freq	In Py	Yj	In Py (Yj)	Yj^2	Zj	Log Dec	Zeta	Nat Freq	Nat Freq
s	m/s^2	s	Hz								rad/s	Hz
2.26418	9.325333502	0	0	2.232735	0	0	0	0.254958	1.5	0.232	3154.209	502.008
2.26582	6.071567994	0.001641	609.5238	1.803617	1	1.803617	1	-1.24504				
2.268164	3.416182444	0.002344	426.6667	1.228524	2	2.457047	4	-2.74504				
Sum	18.81308394			5.264875	3	8.264875	5					

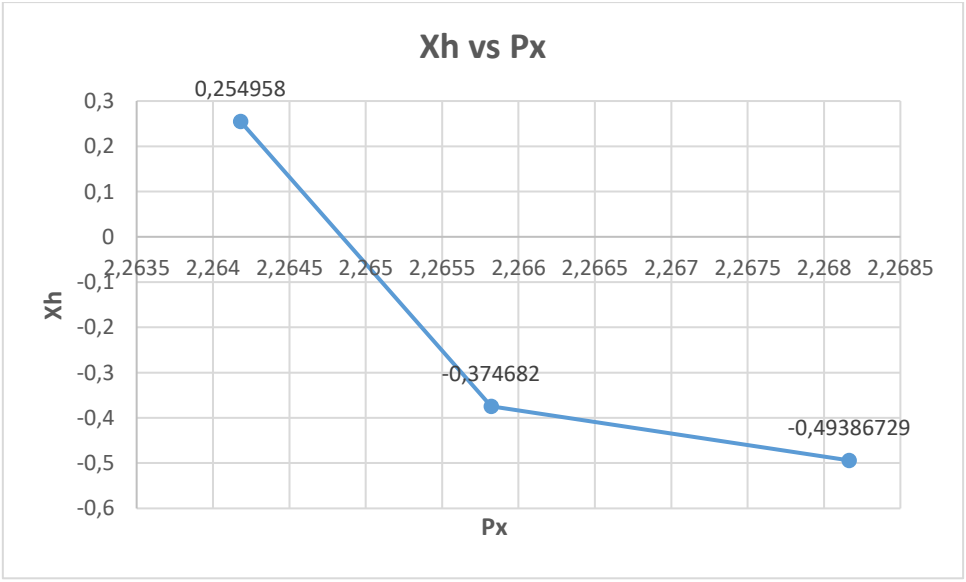

Figure C30: (Xh) vs (Px)

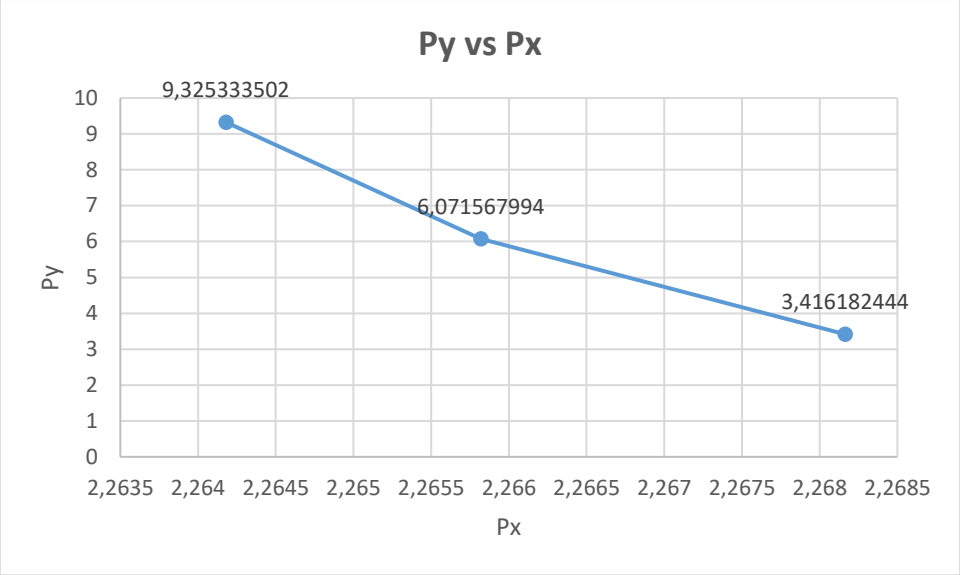

Figure C31: (Py) vs (Px)

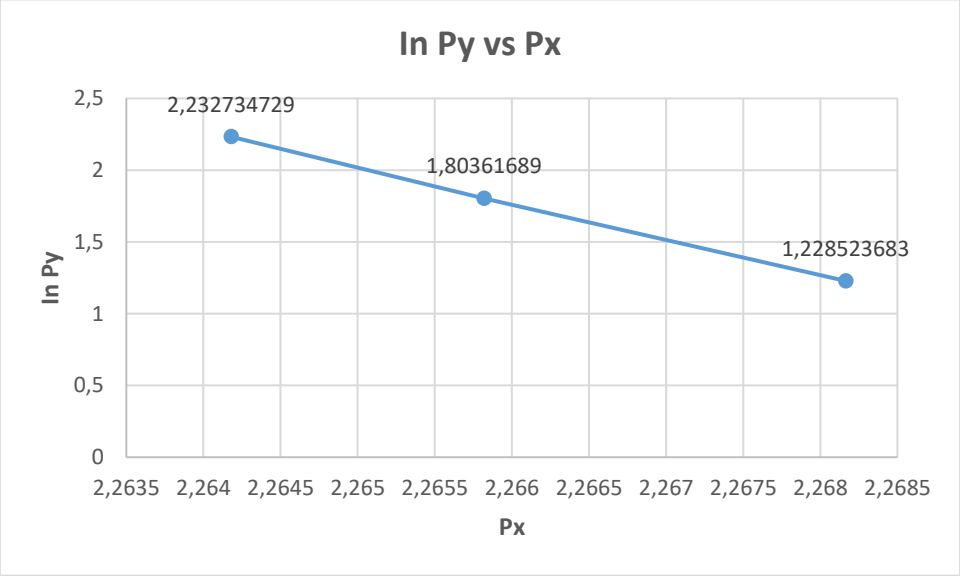

Figure C32: (In Py) vs (Px)

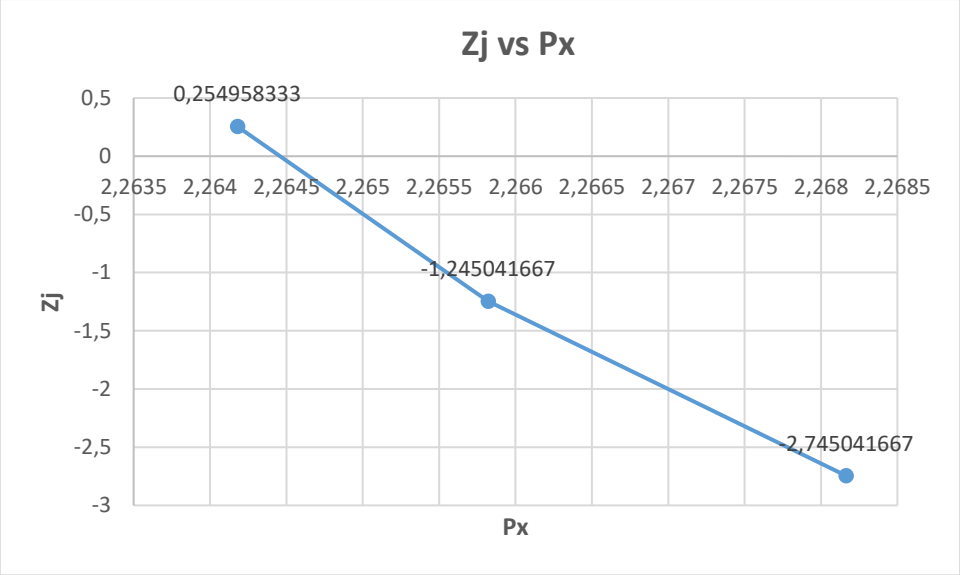

Figure C33: (Zj) vs (Px)

- Figure C30 to C32 in the X-value expanded and the Y-value diminished.
  This means:
- The value of Xh diminished as the time (Px) increased which subsequently implied Xh was inversely corresponding to the time (Px).
- The value of acceleration (Py) decreased as the time (Px) increased which meant Py was inversely proportional to the time (Px).
- The value of Acceleration (In Py) decreased as the time (Px) increased which meant In Py was inversely proportional to the time (Px).

- (Figure C30-C33) obtained from the different results of the Tern conductor where the cable tension of 33 kN appeared to be a similar shape. The value of Zj decreased as the time (Px) increased which meant Zj was inversely proportional to the time (Px).

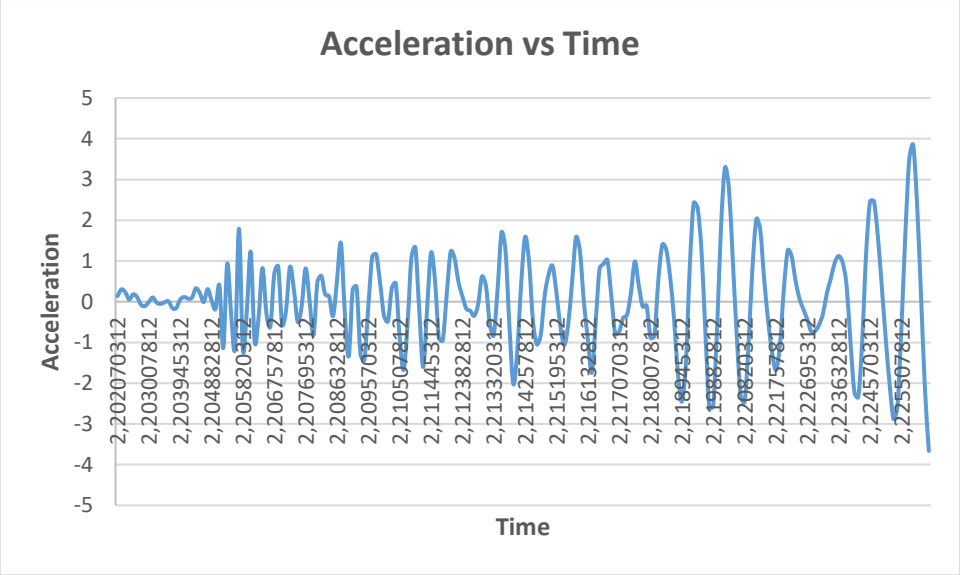

Figure C34: Free Vibration, Accelerometer 0, Mode 3, 33 kN (Test 1) Peak 1

The results in Table C8 below were calculated using results obtained from Figure 195 and were as follow:

The first row in Table C8 below displayed the calculated results. Px was the time (ms) and Py was the acceleration (m/s^-2) where both values were used to calculate the information of Table C8. The first loop used the least-squares method, the log decrement was 1.5, the damping factor was 0.232, and the natural frequency was identified as 6698.492 rad/s.

Table 8: Calculated Data Collected in Figure C34

Px	Py	Period	Freq	ln Py	Yj	ln Py (Yj)	Yj^2	Zj	Log Dec	Zeta	Nat Freq	Nat Freq
s	m/s^2	s	Hz								rad/s	Hz
2.220234	3.293750414	0	0	1.192027	0	0	0	-0.79216	1.5	0.232	6698.492	1066.098
2.221172	2.024757957	0.000938	1066.667	0.70545	1	0.70545	1	-2.29216				
2.222109	1.253624237	0.000938	1066.667	0.226039	2	0.452077	4	-3.79216				
Sum	6.572132608			2.123516	3	5.123516	5					

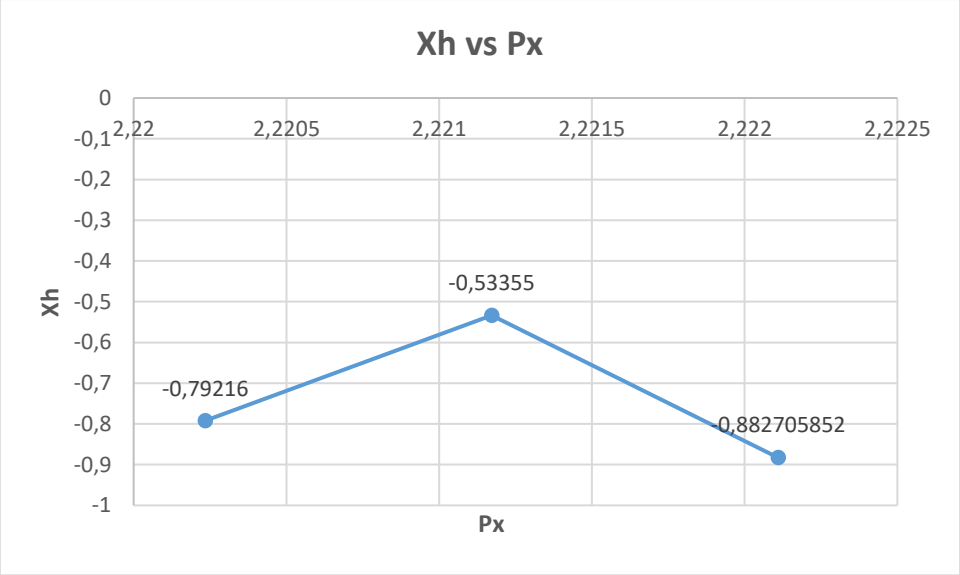

Figure C35: (Zj) vs (Px)

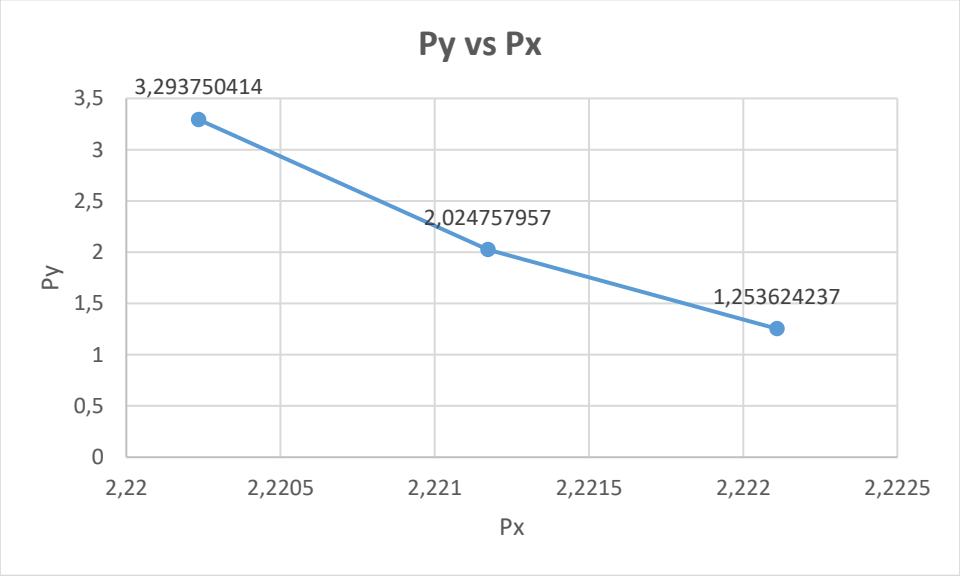

Figure C36: (Py) vs (Px)

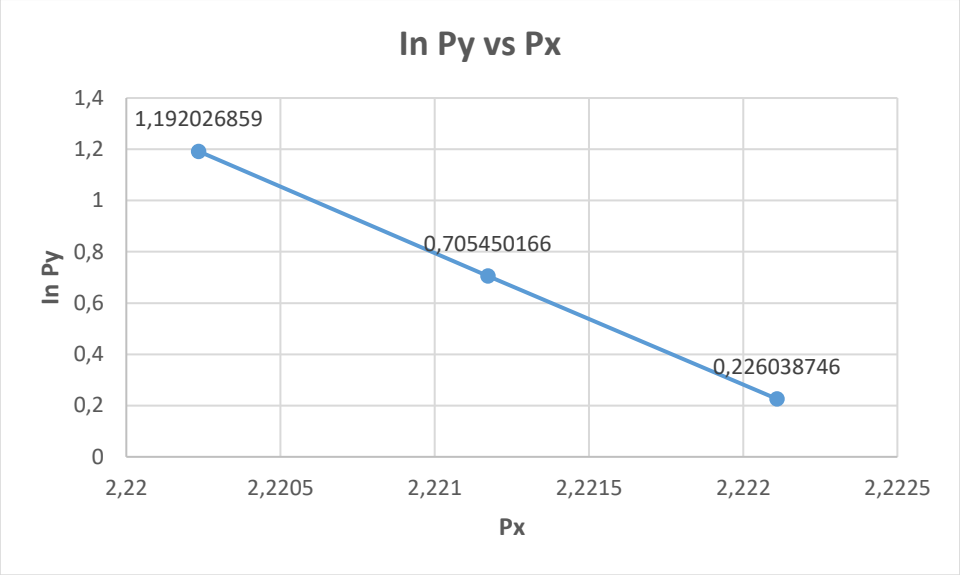

Figure C37: (In Py) vs (Px)

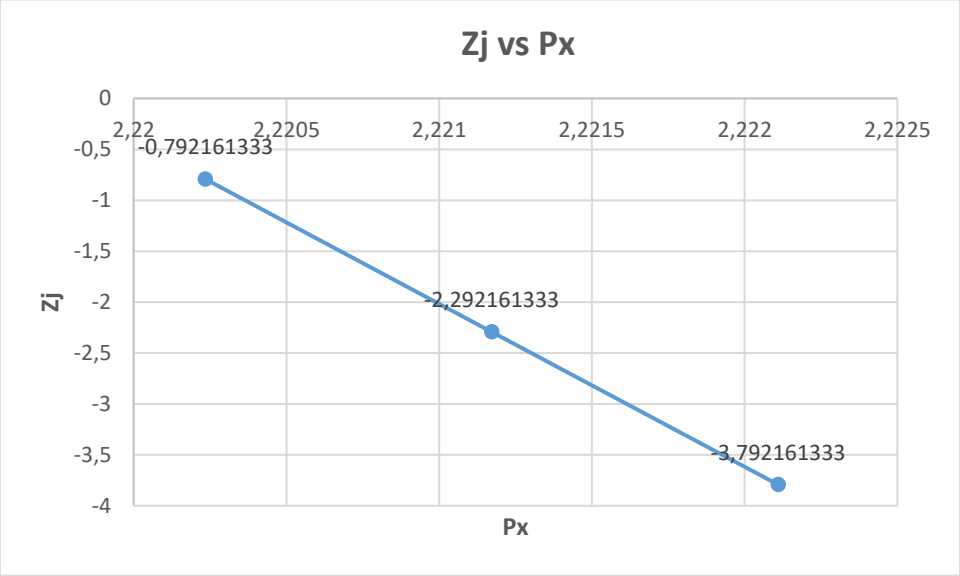

Figure C38: (In Py) vs (Px)

- Figure C35 to C37 in the X-value expanded and the Y-value diminished.
  This means:
- The value of Xh diminished as the time (Px) increased which subsequently implied Xh was inversely corresponding to the time (Px).
- The value of acceleration (Py) decreased as the time (Px) increased which meant Py was inversely proportional to the time (Px).

- The value of Acceleration (In Py) decreased as the time (Px) increased which meant In Py was inversely proportional to the time (Px).

(Figure C35-C38) obtained from the different results of the Tern conductor where the cable tension of 33 kN appeared to be a similar shape. The value of Zj decreased as the time (Px) increased which meant Zj was inversely proportional to the time (Px).

Results for Free Vibration, Accelerometer 3, Mode 1, (Test 1), 33kN Peak 2

The results in Table C9 below were calculated using results obtained from Figure C34 and were as follow:

The first row in Table C9 below displayed the calculated results. Px was the time (ms) and Py was the acceleration (m/s^-2) where both values were used to calculate the information of Table C9. The first loop used the least-squares method, the log decrement was 1.5, the damping factor was 0.232, and the natural frequency was identified as 17849.96 rad/s.

Table C9: Calculated Data Collected in Figure C34

Px	Py	Period	Freq	In Py	Yj	In Py (Yj)	Yj^2	Zj	Log Dec	Zeta	Nat Freq	Nat Freq
s	m/s^2	s	Hz								rad/s	Hz
2.205703	1.791273143	0	0	0.582927	0	0	0	-1.30317	1.5	0.232	17849.96	2840.909
2.206055	1.221629183	0.000352	2844.448	0.200185	1	0.200185	1	-2.80317				
2.206406	0.824797757	0.000352	2844.44	-0.19262	2	-0.38523	4	-4.30317				
Sum	3.837700083			0.590495	3	3.590495	5					

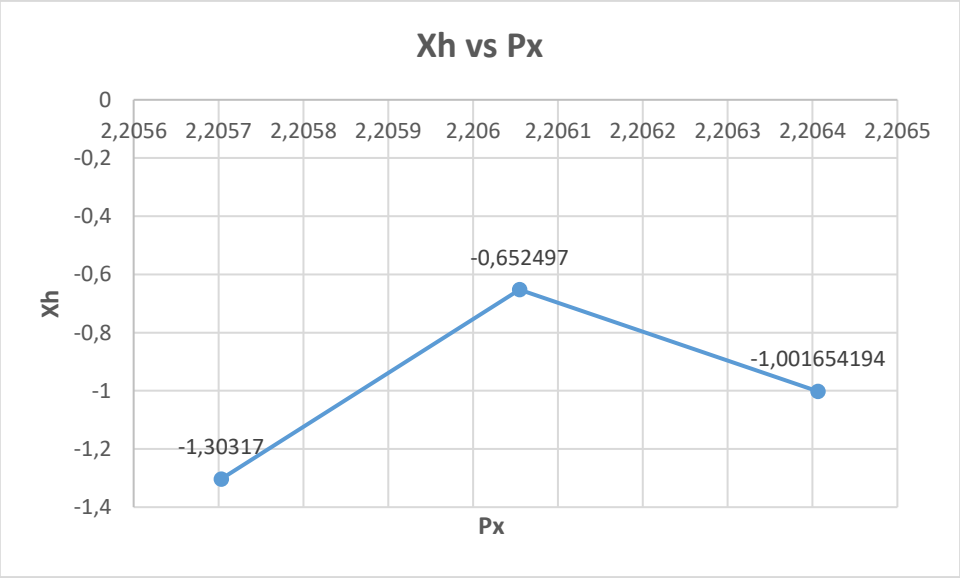

Figure C39: (Xh) vs (Px)

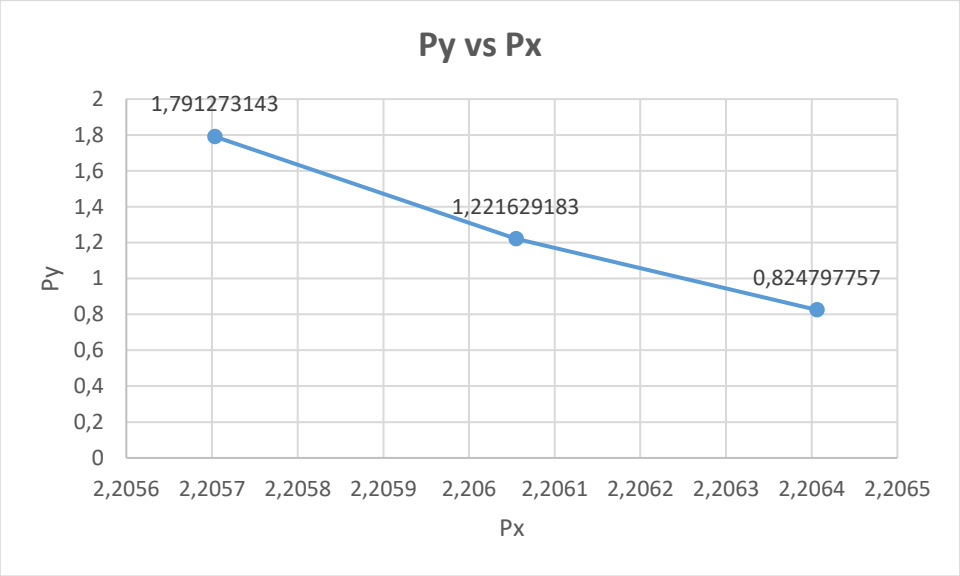

Figure C40: (Py) vs (Px)

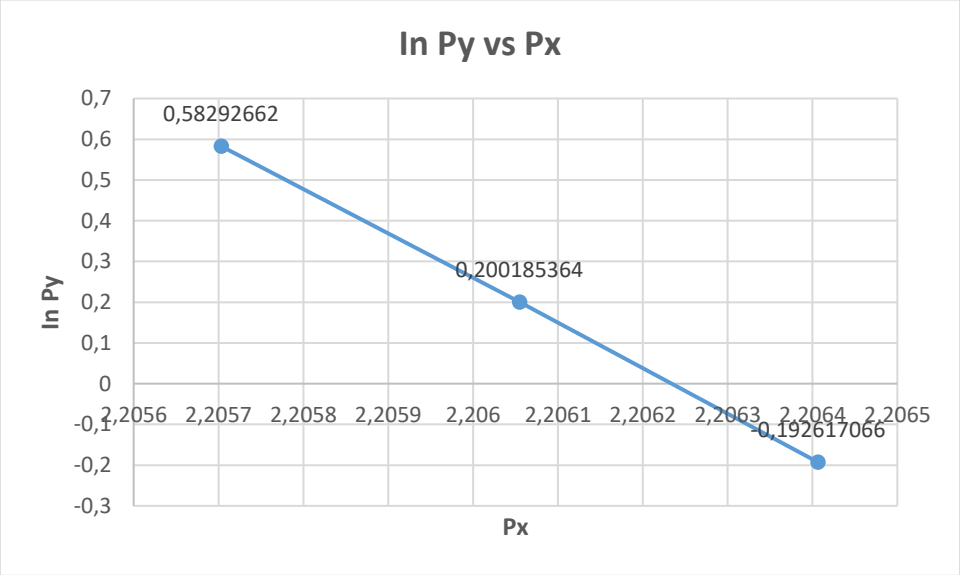

Figure C411: (In Py) vs (Px)

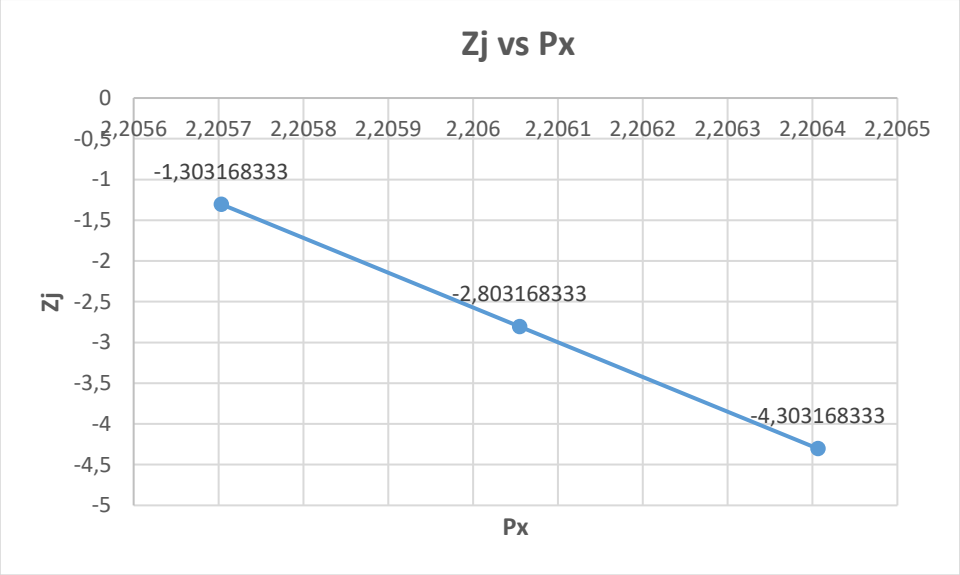

Figure C42: (Zj) vs (Px)

- Figure C39 to C41 in the X-value expanded and the Y-value diminished.

  This means:
- The value of Xh diminished as the time (Px) increased which subsequently implied Xh was inversely corresponding to the time (Px).
- The value of acceleration (Py) decreased as the time (Px) increased which meant Py was inversely proportional to the time (Px).
- The value of Acceleration (In Py) decreased as the time (Px) increased which meant In Py was inversely proportional to the time (Px).

- (Figure C39-C42) obtained from the different results of the Tern conductor where the cable tension of 33 kN appeared to be a similar shape. The value of Zj decreased as the time (Px)increased which meant Zj was inversely proportional to the time (Px).

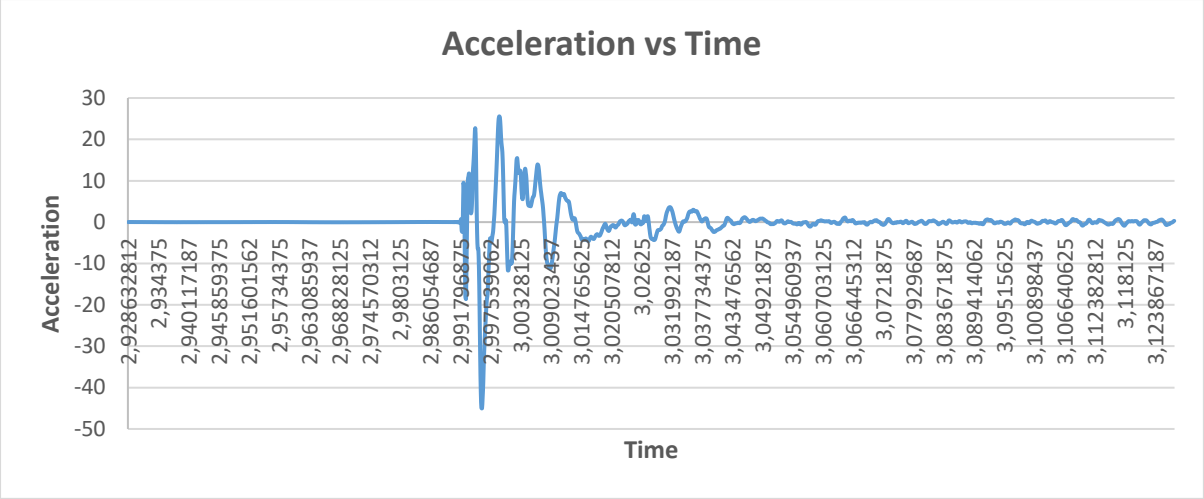

Figure C43: Free Vibration, Accelerometer 0, Mode 1, 39 kN (Test 1)

The results in Table C10 below were calculated using results obtained from Figure C43 and were as follow:

The first row in Table C10 below displayed the calculated results. Px was the time (ms) and Py was the acceleration (m/s^-2) where both values were used to calculate the information of Table C10. The first loop used the least-squares method, the log decrement was 1.5, the damping factor was 0.232, and the natural frequency was identified as 2664.625 rad/s.

Table C10: Calculated Data Collected in Figure C43

Px	Py	Period	Freq	In Py	Yj	In Py (Yj)	Yj^2	Zj	Log Dec	Zeta	Nat Freq	Nat Freq
s	m/s^2	s	Hz								rad/s	Hz
2.999268	25.259254	0	0	3.229193	0	0	0	1.320008	1.5	0.232	2664.625	424.0882
3.002578	15.48360618	0.003311	302.0578	2.739782	1	2.739782	1	-0.17999				
3.003984	12.07399664	0.001406	711.1111	2.491054	2	4.982108	4	-1.67999				
Sum	52.81685682			8.460028	3	11.46003	5					

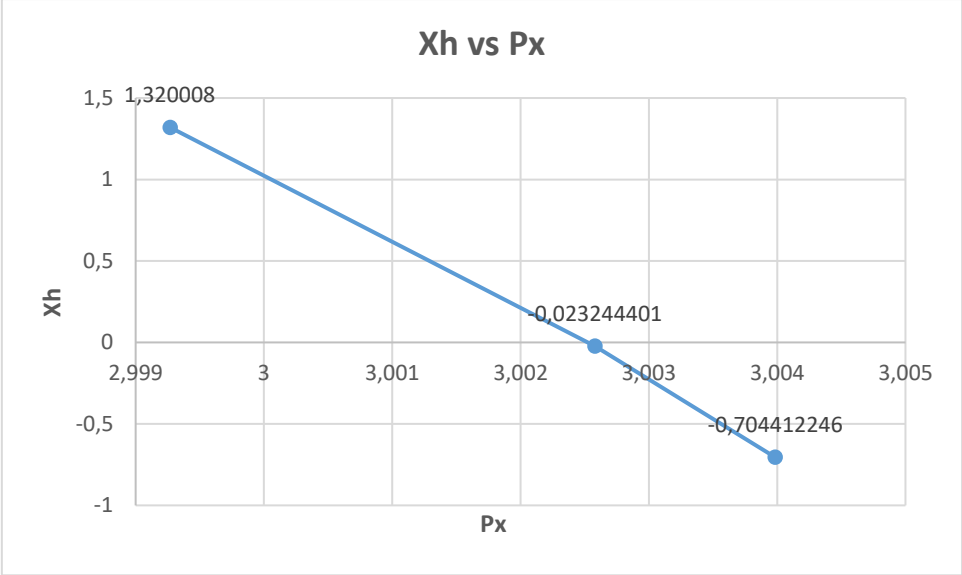

Figure C44: (Xh) vs (Px)

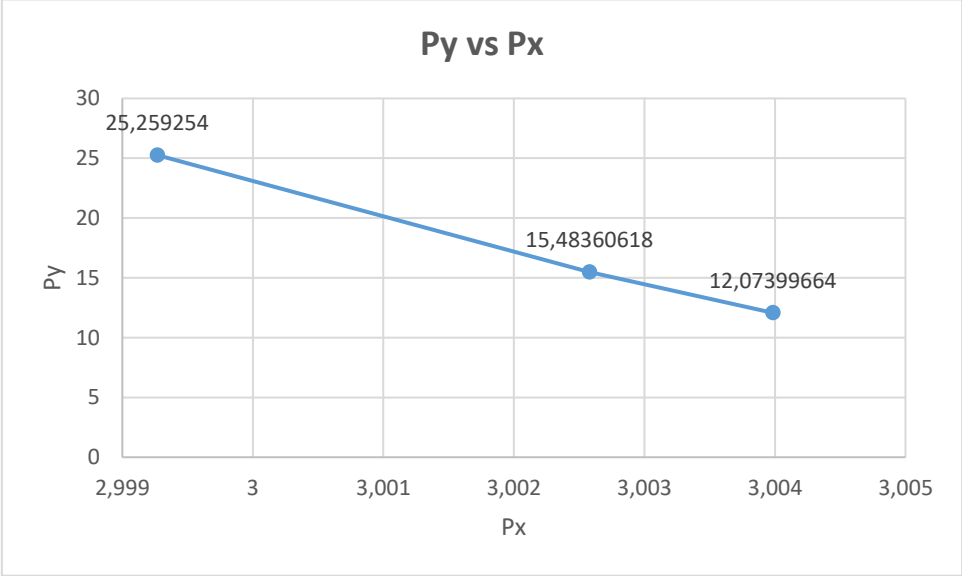

Figure C45: (Py) vs (Px)

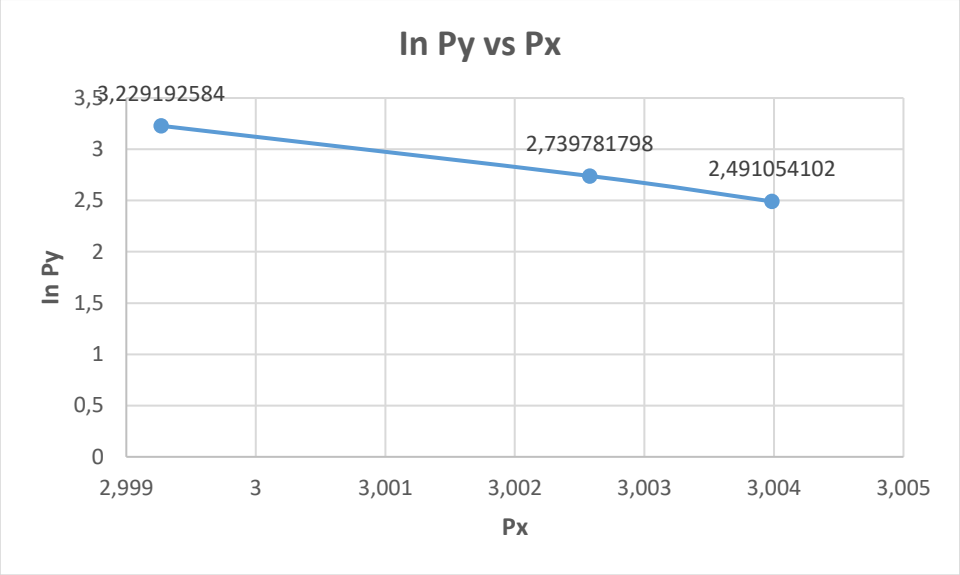

Figure C46: (In Py) vs (Px)

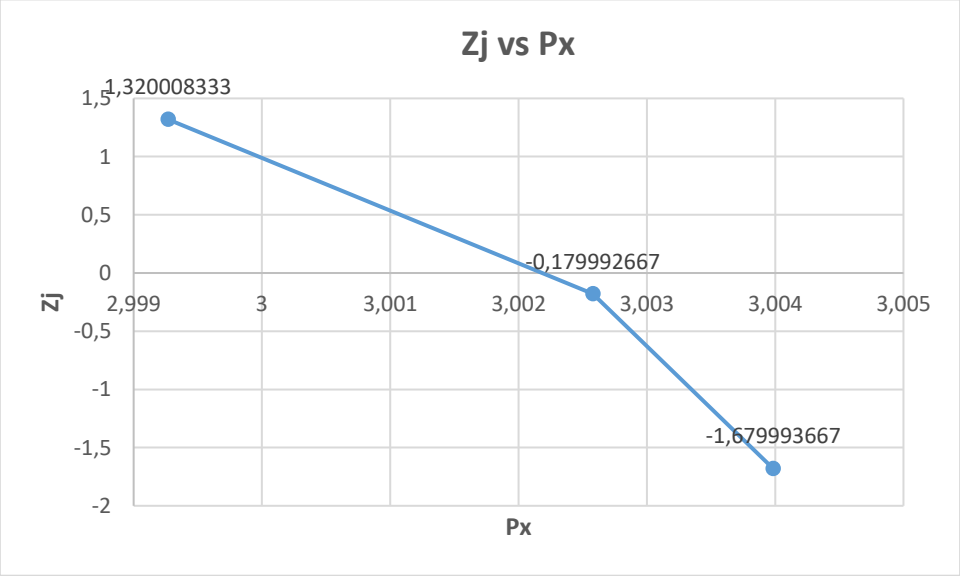

Figure C47: (Zj) vs (Px)

- Figure C44 to C46 in the X-value expanded and the Y-value diminished.
  This means:
- The value of Xh diminished as the time (Px) increased which subsequently implied Xh was inversely corresponding to the time (Px).
- The value of acceleration (Py) decreased as the time (Px) increased which meant Py was inversely proportional to the time (Px).

- The value of Acceleration (In Py) decreased as the time (Px) increased which meant In Py was inversely proportional to the time (Px).

- (Figure C44-C47) obtained from the different results of the Tern conductor where the cable tension of 39 kN appeared to be a similar shape. The value of Zj decreased as the time (Px)increased which meant Zj was inversely proportional to the time (Px).

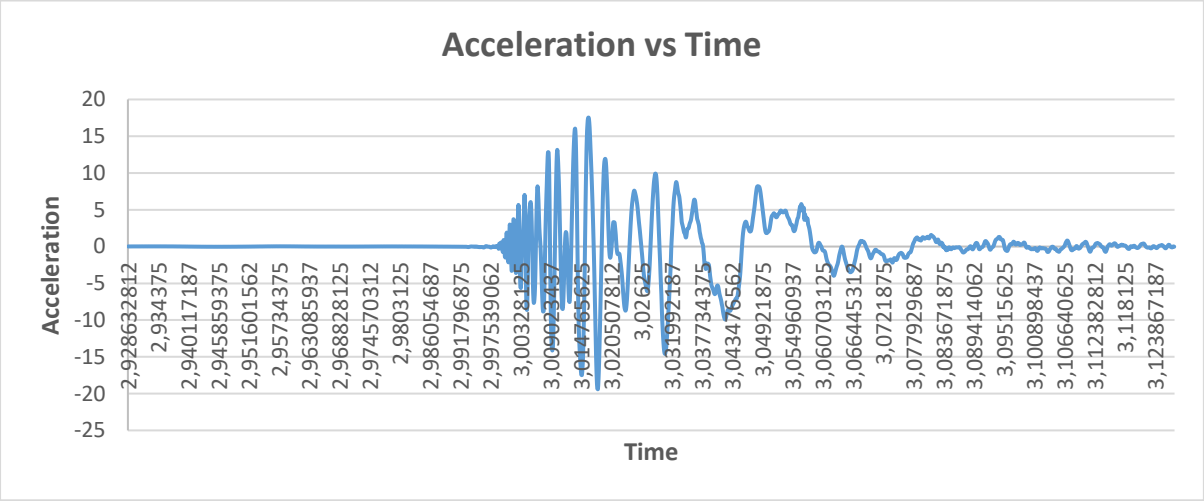

Figure C48: Free Vibration, Accelerometer 1, Mode 1, 39 kN (Test 1)

The results in Table C11 below were calculated using results obtained from Figure C48 and were as follow:

The first row in Table C11 below displayed the calculated results. Px was the time (ms) and Py was the acceleration (m/s^-2) where both values were used to calculate the information of Table C11. The first loop used the least-squares method, the log decrement was 1.5, the damping factor was 0.232, and the natural frequency was identified as 2553.103 rad/s.

Table C11: Calculated Data Collected in Figure C48

Px	Py	Period	Freq	In Py	Yj	In Py (Yj)	Yj^2	Zj	Log Dec	Zeta	Nat Freq	Nat Freq
s	m/s^2	s	Hz								rad/s	Hz
3.016172	17.53325513	0	0	2.864099	0	0	0	0.675526	1.5	0.232	2553.103	406.3389
3.019336	11.92635226	0.003164	316.0494	2.47875	1	2.47875	1	-0.82447				
3.021094	3.266528826	0.001758	568.8887	1.183728	2	2.367456	4	-2.32447				
Sum	32.72613622			6.526578	3	9.526578	5					

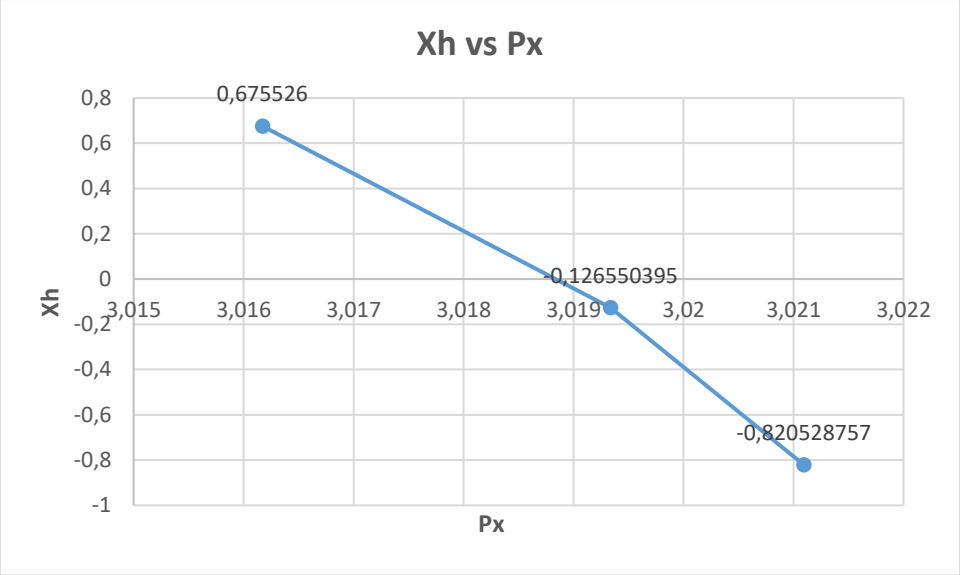

Figure C49: (Xh) vs (Px)

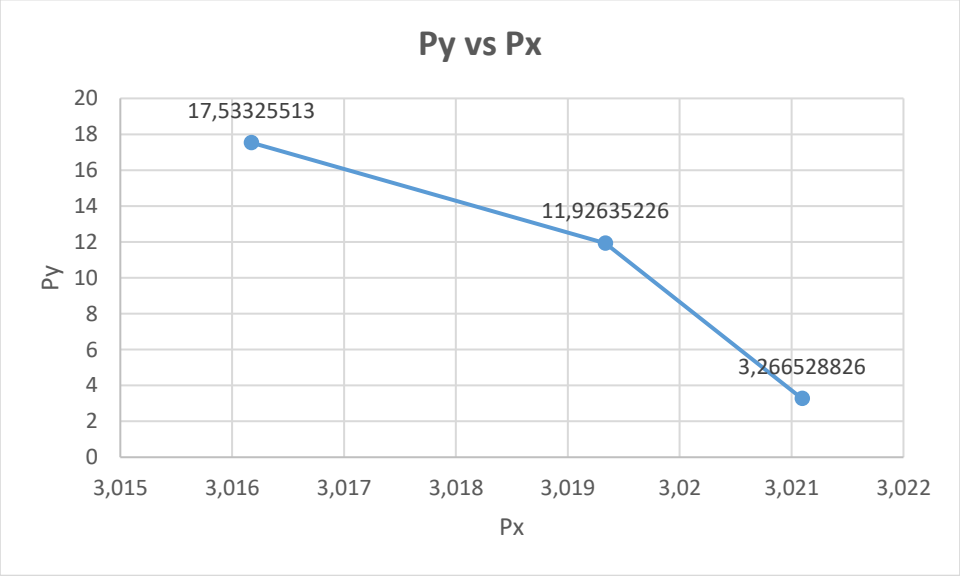

Figure C50: (Py) vs (Px)

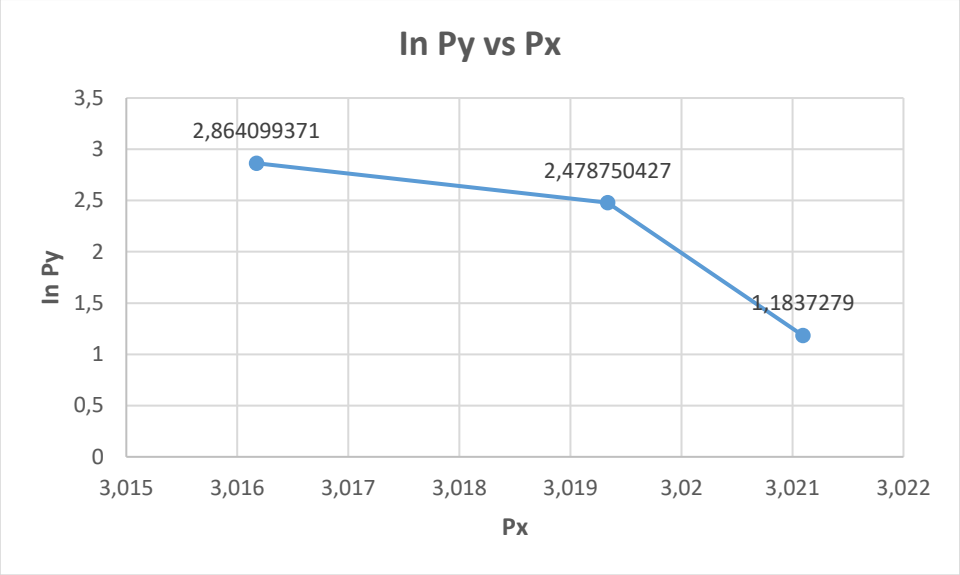

Figure C51: (InPy) vs (Px)

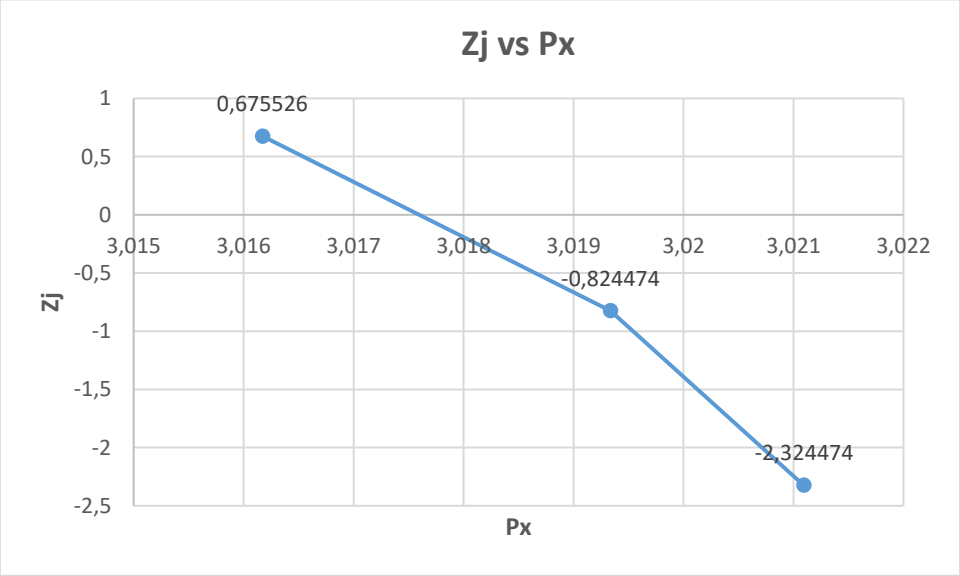

Figure C52: (Zj) vs (Px)

- Figure C49 to C51 in the X-value expanded and the Y-value diminished.
  This means:
- The value of Xh diminished as the time (Px) increased which subsequently implied Xh was inversely corresponding to the time (Px).
- The value of acceleration (Py) decreased as the time (Px) increased which meant Py was inversely proportional to the time (Px).

- The value of Acceleration (In Py) decreased as the time (Px) increased which meant In Py was inversely proportional to the time (Px).

- (Figure C49-C52) obtained from the different results of the Tern conductor where the cable tension of 39 kN appeared to be a similar shape. The value of Zj decreased as the time (Px)increased which meant Zj was inversely proportional to the time (Px).

RESULTS FOR FREE VIBRATION METHOD ON ACSR BERSFORT CONDUCTOR

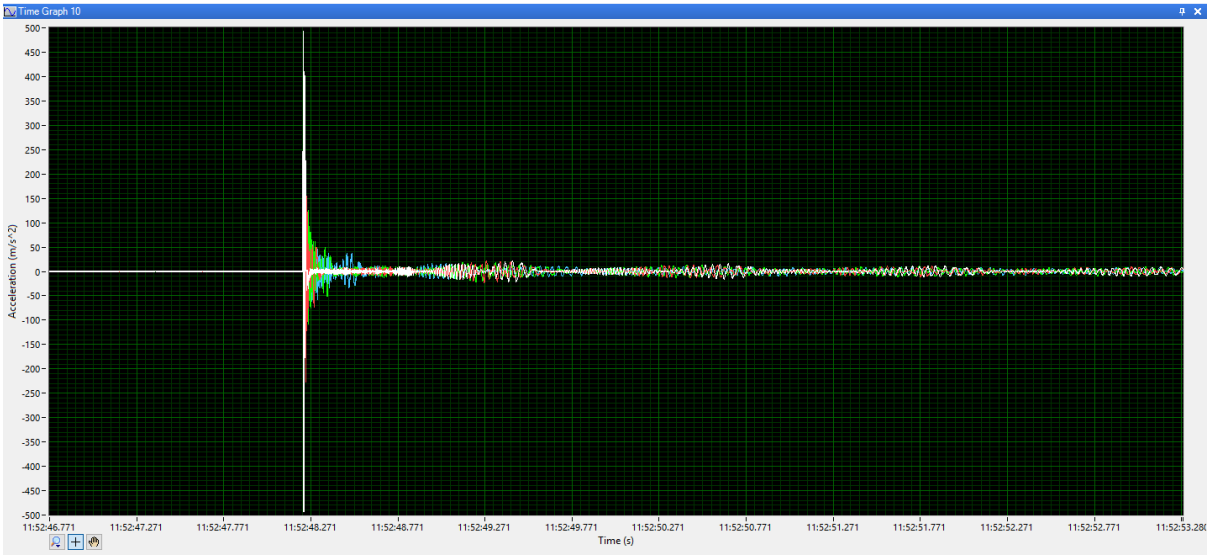

Figure D1: Free Vibration, Accelerometer (All) Mode 1, 36 kN (Test2) National Instrument Desk

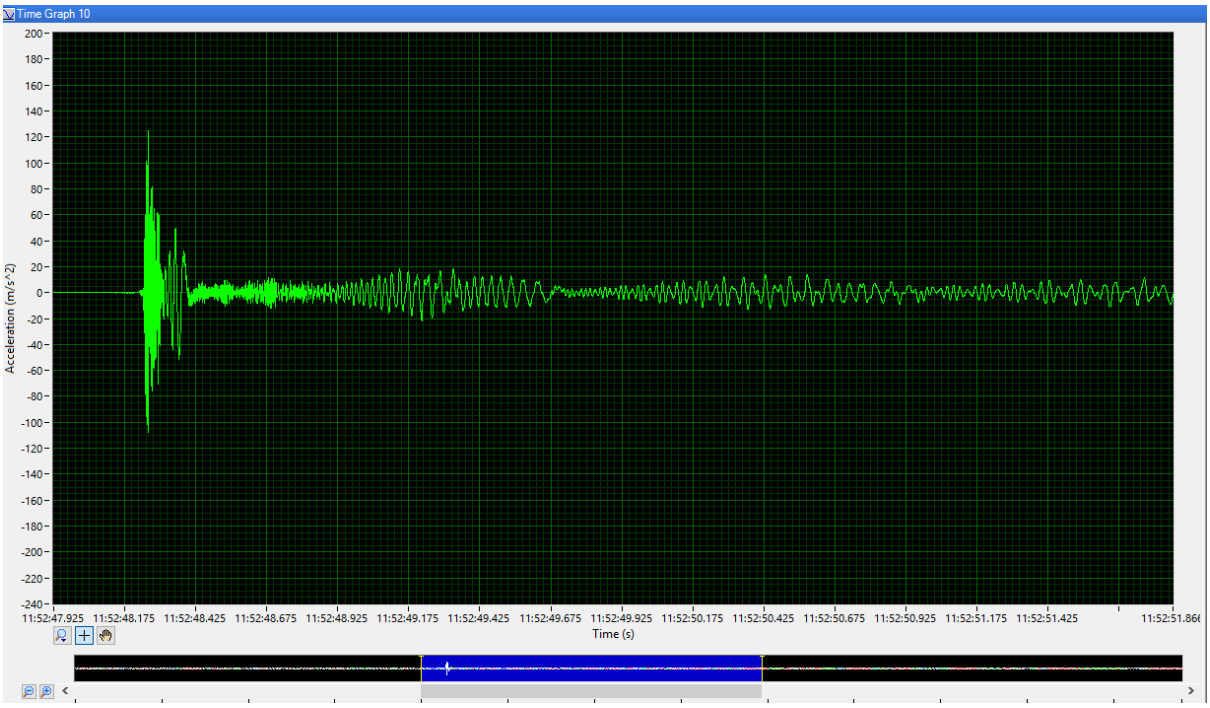

Figure D2: Free Vibration, Accelerometer (2) Mode 1, 36 kN (Test2) National Instrument Desk

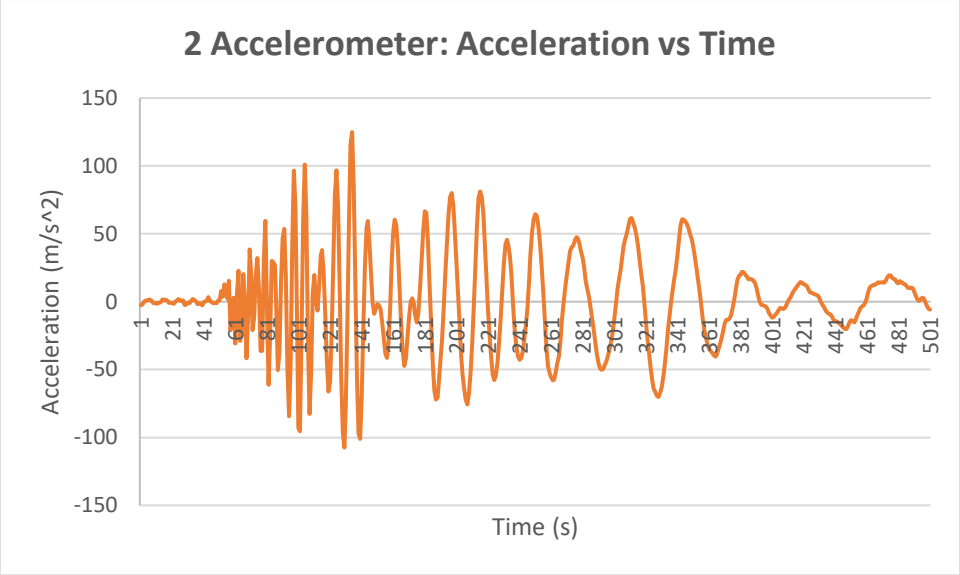

Figure D3: Free Vibration, Accelerometer 2, Mode 1, 36 kN (Test 2) Peak 1

The results in Table D1 below were calculated using results obtained from Figure D3 and were as follow:

The first row in Table D1 below displayed the calculated results. Px was the time (ms) and Py was the acceleration (m/s^-2) where both values were used to calculate the information of Table D1. The first loop used the least-squares method, the log decrement was 1.5, the damping factor was 0.232, and the natural frequency was identified as 35.7 rad/s.

Table D1: Calculated Data Collected in Figure D3

Px	Py	Period	Freq	In Py	Yj	In Py (Yj)	Yj^2	Zj	Log Dec	Zeta	Nat Freq	Nat Freq
ms	x10^-3 m/s^2	ms	Hz								rad/s	Hz
0	209.407	0	0	5.34428	0	0	0	3.377893	1.5	0.232	35.7	5.682
0.176	106.243	0.176	5.681818	4.665729	1	4.665729	1	1.877893				
0.352	101.867	0.176	5.681818	4.623668	2	9.247336	4	0.377893				
Sum	417.517			14.63368	3	17.63368	5					

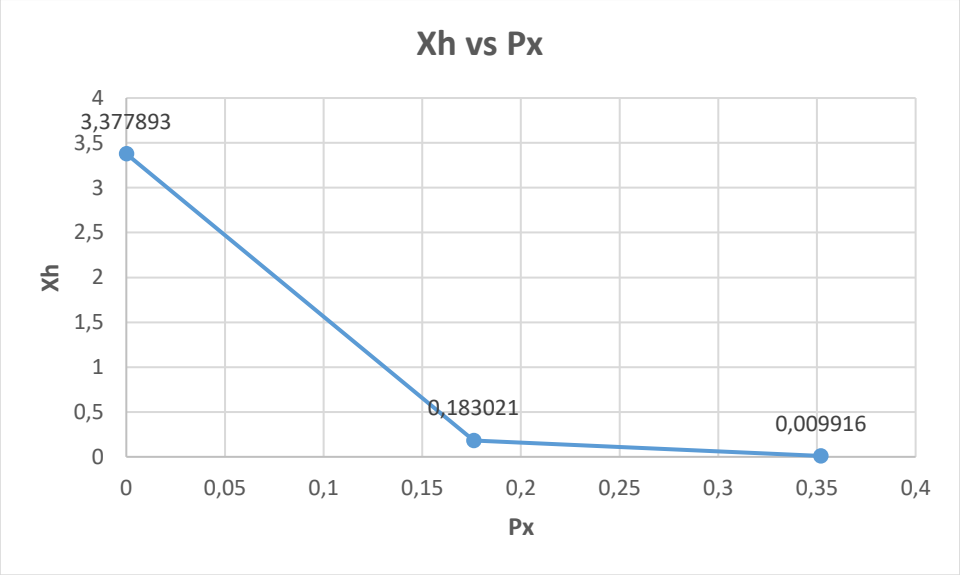

Figure D4: (Xh) vs (Px)

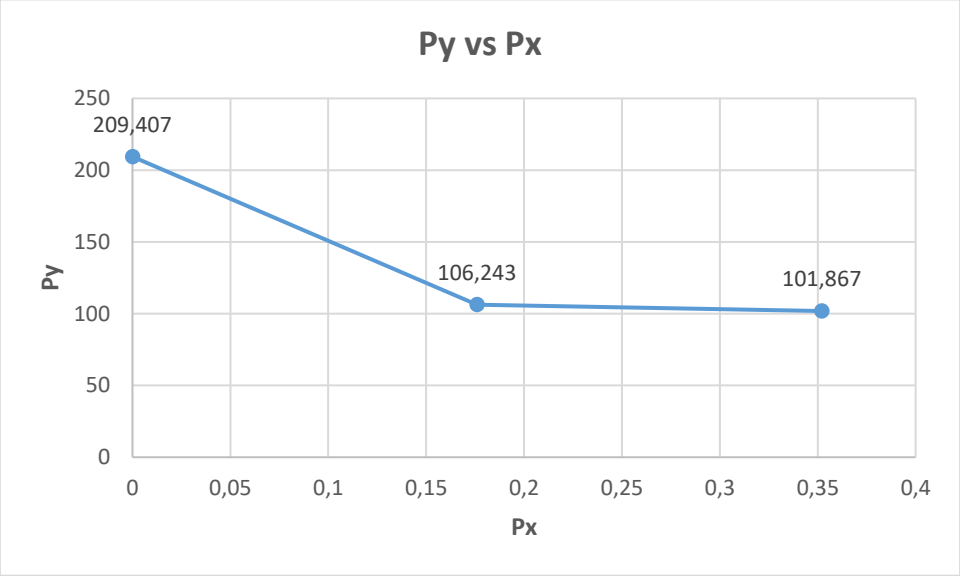

Figure D5: (Py) vs (Px)

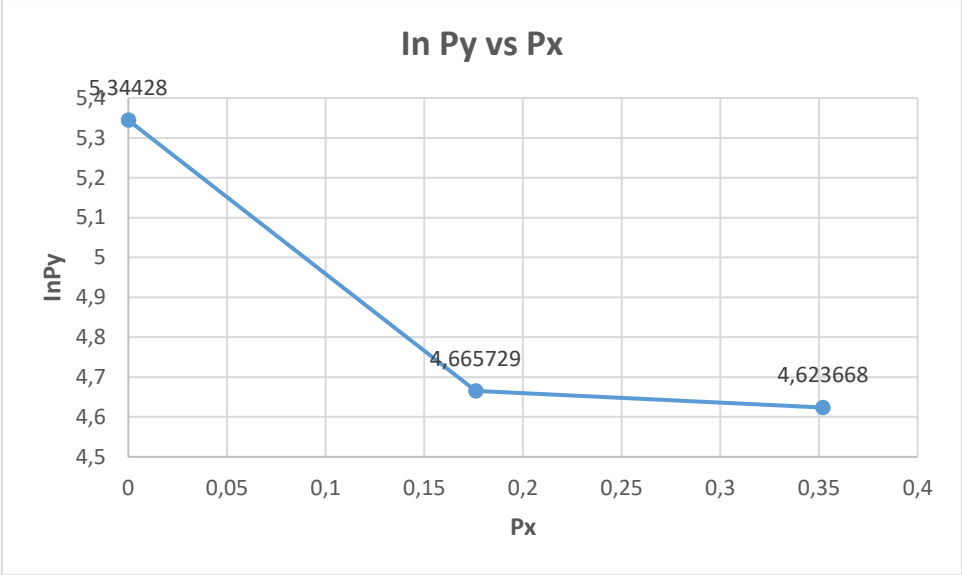

Figure D6: (In Py) vs (Px)

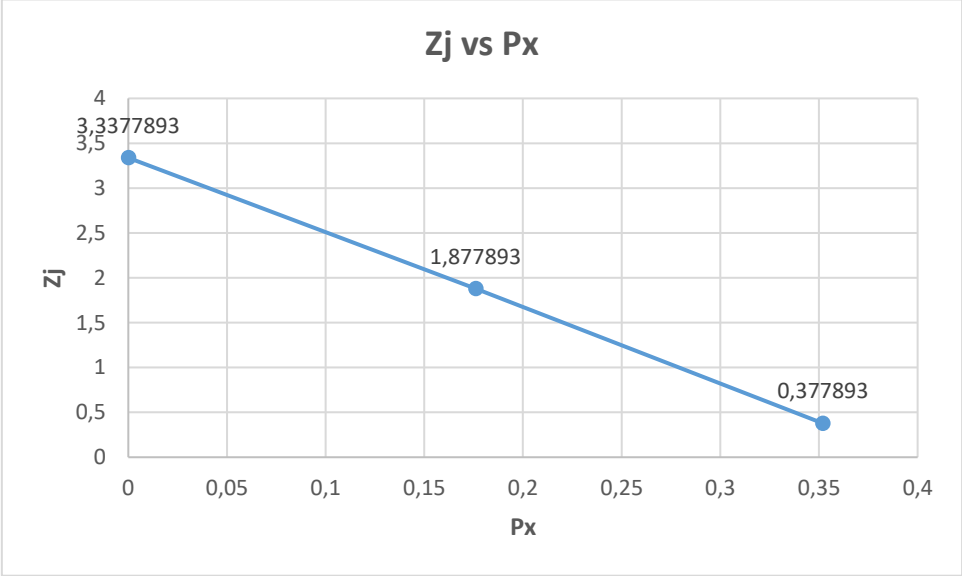

Figure D7: (Zj) vs (Px)

- Figure D4 to D6 in the X-value expanded and the Y-value diminished.
  This means:
- The value of Xh diminished as the time (Px) increased which subsequently implied Xh was inversely corresponding to the time (Px).
- The value of acceleration (Py) decreased as the time (Px) increased which meant Py was inversely proportional to the time (Px).

- The value of Acceleration (In Py) decreased as the time (Px) increased which meant In Py was inversely proportional to the time (Px).

- (Figure D4-D7) obtained from the different results of the Tern conductor where the cable tension of 36 kN appeared to be a similar shape. The value of Zj decreased as the time (Px)increased which meant Zj was inversely proportional to the time (Px).

-

Results for Free Vibration, Accelerometer 2, Mode 1, (Test 2), 36kN Peak 2

The results in Table D2 below were calculated using results obtained from Figure D3 and were as follow:

The first row in Table D2 below displayed the calculated results. Px was the time (ms) and Py was the acceleration (m/s^-2) where both values were used to calculate the information of Table D2. The first loop used the least-squares method, the log decrement was 1.5, the damping factor was 0.232, and the natural frequency was identified as 71.4 rad/s.

Table D2: Calculated Data Collected in Figure D3

Period	Freq	In Py	Yj	In Py (Yj)	Yj^2	Zj	Log Dec	Zeta	Nat Freq	Nat Freq
ms	Hz								rad/s	Hz
0	0	5.027728	0	0	0	3.383047	1.5	0.232	71.4	11.36
0.176	5.681818	4.834033	1	4.834033	1	1.883047				
0.176	5.681818	4.787375	2	9.57475	4	0.383047				
		14.64914	3	17.64914	5					

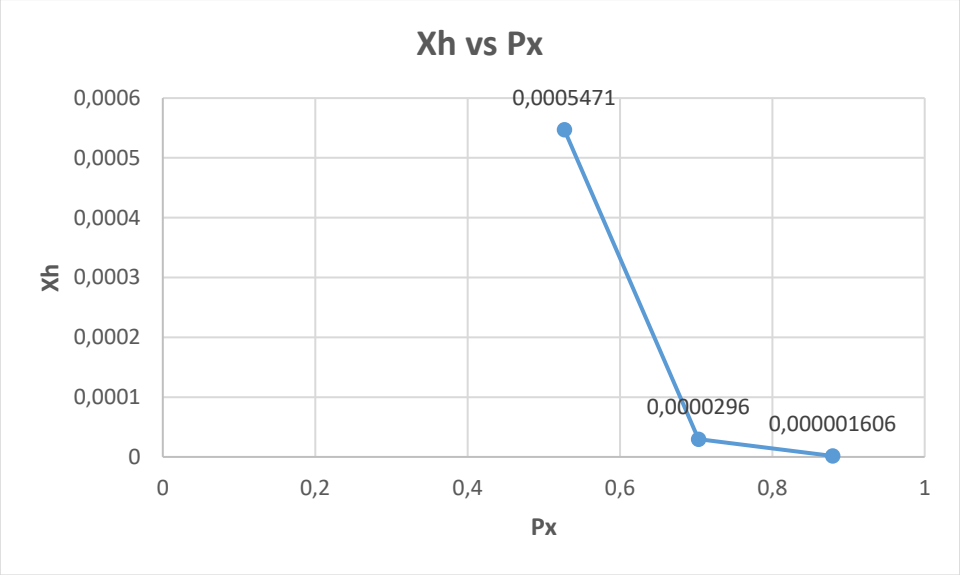

Figure D8: (Xh) vs (Px)

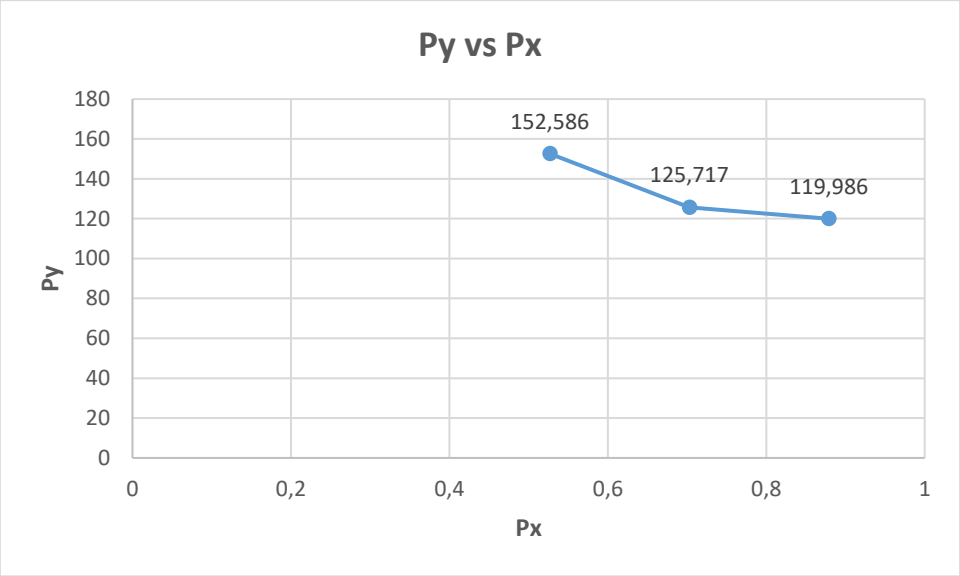

Figure D9: (Py) vs (Px)

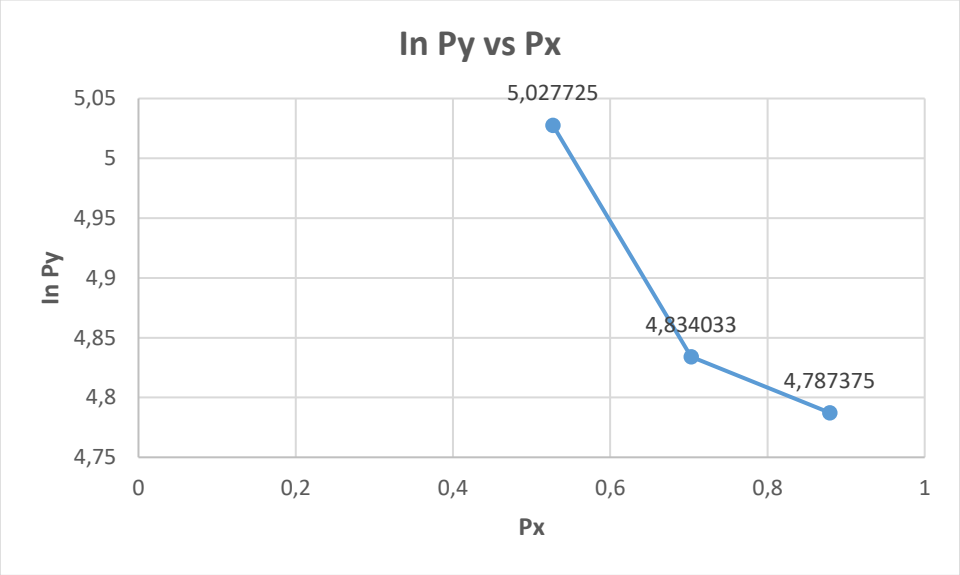

Figure D10: (In Py) vs (Px)

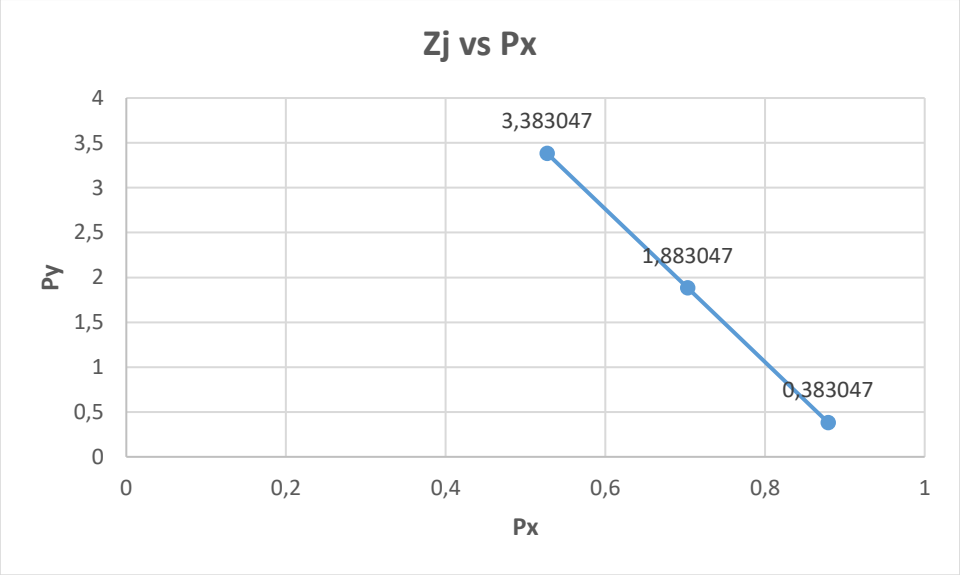

Figure D11: (Zj) vs (Px)

- Figure D8 to D10 in the X-value expanded and the Y-value diminished.

  This means:
- The value of Xh diminished as the time (Px) increased which subsequently implied Xh was inversely corresponding to the time (Px).
- The value of acceleration (Py) decreased as the time (Px) increased which meant Py was inversely proportional to the time (Px).
- The value of Acceleration (In Py) decreased as the time (Px) increased which meant In Py was inversely proportional to the time (Px).

- (Figure D8-D11) obtained from the different results of the Tern conductor where the cable tension of 36 kN appeared to be a similar shape. The value of Zj decreased as the time (Px)increased which meant Zj was inversely proportional to the time (Px).

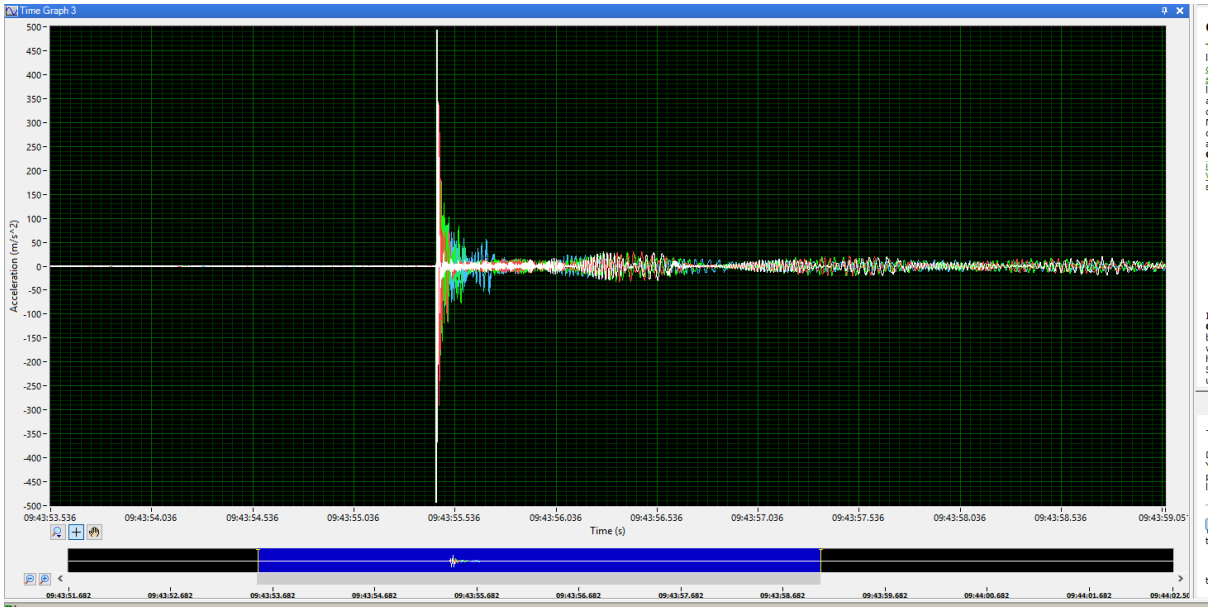

Figure D12: Free Vibration, Accelerometer (All) Mode 1, 45 kN (Test1) National Instrument Desk

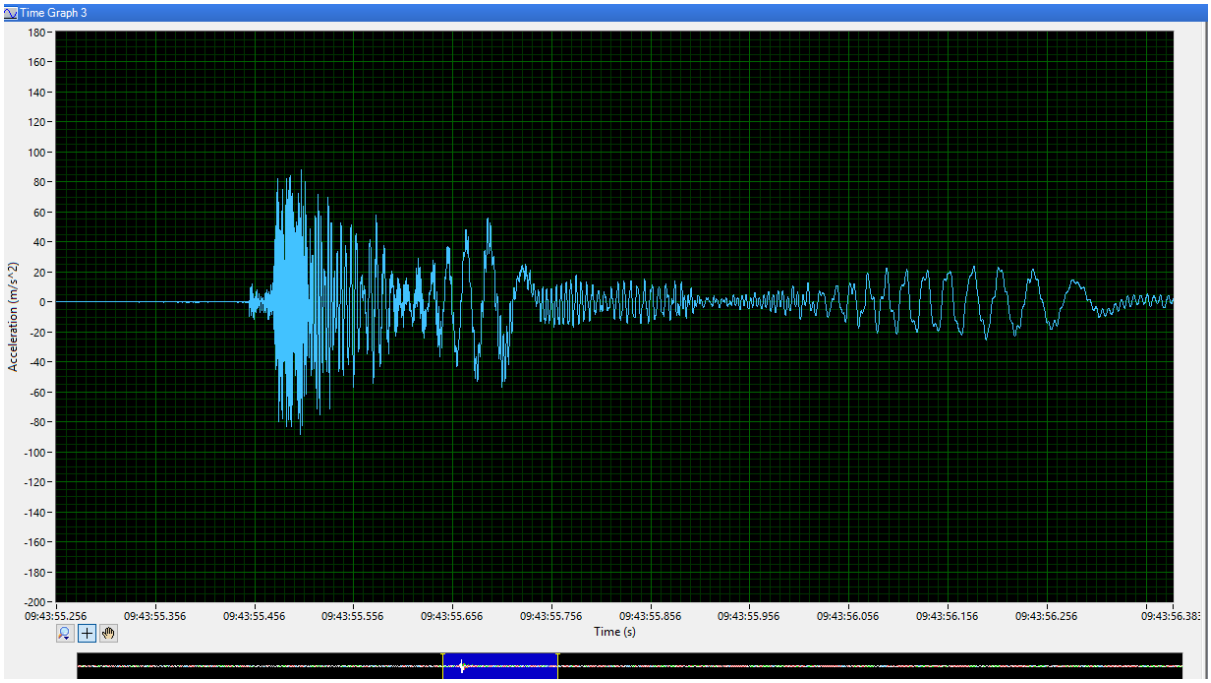

Figure D13: Free Vibration, Accelerometer (3) Mode 1, 45 kN (Test1) National Instrument Desk

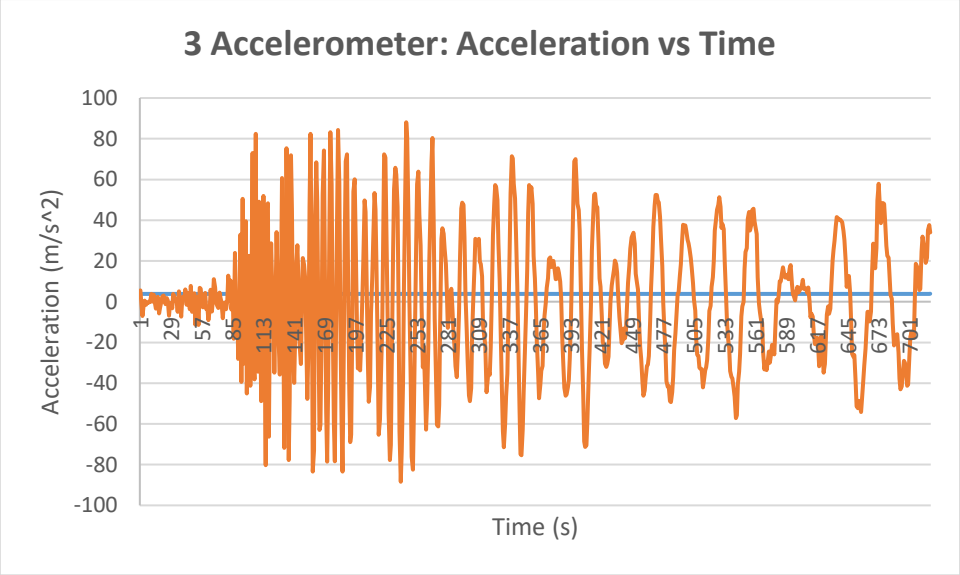

Figure D14: Free Vibration, Accelerometer 3, Mode 1, 45 kN (Test 1) Peak 1

The results in Table D3 below were calculated using results obtained from Figure D14 and were as follow:

The first row in Table D3 below displayed the calculated results. Px was the time (ms) and Py was the acceleration (m/s^-2) where both values were used to calculate the information of Table D3. The first loop used the least-squares method, the log decrement was 1.5, the damping factor was 0.232, and the natural frequency was identified as 71.4 rad/s.

Table D3: Calculated Data Collected in Figure D14

Px	Py	Period	Freq	In Py	Yj	In Py (Yj)	Yj^2	Zj	Log Dec	Zeta	Nat Freq	Nat Freq
ms	x10^-3 m/s^2	ms	Hz								rad/s	Hz
0	333.207	0	0	5.808764	0	0	0	4.233083	1.5	0.232	71.4	11.36
0.176	303.617	0.176	5.681818	5.715767	1	5.715767	1	2.733083				
0.352	291.407	0.176	5.681818	5.674721	2	11.34944	4	1.233083				
Sum	928.231			17.19925	3	20.19925	5					

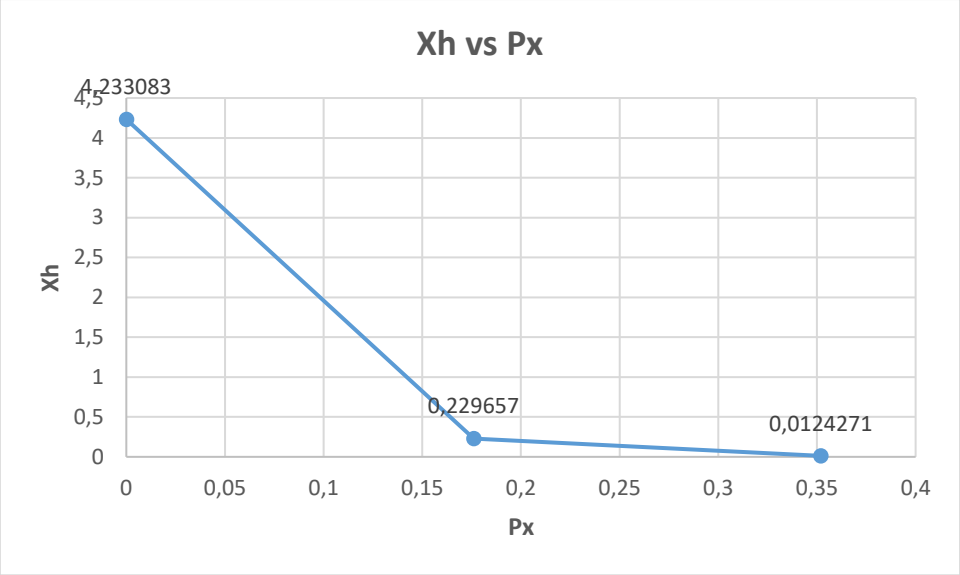

Figure D15: (Xh) vs (Px)

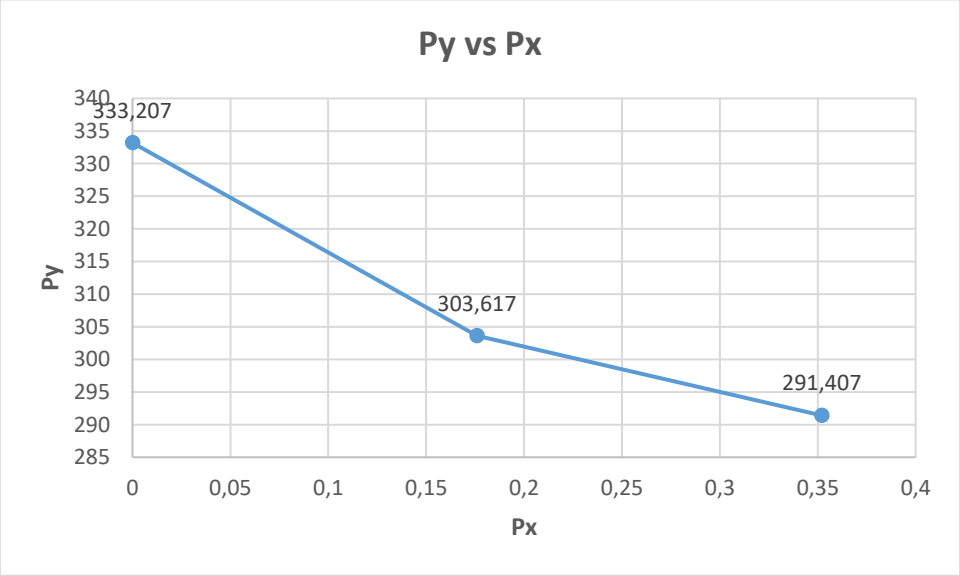

Figure D16: (Py) vs (Px)

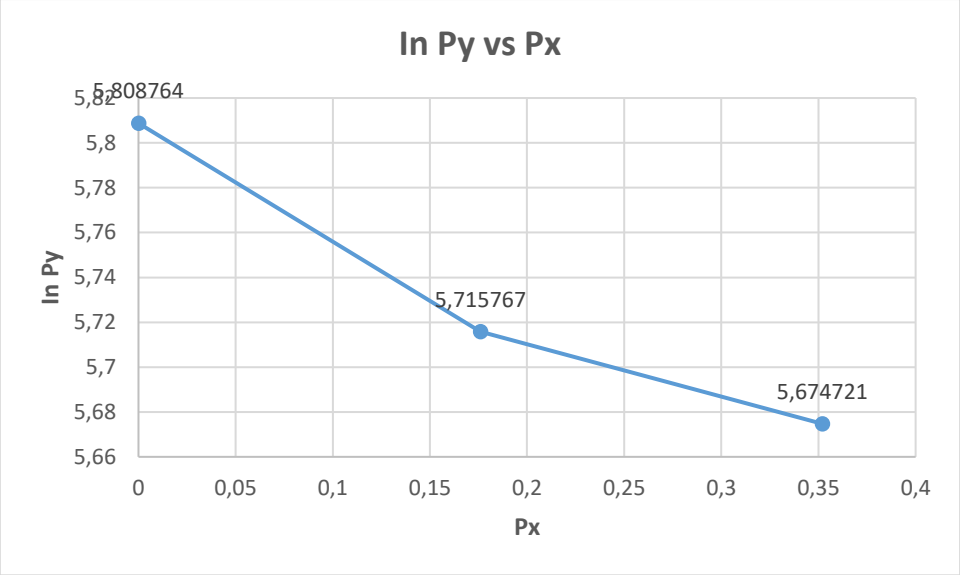

Figure D17: (In Py) vs (Px)

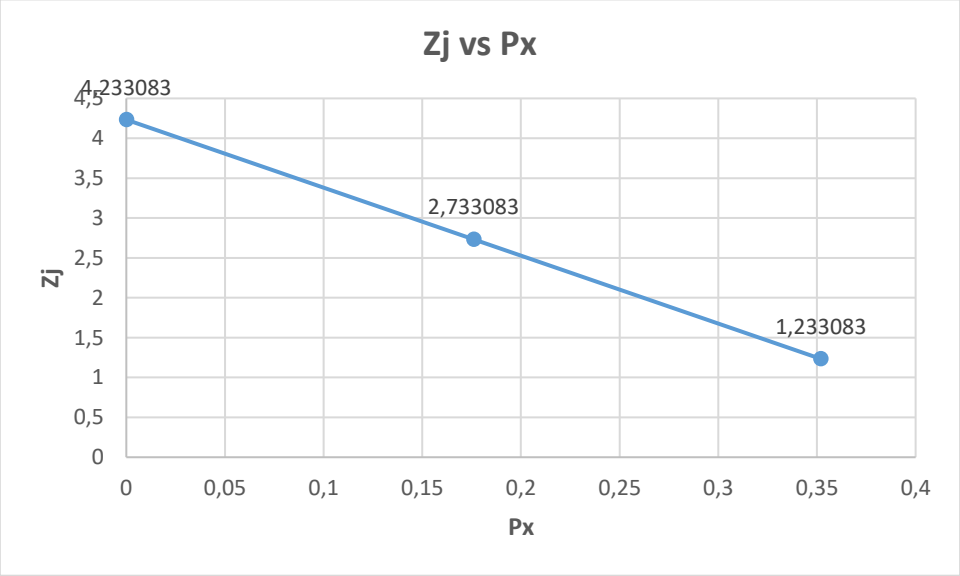

Figure D18: (Zj) vs (Px)

- Figure D15 to D17 in the X-value expanded and the Y-value diminished.
  This means:
- The value of Xh diminished as the time (Px) increased which subsequently implied Xh was inversely corresponding to the time (Px).
- The value of acceleration (Py) decreased as the time (Px) increased which meant Py was inversely proportional to the time (Px).

- The value of Acceleration (In Py) decreased as the time (Px) increased which meant In Py was inversely proportional to the time (Px).

- (Figure D15-D18) obtained from the different results of the Tern conductor where the cable tension of 45 kN appeared to be a similar shape. The value of Zj decreased as the time (Px)increased which meant Zj was inversely proportional to the time (Px).

Results for Free Vibration, Accelerometer 3, Mode 1, (Test 1), 45 kN Peak 2

The results in Table D4 below were calculated using results obtained from Figure D14 and were as follow:

The first row in Table D4 below displayed the calculated results. Px was the time (ms) and Py was the acceleration (m/s^-2) where both values were used to calculate the information of Table D4. The first loop used the least-squares method, the log decrement was 1.5, the damping factor was 0.232, and the natural frequency was identified as 71.4 rad/s.

Table D4: Calculated Data Collected in Figure D14

Px	Py	Period	Freq	In Py	Yj	In Py (Yj)	Yj^2	Zj	Log Dec	Zeta	Nat Freq	Nat Freq
ms	x10^-3 m/s^2	ms	Hz								rad/s	Hz
0.527	371.038	0	0	5.916304	0	0	0	4.245287	1.5	0.232	71.4	11.36
0.703	355.641	0.176	5.681818	5.873922	1	5.873922	1	5.745287				
0.879	231.744	0.176	5.681818	5.445633	2	10.89127	4	7.245287				
Sum	958.423			17.23586	3	20.23586	5					

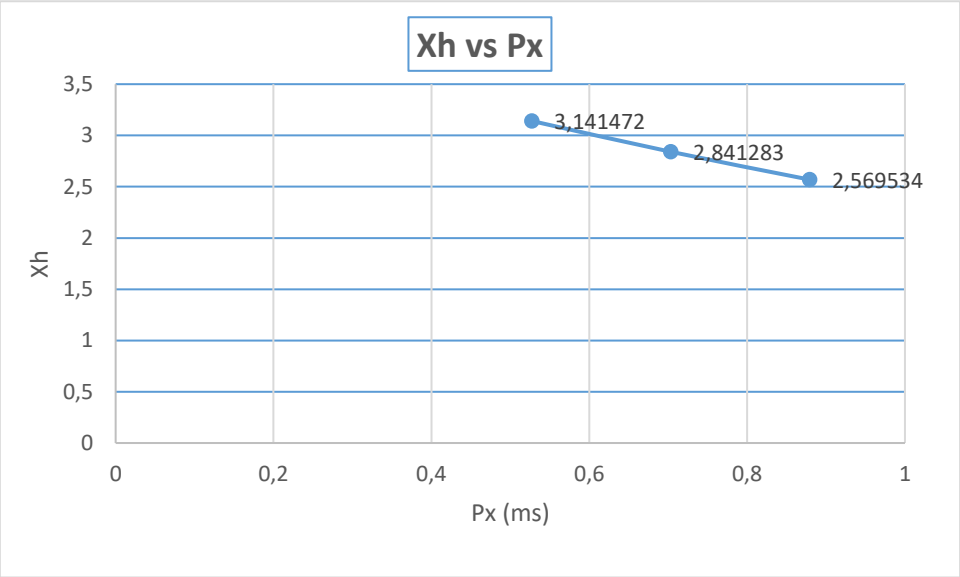

Figure D19: (Xh) vs (Px)

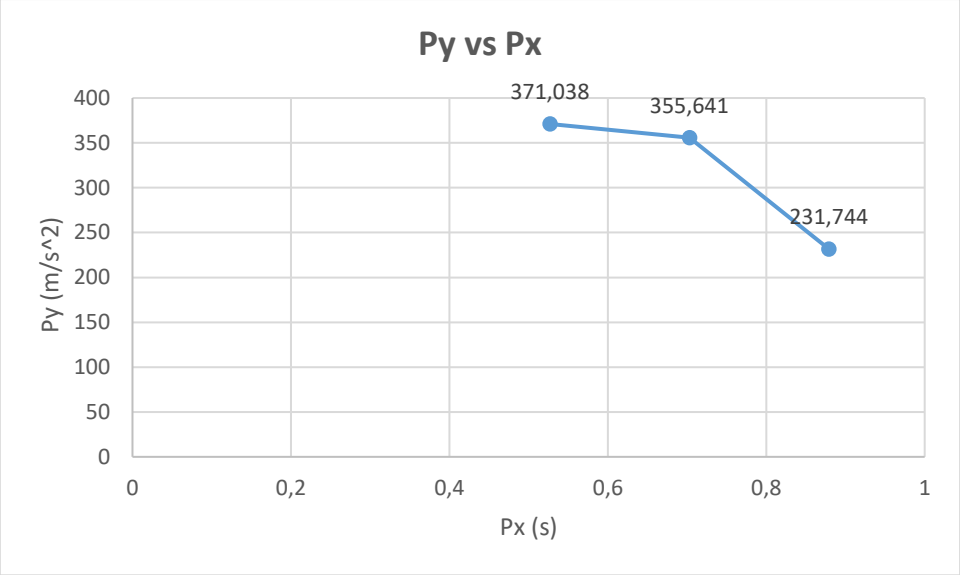

Figure D20: (Py) vs (Px)

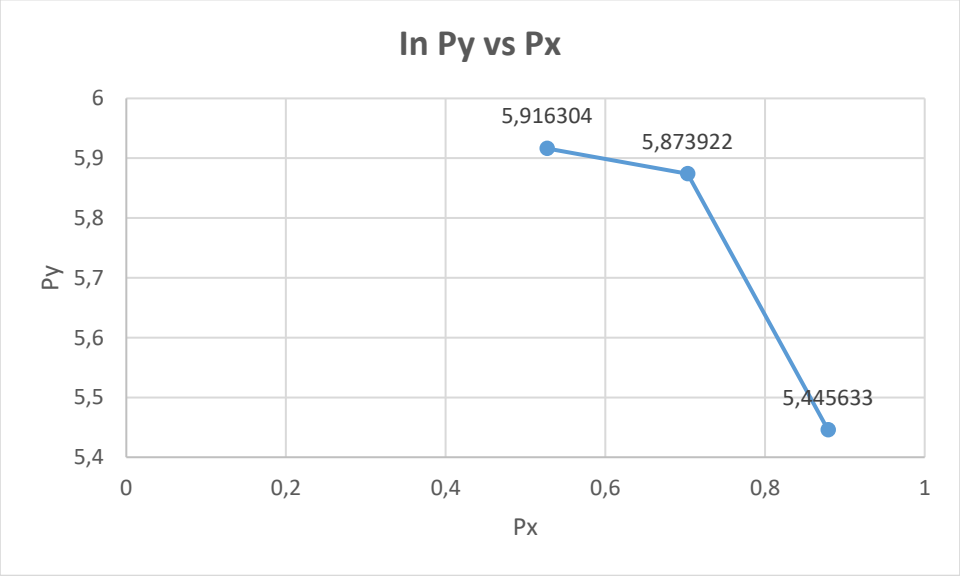

Figure D21: (In Py) vs (Px)

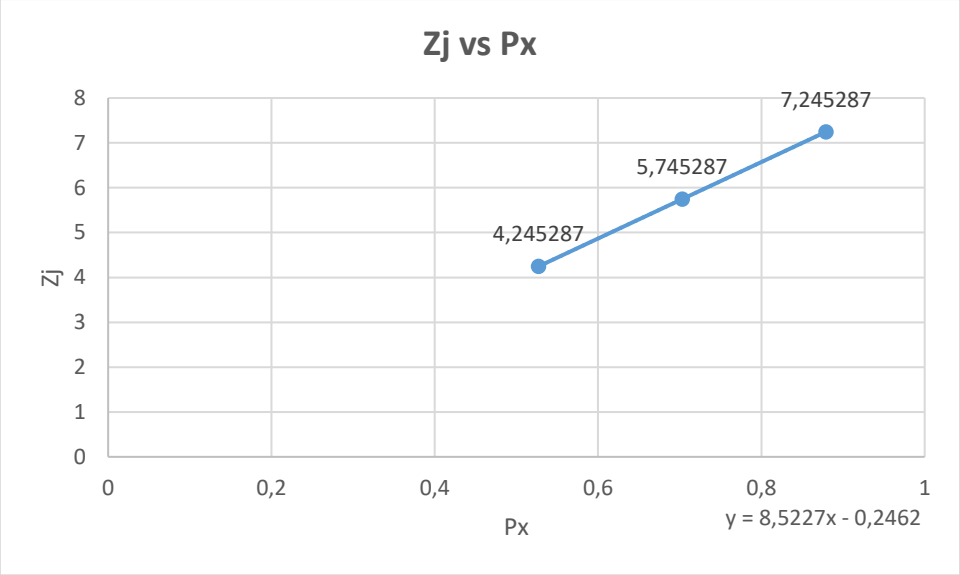

Figure D22: (Zj) vs (Px)

- Figures D19 to D21 in the X-value expanded and the Y-value diminished.
  This means:
- The value of Xh diminished as the time (Px) increased which subsequently implied Xh was inversely corresponding to the time (Px).
- The value of acceleration (Py) decreased as the time (Px) increased which meant Py was inversely proportional to the time (Px).
- The value of Acceleration (In Py) decreased as the time (Px) increased which meant In Py was inversely proportional to the time (Px).

- (Figure D19-D22) obtained from the different results of the Tern conductor where the cable tension of 45 kN appeared to be a similar shape. The value of Zj decreased as the time (Px)increased which meant Zj was inversely proportional to the time (Px).

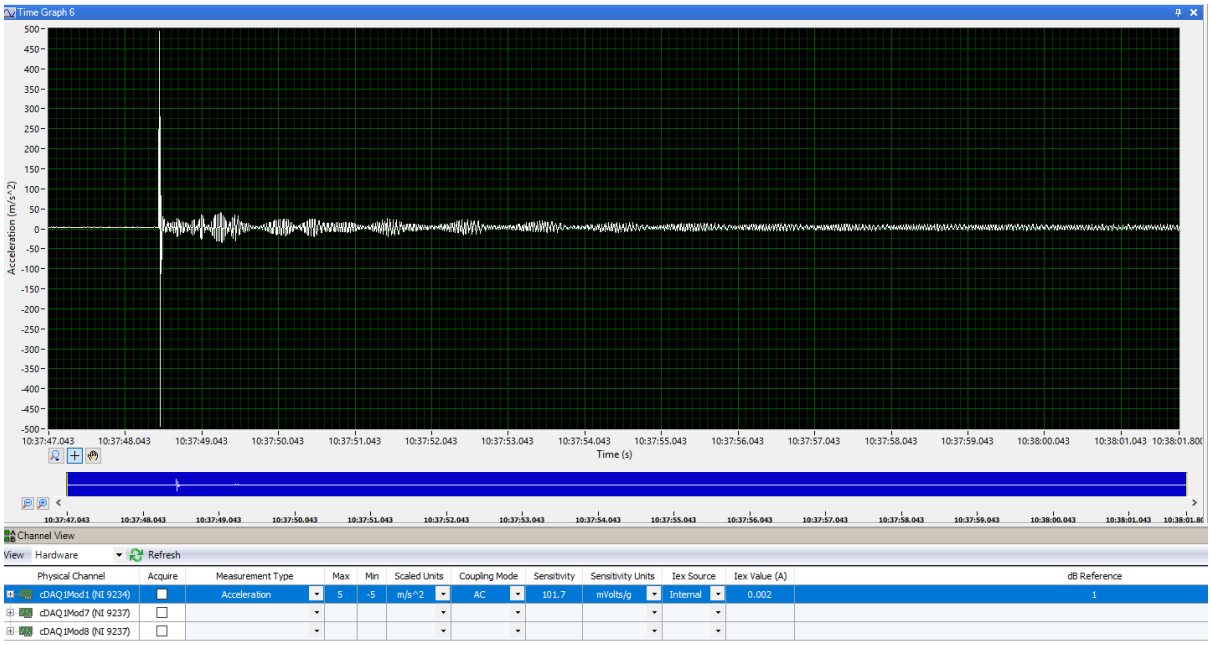

Figure D23: Free Vibration, Accelerometer (1) Mode 1, 24 kN (Test2) National Instrument Desk

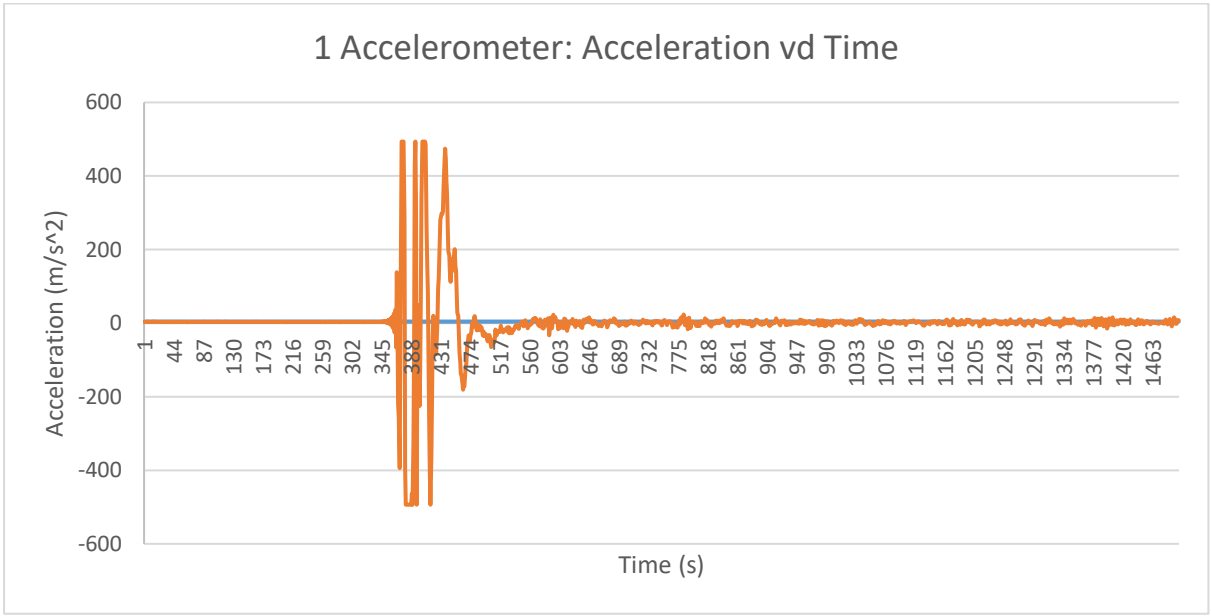

Figure D24: Free Vibration, Accelerometer 1, Mode 1, 54 kN (Test 2)

The results in Table D5 below were calculated using results obtained from Figure 186 and were as follow:

The first row in Table D5 below displayed the calculated results. Px was the time (ms) and Py was the acceleration (m/s^-2) where both values were used to calculate the information of Table

D5. The first loop used the least-squares method, the log decrement was 1.5, the damping factor was 0.232, and the natural frequency was identified as 71.4 rad/s.

Table D5: Calculated Data Collected in Figure D24

Px	Py	Period	Freq	ln Py	Yj	ln Py (Yj)	Yj^2	Zj	Log Dec	Zeta	Nat Freq	Nat Freq
ms	x10^-3 m/s^2	ms	Hz								rad/s	Hz
0	338.331	0	0	5.824025	0	0	0	4.190793	1.5	0.232	71.4	11.36
0.176	325.424	0.176	5.681818	5.785129	1	5.785129	1	2.690793				
0.352	235.856	0.176	5.681818	5.463221	2	10.92644	4	1.190793				
Sum	899.611			17.07238	3	20.07238	5					

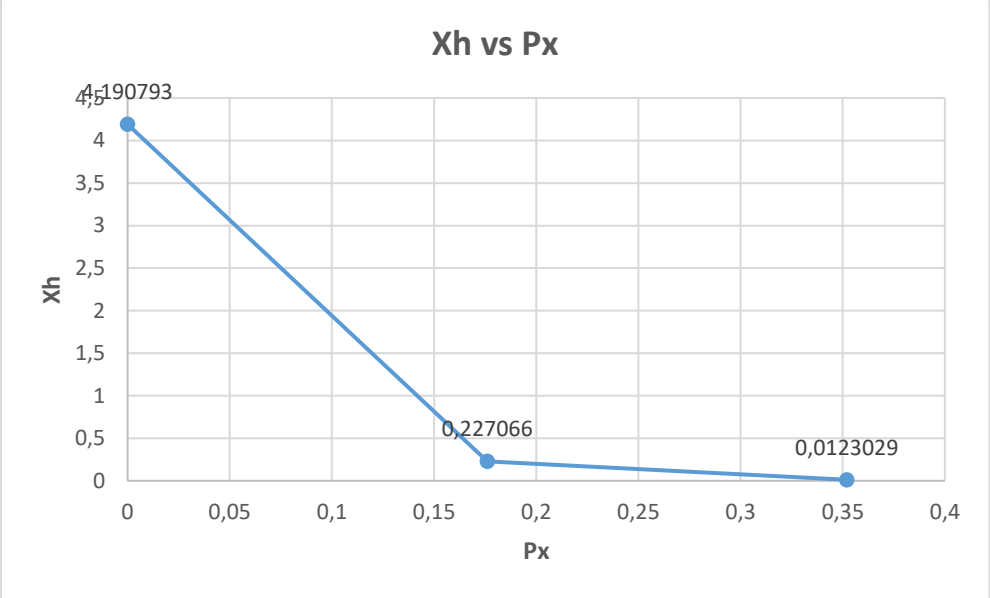

Figure D25: (Xh) vs (Px)

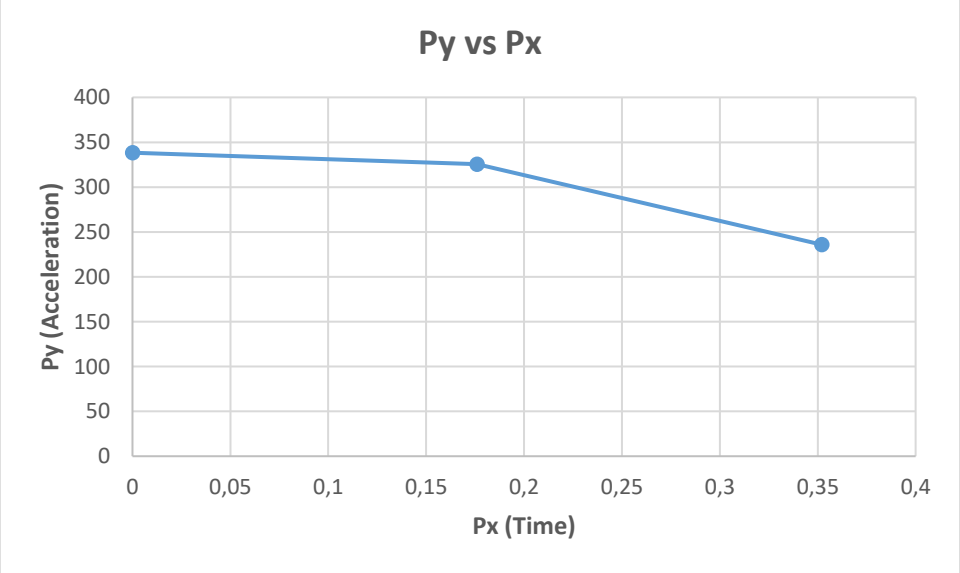

Figure D26: (Py) vs (Px)

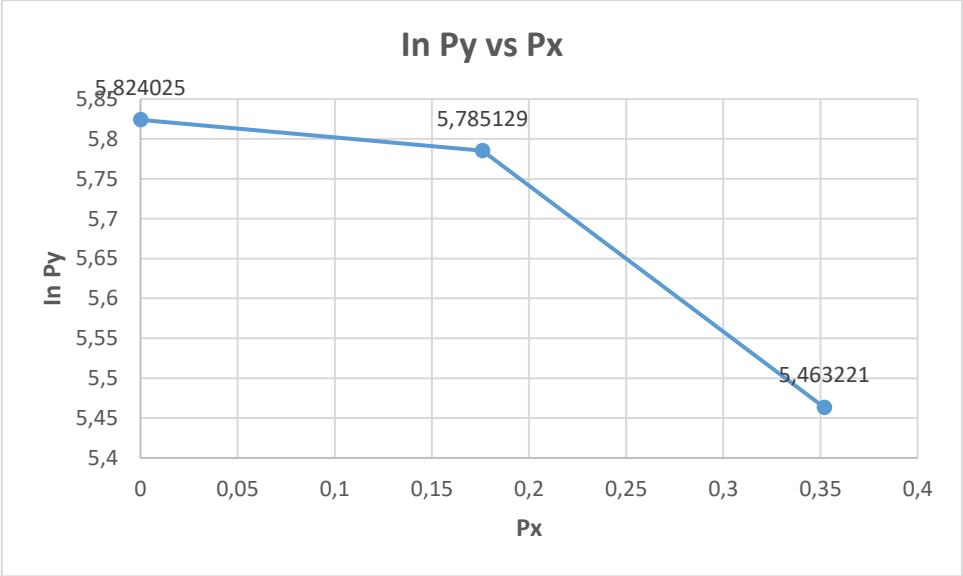

Figure D27: (In Py) vs (Px)

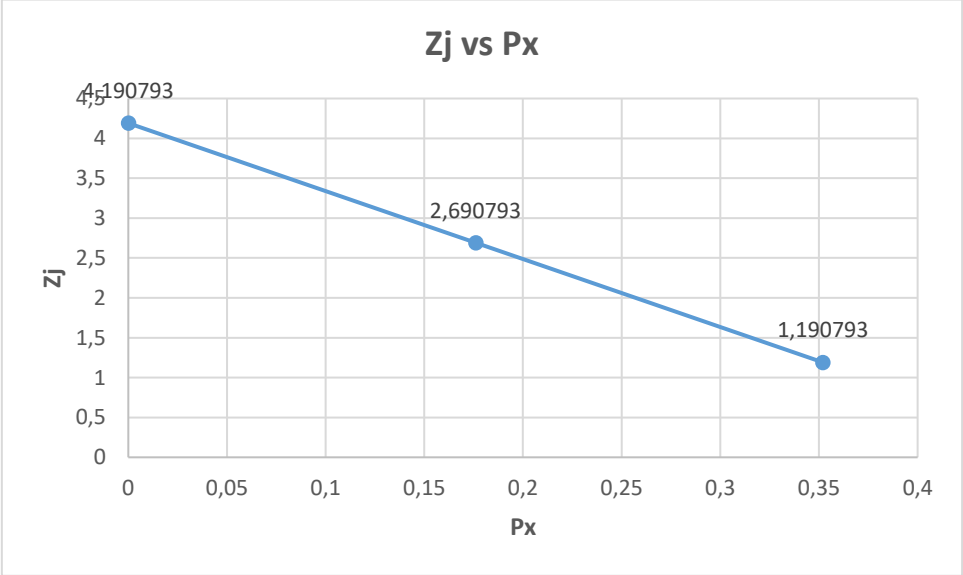

Figure D28: (In Py) vs (Px)

- Figure D25 to D27 in the X-value expanded and the Y-value diminished.

  This means:
- The value of Xh diminished as the time (Px) increased which subsequently implied Xh was inversely corresponding to the time (Px).
- The value of acceleration (Py) decreased as the time (Px) increased which meant Py was inversely proportional to the time (Px).

- The value of Acceleration (In Py) decreased as the time (Px) increased which meant In Py was inversely proportional to the time (Px).

- (Figures D25-D28) obtained from the different results of the Tern conductor where the cable tension of 54 kN appeared to be a similar shape. The value of Zj decreased as the time (Px)increased which meant Zj was inversely proportional to the time (Px).